

# **Epigenetics And Chromosome Segregation In Human Pre-implantation Embryos**

**Christine van de Werken**

## **Epigenetics And Chromosome Segregation In Human Pre-implantation Embryos**

Thesis, Erasmus University Rotterdam, The Netherlands

The research presented in this dissertation was performed at the Department of Obstetrics & Gynaecology, Erasmus MC Rotterdam, The Netherlands

The research for this thesis was performed within the framework of the Erasmus Postgraduate School Molecular Medicine.



This thesis was financially supported by the Department of Obstetrics & Gynaecology, Erasmus MC Rotterdam, The Netherlands

Printing of this thesis was further financially supported by Origio Benelux B.V.

ISBN/EAN: 978-94-6259-726-6

Cover: iStock.com

Lay-out by: Legatron Electronic Publishing, Rotterdam, the Netherlands

Printed by: Ipskamp Drukkers, Enschede, the Netherlands

© Christine van de Werken, 2015

All rights reserved. No part of this thesis may be reproduced or transmitted in any form, by any means, without the prior written permission of the author, or where appropriate, of the publisher of the articles and figures.

# Epigenetics And Chromosome Segregation In Human Pre-implantation Embryos

Epigenetica en chromosoomsegregatie in humane pre-implantatie embryo's

Proefschrift

ter verkrijging van de graad van doctor aan de  
Erasmus Universiteit Rotterdam  
op gezag van de  
rector magnificus

prof.dr. H.A.P. Pols

en volgens besluit van het College voor Promoties.  
De openbare verdediging zal plaatsvinden op  
woensdag 30 september 2015 om 11.30 uur

door

**Christine van de Werken**  
geboren te Werkendam

## Promotiecommissie

**Promotor:** Prof.dr. J.S.E. Laven

**Overige leden:** Prof.dr. J.H. Gribnau  
Prof.dr. R.M.W. Hofstra  
Prof.dr. S.M.A. Lens

**Copromotor:** Dr.ir. E.B. Baart

**Paranimfen:** Elisa van de Werken  
Cindy Eleveld

Aan iedereen  
die wacht op een voorjaarszon  
Aan iedereen  
die zachtjes op een wonder hoopt  
Aan iedereen  
die alles weglacht en altijd wegloopt  
Aan iedereen  
die dacht dat 'ie niet dapper durft te zijn

*Bløf, Aan Iedereen Die Wacht, 2009*



## Table of Contents

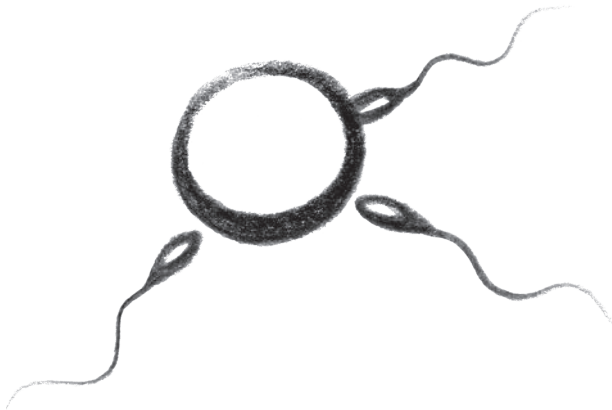
<b>Chapter 1</b>	General introduction	9
<b>Chapter 2</b>	Paternal heterochromatin formation in human embryos is H3K9/HP1 directed and primed by sperm-derived histone modifications	23
<b>Chapter 3</b>	A role for Aurora C in the chromosomal passenger complex during human preimplantation embryo development	63
<b>Chapter 4</b>	A universal method for sequential immunofluorescent analysis of chromatin and chromatin-associated proteins on chromosome spreads	91
<b>Chapter 5</b>	Chromosome segregation regulation in human zygotes: altered mitotic histone phosphorylation dynamics underlying centromeric targeting of the chromosomal passenger complex	113
<b>Chapter 6</b>	General discussion	147
<b>Chapter 7</b>	Summary	157
	Nederlandse samenvatting	161
<b>Addendum</b>	PhD portfolio	167
	Dankwoord	169
	Curriculum Vitae	173





# CHAPTER 1

## General introduction



## Introduction

Around 5 million children have been born worldwide through the use of in vitro fertilization (IVF), an assisted reproductive technology first used successfully in 1978 [1]. In Europe in 2009, the mean pregnancy rate per embryo transfer was around 32% [2]. In order to achieve even better results in the future, we need to gain knowledge on all aspects of the treatment, including early embryo development. Understanding processes underlying pre-implantation embryo development will lead to improvements in embryo culture and selection, and thereby eventually to increased pregnancy rates.

It has been known that some aspects of cells in a pre-implantation embryo are very different from somatic cells, such as cell cycle regulation, gene expression profiles, chromatin dynamics and chromosome segregation. Therefore, studying embryonic cells is crucial for our understanding of pre-implantation development. In this thesis, we describe the research we performed in human pre-implantation embryos derived from IVF.

Chromosomal abnormalities are detected at high frequencies in human IVF-embryos. The aim of our research was to investigate processes possibly underlying these abnormalities: the regulation of chromosome segregation and the organization of chromatin structure.

### Chromosomal abnormalities in pre-implantation embryos

In every cell of a human body, 23 pairs of chromosomes contain the genetic material, the DNA. During every mitotic cell division, duplicated chromosomes are equally separated over the two daughter cells, a process called chromosome segregation. Tight regulation of chromosome segregation is essential in order to prevent aneuploidy (an incorrect number of chromosomes) and maintain genetic integrity. In somatic cells, several mechanisms cooperate to prevent chromosome missegregation. Surprisingly, chromosomal abnormalities are detected at high frequencies in human pre-implantation embryos [3-14], resembling the genetic instability observed in human cancers [11,15]. This suggests a decreased functionality or even a lack of the somatic mechanisms guarding chromosome segregation during the first mitotic divisions of an embryo [7]. Next to that, histone modifications, epigenetic marks that are important for chromatin structure and correct chromosome segregation, are different in oocytes and spermatozoa and need to be re-established in early embryos. The research described in this thesis aimed to investigate both the mechanisms regulation chromosome segregation and the re-establishment of epigenetics marks in human pre-implantation embryos, in order to shed light on the possible causes of chromosomal abnormalities. The following paragraphs give a concise description of mitosis, epigenetics an chromatin organization, regulation of chromosome segregation, and the investigated processes.

### Mitosis

The cell cycle consist of four phases. In the G1 phase, the cell prepares for DNA replication. In the subsequent S phase, DNA replication takes place. Thereafter, in the G2 phase, the cell prepares for division. These three phases together are also called interphase. After G2 the fourth cell cycle phase, called mitosis, begins. During mitosis, duplicated chromosomes are separated and the cell divides [16-17].

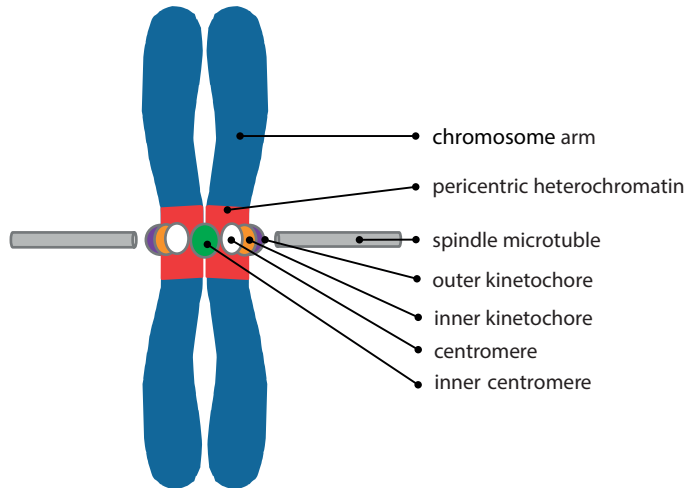


Figure 1 — Schematic representation of a chromosome at the time of cell division. Indicated are the centromeres and kinetochores, at which the spindles attach.

Mitosis consists of five phases. During prophase, chromosomes in the nucleus condense and the centrosomes separate and start to form the mitotic spindle. During prometaphase, the nuclear envelope breaks down and the spindle attaches to the kinetochores of the condensed chromosomes (Figure 1). Attached chromosomes then move to the equatorial plane, resulting in alignment at the metaphase plate during metaphase. Once this alignment is achieved, the anaphase promoting complex/cyclosome (APC/C) is activated and anaphase begins. During anaphase, chromosome segregation takes place: sister chromatids are separated to opposite sites of the cell. Eventually, in telophase, a cleavage furrow forms and the cell divides. Also, the nuclear envelopes are reformed and the chromosomes decondense, resulting in two new interphase nuclei [18-19]. Figure 2 illustrates these phases of mitosis in the first mitotic division of an embryo.

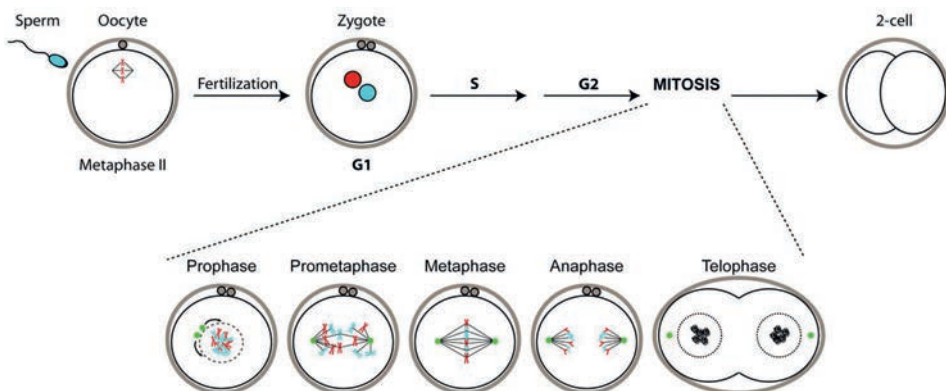
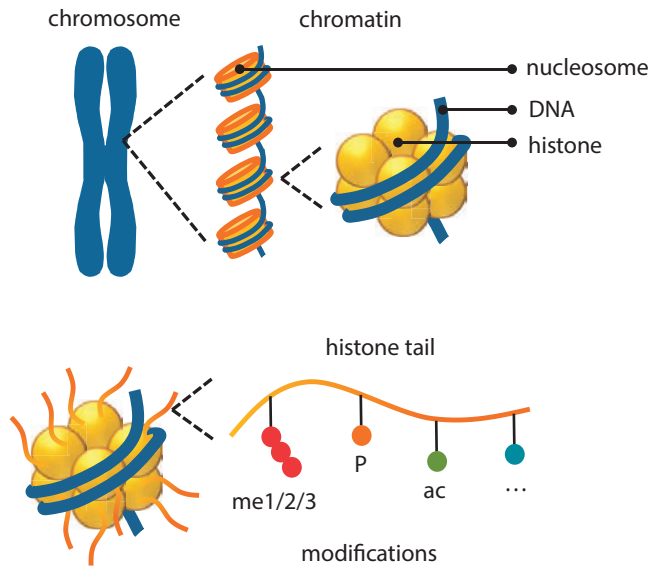


Figure 2 — Schematic representation of the first mitotic cell cycle of an embryo. After fertilization of an oocyte by a sperm cell, one paternal and one maternal pronucleus are formed in the zygote during the G1 phase. After S phase en G2 phase, mitosis begins, eventually resulting in the first cell division. (Adopted from [20])

## Epigenetics and chromatin organization

The term ‘epigenetics’ refers to heritable marks and changes in the genome, which do not alter the underlying DNA sequence. Epigenetic marks, such as DNA methylation [21] and histone modifications [22-26], determine the structure of chromatin and chromosomes, which is essential for nuclear architecture, cell potency, gene expression and chromosome segregation. In this paragraph, we briefly describe the structure of chromatin and the characteristics and function of the most prominent chromatin domains.



**Figure 3** — Schematic representation of the structure of a chromosome. DNA is wrapped around a histone octamer, together called nucleosome, forming the basic repeating subunit of chromatin. Amino acids in the histone tails are subject to posttranslational enzymatic modifications, such as (mono-/di-/tri-) methylation, phosphorylation, and acetylation.

In every somatic cell nucleus, DNA is wrapped around a histone octamer, together called a nucleosome, forming the basic repeating subunit of chromatin (Figure 3). Nucleosomes consist of eight histones of different types: two histone H2A-H2B dimers and one histone H3-H4 tetramer, and are linked by histone H1 and linker DNA. The presence of certain histone variants and post-translational modifications at amino acid residues in the N-terminal tail of histones influence the structure of chromatin. Examples of such histone variants are H2AZ, H3.3 and CENP-A. Histone modifications are for example methylation, phosphorylation, ubiquitination and acetylation (Figure 3). Both histone variants and histone modifications have distinct biochemical properties, which result in a certain configuration of chromatin. Together with chromatin-associated proteins and non-coding RNAs, this determines chromatin structure and defines chromatin domains [22-26].

Functional chromatin domains are essential to maintain chromosome structure and to regulate gene expression.

The two most prominent chromatin domains are euchromatin and heterochromatin. Euchromatin is an 'open', decondensed form of chromatin, associated with transcription. It is characterized by di- and trimethylation of histone H3 at lysine 4 and lysine 36 (H3K4me2/3, H3K36me2/3). Heterochromatin is a condensed, silenced form of chromatin, associated with transcriptional repression. There are two forms of heterochromatin: constitutive and facultative heterochromatin, each characterized by different epigenetic marks.

### **Heterochromatin**

Facultative heterochromatin is associated with the regulation of gene expression and can, depending on the situation, also become transcriptionally active. It is formatted by Polycomb group (PcG) proteins. These proteins catalyze the monoubiquitination of lysine 119 on histone H2A (H2AK119Ub1) [27] and the di- and trimethylation of lysine residue 27 of histone H3 (H3K27me2/3) [28-29]. PcG proteins are essential regulators in development; they play a crucial role in cell fate decisions and differentiation [29-32].

Constitutive heterochromatin (cHC) is mostly associated with structural functions, for example defining the centromeres (Figure 1) and telomeres. These chromatin domains do not change, but remain condensed throughout the cell cycle and are inherited by the daughter cells after cell division. cHC is modified by Suv39h1/h2 histone methyltransferases (HMTs) [33-35], which trimethylate histone H3 at lysine 9 (H3K9me3). H3K9me3 subsequently recruits heterochromatin protein 1 (HP1) [36-37] and HMTs which trimethylate histone H4 at lysine 20 (H4K20me3) [38] and histone H3 at lysine 64 (H3K64me3) [39]. H3K9me3 also recruits DNA methyltransferases, eventually leading to establishment of a condensed, transcriptionally repressed state [33,38,40-41].

### **Pericentric heterochromatin and chromosome segregation**

A cHC domain important for chromosome segregation is pericentric heterochromatin (pHC) [34]. These chromatin domains are located adjacent to the centromeric region of each chromosome (Figure 1) and characterized by classic cHC marks, such as H3K9me3, H4K20me3 and abundant DNA methylation [42].

During mitosis, different protein complexes are formed in the centromeric region of chromosomes, such as the kinetochores, which bind the microtubules of the mitotic spindle, and the (inner) centromeres, which connect the sister chromatids (Figure 1) [43]. These complexes are crucial for correct chromosome segregation, not only because of their structural role, but also because they are part of the mitotic checkpoint (see below). The localization of the centromeres is specified by chromatin regions that contain certain histone modifications and histone variants, such as the centromere-specific histone H3 variant CENP-A (CenH3) [25]. pHC plays a role in the formation of these regions. It also limits CENP-A incorporation, thereby serving as a boundary for the centromeric region and ensuring precise CENP-A localization [25]. This is crucial for correct centromere function and chromosome segregation, as both overexpression of CENP-A and disruption of pHC marks have been linked to chromosome missegregation [34,44].

As pHC is essential for correct chromosome segregation, we aimed to investigate pHC dynamics in human pre-implantation embryos. These dynamics might differ from what has been described for somatic cells, since chromatin structure and domains have to be re-established after fertilization (see below).

### Chromatin structure re-establishment in pre-implantation embryos

At the time of fertilization, the parental gametes, the oocyte and the spermatozoon, are very dissimilar. This extends to the structure of their chromatin. Maternal DNA is present in nucleosomes, as in somatic cells, and is marked with histone modifications inherited from the oocyte. In contrast, the DNA in the spermatozoon is wrapped around protamines, as a result from the histone-to-protamine exchange during spermatogenesis (Figure 3). Protamine-based chromatin is much more condensed than nucleosome-based chromatin, enabling the formation of the very small sperm head. During the first stages of pre-implantation development, dramatic changes occur in chromatin organization: the paternal protamines are replaced by maternally provided histones and these histones are modified in order to re-establish the paternal chromatin structure and form a functional embryonic genome (Figure 4).

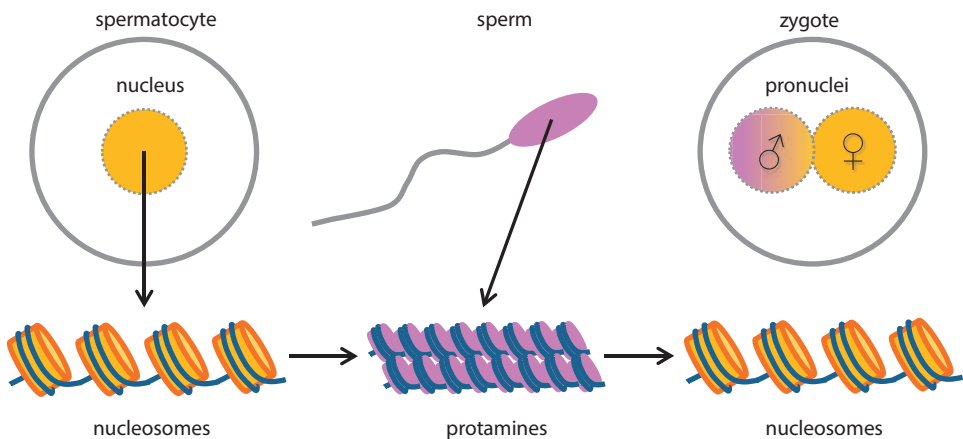


Figure 4 — Schematic representation of the configuration of chromatin from spermatocytes to zygotes, showing the transition from nucleosomes to protamines during spermatogenesis and the re-establishment of a nucleosome-based chromatin structure in the zygote.

Mechanisms of chromatin structure re-establishment have been studied extensively in mouse embryos, especially for pHC (for reviews see [45-48]). In short, pHC in mouse spermatozoa is largely devoid of canonical cHC marks and the paternal pHC signature has to be re-established after fertilization. The H3K9/HP1 pathway has been shown not to be involved in this process. Instead, maternally provided PRC1 and PRC2 transiently establish pHC, which becomes marked with

H3K27me3 [49-50]. During the 8-cell stage the H3K9/HP1 pathway takes over and the two parental genomes become equivalent for H3K9me3 [50-51]. Other pHC associated marks, such as H3K64me3 and H4K20me3, remain undetected until after compaction and implantation, respectively [39,52-53]. Thus, in mouse pre-implantation embryos the PRC1/2 pathway operates as a transient backup mechanism for pHC formation [50].

Although findings in early mouse embryos are often assumed to be universal for mammalian embryos [47-48,54], epigenetic regulation of early development is known to differ between mammals [55]. Importantly, it is not known how the process of pHC re-establishment is regulated in human pre-implantation embryos. As mentioned above, we aimed to investigate the dynamics of pHC in human embryos. Interestingly, during human spermatogenesis not all nucleosomes are replaced by protamines. Whereas mouse spermatozoa retain 1% of their histones [56], this percentage is reported to be higher and more variable in human spermatozoa (4-30%) [57-60]. Therefore, for several years researchers have speculated about an epigenetic contribution of human spermatozoa to embryo development. In our study, we investigated the mechanism of pHC re-establishment in human pre-implantation embryos and the possible contribution of sperm-derived histones to this process.

### Regulation of chromosome segregation

In order to prevent missegregation of chromosomes during mitosis (see above), the onset of anaphase has to be delayed as long as chromosomes are not or not correctly attached to the mitotic spindle. As described above, the APC/C regulates anaphase entry. In case of the presence of unattached chromosomes, the mitotic checkpoint complex (MCC) inhibits the APC/C. The MCC consists of diverse proteins (Mad2, Bub3, BubR1) which localize at the unattached kinetochore and inhibit Cdc20, an essential cofactor of APC/C. Once all chromosomes have reached attachment, the MCC is inactivated and APC/C is no longer inhibited, enabling anaphase onset (Figure 5) [61].

The chromosomal passenger complex (CPC) consists of Survivin, Borealin, INCENP and Aurora kinase B (Aurora B / AURKB), and has diverse roles during mitosis, for example in chromosome condensation and cytokinesis [61,63-66]. At the start of mitosis, Aurora B phosphorylates histone H3 at serine 10 (H3pS10) (Figure 5) along the chromosome arms (Figure 1). Later, during prometaphase, the CPC localizes to the inner centromeric region, where it exerts its role in the correction of misattached chromosomes (non-bipolar attachments: for review see [66]). Recently, it has been proposed that the localization of the CPC at the inner centromere is regulated by two histone modifications, phosphorylation of histone H2A at threonine 120 (H2ApT120) and phosphorylation of histone H3 at threonine 3 (H3pT3), which are catalyzed by Bub1 and Haspin respectively [67-68] (Figure 5). Aurora B in turn phosphorylates and thereby further activates Haspin, leading to a positive feedback loop for accumulation of the CPC at the inner centromere [69] (Figure 5). At the centromere, the CPC regulates kinetochore-microtubule attachments. Incorrect attachments, for example when both sister chromatids are attached to the same spindle pole, are destabilized by the CPC in order to promote correct attachments. This destabilization also leads to unattached kinetochores, which activate the MCC (Figure 5). Destabilization of incorrect attachments is thought to be mediated by Aurora B, which phosphorylates diverse targets at the kinetochore-microtubule interface, leading

to the release of the incorrect attached microtubule (Figure 5). When a correct, bipolar attachment is established, the pulling forces of the microtubules result in tension over the connected sister chromatids, and it is thought that Aurora B can then no longer reach its phosphorylation targets, resulting in a stable attachment [61]. This model for the localization and mechanism of action of the CPC is currently under debate. It is not yet completely clear whether inner centromeric localization of the CPC is necessary for correction of chromosome-spindle misattachments. Also, Aurora B might signal directly to the MCC in other, more direct ways [70-72]. For a detailed review of these possibilities, see [73].

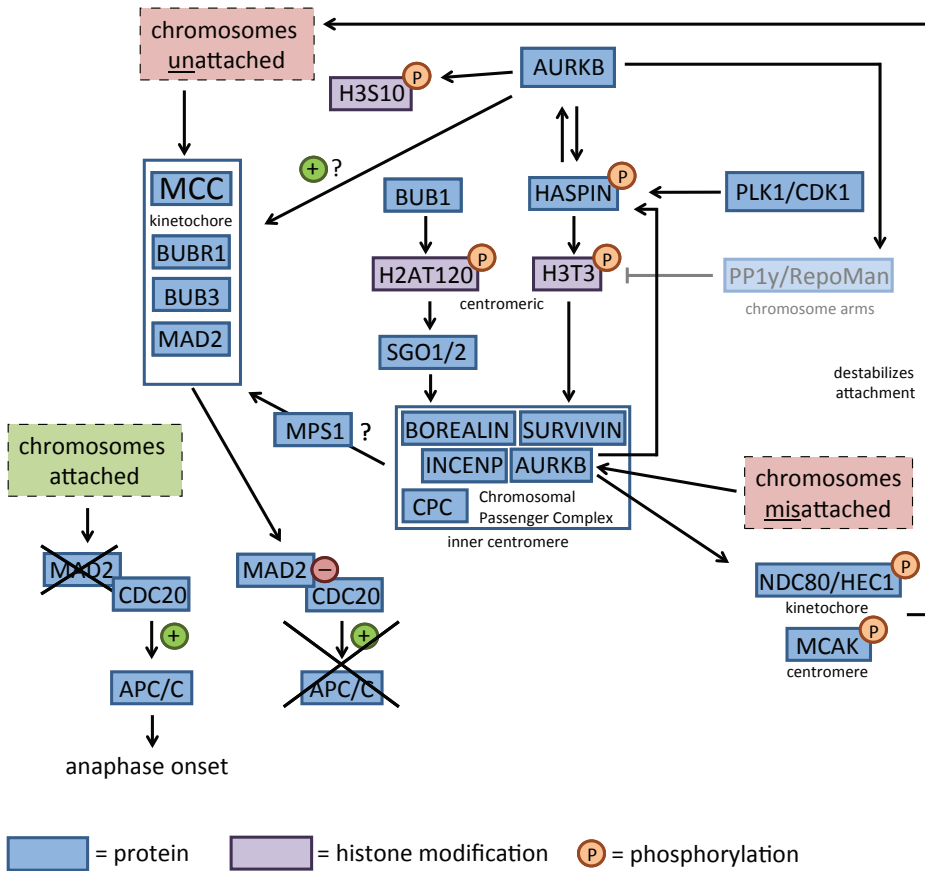


Figure 5 — Scheme of the regulation of mitotic progression by the mitotic checkpoint complex (MCC) and the chromosomal passenger complex (CPC). See text for explanation.

Together, the CPC and the MCC ensure the inhibition of the APC/C as long as not all chromosomes are correctly attached to the spindle. Thereby, these protein complexes are crucial to prevent chromosome missegregation. As described above, chromosomal abnormalities are common in



human pre-implantation embryos. Therefore, it has been suggested that there may be a decreased or even absence of mitotic checkpoint function in early embryos [7]. In our studies, we aimed to investigate the expression and localization of the chromosomal passenger complex in order to shed light on the possible underlying causes of chromosomal abnormalities in human embryos.

### Research on human pre-implantation embryos

The Dutch 'embryo law' does not permit the use of good quality embryos that are intended for patient treatment and the fertilization of oocytes with the aim to create embryos for research. Therefore, in our studies into the earliest stages of pre-implantation embryo development we are limited to tripronuclear (3PN) zygotes and embryos resulting from 3PN zygotes. These zygotes mostly originate from an oocyte that is fertilized by two spermatozoa, resulting in one maternal pronucleus and two paternal pronuclei [74-76]. 3PN zygotes proceed through the first divisions normally and are capable of implantation, thus providing an ethically acceptable and relevant model for the first stages of pre-implantation embryo development [77-78]. To study later stages of development, from embryonic day 3 onwards, we are able to use good quality embryos that were first cryopreserved for patient treatment and later donated for research by these patients.

As may be clear from what is described above, human pre-implantation embryos for research are scarce and precious. This is a challenge for us, researchers, as we have to perform experiments with as little embryos as possible. Next to that, we have to optimize every experimental protocol for use on single embryos. When studying protein expression for example, we are not able to use the Western Blot technique, because we do not have enough cells. Instead, we use immunofluorescence, a less sensitive and quantitative technique through which we visualise protein expression and localization in single cells of single embryos. In order to optimize the use of our scarce material, in one of our studies we aimed to develop a method to perform sequential immunofluorescent analyses on the same preparation. Next to that, we optimized a protocol for gene expression analysis by RT-qPCR for application on single embryos in order to study gene expression in our studies.

In summary, research involving human pre-implantation embryos derived from IVF knows both ethical and methodological challenges. Despite these difficulties, we aim to increase our knowledge of human embryo development, as this will lead to the optimization of IVF procedures in the future. Aims and outline of this thesis

The aim of the research described in this thesis was to get more insight in mechanisms regulating chromosome segregation and chromatin organization in human pre-implantation embryos.

In **chapter 2** we investigated how cHC is marked and re-established in human pre-implantation embryos. Our results demonstrate that human sperm cells retain histones with cHC marks, which contribute to paternal chromatin formation in embryos. These results show a mechanism for a paternal epigenetic contribution to embryo development.

In order to gain knowledge on the mechanisms regulating chromosome segregation, and possibly explaining the high rates of missegregation observed in human embryos, in **chapter 3** we investigated the expression of CPC subunits. In contrast to somatic cells, in which Aurora kinase B is the enzymatic subunit of the CPC, in human pre-implantation embryos we found Aurora kinase C to

be the main enzymatic subunit. Further investigations into CPC localization are described in chapter 5.

In **chapter 4** we describe a method we developed, which enables us to perform sequential immunofluorescent stainings on the same material. This is of great value, because it allows investigation of co-localization of proteins and it saves our scarce material, human pre-implantation embryos.

In order to further elucidate the mechanism guarding chromosome segregation, in **chapter 5** we investigated the dynamics of histone modifications that define CPC localization. Our results suggest that in human zygotes the mechanism regulating targeting of the CPC to the inner centromeres partially differs from that described in somatic cells.

In **chapter 6** we summarize the most important conclusions from the studies described in the previous chapters and we discuss the implications for future research.

## References

1. ESHRE. *Assisted reproductive technology and intrauterine inseminations in Europe, 2009: results generated from European registers by ESHRE*. in *2012 Annual Meeting of ESHRE*. 2012. Istanbul, Turkey.
2. Ferraretti, A.P., et al., *Assisted reproductive technology in Europe, 2009: results generated from European registers by ESHRE*. Hum Reprod, 2013.
3. Magli, M.C., et al., *Chromosome mosaicism in day 3 aneuploid embryos that develop to morphologically normal blastocysts in vitro*. Hum Reprod, 2000. **15**(8): p. 1781-6.
4. Wells, D. and J.D. Delhanty, *Comprehensive chromosomal analysis of human preimplantation embryos using whole genome amplification and single cell comparative genomic hybridization*. Mol Hum Reprod, 2000. **6**(11): p. 1055-62.
5. Bielanska, M., S.L. Tan, and A. Ao, *Chromosomal mosaicism throughout human preimplantation development in vitro: incidence, type, and relevance to embryo outcome*. Hum Reprod, 2002. **17**(2): p. 413-9.
6. Coonen, E., et al., *Anaphase lagging mainly explains chromosomal mosaicism in human preimplantation embryos*. Hum Reprod, 2004. **19**(2): p. 316-24.
7. Los, F.J., D. Van Opstal, and C. van den Berg, *The development of cytogenetically normal, abnormal and mosaic embryos: a theoretical model*. Hum Reprod Update, 2004. **10**(1): p. 79-94.
8. Delhanty, J.D., *Mechanisms of aneuploidy induction in human oogenesis and early embryogenesis*. Cytogenet Genome Res, 2005. **111**(3-4): p. 237-44.
9. Baart, E.B., et al., *Preimplantation genetic screening reveals a high incidence of aneuploidy and mosaicism in embryos from young women undergoing IVF*. Human reproduction (Oxford, England), 2006. **21**(1): p. 223-233.
10. Baart, E.B., et al., *FISH analysis of 15 chromosomes in human day 4 and 5 preimplantation embryos: the added value of extended aneuploidy detection*. Prenatal diagnosis, 2007. **27**(1): p. 55-63.
11. Vanneste, E., et al., *Chromosome instability is common in human cleavage-stage embryos*. Nature medicine, 2009. **15**(5): p. 577-583.
12. Santos, M.A., et al., *The fate of the mosaic embryo: chromosomal constitution and development of Day 4, 5 and 8 human embryos*. Hum Reprod, 2010. **25**(8): p. 1916-26.
13. van Echten-Arends, J., et al., *Chromosomal mosaicism in human preimplantation embryos: a systematic review*. Hum Reprod Update, 2011. **17**(5): p. 620-7.
14. Dekel-Naftali, M., et al., *Chromosomal integrity of human preimplantation embryos at different days post fertilization*. J Assist Reprod Genet, 2013. **30**(5): p. 633-48.
15. Voet, T., E. Vanneste, and J.R. Vermeesch, *The human cleavage stage embryo is a cradle of chromosomal rearrangements*. Cytogenet Genome Res, 2011. **133**(2-4): p. 160-8.
16. Norbury, C. and P. Nurse, *Animal cell cycles and their control*. Annu Rev Biochem, 1992. **61**: p. 441-70.
17. Vermeulen, K., D.R. Van Bockstaele, and Z.N. Berneman, *The cell cycle: a review of regulation, deregulation and therapeutic targets in cancer*. Cell Prolif, 2003. **36**(3): p. 131-49.
18. Pines, J. and C.L. Rieder, *Re-staging mitosis: a contemporary view of mitotic progression*. Nat Cell Biol, 2001. **3**(1): p. E3-6.
19. Carmena, M. and W.C. Earnshaw, *The cellular geography of aurora kinases*. Nat Rev Mol Cell Biol, 2003. **4**(11): p. 842-54.
20. da Avó Ribeiro dos Santos, M., *Chromosomal mosaicism: underlying mechanisms and consequences for early human embryo development*, in *Department of Reproductive Medicine and Gynecology, University Medical Center Utrecht, The Netherlands*. 2013, Utrecht University: Utrecht. p. 187.
21. Jin, B., Y. Li, and K.D. Robertson, *DNA methylation: superior or subordinate in the epigenetic hierarchy?* Genes Cancer, 2011. **2**(6): p. 607-17.
22. Kamakaka, R.T. and S. Biggins, *Histone variants: deviants?* Genes Dev, 2005. **19**(3): p. 295-310.
23. Bhaumik, S.R., E. Smith, and A. Shilatifard, *Covalent modifications of histones during development and disease pathogenesis*. Nat Struct Mol Biol, 2007. **14**(11): p. 1008-16.
24. Kouzarides, T., *Chromatin modifications and their function*. Cell, 2007. **128**(4): p. 693-705.

25. Boyarchuk, E., R. Montes de Oca, and G. Almouzni, *Cell cycle dynamics of histone variants at the centromere, a model for chromosomal landmarks*. *Curr Opin Cell Biol*, 2011. **23**(3): p. 266-76.
26. Suganuma, T. and J.L. Workman, *Signals and combinatorial functions of histone modifications*. *Annu Rev Biochem*, 2011. **80**: p. 473-99.
27. Eskeland, R., et al., *Ring1B compacts chromatin structure and represses gene expression independent of histone ubiquitination*. *Mol Cell*, 2010. **38**(3): p. 452-64.
28. Hublitz, P., M. Albert, and A.H. Peters, *Mechanisms of transcriptional repression by histone lysine methylation*. *Int J Dev Biol*, 2009. **53**(2-3): p. 335-54.
29. Margueron, R. and D. Reinberg, *The Polycomb complex PRC2 and its mark in life*. *Nature*, 2011. **469**(7330): p. 343-9.
30. Ringrose, L. and R. Paro, *Epigenetic regulation of cellular memory by the Polycomb and Trithorax group proteins*. *Annu Rev Genet*, 2004. **38**: p. 413-43.
31. Simon, J.A. and R.E. Kingston, *Mechanisms of polycomb gene silencing: knowns and unknowns*. *Nat Rev Mol Cell Biol*, 2009. **10**(10): p. 697-708.
32. Morey, L., et al., *Nonoverlapping functions of the polycomb group cbx family of proteins in embryonic stem cells*. *Cell Stem Cell*, 2012. **10**(1): p. 47-62.
33. Rea, S., et al., *Regulation of chromatin structure by site-specific histone H3 methyltransferases*. *Nature*, 2000. **406**(6796): p. 593-9.
34. Peters, A.H., et al., *Loss of the Suv39h histone methyltransferases impairs mammalian heterochromatin and genome stability*. *Cell*, 2001. **107**(3): p. 323-37.
35. Peters, A.H. and D. Schubeler, *Methylation of histones: playing memory with DNA*. *Curr Opin Cell Biol*, 2005. **17**(2): p. 230-8.
36. Bannister, A.J., et al., *Selective recognition of methylated lysine 9 on histone H3 by the HP1 chromo domain*. *Nature*, 2001. **410**(6824): p. 120-4.
37. Lachner, M., et al., *Methylation of histone H3 lysine 9 creates a binding site for HP1 proteins*. *Nature*, 2001. **410**(6824): p. 116-20.
38. Schotta, G., et al., *A silencing pathway to induce H3-K9 and H4-K20 trimethylation at constitutive heterochromatin*. *Genes Dev*, 2004. **18**(11): p. 1251-62.
39. Daujat, S., et al., *H3K64 trimethylation marks heterochromatin and is dynamically remodeled during developmental reprogramming*. *Nat Struct Mol Biol*, 2009. **16**(7): p. 777-81.
40. Lehnertz, B., et al., *Suv39h-mediated histone H3 lysine 9 methylation directs DNA methylation to major satellite repeats at pericentric heterochromatin*. *Curr Biol*, 2003. **13**(14): p. 1192-200.
41. Grewal, S.I. and S. Jia, *Heterochromatin revisited*. *Nat Rev Genet*, 2007. **8**(1): p. 35-46.
42. Fodor, B.D., et al., *Mammalian Su(var) genes in chromatin control*. *Annu Rev Cell Dev Biol*, 2010. **26**: p. 471-501.
43. Kiyomitsu, T., et al., *Inner centromere formation requires hMis14, a trident kinetochore protein that specifically recruits HP1 to human chromosomes*. *J Cell Biol*, 2010. **188**(6): p. 791-807.
44. Slee, R.B., et al., *Cancer-associated alteration of pericentromeric heterochromatin may contribute to chromosome instability*. *Oncogene*, 2012. **31**(27): p. 3244-53.
45. Burton, A. and M.E. Torres-Padilla, *Epigenetic reprogramming and development: a unique heterochromatin organization in the preimplantation mouse embryo*. *Brief Funct Genomics*, 2010. **9**(5-6): p. 444-54.
46. Duffie, R. and D. Bourc'his, *Parental epigenetic asymmetry in mammals*. *Curr Top Dev Biol*, 2013. **104**: p. 293-328.
47. Fadloun, A., A. Eid, and M.E. Torres-Padilla, *Mechanisms and dynamics of heterochromatin formation during Mammalian development: closed paths and open questions*. *Curr Top Dev Biol*, 2013. **104**: p. 1-45.
48. Nestorov, P., M. Tardat, and A.H. Peters, *H3K9/HP1 and Polycomb: Two Key Epigenetic Silencing Pathways for Gene Regulation and Embryo Development*. *Curr Top Dev Biol*, 2013. **104**: p. 243-91.
49. Santos, F., et al., *Dynamic chromatin modifications characterise the first cell cycle in mouse embryos*. *Dev Biol*, 2005. **280**(1): p. 225-36.
50. Puschendorf, M., et al., *PRC1 and Suv39h specify parental asymmetry at constitutive heterochromatin in early mouse embryos*. *Nature genetics*, 2008. **40**(4): p. 411-420.

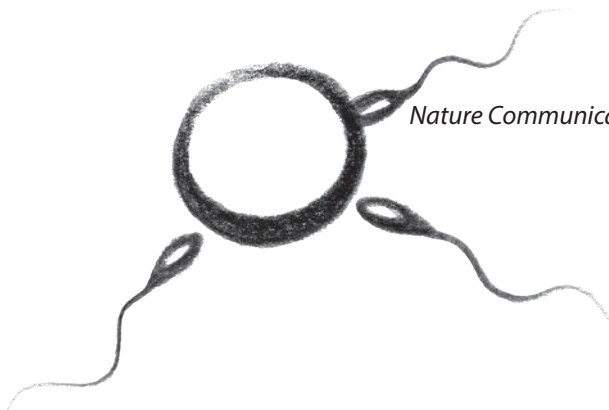
51. Merico, V., et al., *Epigenomic differentiation in mouse preimplantation nuclei of biparental, parthenote and cloned embryos*. Chromosome Res, 2007. **15**(3): p. 341-60.
52. Wongtawan, T., et al., *Histone H4K20me3 and HP1 alpha are late heterochromatin markers in development, but present in undifferentiated embryonic stem cells*. J Cell Sci, 2011. **124**(Pt 11): p. 1878-90.
53. Lange, U.C., et al., *Dissecting the role of H3K64me3 in mouse pericentromeric heterochromatin*. Nat Commun, 2013. **4**: p. 2233.
54. Probst, A.V. and G. Almouzni, *Heterochromatin establishment in the context of genome-wide epigenetic reprogramming*. Trends Genet, 2011. **27**(5): p. 177-85.
55. Okamoto, I., et al., *Eutherian mammals use diverse strategies to initiate X-chromosome inactivation during development*. Nature, 2011. **472**(7343): p. 370-4.
56. Balhorn, R., B.L. Gledhill, and A.J. Wyrobek, *Mouse sperm chromatin proteins: quantitative isolation and partial characterization*. Biochemistry, 1977. **16**(18): p. 4074-80.
57. Tanphaichitr, N., et al., *Basic nuclear proteins in testicular cells and ejaculated spermatozoa in man*. Exp Cell Res, 1978. **117**(2): p. 347-56.
58. Gusse, M., et al., *Purification and characterization of nuclear basic proteins of human sperm*. Biochim Biophys Acta, 1986. **884**(1): p. 124-34.
59. Gatewood, J.M., et al., *Isolation of four core histones from human sperm chromatin representing a minor subset of somatic histones*. J Biol Chem, 1990. **265**(33): p. 20662-6.
60. Bench, G.S., et al., *DNA and total protamine masses in individual sperm from fertile mammalian subjects*. Cytometry, 1996. **23**(4): p. 263-71.
61. Vader, G., A.F. Maia, and S.M. Lens, *The chromosomal passenger complex and the spindle assembly checkpoint: kinetochore-microtubule error correction and beyond*. Cell Div, 2008. **3**: p. 10.
62. Adams, R.R., M. Carmena, and W.C. Earnshaw, *Chromosomal passengers and the (aurora) ABCs of mitosis*. Trends Cell Biol, 2001. **11**(2): p. 49-54.
63. Vagnarelli, P. and W.C. Earnshaw, *Chromosomal passengers: the four-dimensional regulation of mitotic events*. Chromosoma, 2004. **113**(5): p. 211-222.
64. Ruchaud, S., M. Carmena, and W.C. Earnshaw, *Chromosomal passengers: conducting cell division*. Nature reviews.Molecular cell biology, 2007. **8**(10): p. 798-812.
65. Carmena, M., et al., *The chromosomal passenger complex (CPC): from easy rider to the godfather of mitosis*. Nat Rev Mol Cell Biol, 2012. **13**(12): p. 789-803.
66. Kops, G.J., B.A. Weaver, and D.W. Cleveland, *On the road to cancer: aneuploidy and the mitotic checkpoint*. Nature reviews.Cancer, 2005. **5**(10): p. 773-785.
67. Perera, D. and S.S. Taylor, *Sgo1 establishes the centromeric cohesion protection mechanism in G2 before subsequent Bub1-dependent recruitment in mitosis*. J Cell Sci, 2010. **123**(Pt 5): p. 653-9.
68. Yamagishi, Y., et al., *Two histone marks establish the inner centromere and chromosome bi-orientation*. Science, 2010. **330**(6001): p. 239-43.
69. Wang, F., et al., *A positive feedback loop involving Haspin and Aurora B promotes CPC accumulation at centromeres in mitosis*. Curr Biol, 2011. **21**(12): p. 1061-9.
70. Santaguida, S., et al., *Evidence that Aurora B is implicated in spindle checkpoint signalling independently of error correction*. EMBO J, 2011. **30**(8): p. 1508-19.
71. Saurin, A.T., et al., *Aurora B potentiates Mps1 activation to ensure rapid checkpoint establishment at the onset of mitosis*. Nat Commun, 2011. **2**: p. 316.
72. Wang, F., et al., *Haspin inhibitors reveal centromeric functions of Aurora B in chromosome segregation*. J Cell Biol, 2012. **199**(2): p. 251-68.
73. van der Horst, A. and S.M. Lens, *Cell division: control of the chromosomal passenger complex in time and space*. Chromosoma, 2014. **123**(1-2): p. 25-42.
74. Plachot, M., et al., *Cytogenetic analysis and developmental capacity of normal and abnormal embryos after IVF*. Hum Reprod, 1989. **4**(8 Suppl): p. 99-103.

75. Staessen, C. and A.C. Van Steirteghem, *The chromosomal constitution of embryos developing from abnormally fertilized oocytes after intracytoplasmic sperm injection and conventional in-vitro fertilization*. Hum Reprod, 1997. **12**(2): p. 321-7.
76. van der Heijden, G.W., et al., *Parental origin of chromatin in human monopronuclear zygotes revealed by asymmetric histone methylation patterns, differs between IVF and ICSI*. Molecular reproduction and development, 2009. **76**(1): p. 101-108.
77. Avo Santos, M., et al., *A role for Aurora C in the chromosomal passenger complex during human preimplantation embryo development*. Hum Reprod, 2011. **26**(7): p. 1868-81.
78. Mantikou, E., et al., *Temporal and developmental-stage variation in the occurrence of mitotic errors in tripronuclear human preimplantation embryos*. Biol Reprod, 2013. **89**(2): p. 42.

# CHAPTER 2

## **Paternal heterochromatin formation in human embryos is H3K9/HP1 directed and primed by sperm-derived histone modifications**

Christine van de Werken, Godfried W. van der Heijden, Cindy Eleveld,  
Miriam Teeuwssen, Mareike Albert, Willy M. Baarends, Joop S.E. Laven, Antoine  
H.F.M. Peters, Esther B. Baart



*Nature Communications, 2014. 5: p. 5868*

## Abstract

The different configurations of maternal and paternal chromatin, acquired during oogenesis and spermatogenesis, have to be rearranged after fertilization to form a functional embryonic genome. In the paternal genome, nucleosomal chromatin domains are re-established after the protamine-to-histone exchange. We investigated the formation of constitutive heterochromatin (cHC) in human pre-implantation embryos. Our results show that histones carrying canonical cHC modifications are retained in cHC regions of sperm chromatin. These modified histones are transmitted to the oocyte and contribute to the formation of paternal embryonic cHC. Subsequently, the modifications are recognized by H3K9/HP1 pathway maternal chromatin modifiers and propagated over the embryonic cleavage divisions. These results are in contrast to what has been described for mouse embryos, in which paternal cHC lacks canonical modifications and is initially established by Polycomb group proteins. Our results show intergenerational epigenetic inheritance of the cHC structure in human embryos.



## Introduction

Fertilization marks the fusion of two specialized gametes, oocyte and sperm. In mammalian zygotes, the maternal and paternal genome exist in an asymmetric chromatin configuration. Extensive reorganization of chromatin to the embryonic configuration is crucial for developmental potency [1]. During this process, some information of parental origin needs to be retained in order to maintain imprinting [2]. Other chromatin domains, such as the constitutive heterochromatin (cHC), need to be reorganized to the somatic configuration in order to function properly [3-4].

Constitutive HC assembles mostly on telomeric, centromeric and pericentric regions, remains condensed throughout the cell cycle and is important for genome stability and chromosome segregation [5]. DNA sequences underlying cHC differ between species, but mainly consist of repeats and transposons. In mouse, most of the cHC is located pericentrically (pericentric heterochromatin (pHC)), a region with major satellite DNA repeats. In human, cHC is more dispersed across the genome [6]; classic satellite II and III DNA repeats localize to the pericentric region, but also to large blocks of cHC on chromosomes 1, 9, 16, the acrocentric chromosomes and Y [7], also referred to as “knobs” [5].

The H3K9/HP1 pathway underlies formation of cHC. A central event is tri-methylation of histone H3 at lysine 9 (H3K9me3) by histone methyltransferases (HMTs) Suv39h1 and Suv39h2 [5,8-9]. H3K9me3 serves as a docking place for binding of heterochromatin protein 1 (HP1) isoforms, which results in chromatin compaction [5]. Subsequently, HP1 binds Suv4-20h1/2 HMTs, which trimethylate histone H4 at lysine 20 (H4K20me3) to further establish a compact chromatin structure [5,10]. Through an unidentified mechanism, H3K9me3 also facilitates tri-methylation of histone H3 at lysine 64 (H3K64me3), which has been suggested to stabilize cHC [11-12]. The H3K9/HP1 pathway is interwoven with methylation of DNA, another mechanism for gene silencing prominent in cHC [5,10]. Together, all modifications eventually lead to the establishment of a condensed, transcriptionally repressed state that is epigenetically heritable through cell division.

In mammalian oocytes, the maternal genome is marked by high levels of histone lysine methylation, whereas in spermatozoa the paternal genome is compacted with small proteins named protamines [13]. Current knowledge of resolution of this epigenetic asymmetry in early mammalian embryos is mainly based on mouse models [1]. Paternal pHC in mouse spermatozoa and zygotes is largely devoid of canonical cHC marks [14]. Re-establishment of the canonical pHC configuration is not performed by the H3K9/HP1 pathway. Instead, during the earliest embryonic stages, maternally provided Polycomb repressive complex 1 (PRC1) localizes to paternal pHC, which subsequently becomes enriched for Polycomb repressive complex 2 (PRC2)-mediated trimethylation of histone H3 on lysine 27 (H3K27me3) [3,15]. The core PRC1 complex contains an E3 ligase Ring1a/b, which interacts with one of the orthologs of the *Drosophila* posterior sex combs (PSC) (Mel18, Bmi1 or Nspc1), a Polyhomeiotic (PH) ortholog (Phc1, Phc2 or Phc3), and a Polycomb ortholog (Cbx2, Cbx4, Cbx6, Cbx7 or Cbx8) [16]. The PRC2 core complex contains one of the HMTs Ezh1 or Ezh2, together with the regulatory subunits Suz12 and Eed [17]. In somatic cells, Polycomb complexes are known to regulate formation of facultative heterochromatin, a type of heterochromatin which is able to undergo changes in configuration in the context of regulation of gene expression. Thus,

in mouse pre-implantation embryos the paternal pericentric DNA temporarily assumes a facultative heterochromatin packaging, to circumvent the inactivity of the H3K9/HP1 pathway. The PRC1/2 pathway thereby operates as a transient backup mechanism for pHC formation [3]. During the 8-cell stage of mouse embryo development, the H3K9/HP1 pathway takes over again and the pHC of both parental origins gradually becomes equivalent for H3K9me3 [3,18]. Other pHC associated marks, such as H3K64me3 and H4K20me3, remain undetected at paternal chromatin until after compaction and implantation, respectively [11-12,19].

In this study we addressed chromatin dynamics on cHC during human pre-implantation embryo development. Our results identify striking differences with mouse: cHC in human embryos is not re-established by PRC1/2 action, but is transmitted and maintained by actors of the canonical H3K9/HP1 pathway. We show that human spermatozoa retain and transmit nucleosomes with cHC marks, such as H3K9me3, to the embryo. These paternal marks are subsequently bound by maternal HP1 and propagated over cell divisions. Based on this we propose a model in which paternal cHC is transmitted intergenerationally.

## Methods

### Collection and culture of human gametes and embryos

All human surplus material was donated for research according to guidelines of the local ethical committee. Surplus embryos and oocytes were donated with patients' written informed consent after approval by the Dutch Central Committee on Research Involving Human Subjects (CCMO – NL28739.000.09).

Ovarian stimulation, oocyte retrieval, IVF procedures and assessment of embryo morphology were performed as described [53]. Supernumerary good-quality embryos were cryopreserved. Cryopreservation was performed in a controlled rate freezer (in straws in culture medium with 1.5M dimethyl sulfoxide (DMSO)). Straws were cooled to  $-6^{\circ}\text{C}$  before seeding and subsequently cooled to  $-40^{\circ}\text{C}$  at  $0.3^{\circ}\text{C}/\text{min}$ . Finally, straws were cooled rapidly at  $-25^{\circ}\text{C}/\text{min}$  to  $-140^{\circ}\text{C}$ , before immersion in liquid nitrogen and storage in nitrogen vapour. After donation for research, thawing of embryos was performed at room temperature by consecutive washes in decreasing DMSO concentrations in G-MOPS Plus medium (Vitrolife).

Oocytes which failed to fertilize after IVF (OPN) were obtained 18 h post insemination at embryonic day (E) 1. Trippronuclear (3PN) embryos were used to study embryo development from E1 to E2. Surplus cryopreserved pre-implantation embryos of good quality were used to study embryonic developmental stages from E3 to E5 (for overview of stages see Supplementary Figure 1a). Embryo culture was performed in G1 Plus medium (Vitrolife) from E1 to E3 and thereafter in G2 Plus medium (Vitrolife) according to instructions of the manufacturer. Human surplus spermatozoa were obtained from IVF patients meeting the criteria for normospermia (WHO, 2010). These sperm samples underwent routine workup by layering on a discontinuous silica gel gradient (PureSperm, Nidacon International) and centrifugation at 1100rpm for 20 min. The resulting pellet was washed with G-IVF Plus medium (Vitrolife) at 1600rpm for 10 min and kept in 0.5mL G-IVF at  $37^{\circ}\text{C}$ , 6%  $\text{CO}_2$  in air.

Human U2OS cells (a gift from Dr. Kops [54]) were grown in Dulbecco's Modified Eagle's Medium (DMEM, Sigma) supplemented with 10% fetal bovine serum (FBS, Sigma) and 100 U/mL penicillin, 100 µg/mL streptomycin (Invitrogen) and cultured at 37°C in a humidified chamber in the presence of 5% CO<sub>2</sub>. Cells were plated on poly-D-Lysine-coated 12-mm coverslips, fixed with methanol at -20°C for 10 min and then permeabilized with 0.2% TritonX-100 in phosphate buffered saline (PBS).

### Antibodies

The following antibodies were used: rabbit polyclonal antibodies against H3K9me3 (1:500; Abcam ab8898), tetra-acetyl-Histone H4 (1:100; Upstate 06-598), H4K5ac (1:500; Abcam ab51997), H4K8ac (1:500; Upstate, 06-760), H4K12ac (1:500; Upstate 06-761), H4K20me3 (1:500; [55]), H3K64me3 (1:20; [11]) and H3K27me3 (1:200; [55]), mouse monoclonal antibodies against RING1A (1:200; Millipore 05-1362), RING1B (1:400; [56]), PHC2 (1:50; [57]), EZH2 (undiluted; [58]), EED (undiluted; [58]), HP1α (1:500; Euromedex 2HP-1H5-AS) and H3 (1:1000; Active Motif 39763); rat monoclonal antibodies against H4K12ac (1:50; SciLight Biotechnology C2077001) and HP1β (1:500; Serotec MCA1946); and human anti-centromere antibodies (ACA) (human centromere antiserum; 1:1000, Fitzgerald Industries).

Primary antibodies were detected by labelling with the appropriate secondary antibodies conjugated with Alexa Fluor 488, 555, 594 or 633 (Invitrogen).

### Fixation and immunofluorescence of embryos

After removal of the zona pellucida by incubation with Acidic Tyrode's Solution (Sigma), embryos were washed twice in G-MOPS, fixed for 15 min in 4% paraformaldehyde (PFA) in PBS (pH 7.4) and permeabilized with 0.2% Triton-X 100 in PBS for 15 min at room temperature. Embryos were incubated in blocking solution (0.1% Tween-20 in PBS containing 2% bovine serum albumin (BSA) and 5% normal goat serum (NGS)) for 4h at room temperature, followed by incubation with primary antibodies in blocking solution overnight at 4°C. Embryos were washed three times for 20 min in 0.1% Tween-20 in PBS containing 2% BSA before application of secondary antibodies. These were diluted 1:200 in blocking solution and embryos were incubated for 1h at room temperature, followed by three washing steps in 0.1% Tween-20 in PBS containing 2% BSA. Double antibody stainings were performed by mixing appropriate primary antibodies for simultaneous incubation, followed by detection with different secondary antibodies. Embryos were mounted on coverslips with Vectashield with 750 ng/ml 4,6-diamidino-2-phenylindole (DAPI) for DNA counterstaining (Vector Laboratories) [3].

For live staining of DNA in 3PN zygotes, zygotes were incubated in medium containing 1 µg/mL Hoechst 33342 and imaged directly.

To obtain chromosome spreads, embryos were incubated with 1.5 µg/ml colcemid (Invitrogen) for 8-16h to arrest cells at prometaphase. After zona pellucida removal, arrested embryos were incubated in hyposolution (25% fetal calf serum (FCS) in 0.5% sodium citrate) for 5 min and subsequently transferred to a drop of fixative (1% PFA with 0.2% Triton X-100, pH 9.2) on a glass slide. After horizontal drying for 1 hour, slides were washed with 0.08% Photo-Flo (Kodak) and air-dried

[59]. Slides with chromosome spreads were stored at -20°C until use. Surface spread preparations were processed for immunofluorescence as described above without permeabilization.

For each embryonic stage and antibody investigated 5-10 embryos were analysed unless otherwise stated.

### Single oocyte and embryo RT-qPCR

mRNA levels were quantified in single oocytes and pre-implantation embryos at the following eight developmental stages: metaphase II oocytes (E0; n=7); zygotes (E1; n=5); 2 cell embryos (E1.5; n=5), 4 cell (E2; n=4), 8 cell (E3; n=5), 12-16 cell (E3.5; n=5), morula (E4; n=4), and blastocyst (E5; n=5) (Supplementary Fig. 1a). Human embryonic stem cells (hESCs) (WA01 (H1) Lot 11, WiCell Research Institute) were used as a control.

For quantitative RT-PCR (RT-qPCR) of single oocyte/embryos, the Taqman® PreAmp Cells-to-Ct Kit (Applied Biosystems) was used according to the manufacturer's protocol with minor adjustments [21]. The zona pellucida was removed from the oocytes and embryos by incubation in 0.1% protease (Sigma) in G-MOPS medium for 3 min, prior to washing in G-MOPS medium and PBS. Lysis was performed for 5 min in 20 µl of Taqman® PreAmp Cells-to-Ct lysis solution and terminated by addition of 2 µl of stop solution. After 2 min of incubation the lysate was stored at -20°C until further processing within 1 week. Small pieces of hESC colonies containing 500-1000 cells were washed in PBS, and transferred to 50 µl Taqman® PreAmp Cells-to-Ct Lysis solution and terminated by addition of 5 µl Stop solution. RNA was reverse transcribed to cDNA within an hour at 37°C by adding 25 µl of 2× RT Buffer and 2.5 µl of 20× RT Enzyme Mix to each lysate, prior to inactivating the enzyme for 5 min at 95°C. For sequence-specific preamplification of cDNA, Taqman Gene Expression Assays (Assays-on-demand, Applied Biosystems) were pooled and diluted 1:100 with 1× TE buffer (10 mM Tris-HCl, 5 mM EDTA; pH 7.5) to a final concentration of 180nM of each primer. The following assays (Applied Biosystems) were used: *ZP3* (Assay ID: Hs00610623\_m1, amplicon size: 74 bp), *HPRT1* (Hs99999909\_m1, 100 bp), *SOX2* (Hs01053049\_s1, 91 bp), *OCT4* (Hs00999632\_g1, 77 bp), *BMI1* (Hs00180411\_m1, 105 bp), *MEL18* (Hs00810639\_m1, 64 bp), *RING1A* (Hs00968517\_m1, 71 bp), *RING1B* (Hs00200541\_m1, 82 bp), *PHC2* (Hs00189460\_m1, 114 bp), *CBX2* (Hs00364145\_m1, 93 bp), *CBX7* (Hs00545603\_m1, 54 bp), *CBX8* (Hs00221034\_m1, 64 bp), *EZH1* (Hs00157470\_m1, 65 bp), *EZH2* (Hs00544830\_m1, 86 bp), and *EED* (Hs00537777\_m1, 110 bp). Assays were selected to be exon spanning and to recognize most of the validated (Ref Seq) splice variants of each gene of interest.

To 12.5 µl of cDNA, 25 µl of Taqman® PreAmp Master Mix and 12.5 µl of 0.2× pooled Taqman® Gene Expression Assays were added. After 10 cycles of preamplification (10 min at 95°C, followed by 10× 15 s at 95°C and 4 min at 60°C), the preamplified cDNA (50 µl) was diluted with 100 µl of 0.5× TE buffer. qPCR was performed on an ABI Prism 7000 Sequence Detecting System (Applied Biosystems) using 10 µl of 2× Taqman® Gene Expression Master Mix, 1 µl of Taqman® Gene Expression Assay and 5 µl of nuclease-free water added to 4 µl of diluted preamplified cDNA. The two-step cycling parameters were as follows: one cycle of 2 min at 50°C, followed by one cycle of 10 min at 95°C to activate the polymerase and 40 cycles of 15 s at 95°C and 1 min at 60°C [21]. Results were analysed using Sequence Detection Software version 1.2.3 (Applied Biosystems) and expressed as cycle threshold (Ct) values (Supplementary Figure 3a). As a pre-amplification reaction of 10 cycles was

performed, the detection limit of the qPCR was set at a cycle threshold value of 30 or less. Presence of a single PCR-product of expected amplicon size was verified by 2% agarose gel electrophoresis (Supplementary Figure 3b).

### **Heterologous intra cytoplasmic sperm injection**

All institutional and national guidelines for the care and use of laboratory animals were followed and mouse experiments were approved by the local committee on animal experiments, DEC Consult. B6D2 F1 female mice (Harlan) were used as oocyte donors and superovulation was induced by i.p. injection of 7.5 IU pregnant mare's serum gonadotrophin (Intervet) followed by 7.5 IU human chorionic gonadotropin (hCG; Intervet) 48 h later [60-61]. Oocytes were isolated from the oviducts 13 h after hCG, and cumulus cells were removed by brief incubation in G-MOPS medium containing 80 IU/mL hyaluronidase (Sigma). Thereafter, the oocytes were washed and kept until after injection in freshly prepared mem-alpha medium (Life Technologies), supplemented with 10% (v/v) FCS, 21  $\mu$ M HEPES, 12.2  $\mu$ M sodium lactate, 1  $\mu$ M sodium pyruvate and 1  $\mu$ M L-glutamin. Microinjection was performed using an inverted microscope equipped with an ICSI micromanipulation set-up (Narishige) and a piezo-actuated injector (Burleigh). An XYclone laser system (Hamilton Thorne) was used to breach the zona pellucida. Prior to installation a small volume of mercury (Sigma) was inserted in an Straight Piezo Drill Micropipette (Humagen). Spermatozoa were used either directly after collection from the epididymis or, to prevent oocyte activation, after heat inactivation (incubation at 50°C for 30 min [62]). For each injection series, an aliquot of spermatozoa was transferred to medium containing 12% polyvinyl pyrrolidone (Irvine Scientific). Spermatozoa were immobilized with a short piezo pulse applied to the neck piece. Injections were performed at room temperature. Injected oocytes were warmed to 37°C and transferred after 5-10 min to G1 medium (Vitrolife) for culture at 37°C, 5% CO<sub>2</sub> in air. Oocytes injected with heat-inactivated spermatozoa (n=60) were fixed 22 hours after injection with 4% PFA as described above. Oocytes injected with normal spermatozoa were either fixed with 4% PFA 12-15 hours after injection (n=60) or transferred to medium containing 1.5  $\mu$ g/ml colcemid and processed for chromosome spreads 7-9 hours later as described above (n=60).

### ***In vitro* sperm decondensation**

Sperm head decondensation was achieved as described [48], with some modifications. First, 5  $\mu$ L of a spermatozoa suspension was brought on a glass slide and spread out using the side of the pipet tip. After drying, the slides were incubated in decondensation buffer (2.5mM dithiothreitol (DTT) (Sigma), 0.2% Triton X-100 (Sigma) in PBS) for 10 min, followed by incubation for 3, 4 and 5 min with 0.5% (v/v) heparin (5000U/mL, LEO Pharma BV) in decondensation buffer. Subsequently the slides were fixed in 4% PFA for 15 min, air dried, washed in Photo-Flo, and air dried. Slides were processed for immunofluorescence immediately as described above, starting with two washes in PBS-T. For each sperm sample, the optimal decondensation time was determined by sperm head morphology and ACA antibody accessibility. Preparations with optimal decondensation were used for further analysis. The presence of each histone modification under investigation was assessed in at least 100 sperm cells with clearly distinguishable ACA staining, from at least three separate donors.

To obtain sperm DNA in a chromatin fiber-like structure, 5  $\mu\text{L}$  of a spermatozoa suspension was added to 80  $\mu\text{L}$  decondensation buffer, as described above and incubated for 10-20 min. Heparin was added to a concentration of 0.5% (v/v) and incubated for 10 min. Of this decondensed spermatozoa suspension, 5  $\mu\text{L}$  was brought on a glass slide, spread out using the side of the pipet tip, and air dried. Slides were fixed in 4% PFA for 15 min and processed for immunofluorescence as described above.

### **Immunofluorescence – Fluorescent *In Situ* Hybridization**

For immuno-FISH on *in vitro* decondensed spermatozoa, slides were first processed for FISH. The DNA probes used were Satellite DNA II/III probes for chromosomes 1 (pUC1.77 [63]), 9 (pHuR98 [64-65]), 16 (pHuR195 [64-65]), and Y (RPN1305X [66]), and alpha satellite DNA probes for chromosomes 7 (pa7tl [67]) and X (pBamX5 [68]). Probes were fluorescently labelled using a BioPrime DNA labelling kit (Invitrogen), according to the instructions of the manufacturers. A hybridization mixture containing 1 ng/ $\mu\text{L}$  of labeled probe in 50% formamide, 10% dextran sulfate, 1% Tween-20 and 0.1  $\mu\text{g}/\text{ml}$  Human Cot-1 DNA (Invitrogen) in 2 $\times$  standard saline citrate (SSC) was applied to each slide under a coverslip. Slides were denatured at 75°C for 3 min and hybridization was performed in a humid box at 37°C for 6 h. After hybridization, slides were washed in 2 $\times$  SSC/0.05% Tween-20 for 2 min at 42°C, 0.4  $\times$ SSC for 6 min at 60°C and in 2 $\times$  SSC/0.05% Tween 20 for 2 min at room temperature. The slides were rinsed once in PBS before proceeding to immunofluorescence of H3K9me3 as described above. Immuno-FISH was imaged simultaneously and for each probe co-localization for H3K9me3 and satellite DNA was measured in 10-12 randomly selected sperm cells from at least three separate donors.

For immuno-FISH on chromosome spreads of unfertilized oocytes or 3PN zygotes (5-7 per probe combination), slides were first processed for immunofluorescence of H3K9me3 as described above. Chromosome spreads were subsequently imaged and positions of chromosomes were recorded in the form of the XY-position of the microscope table. These coordinates were used to find the same chromosomes after FISH. Subsequently, FISH was performed as described [69] for either Satellite DNA II/III probes for chromosome 1 (pUC1.77 [63]) in combination with 9 (pHuR98 [64-65]), or 16 (pHuR195 [64-65]) in combination with Y (RPN1305X [66]). Probes were hybridized overnight followed by post-hybridization washes and imaging of the FISH signals.

### **Imaging and image analysis**

Immunofluorescent images from whole mount embryos, heterologous zygotes, chromosome spreads and immuno-FISH on *in vitro* decondensed spermatozoa were acquired using a Zeiss Axio Imager M2 confocal laser scanning microscope, equipped with four diode lasers (405, 488, 555, 639 nm), an Axiocam camera, and Zen 2009 (Carl Zeiss) software. For embryos, we recorded Z-series of 5  $\mu\text{m}$  slices and for chromosome spreads, we recorded Z-series of 0.5  $\mu\text{m}$  slices. Images were processed with Image J (version 1.42n) and Adobe Photoshop CS3 software.

Imaging for immuno-FISH on chromosome spreads was performed on a Zeiss Axio Imager M1 microscope (Carl Zeiss), equipped with a CoolCube 1m camera (MetaSystems), and Isis FISH Imaging System software (version 5.4.7, MetaSystems). Images of immunofluorescence and FISH were obtained in two rounds of imaging and merged using Image J. With the ROI Manager in Image J,

a selected area of one image was copied to the other images. Subsequently, selected areas were cropped and merged.

For visualization of co-localization between H3K9me3 and satellite DNA the distribution of fluorescence intensities were plotted using the Straight lines selection tool in Image J. Subsequently, using the Analyze - Plot Profile tool, the distribution of fluorescence intensities along the selected line was obtained. Sperm cells were divided in three categories according to their profiles for H3K9me3 and satellite DNA: 1) profiles where the peak intensities for H3K9me3 and FISH signal completely overlap, 2) profiles where the peak intensities are within a 1  $\mu\text{m}$  distance and 3) profiles where the peak intensities are further apart.

## Results

### Pronuclear morphology and cHC localization in human zygotes

To determine the localization of cHC in human zygotes, pronuclear morphology was studied. Due to restrictions on the use of human embryos for research we were limited to trippronuclear (3PN) zygotes and embryos resulting from 3PN zygotes to study embryos at Embryonic day (E) 1 and 2 (for overview of stages and source of embryos see Supplementary Figure 1a). Trippronuclear zygotes mostly originate from an oocyte that is fertilized by two spermatozoa, resulting in one maternal pronucleus and two paternal pronuclei [20]. Occasionally, when polar body extrusion fails, a 3PN zygote contains two maternal pronuclei and one paternal pronucleus. 3PN zygotes proceed through the first divisions normally and are capable of implantation, thus providing an ethically acceptable and relevant model for the first stages of pre-implantation embryo development [21-22]. From E3 onwards, embryos developed from diploid (2PN) zygotes and donated for research were used (Supplementary Figure 1a).

Pronuclear morphology of human zygotes differs from mouse zygotes. In late stage mouse zygotes (G2 phase, also indicated as PN4/5 stage [23]), pronuclei are spherical and the DNA is spread throughout the pronucleus. A 4'-6-diamidino-2-phenylindole (DAPI)-intense ring-like structure around the nucleolar precursor body (NPB) contains the pHC [3-4] (Figure 1a). Human pronuclei also appear spherical under a stereomicroscope (Figure 1b). However, when pronuclei are examined at G2 phase (18-20 hours after fertilization [24], Supplementary Figure 1a) by DNA staining, the DNA content concentrates in the direction of the opposing pronucleus in both live and fixed conditions, resulting in a crescent shape (Figure 1c,d). The NPBs are also contained in DAPI-rich ring-like structures, but are smaller and more numerous when compared to mouse NPBs at that stage. In addition, a few DAPI-rich knobs are observed, similar in appearance to cHC blocks in human somatic cells [5]. Using human autoantibodies against the centromeres (ACA), we show that the centromeres are situated in close proximity to both the rings and knobs (Figure 1d). This confirms that these DAPI-rich chromatin domains are located pericentrically and are likely to contain cHC in human embryos.

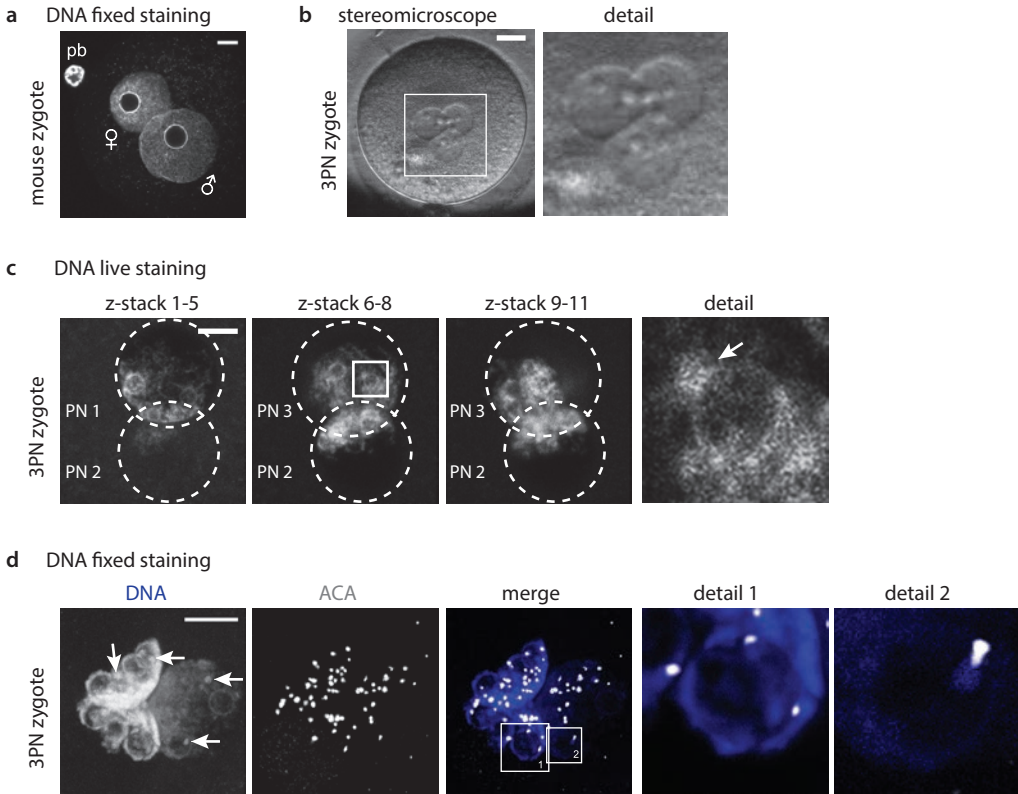


**Figure 1 — Pronuclear morphology of human zygotes differs from mouse zygotes.** (a) Representative confocal image of a mouse zygote fixed 12-15 h post fertilization (G2 phase) with typical pronuclear morphology as observed by DNA staining (DAPI;  $n=10$ ). Shown is a full projection of Z-sections. Pronuclei contain a ring-like structure called nucleolar precursor body (NPB) and pericentric heterochromatin can be observed as a ring with intense DAPI staining, surrounding the NPB. Paternal (♂) and maternal (♀) pronuclei are indicated, as is the polar body (pb). Scale bar, 10  $\mu\text{m}$ . (b) Stereo micrograph of a human 3PN zygote showing typical pronuclear morphology. Detail shows a magnification of the boxed area. Scale bar, 20  $\mu\text{m}$ . (c) Representative confocal image of a human zygote 18-20 h post insemination (G2 phase) with typical pronuclear morphology as observed by live staining with Hoechst 33342 ( $n=6$ ). Shown are three projections of consecutive Z-sections through the three pronuclei. DNA inside each pronucleus is contracted into a crescent shape containing several ring-like structures and denser stained “knobs”. Detail shows a magnification of a single Z-section through the boxed ring-like structure with attached knob (arrow). Scale bar, 10  $\mu\text{m}$ . (d) Representative confocal image of a human zygote fixed 18-20 h post insemination (G2 phase) with typical pronuclear morphology ( $n=10$ ). Shown is a full projection of Z-sections with DNA staining (DAPI; blue) and immunolocalization of the centromeres (ACA; white). Pronuclear morphology is not affected by fixation and DNA is observed in the same crescent shape with ring-like structures and DAPI-intense knobs (arrows). Centromeres are localized preferentially on the ring or in close proximity to a knob. Detail 1 and 2 show magnifications of a single Z-section through the boxed ring-like structure and knob, respectively. Scale bar, 10  $\mu\text{m}$ .



### PRC1/2 are not associated with cHC in cleavage stages

Protein localization of PRC1 and PRC2 subunits was performed by immunofluorescence in 3PN zygotes fixed at G2 phase. The enzymatic PRC1 subunit RING1B was not detected (Figure 2a), whereas typical RING1B foci [25] were observed in nuclei from hU2OS cells and human blastocysts (Supplementary Figure 2a). Similar results were obtained for two other PRC1 subunits, RING1A and PHC2 (Supplementary Figure 2b,c), as well as for the core-components of PRC2, EZH2 (Figure 2b) and EED (Supplementary Figure 2d).

Subsequently, we characterized PRC2 activity by investigating the histone modification it catalyzes: H3K27me3. Immunodetection of H3K27me3 in 3PN zygotes at the G2 phase revealed a clear asymmetry for H3K27me3 staining, with one pronucleus showing intense staining throughout, whereas in the other two pronuclei staining levels were barely detectable (Figure 2c). These results are in accordance with our previous findings [20] and those of Zhang and colleagues [26]. Since metaphase II chromosomes in oocytes show high levels of H3K27me3 [26] and in analogy to what has been described in mouse [15,27] and other species [28-29], we propose the pronucleus with strong H3K27me3 staining to be of maternal origin.

In mouse zygotes, paternal pHC becomes increasingly enriched for H3K27me3 by PRC2 activity during G2 phase [3,30]. In contrast, in human zygotes arrested at the prometaphase stage, H3K27me3 levels remained barely detectable on paternal chromosomes, also at pericentric regions (Figure 2d). To determine whether PRC2 activity is upregulated during subsequent development, we performed immunostaining on whole-mount embryos of all stages of pre-implantation development from the zygote at E1 to the blastocyst at E5 (for overview of stages and source of embryos see Supplementary Figure 1a). On E1 and E2, H3K27me3 staining was restricted to one side of the nucleus, presumably marking the maternal chromatin. Overall levels of H3K27me3 decreased to become barely detectable at E3. From E4 onwards H3K27me3 levels increased and staining was distributed throughout the entire nucleus (Figure 2e). To exclude differences caused by the triploid state of the embryos examined at E1 and E2, we compared embryos at E3 and E4 developed from normal, dipronuclear zygotes (Figure 2e) with those developed from 3PN zygotes (Supplementary Figure 2e) and observed no differences. The lack of PRC2 activity at E1-3 is thus unlikely to be related to the triploid state of the embryos investigated.

Next, we analyzed the abundance of mRNA transcripts for subunits of PRC1 and PRC2 by RT-qPCR in oocytes and embryos of eight developmental stages (for overview of stages see Supplementary Figure 1a). The mRNA expression of most PRC1 and PRC2 subunits followed similar patterns throughout pre-implantation development: levels decreased from oocytes to the 8-cell stage at E3 and increased again from E3.5 onwards (Supplementary Figure 3a), concomitant with the above described increase in trimethylation levels of H3K27.

Although observed high levels of H3K27me3 on maternal chromatin indicates PRC2 activity at some point during oocyte development, our failure to detect PRC1 and PRC2 at the paternal chromatin suggests the absence of these complexes in the zygote and the early embryo. Alternatively, our observations can also be explained by an inability of PRC complexes to target paternal chromatin. To differentiate between these possibilities we injected human spermatozoa into mouse oocytes, resulting in heterologous zygotes (Supplementary Figure 1b). When fixed at late G2 phase, the

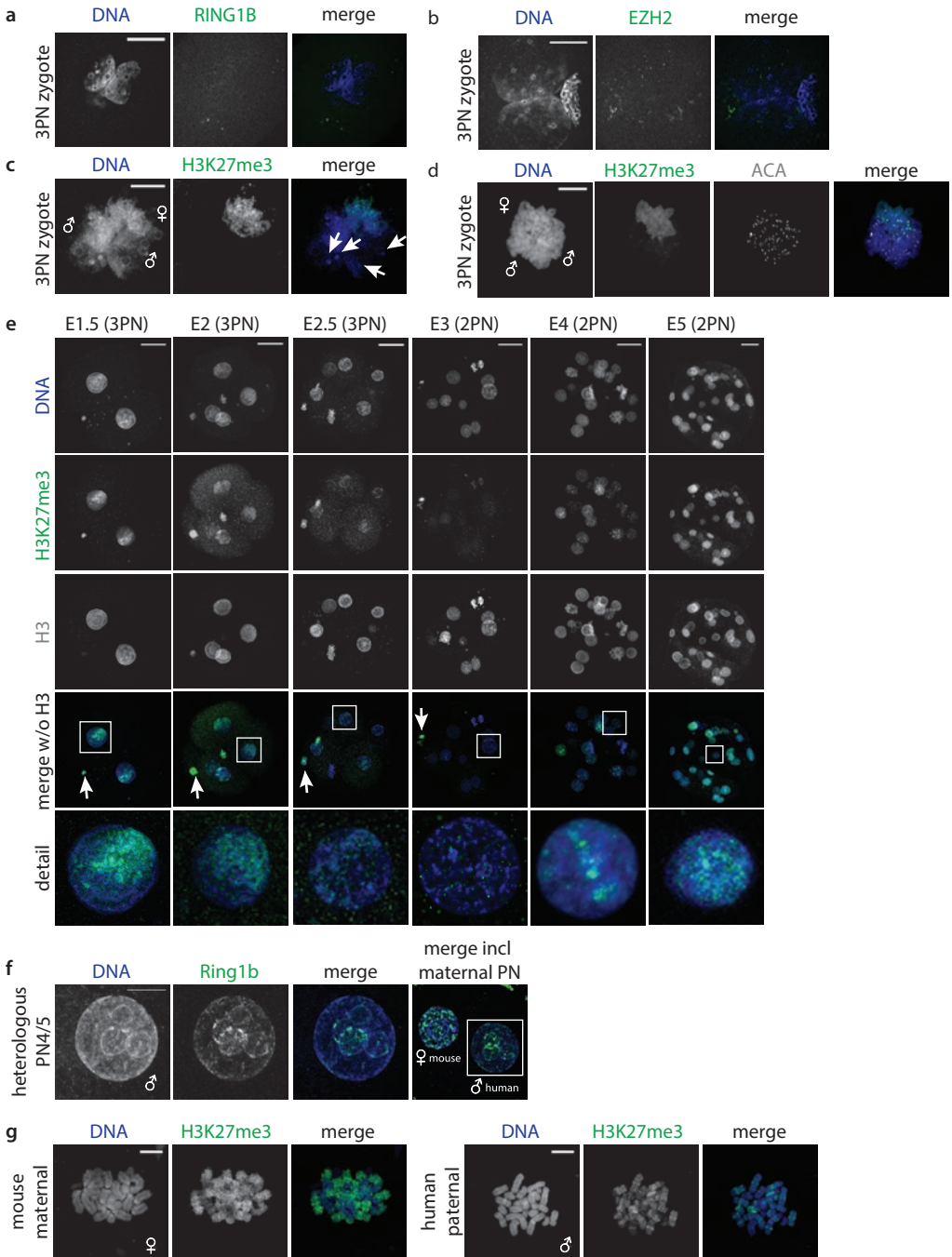


**Figure 2 — Polycomb Repressive Complex 1 and 2 are not associated with paternal cHC in cleavage stage human embryos.** (a-c) Representative confocal images of human 3PN zygotes fixed at G2 phase. Shown are full projections of Z-sections. (a, b) Zygotes immunostained with PRC1 subunit RING1B (n=10) and PRC2 subunit EZH2 (n=5) antibodies (green). No signal is observed to localize to the pronuclei. Scale bars, 30  $\mu$ m. (c) Immunolocalization of H3K27me3 (green) in a 3PN zygote (n=15). Paternal (♂) and maternal (♀) pronuclei are indicated. H3K27me3 is detected broadly on maternal chromatin and only very low levels are observed on paternal chromatin with no enrichment at DAPI-intense, heterochromatic rings or knobs (arrows). Scale bar, 10  $\mu$ m. (d) Representative chromosome spread of a 3PN zygote (n=5) arrested at prometaphase showing immunolocalization of H3K27me3 (green) and centromeres (ACA; white). Paternal (♂) and maternal (♀) chromosomes are indicated. H3K27me3 is detected broadly on maternal chromosomes and no H3K27me3 enrichment is observed at paternal pericentric regions. Scale bar, 10  $\mu$ m. (e) Representative full projections of confocal Z-sections of human embryos at indicated stages (n=5-10 per embryonic stage). From embryonic day (E) 1 to 3, nuclei show an asymmetric staining pattern for H3K27me3 (green). Compared to overall H3 levels as detected by a histone H3 antibody (white), H3K27me3 levels decrease gradually with each cell division. At E4, H3K27me3 is clearly detected throughout all nuclei. Arrows indicate the polar body, where H3K27me3 remains high. Detail shows a magnification of the boxed nucleus. Scale bars, 30  $\mu$ m. (f) Mouse oocytes injected with human spermatozoa, fixed at PN4/5 stage (G2 phase). Shown is a representative confocal image of immunolocalization of Ring1b (green) in a heterologous zygote (n=30). Human paternal (♂) and mouse maternal (♀) pronuclei are indicated. The human paternal pronucleus assumes a mouse-like morphology and Ring1b is detected at distinct regions on the DAPI-intense ring around the nucleolar precursor bodies. Scale bar, 10  $\mu$ m. (g) Representative chromosome spread from a heterologous zygote (n=5) arrested at prometaphase with immunolocalization of H3K27me3 (green). Human paternal (♂) and mouse maternal (♀) chromosomes are indicated. On human paternal chromosomes, H3K27me3 is detected and shows enrichment at distinct chromosome bands. Scale bars, 10  $\mu$ m.

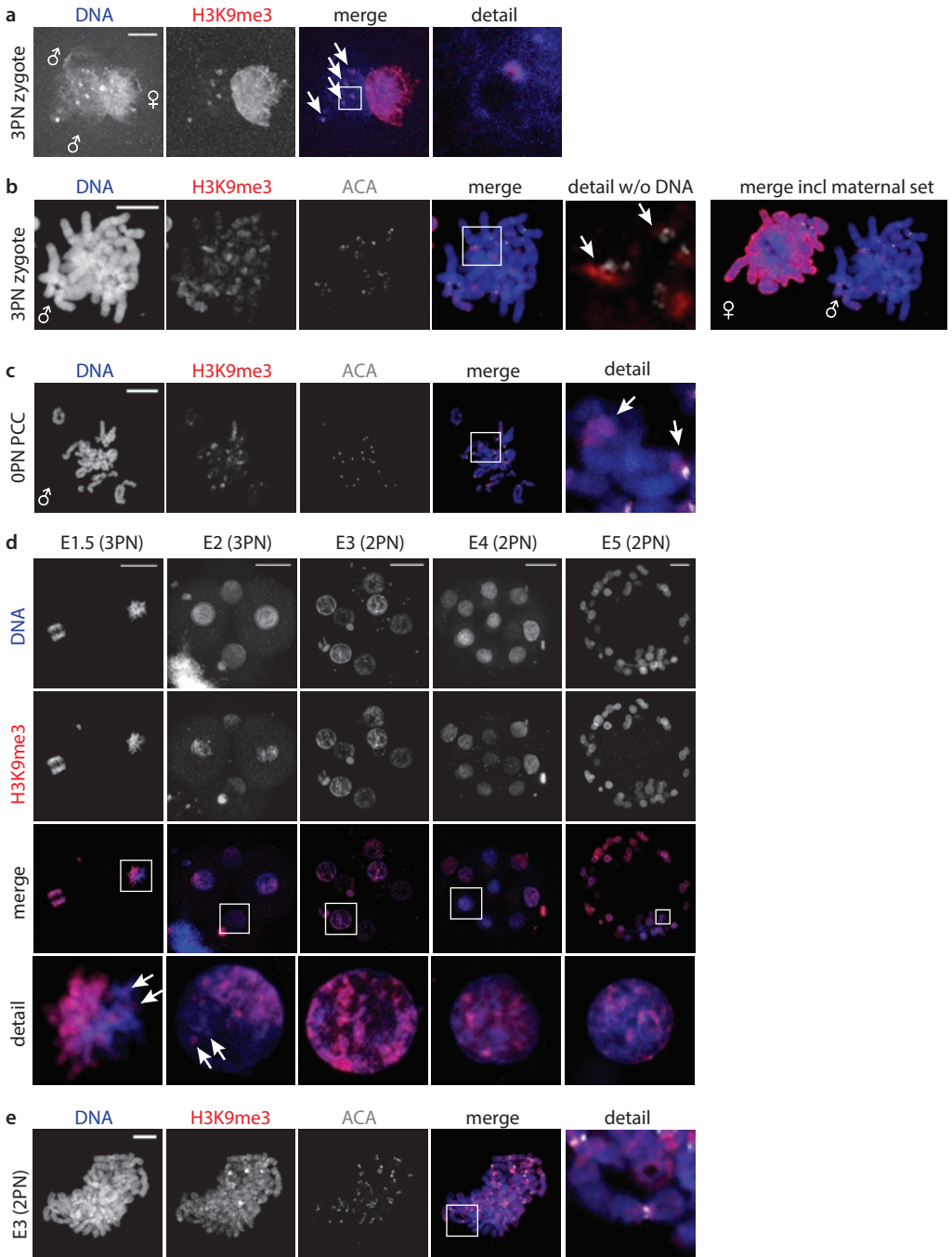
human paternal pronucleus was observed to have adopted a mouse-like pronuclear morphology. We detected Ring1b staining at the ring surrounding the NPBs (Figure 2f). This shows that mouse maternal Ring1b is able to access human paternal chromatin. When heterologous zygotes were arrested and fixed at prometaphase, H3K27me3 was detected in a banding pattern on human paternal chromatin in heterologous zygotes (Figure 2g). This is in contrast to barely detectable levels on paternal prometaphase chromosomes in human zygotes (Figure 2d). These results indicate that human sperm chromatin is intrinsically able to undergo PRC1/2 processing. Although we cannot completely rule out the possibility that the observed change in pronuclear structure positively affects accessibility of paternal cHC in heterologous zygotes, the low abundance of PRC1 and PRC2 transcripts and the dilution of maternal H3K27me3 over divisions, suggests an absence of active PRC1/2 in early human embryos. Altogether, our results suggest that the PRC1/2 pathway does not have a role in paternal cHC establishment in human pre-implantation embryos.

### H3K9me3 marks paternal chromatin on DAPI-rich regions

As the PRC1/2 pathway does not seem to be involved in build-up of cHC in early human embryos, we investigated the canonical H3K9/HP1 pathway by immunostaining for H3K9me3. In human 3PN zygotes at the late G2 phase, maternal pronuclei are abundantly marked by H3K9me3, as described before [20] (Figure 3a). Although signal in the paternal pronuclei was overall much lower, we did observe strong enrichment of H3K9me3 at the DAPI-rich knobs (Figure 3a). This parental asymmetry in H3K9me3 was confirmed by staining of prometaphase chromosome spreads: on paternal chromosomes enrichment was detected between the centromeres and on a few chromosome bands (Figure 3b).

Next, we investigated if our observations for H3K9me3 on the paternal chromatin in post-S-phase human zygotes resulted from *de novo* H3K9 methyltransferase activity during S-phase. In approximately 10% of IVF oocytes that fail to fertilize after IVF, a sperm cell has penetrated, but failed to activate the oocyte [31]. Such spermatozoa frequently undergo a condensation of the paternal chromatin into chromatids, called premature chromatid condensation (PCC). In oocytes with sperm-PCC, we detected strong H3K9me3 enrichment on paternal chromatids at pericentric regions and heterochromatic knobs (Figure 3c), indicating that this mark is independent of DNA replication in S-phase.

**Figure 3 — H3K9me3 is detected on DAPI-dense regions in paternal chromatin from cleavage stage human embryos.** (a) Representative confocal image of a human 3PN zygote fixed at G2 phase (n=15). Shown is a full projection of Z-sections with immunolocalization of H3K9me3 (red). Paternal (♂) and maternal (♀) pronuclei are indicated. H3K9me3 is detected broadly on maternal chromatin and on paternal chromatin enrichment of H3K9me3 is detected at DAPI-intense, heterochromatic, regions (arrows). Detail shows a magnification of the boxed region. Scale bar, 10 µm. (b) Representative chromosome spread of a 3PN zygote arrested at prometaphase (n=30) showing immunolocalization of H3K9me3 (red) and centromeres (ACA; white). Paternal (♂) and maternal (♀) chromosomes are indicated. H3K9me3 is detected broadly on maternal chromosomes. On paternal chromosomes, H3K9me3 is observed at inner centromeric regions (arrows) and some distinct chromosome bands (arrows). Detail shows a magnification of the boxed chromosomes. Scale bar, 10 µm. (c) Representative chromosome spread of a human oocyte 18-20 h post insemination with fertilization failure (OPN) and presence of paternal chromatids after premature chromatid condensation (PCC; n=10). Shown is immunolocalization of H3K9me3 (red) and centromeres (ACA; white) on paternal chromatids. H3K9me3 is detected at distinct regions around the centromeres. Detail shows a magnification of the boxed chromatid (arrows indicate examples of the pericentromere and a H3K9me3 enriched band). Scale bar, 10 µm. (d) Representative full projections of confocal Z-sections of human embryos at indicated stages (n=5-10 per embryonic stage). On embryonic day (E) 1.5 and E2, H3K9me3 (red) is detected in an asymmetric pattern similar to the zygote. Levels on maternal chromatin remain high and arrows indicate H3K9me3 enriched regions on paternal chromatin. From E3 onwards, H3K9me3 was detected throughout the nucleus. Detail shows a magnification of the boxed nucleus. Scale bars, 30 µm. (e) Representative chromosome spread of an embryo at E3.5 arrested at the prometaphase of the 4<sup>th</sup> cleavage division with immunolocalization of H3K9me3 (red) and centromeres (ACA; white) (n=5). H3K9me3 was detected in a banding pattern on all chromosomes with enrichment at pericentric regions. Detail shows a magnification of the boxed chromosomes. Scale bar, 10 µm.



To determine the fate of H3K9me3 on paternal chromatin in the zygote, we performed immunostaining of H3K9me3 on whole-mount embryos of all stages of pre-implantation development (Supplementary Figure 1a). In nuclei from E1 and E2 embryos, H3K9me3 staining was restricted to one side of the nucleus, presumably marking the maternal chromatin (Figure 3d). In contrast to H3K27me3, levels on maternal chromatin remained high during these stages and DAPI-rich domains in the paternal chromatin remained positive for H3K9me3. From the 8-cell stage on, H3K9me3 was detected throughout the nucleus at DAPI-rich domains (Figure 3d). These findings were confirmed by H3K9me3 staining of prometaphase chromosomes of 8-cell (E3) embryos arrested at the prometaphase stage of the fourth cleavage division; the difference between maternal and paternal chromosomes was no longer obvious (Figure 3e). Taken together, these results show that H3K9me3 marks the paternal cHC in the zygote and suggest that this modification is maintained during subsequent cleavage divisions.

### **H3K9me3 marks satellite DNA repeats in human spermatozoa**

In mouse spermatogenesis, pHC becomes devoid of H3K9me3 as elongation is completed and the mark is also not detected on the paternal chromatin in the zygote directly after fertilization [14,27]. However, in human spermatozoa, H3K9me3 enrichment has been observed at the pericentric region of chromosome 16 using ChIP-PCR [32]. To further investigate the presence of H3K9me3 in mature human spermatozoa, we performed immunolocalization of H3K9me3 and the centromeres (ACA) after *in vitro* decondensation. In virtually all spermatozoa H3K9me3 was prominently detected around the centromeres (Figure 4a). To investigate the location of retained H3K9me3 in more detail, human spermatozoa were subjected to extreme *in vitro* decondensation to obtain sperm chromatin in a fiber-like configuration. Whereas H3 was detected broadly, H3K9me3 was detected directly around the centromere, confirming its pericentric localization (Figure 4b).

In mouse elongating spermatids, pHC domains that still contain residual H3K9me3-bearing nucleosomes, also become enriched for nucleosomes with acetylation of histone H4 [14,33]. Although these modifications appear to be mutually exclusive at the nucleosome level, pHC temporarily exists in a bivalent state that may contribute to the reprogramming process [33]. To investigate if cHC in mature human spermatozoa exists in a similar bivalent state, H4 acetylation was detected by immunofluorescence. Acetylation of lysines 5, 8, and 12 of histone H4 (H4K5ac, H4K8ac, and H4K12ac), as well as a tetra-acetylated form of H4 (H4ac4) localized in a cap-like pattern, as described for human elongating spermatids [34] (Supplementary Figure 4). In contrast to mouse, acetylated forms of H4 were not specifically enriched around the centromeres and H4K12ac was not confined to H3K9me3 positive pHC domains (Figure 4c).

To investigate if human DNA repeat sequences underlying cHC are marked by H3K9me3 in sperm cells, we performed a combination of immunofluorescent analysis of H3K9me3 and fluorescent *in situ* hybridization (immuno-FISH). We investigated  $\alpha$ -satellite repeats located on chromosomes 7 and X and Sat II/III sequences of chromosomes 1, 9, 16, and Y. With exception of the X  $\alpha$ -satellite, all repeat sequences investigated were observed to localize partially or completely to the region enriched for H3K9me3 in the majority of sperm cells investigated (Figure 4e and 4f, Supplementary Figure 5). These results demonstrate that DNA repeat sequences that form the cHC in humans are

enriched for H3K9me3 in sperm cells. To investigate if this is also the case after fertilization, we performed immuno-FISH on sperm-PCC in unfertilized oocytes and on paternal chromosomes of human zygotes arrested at prometaphase (Figure 4g). Probe signals for Sat II and III sequences on chromosomes 1, 9, 16, and Y were observed to consistently co-localize with the H3K9me3-positive regions. The satellite III repeat region located to the knob on the long arm of the Y chromosome is completely marked by H3K9me3.

Thus, DNA repeat sequences underlying cHC are enriched for H3K9me3 on paternal chromatin before and after fertilization. This suggests the delivery of these sequences in a canonical, heterochromatic conformation from the spermatozoon to the embryo.

### **Sperm contributes modified histones marking cHC to zygotes**

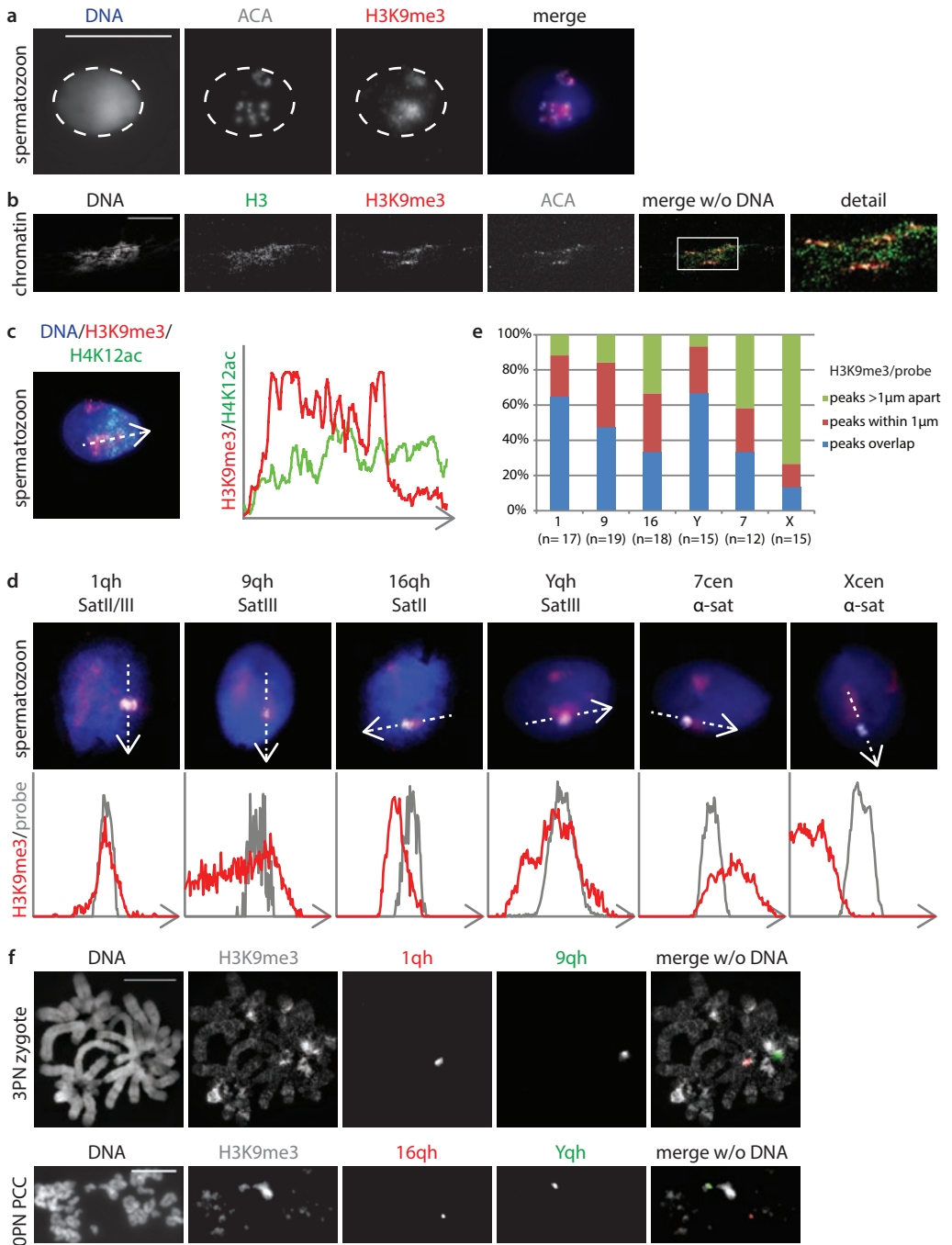
Instead of the suggested inheritance of modified histones, our findings might also be explained by a scenario wherein paternally inherited nucleosomes are replaced by maternal ones, which are subsequently modified by maternal SUV39H1/2 activity. In mouse oocytes, Suv39h mediated modification of H3K9 is not active on paternal constitutive heterochromatin [3]. Any H3K9me3 observed on human paternal chromatin after heterologous ICSI in mouse oocytes would thus be of sperm origin. First, we injected heat inactivated human spermatozoa (for experimental set up of heterologous ICSI see Supplementary Figure 1b), which have lost the ability to activate the oocyte [35] and directly undergo PCC after injection. In mouse oocytes with human sperm-PCC, we detected distinct H3K9me3-rich regions on the human paternal chromatids (Figure 5a), identical to sperm-PCC in human oocytes (Figure 3c). Next, we injected normal human spermatozoa (Supplementary Figure 1b) and investigated zygotes at the late G2 phase. The human paternal pronucleus exhibited distinct domains of H3K9me3 on the DAPI-rich rings around the NPBs (Figure 5b), whereas this mark is absent from mouse paternal chromatin at this stage [3]. PRC1 is not targeted to the H3K9me3 positive domains, as these two types of heterochromatin do not overlap on both PCC and the paternal pronucleus at G2 (Figure 5a,b). This reinforces previous findings that H3K9me3 impairs PRC1 targeting [3]. In heterologous zygotes arrested at prometaphase, the H3K9me3 staining pattern was similar to the one observed on human 3PN zygotes. Distinct H3K9me3 positive bands were observed on human paternal chromosomes (Figure 5c). Chromosome morphology of these heterologous spreads was generally good, and in some cases allowed (partial) karyotyping based on chromosome size and DAPI-banding pattern (Figure 5d). Strong enrichment of H3K9me3 on heterochromatin knobs was specifically observed on chromosomes 1, 9, 13, 14, 16, 21 and Y, on regions known to contain satellite II and III DNA repeats.

Altogether these data suggest that the H3K9me3 in human spermatozoa is retained during the remodeling that occurs in a mouse oocyte after gamete fusion. Based on our previous observations [36] and the data we presented here, we assume this also to be the case in human zygotes. Therefore, our results indicate a sperm origin of these modified histones in paternal embryonic chromatin.

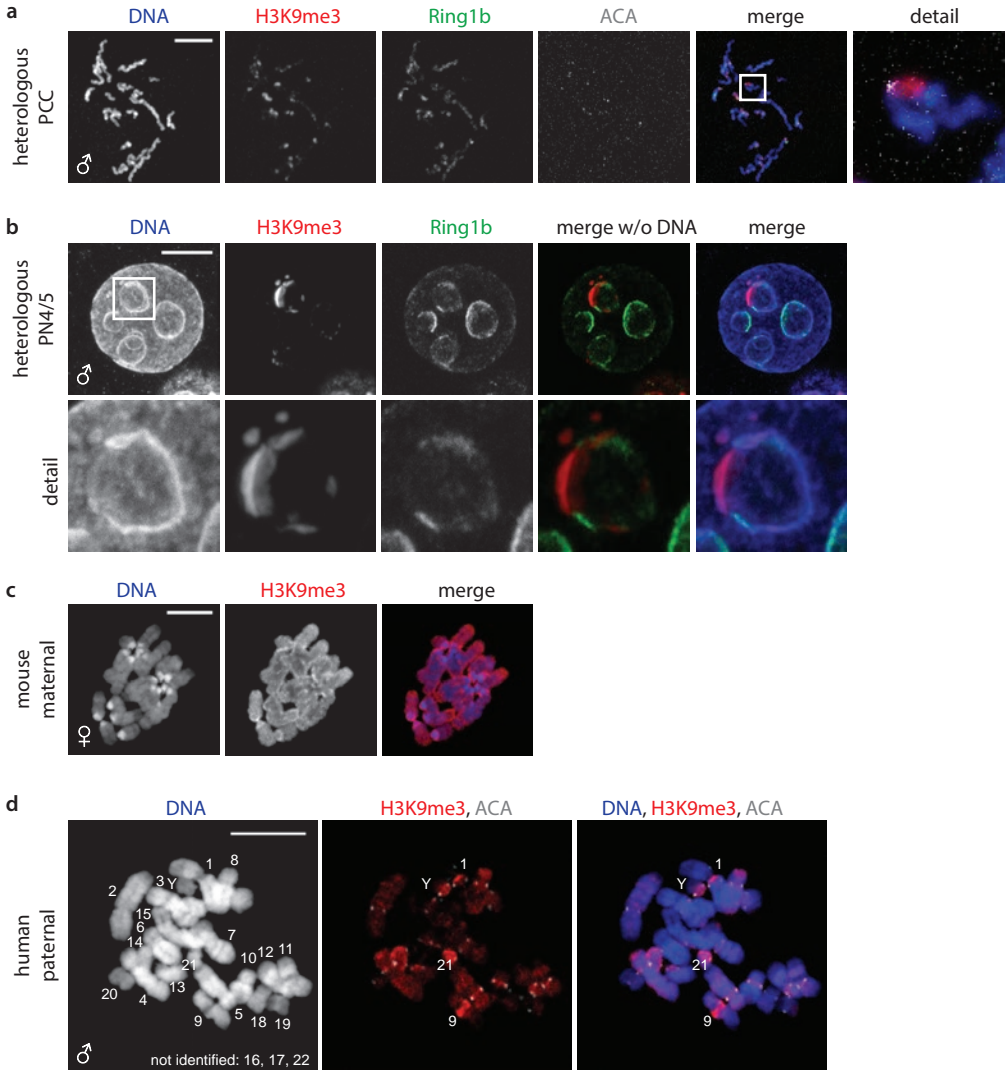
**Figure 4 — H3K9me3 marks satellite DNA sequences at cHC regions on paternal chromatin in spermatozoa and zygotes.** (a) Representative confocal image of a human *in vitro* decondensed spermatozoon. Shown is a full projection of Z-sections with immunolocalization of H3K9me3 (red) and centromeres (ACA; white) (n=100). Enrichment of H3K9me3 surrounding centromeres suggests pericentric localization. Dotted line indicates the nucleus of the spermatozoon. Scale bar, 10  $\mu\text{m}$ . (b) Representative immunofluorescent image of human spermatozoa subjected to extreme *in vitro* decondensation. Chromatin contained in a nucleosomal structure was identified using a histone H3 antibody (green), in combination with immunolocalization of H3K9me3 (red) and centromeres (ACA; white) (n=100). H3K9me3 is detected directly neighbouring ACA signal, indicating pericentric localization. Scale bar, 20  $\mu\text{m}$ . (c) Full projection of Z-sections of a human *in vitro* decondensed spermatozoon with immunolocalization of H3K9me3 (red) and H4K12ac (green) (full set of single channel images in Supplementary Figure 4). Graph shows distribution of fluorescent intensities along the line (c) for H3K9me3 (red) and H4K12ac (green) in arbitrary units. (d) Codetection of H3K9me3 (red) and (peri)centric repeat sequences (white) in *in vitro* decondensed human spermatozoa (n=10-12) by immuno-FISH. DNA probes detecting satellite (Sat) DNA II/III repeat sequences at heterochromatic knobs on chromosomes 1, 9, 16 and Y and  $\alpha$  satellite DNA sequences at centromeric locations (chromosomes 7 and X) are used. Shown are representative merged images of a single Z-section through the probe signal (full set of single channel images in Supplementary Figure 5). Graph shows distribution of fluorescent intensities along the line for H3K9me3 (red) and probe signal (grey) in arbitrary units. Scale bar, 5  $\mu\text{m}$ . (e) Distribution of sperm cells according to their classification based on their profiles shown in (d). (f) Codetection of H3K9me3 and (peri)centric repeat sequences by immuno-FISH on chromosome spreads. Upper panel: representative chromosome spread from the paternal chromosome set of a 3PN zygote arrested at prometaphase hybridized with DNA probes detecting satellite II/III sequences at chromosomes 1 (1qh, red) and 9 (9qh, green) (n=5). Lower panel: representative chromosome spread from paternal chromatids (PCC) in an unfertilized oocyte (OPN; n=7) hybridized with DNA probes detecting satellite II/III sequences at chromosomes 16 (16qh, red) and Y (yqh, green). DNA probes colocalize with areas of strong H3K9me3 (white) enrichment. Scale bars, 10  $\mu\text{m}$ .



2



**Figure 5 — H3K9me3 on paternal embryonic chromatin originates from the human spermatozoon.** To assess the origin of H3K9me3 on human paternal chromatin, human spermatozoa were injected into mouse oocytes. **(a)** Confocal analysis of fixed mouse oocytes 22 h after heterologous ICSI with heat inactivated human sperm (n=30). Shown is a full projection of Z-sections containing paternal chromatids (♂) with immunolocalization of H3K9me3 (red) and Ring1b (green). H3K9me3 is clearly detected at pericentric regions on each chromatid. Scale bar, 10 μm. **(b)** Representative confocal image of the paternal pronucleus of a heterologous zygote fixed 12-15 h after injection (G2 phase; n=30). Shown is a full projection of Z-sections with immunolocalization of H3K9me3 (red) and Ring1b (green). The human paternal pronucleus (♂) assumes a mouse-like morphology (PN4). H3K9me3 and Ring1b are detected in a non-overlapping fashion at distinct regions at the DAPI-intense ring around the nucleolar precursor bodies. Detail shows a magnification of the boxed ring. Scale bar, 10 μm. **(c, d)** Representative chromosome spread of a zygote resulting from heterologous ICSI arrested at prometaphase (n=30). Paternal (♂) and maternal (♀) chromosomes are indicated. Scale bars, 10 μm. **(c)** Mouse maternal chromosomes with immunolocalization of H3K9me3 (red), showing H3K9me3 ubiquitously on maternal chromosomes. **(d)** On paternal chromosomes, immunolocalization of H3K9me3 (red) and centromeres (ACA; white) revealed enrichment of H3K9me3 at the inner centromere of all chromosomes. Partial karyotyping of the paternal chromosomes identified strong enrichment on heterochromatin knobs on chromosomes 1, 9, 13, 14, 21 and Y. Chromosomes 16, 17 and 22 were not unambiguously identified in this spread.



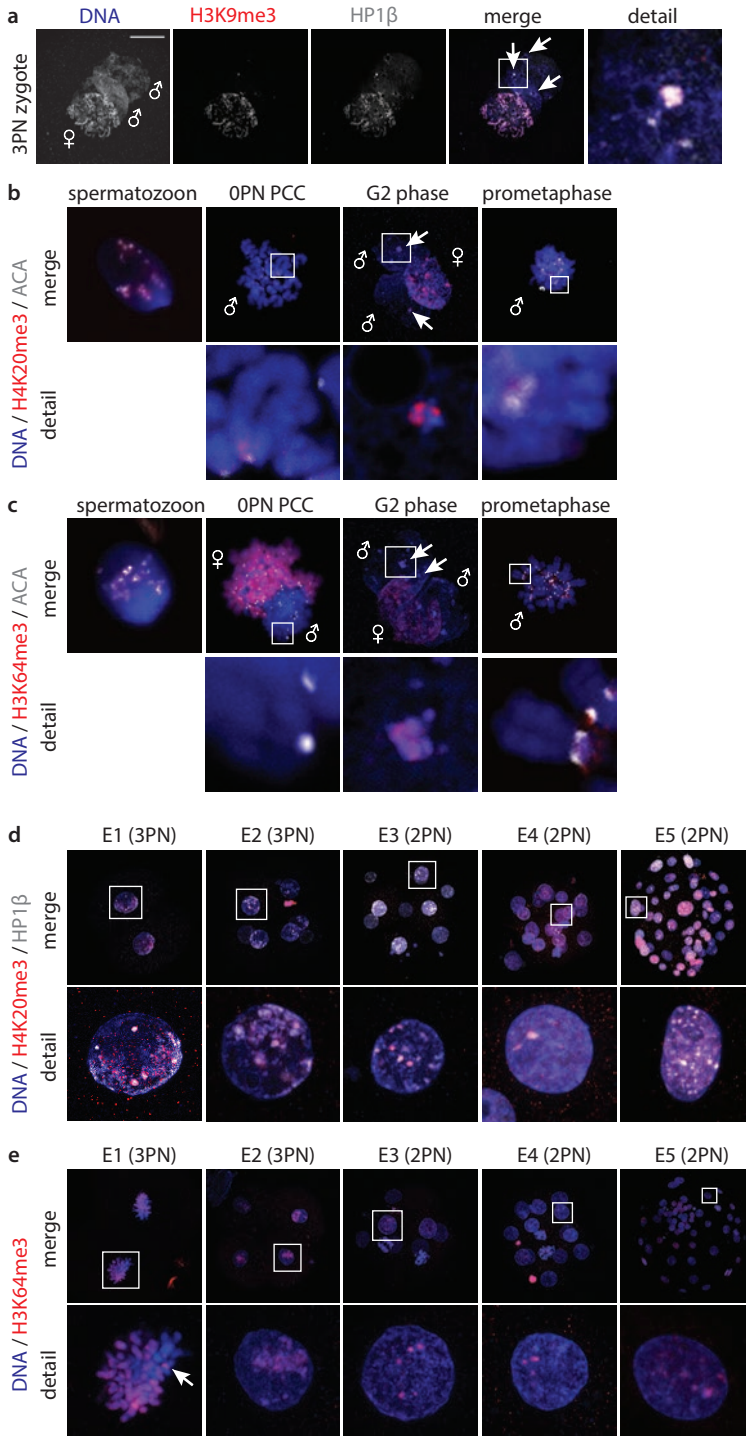


**Figure 6 — Paternal cHC marked by H3K9me3 also contains HP1 $\beta$ , H4K20me3 and H3K64me3.** (a) Representative confocal image of a human 3PN zygote fixed 18-20 h post insemination with immunostaining of H3K9me3 (red) and HP1 $\beta$  (white) (n=5). Paternal (♂) and maternal (♀) pronuclei are indicated. Detail shows a magnification of the boxed region. HP1 $\beta$  was detected broadly on the maternal pronucleus and on heterochromatin knobs on the paternal pronucleus (arrows and detail), co-localizing with H3K9me3 staining. Scale bar, 10  $\mu$ m. (b, c) Representative merged confocal images of a human *in vitro* decondensed spermatozoon, a human 0PN oocyte with PCC, a human 3PN zygote at G2 phase and a human 3PN zygote arrested at prometaphase (n=5-10 per embryonic stage), all immunostained for (b) H4K20me3 (red) and centromeres (ACA; white (excluding G2 phase)) or (c) H3K64me3 (red) and centromeres (ACA; white (excluding G2 phase)). Shown are full projections of Z-sections. Paternal (♂) and maternal (♀) chromatin is indicated. Details shows magnifications of boxed regions. Full set of single channel images in Supplementary Figure 5. Both H4K20me3 and H3K64me3 were detected at pericentric regions in all stages, comparable to H3K9me3 and HP1 $\beta$ , but H3K64me3 staining was less intense in spermatozoa and 0PN PCC. (d, e) Dynamics of H4K20me3, HP1 $\beta$ , and H3K64me3 during human pre-implantation embryo development. Representative merged confocal images of human embryos at indicated developmental stages (n=5-10 per embryonic stage) with immunolocalization of (d) H4K20me3 (red) and HP1 $\beta$  (white) or (e) H3K64me3 (red). Shown are representative merged full projections of confocal Z-sections. Detail shows magnification of the boxed nucleus. Full set of single channel images in Supplemental Figure S6. On embryonic day (E) 1 and E2, all antibodies are detected in an asymmetric pattern similar to their expression the zygote. On condensed chromosomes, paternal H3K64me3 knobs are clearly visible (arrow). Whereas HP1 $\beta$  is observed strongly and throughout the nucleus from E3 onwards, H4K20me3 and H3K64me3 are more confined to DAPI-intense regions.

### Paternal cHC is marked by H3K9me3/HP1 pathway modifications

As described, H3K9me3-binding HP1 proteins (isoforms  $\alpha$ ,  $\beta$ ) and histone modifications H4K20me3 and H3K64me3 are additional markers of cHC. To investigate the extent of cHC formation on the paternal chromatin, we determined the dynamics of these additional markers by immunofluorescent analysis in spermatozoa, unfertilized oocytes with PCC, 3PN zygotes, and all stages of pre-implantation development. As described in mouse [3], we also failed to detect HP1 $\beta$  in *in vitro* decondensed human spermatozoa (data not shown). However, in contrast to mouse, both HP1 $\alpha$  and HP1 $\beta$  were readily detected at the DAPI-rich knobs in paternal pronuclei, co-localizing with H3K9me3 (Figure 6a, Supplementary Figure 6a). HP1 $\beta$  dynamics during embryo development followed the same pattern as H3K9me3, with asymmetric staining in the nucleus at E1 and E2 (Figure 6d, Supplementary Figure 7a). From E3 onwards, staining was observed at DAPI-rich regions throughout the nucleus.

H4K20me3 was detected around the centromeres in decondensed human spermatozoa, similar to H3K9me3. After fertilization, H4K20me3 was detected ubiquitously at maternal chromatin, on DAPI-rich knobs at G2 phase in the paternal pronucleus, and at paternal pericentric regions in PCC and prometaphase chromosomes (Figure 6b, Supplementary Figure 6b). From the 2-cell stage onwards, H4K20me3 remained detectable in a pattern similar to H3K9me3, but staining appeared more constricted to the DAPI-rich regions (Fig. 6d, Supplementary Figure 7a).

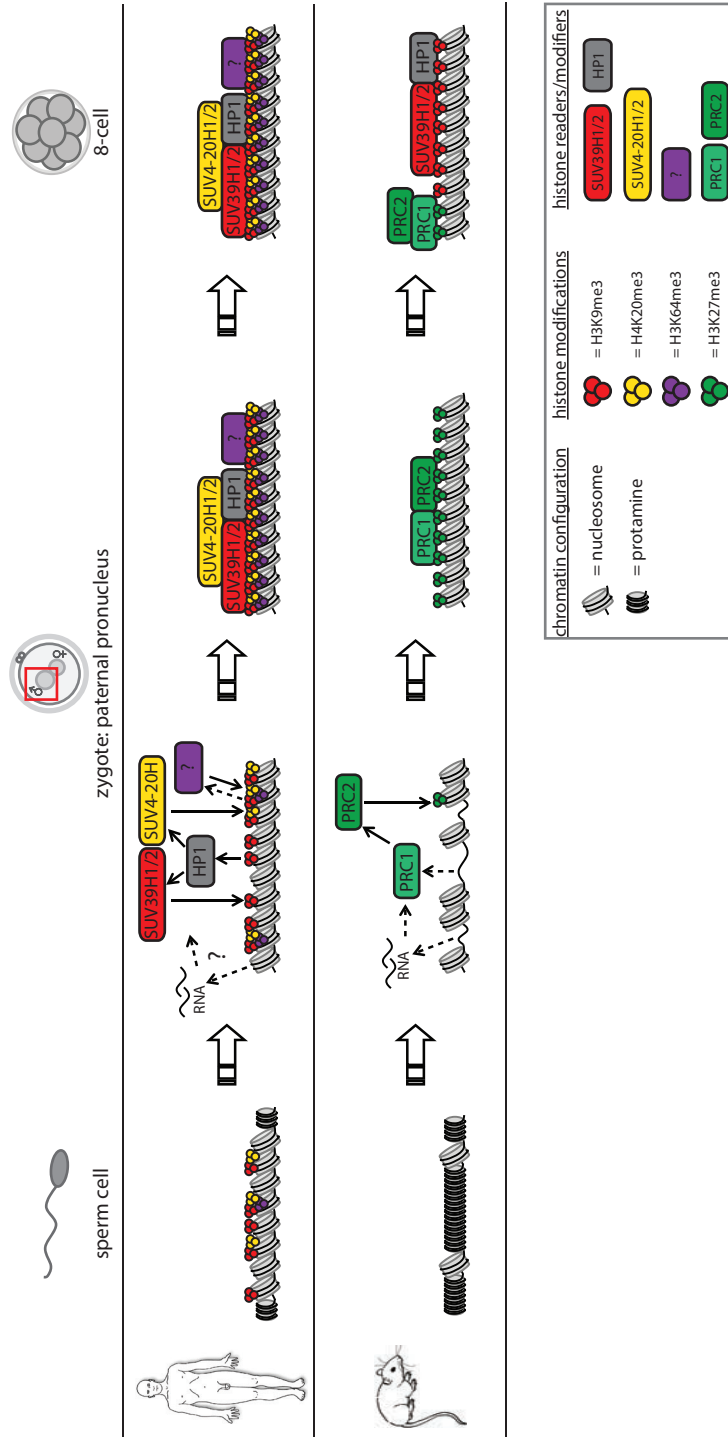


Figure 7 — The build-up of paternal cHC in human embryos is direct by the H3K9/HP1 pathway and primed by sperm-derived histone modifications. Schematic representation of our results and conclusions, and comparison to previous findings in mouse [3]. Whereas in mouse embryos re-establishment of paternal cHC is directed by the PRC1/2 pathway, in human embryos modified histones originating from the spermatozoon allow build-up and maintenance of cHC by the canonical H3K9/HP1 pathway.

H3K64me3 was observed at barely detectable levels in decondensed human spermatozoa. In unfertilized oocytes with paternal PCC, H3K64me3 was detected strongly at maternal chromatin, but barely at paternal chromatin. H3K64me3 levels appeared to increase after S-phase, as staining was observed on DAPI-rich knobs at G2 phase in the paternal pronucleus and prometaphase chromosomes (Figure 6c, Supplementary Figure 6b). From the 2-cell stage onwards, H3K64me3 followed a pattern similar to H4K20me3 (Figure 6e, Supplementary Figure 7b).

These findings show that, in contrast to mouse, paternal cHC in human pre-implantation stage embryos contains a full suit of canonical cHC markers, all of them grouped in the H3K9/HP1 pathway. Since we found that maternal HP1 binds sperm-derived H3K9me3 and that H3K64me3 is increased at H3K9me3-positive regions, our data also shows that the modified histones contributed by the sperm cell enable further establishment and maintenance of cHC by the maternal machinery.

## Discussion

The current work identifies three major mechanistic differences in paternal cHC build-up between mouse and human: 1) human paternal cHC is transmitted from the spermatozoon to the zygote in a canonical conformation, which is subsequently propagated by the H3K9me3/HP1 pathway, 2) in humans, paternal embryonic cHC remains under control of the H3K9/HP1 pathway and cHC is characterized by hallmarks as H4K20me3 and H3K64me3 much earlier in development than in mouse, and 3) a PRC1/2-mediated back-up mechanism, as described in mouse [3], does not seem to play a role.

Based on our results, we propose an intergenerational model for cHC build-up in the early human embryo (Figure 7): nucleosomes bearing H3K9me3 and H4K20me3 are transmitted by the spermatozoon and demarcate cHC domains in the zygote. H3K9me3 is detected and bound by maternally provided HP1 proteins, which in turn bind the SUV39H1/2 and SUV4-20H1/2 KMTs, enabling propagation of these marks. Low levels of H3K64me3 present in the sperm cell can contribute to the feedback loop that reinforces further heterochromatinization [12]. Together this results in the epigenetic propagation of the chromatin conformation of paternal cHC to the next generation.

In mouse, only 1% of sperm DNA remains histone associated [37]. Although transferred to the embryo [14], this low quantity of paternally-inherited nucleosomes might not allow similar protein-based inheritance of heterochromatic DNA. Instead, paternal heterochromatin build-up is initiated through action of PRC1 [3]. Recent findings indicate that the histone demethylase Kdm2b binds to unmethylated CpG islands and directly recruits a subset of PRC1 complexes to chromatin in pluripotent stem cells [38]. This or an analogous binding cascade could enable a DNA-based paternal heterochromatin build-up in mouse embryos [38-39]. Thus, whereas mouse embryos seem to depend on sperm DNA sequence and a maternal store of Polycomb proteins to re-establish paternal cHC, in human embryos cHC is inherited from the sperm cell in the canonical configuration.

In mouse, Polycombs are key to regulation of genes associated with development [40]. Therefore, our failure to detect PRC1/2 activity in human cleavage stage embryos is remarkable. However,

immunofluorescence is not sensitive enough to detect possible presence and maintenance of H3K27me3 at a gene level. Genome wide chromatin analysis of human sperm cells previously identified H3K27me3 enrichment at developmental regulators [32,41]. If transferred to the embryo in a similar fashion as H3K9me3, these marks might be enough to prevent inappropriate gene expression. A global decline in H3K27me3 levels during pre-implantation development has also been described in bovine and porcine cleavage embryos, in which the embryonic stage with the lowest levels of H3K27me3 coincided with EGA [42]. Our findings are consistent with this, as the major wave of human EGA occurs around the 8 cell stage [43]. Global loss of H3K27me3 may thus be required for EGA in species where EGA occurs later than in mouse [42].

In mouse embryos, transcription of major satellites, especially from the paternal genome, has recently been reported to be crucial for rearrangement of pHc [4]. In this light it is interesting that we observed strong H3K9me3 enrichment on satellite II/III DNA repeats on paternal chromatin in both spermatozoa and zygotes. Sat III repeat sequences are primate specific [44] and long non-coding Sat III transcripts have been implicated in developmental regulation [45]. As long non-coding RNAs contribute to heterochromatin assembly during female X chromosome inactivation, Sat III transcripts may have a similar function in cHC maintenance [46]. It remains to be determined if such RNA-based mechanisms are needed for cHC organization in human embryos or if the self-sustaining loop of the full H3K9/HP1 pathway is sufficient.

During mammalian spermiogenesis, histones are replaced by protamines. In humans, 5-15% of the DNA, encompassing specific genes, as well as (peri)centromeric DNA, appear to be protected against this removal and retain a nucleosomal structure (for review see [47]). Studies on human sperm have demonstrated that there is an increase in the nucleosome/protamine ratio when sperm from male factor subfertility patients are compared with sperm from fertile men, confirming incomplete chromatin remodelling during spermatid elongation [48]. Also, differences in composition of retained nucleosomes exist between these groups, with a more dispersed pattern throughout the genome in sperm from subfertility patients [41,48-50]. As we show that sperm-inherited modified histones contribute to cHC formation in the human zygote, the variability observed in retention of nucleosomes may interfere with cHC function in the zygote and impact upon embryo developmental potential.

Frequently, findings on chromatin dynamics in early mouse embryos are assumed to be universal for epigenetic reprogramming in mammalian embryos [51-52]. Our findings highlight the existence of divergent epigenetic developmental programs in mammals. Charting these differences will greatly improve our understanding of how heterochromatin features impact on embryo development.

### **Acknowledgements**

We are grateful to the patients of the IVF unit at the Erasmus MC University Medical Center for participating in this study. We thank Marian Kroos-de Haan, Anneke de Vreeden and Karin van Veen-Buurman for technical assistance, Liliana Ramos for technical advice on sperm decondensation, Diane van Opstal for karyotyping and Gert van Cappellen from the Erasmus MC Optical Imaging Center for help with immunofluorescent quantifications. We thank Catherine Dupont, Geert Kops, Sylvain Daujat and Hikke van Doorninck for materials. This work was funded by a grant from the



Netherlands Organisation for Scientific Research (NWO-Veni: ZonMW 016.096.106) to E.B.B., M.A. was supported by a Boehringer Ingelheim Fonds PhD fellowship, and research in the laboratory of A.H.F.M.P. is supported by the Novartis Research Foundation.

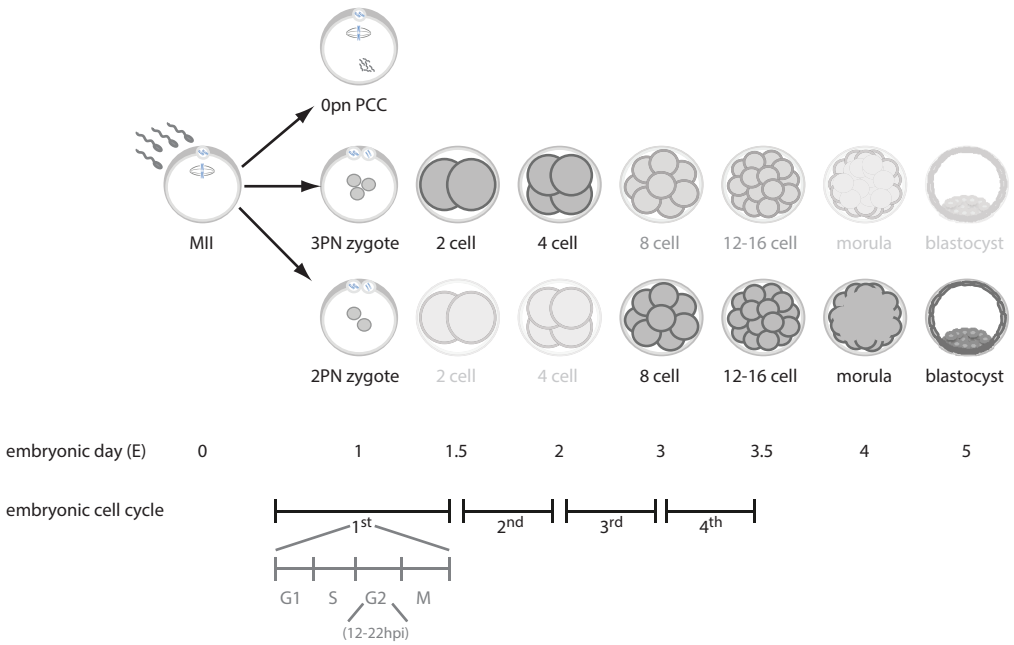
### **Author contributions**

E.B.B. and A.H.F.M.P. conceived the project and designed the experiments. C.W., G.H., C.E., M.T. and M.A. performed the experiments and C.W., G.H., M.A., A.H.F.M.P. and E.B.B. analyzed the data and evaluated results. W.B. provided mouse material and facilities for heterologous ICSI. J.L. was responsible for IVF patients and informed consent for donated human embryos. C.W., G.H. and E.B.B. wrote the manuscript. All authors contributed to manuscript revision and critical discussion.

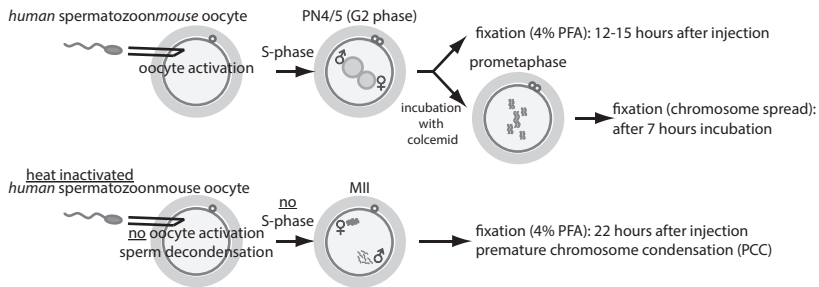
### **Competing financial interests**

The authors declare that they have no conflict of interest.

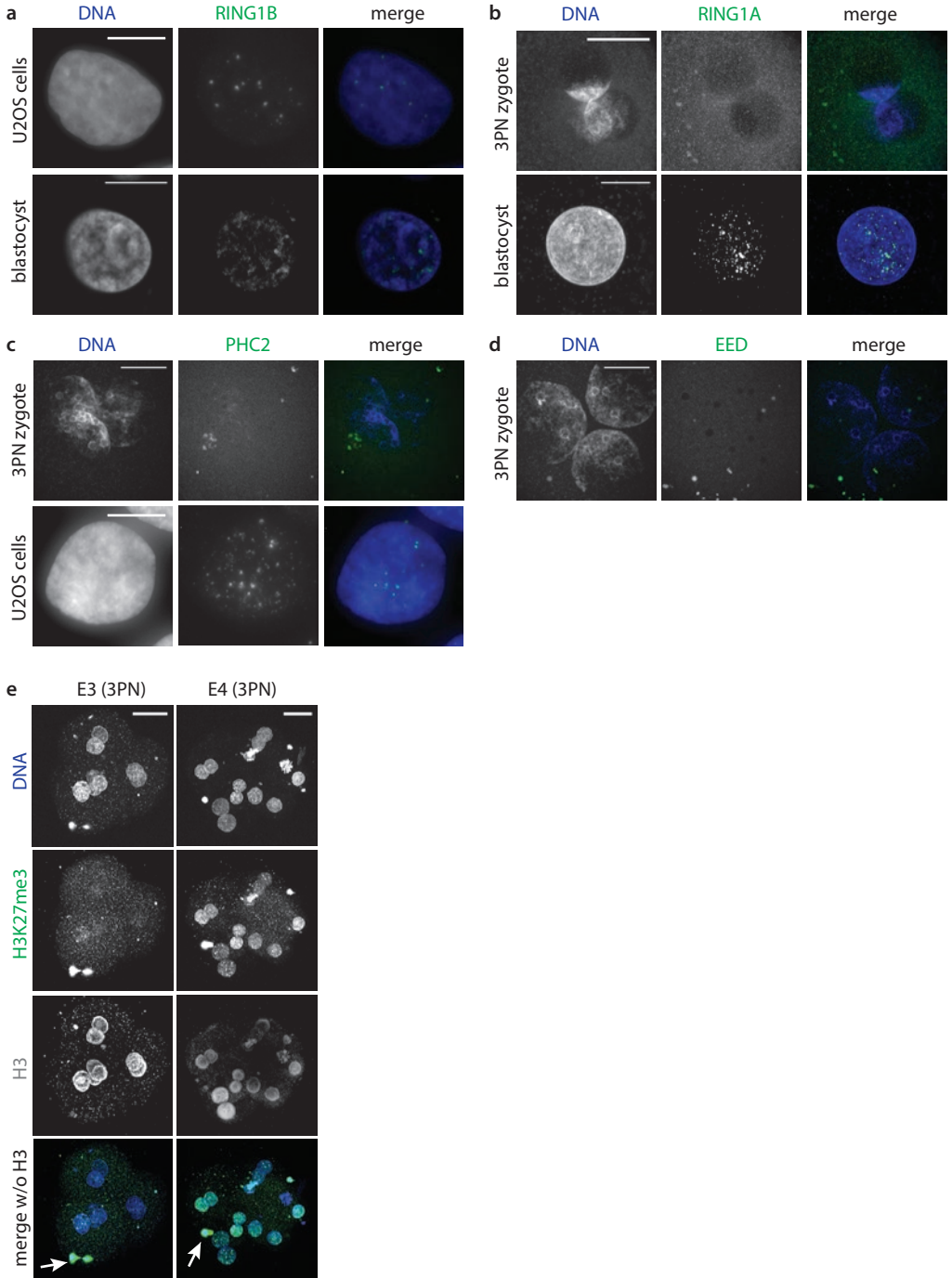
a Human oocytes and embryos used for this study



b Heterologous Intra Cytoplasmic Sperm Injection (ICSI)



**Supplementary Figure 1 — Developmental time-frame for human oocytes and pre-implantation embryos used in this study. (a)** Schematic representation of the stages of oocyte and embryo development used in this study. Oocytes that failed to fertilize were processed on E1 and checked for the presence of paternal chromatids (PCC). Zygotes that displayed three pronuclei (3PN) were either processed directly, incubated in colcemid for prometaphase arrest or allowed to develop until E1 or E2 and processed subsequently. Good quality diploid (2PN) embryos that had been cryopreserved on E3 or E4 were thawed and processed immediately or allowed to develop to E4 or E5 and processed subsequently. **(b)** Schematic representation of heterologous ICSI experiments: mouse oocytes are injected with normal or heat-inactivated human spermatozoa. Oocytes injected with normal spermatozoa are either fixed 12-15 h post injection at the PN4/5 stage (corresponding to G2 phase) or prepared for chromosome spreads after incubation with colcemid to induce prometaphase arrest. Oocytes injected with heat inactivated spermatozoa fail to activate and remain at the metaphase II (MII) stage, while paternal chromatin is condensed into chromatids (PCC).

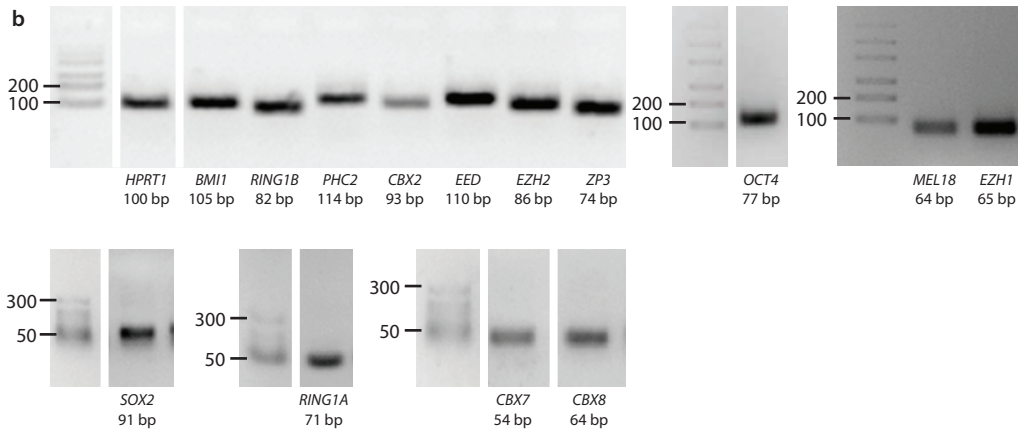


**Supplementary Figure 2 — Polycomb Repressive Complex 1 and 2 are not associated with paternal cHC in human embryos until after E3. (a)** Immunolocalization of PRC1 subunit RING1B (green) in a U2OS cell nucleus and a blastocyst nucleus. Human U2OS cells spontaneously overexpress Polycomb group proteins and serve as a positive antibody control. Shown is an immunofluorescent image of a U2OS cell nucleus containing enrichment of RING1B in typical “polycomb bodies”<sup>25</sup>. Confocal analysis of human blastocysts fixed on E5 also shows several RING1B foci to be present in the nucleus (n=5). Shown is a representative full projection of Z-sections through a single nucleus. Scale bars, 10  $\mu\text{m}$ . **(b)** Immunolocalization of PRC1 subunit RING1A (green) in a 3PN zygote and blastocyst. Representative confocal images of a 3PN zygote fixed 18-20 h post insemination and a blastocyst fixed on E5. Shown are full projections of Z-sections. RING1A is not detected in the zygote (n=5), but several foci can be observed in the blastocyst nucleus (n=5). Scale bars, 30  $\mu\text{m}$  (3PN zygote) and 10  $\mu\text{m}$  (blastocyst). **(c)** Immunolocalization of PRC1 subunit PHC2 (green) in a 3PN zygote and a U2OS cell nucleus. Representative confocal image of a human 3PN zygote fixed 18-20 h post insemination. Full projections of Z-sections fail to detect PHC2 in the zygote (n=5), but several foci can be observed in U2OS cells. Scale bar, 30  $\mu\text{m}$  (3PN zygote), 10  $\mu\text{m}$  (U2OS cell). **(d)** Immunolocalization of PRC2 subunit EED (green) in a 3PN zygote. Representative confocal image of a 3PN zygote fixed 18-20 h post insemination (n=5). Shown is a full projection of Z-sections. EED is not detected at DAPI-dense rings or knobs. Scale bar, 30  $\mu\text{m}$ . **(e)** H3K27me3 dynamics in E3 and E4 embryos originating from 3PN embryos. Shown are representative full projections of confocal Z-sections of embryos fixed at indicated developmental stages (n=5 per stage), with immunolocalization of H3K27me3 (green) and histone H3 (white). Results are the same as in embryos from a 2PN origin (compare with Figure 2e): compared to overall H3 levels, H3K27me3 levels are barely detectable at E3. At E4, high H3K27me3 levels are detected in all nuclei. Arrows indicate the polar body. Scale bars, 30  $\mu\text{m}$ .

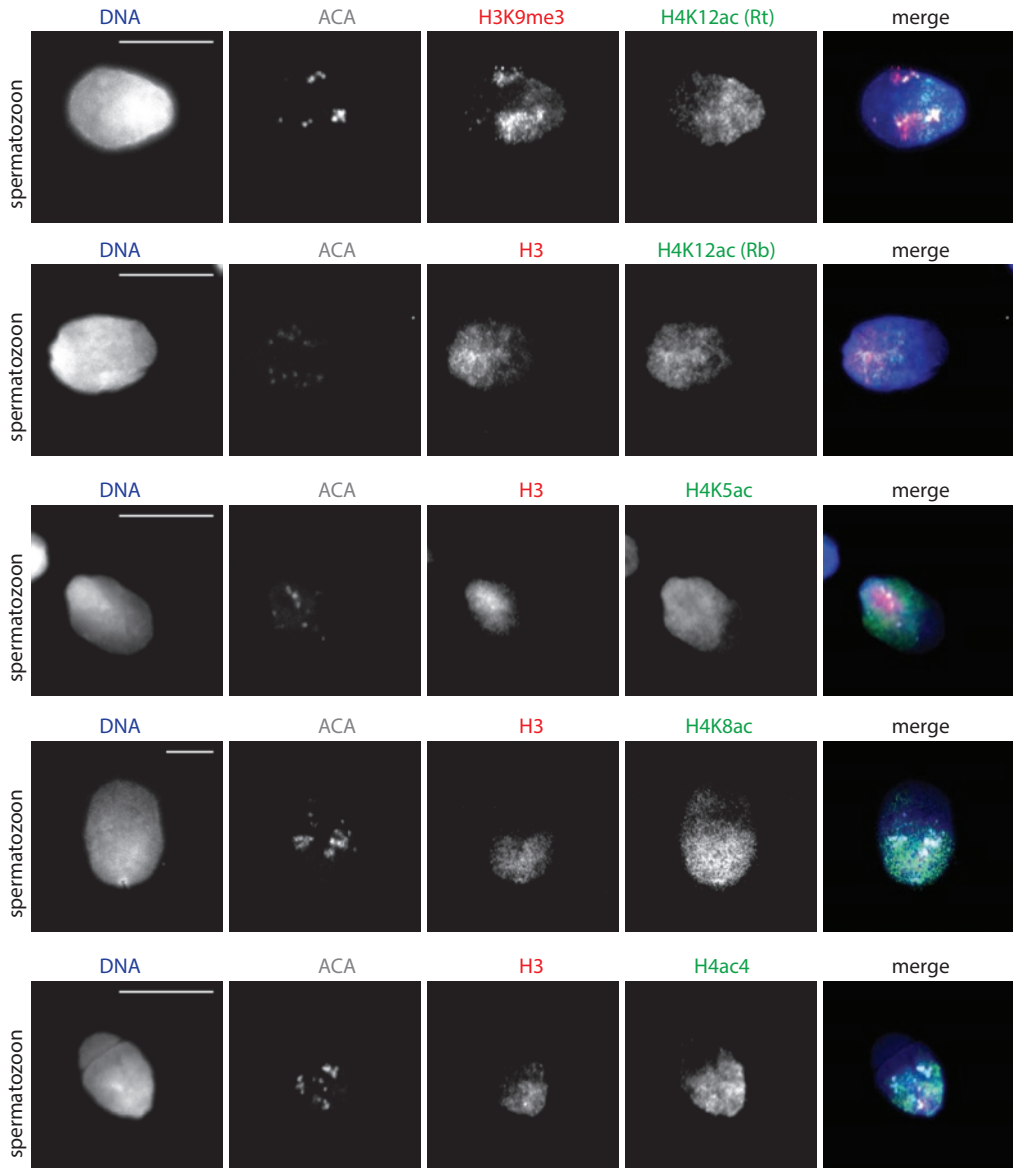
a

GENE	E0	E1	E1.5	E2	E3	E3.5	E4	E5	hESCs	expression		
										highly expressed	Ct value	color
<b>Controls</b>												
ZP3	20	20	23	24	24	26	25	27	25	≤17	green	
HPRT1	23	24	24	27	27	27	25	24	19	18-20	light green	
SOX2	31	31	28	26	26	25	23	24	17	21-23	yellow	
OCT4	27	27	28	27	27	25	23	22	15	24-26	orange	
<b>PRC1</b>												
BMI1	32	34	33	33	30	30	27	26	23	27-29	red-orange	
MEL18	29	29	30	30	30	30	29	25	18	≥30	red	
RING1A	24	24	25	28	27	26	26	24	18			
RING1B	25	26	27	28	27	28	26	25	19			
PHC2	26	26	27	29	29	31	29	25	20			
CBX2	25	26	26	28	27	30	27	26	20			
CBX7	32	32	33	34	34	33	33	31	22			
CBX8	25	24	26	28	28	28	27	27	23			
<b>PRC2</b>												
EZH1	28	29	29	30	31	32	30	29	21			
EZH2	27	27	28	27	27	27	25	24	19			
EED	33	36	35	31	31	30	28	26	23			

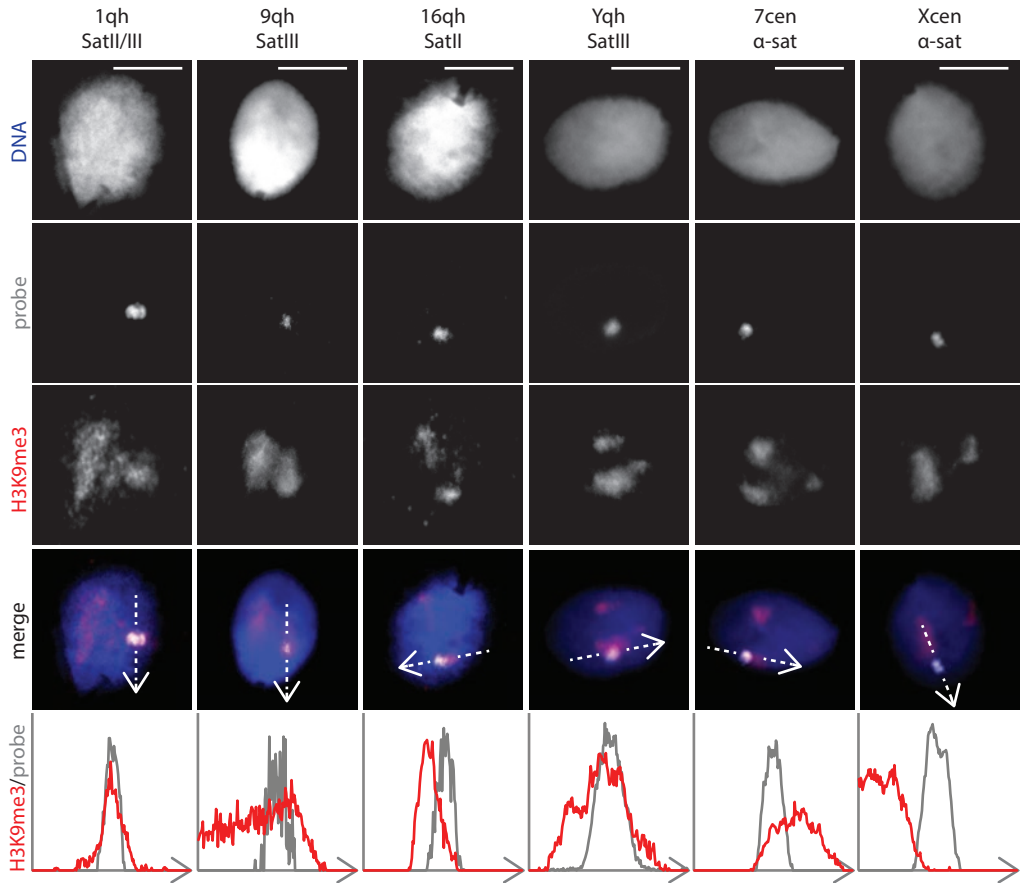
b



**Supplementary Figure 3 —mRNA expression of PRC1/2 subunits in human oocytes and pre-implantation embryos.** (a) mRNA expression levels of control genes and PRC1/2 subunits were quantified by RT-qPCR in single oocytes and pre-implantation embryos at the following eight developmental stages (Supplementary Figure 1): E0 (n=7); E1 (n=5); E1.5 (n=5), E2 (n=4), E3 (n=5), E3.5 (n=5), E4 (n=4), and E5 (n=5). Average cycle threshold (Ct) values are given and results are depicted as colours ranging from green to red, indicating expression levels ranging from high (green) to below detection threshold ( $\geq 30$ ; red). ZP3, expressed only as a maternal transcript, HPRT1, expressed stably in somatic cells, and SOX2 and OCT4, transcription factors whose expression is known to increase during pre-implantation development, were used as controls. RNA isolated from human embryonic stem cells (hESCs) is used to verify detection of all investigated mRNAs with the chosen gene expression assays. Expression of the investigated mRNAs followed similar patterns: levels decreased from E0 to E3 and started increasing again around E4. Exceptions were expression of BMI1 and EED, which was not detected until E4, and CBX7, which was only detected in hESCs. (b) Verification of PCR products on agarose gel. DNA marker sizes are indicated in base pairs. Indicated beneath the gel lanes are the gene and the expected amplicon size in base pairs (bp).



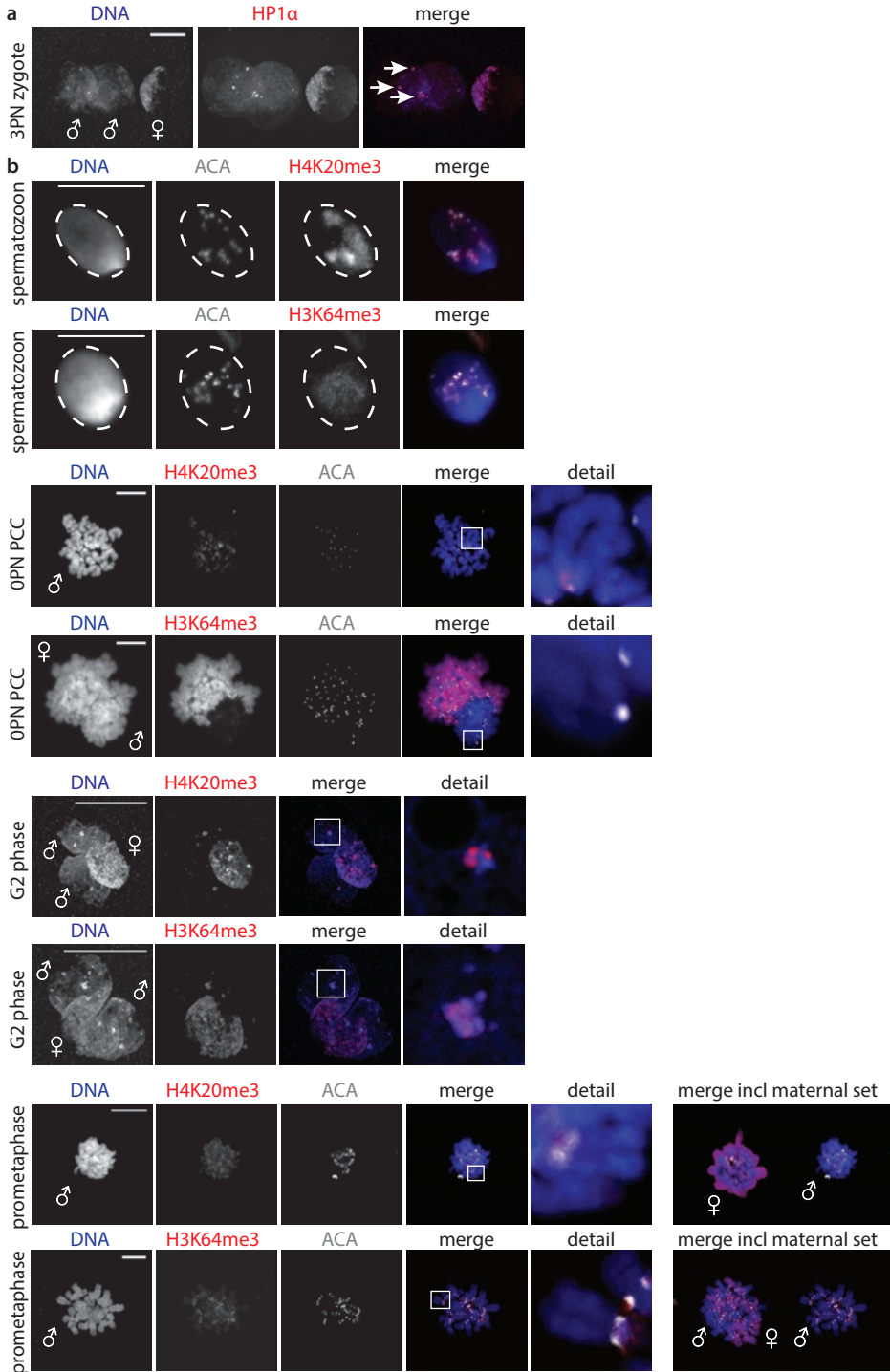
**Supplementary Figure 4 — Acetylated forms of Histone 4 are not enriched at pericentric heterochromatin in mature human spermatozoa.** Representative full projections of confocal Z-sections through human *in vitro* decondensed spermatozoa (n=100 per experiment). Upper panel: Full set of single channel images corresponding to merged image shown in Fig. 4c, with immunolocalization of H3K9me3 (red) and H4K12ac (monoclonal Rat antibody, green) relative to centromeres (ACA; white). H3K9me3 is enriched in the region surrounding the centromeres, but H4K12ac localizes in a cap-like pattern and is not specifically enriched at pHc. Lower panels: Immunolocalization of chromatin contained in a nucleosomal structure using a histone H3 antibody (green), together with H4K12ac (polyclonal Rabbit antibody), H4K5ac, H4K8ac and a tetra-acetylated form of H4 (red) relative to centromeres (ACA; white). All acetylated forms of H4 were observed to be enriched in a cap-like pattern. Scale bar, 10  $\mu$ m.



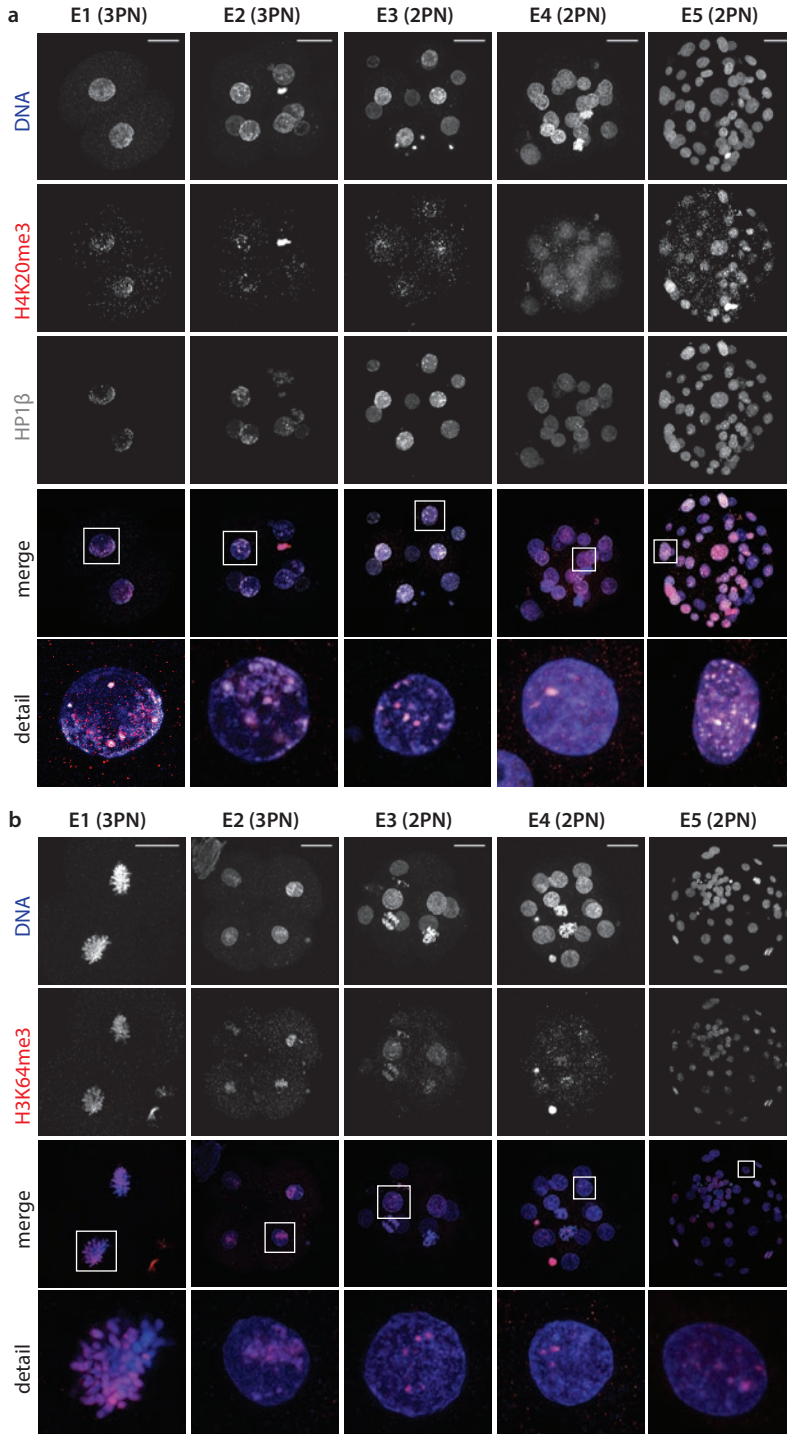
**Supplementary Figure 5 — Codetection of H3K9me3 and (peri)centric repeat sequences in in vitro decondensed human spermatozoa by immuno-FISH.** Full set of single channel images corresponding to merged images shown in Figure 4d. DNA probes detecting satellite (Sat) DNA II or III repeat sequences at pericentric (chromosomes 1, 9, 16 and Y) and  $\alpha$  satellite DNA sequences at centromeric locations (chromosomes 7 and X) are used. Shown are representative single Z-sections for all channels and the merged images. A dotted line was drawn through the probe signal following the length of the H3K9me3 cloud and the distribution of fluorescent intensities along this line were plotted for H3K9me3 (red) and probe signal (grey) in arbitrary units. Scale bar, 5  $\mu$ m.

**Supplementary Figure 6 — Paternal cHC marked by H3K9me3 also contains HP1 $\alpha$ , H4K20me3 and H3K64me3.** (a) Representative confocal image of a human 3PN zygote fixed 18-20 h post insemination (n=10). Shown is a full projection of Z-sections with immunolocalization of HP1 $\alpha$  (red). Paternal ( $\sigma$ ) and maternal ( $\rho$ ) pronuclei are indicated. HP1 $\alpha$  was detected broadly on the maternal pronucleus and on DAPI-dense knobs on the paternal pronucleus (arrows). Scale bar, 30  $\mu$ m. (b) Full set of single channel images corresponding to merged images shown in Figure 6b/c. Dotted line indicates the sperm nucleus. Paternal ( $\sigma$ ) and maternal ( $\rho$ ) chromatin is indicated. Detail shows a magnification of the boxed regions. Scale bar, 10  $\mu$ m (all stages) and 30  $\mu$ m (G2 phase).





2



Supplementary Figure 7 — cHC markers HP1 $\beta$ , H4K20me3 and H3K64me3 are maintained during pre-implantation development. (a, b) Full set of single channel images corresponding to merged images shown in Figure 6d/e. Detail shows a magnification of the boxed nucleus. Scale bars, 30  $\mu$ m.

## References

1. Burton, A. and M.E. Torres-Padilla, *Chromatin dynamics in the regulation of cell fate allocation during early embryogenesis*. Nat Rev Mol Cell Biol, 2014. **15**(11): p. 723-35.
2. Surani, M.A., *Reprogramming of genome function through epigenetic inheritance*. Nature, 2001. **414**(6859): p. 122-8.
3. Puschendorf, M., et al., *PRC1 and Suv39h specify parental asymmetry at constitutive heterochromatin in early mouse embryos*. Nature genetics, 2008. **40**(4): p. 411-420.
4. Probst, A.V., et al., *A strand-specific burst in transcription of pericentric satellites is required for chromocenter formation and early mouse development*. Dev Cell, 2010. **19**(4): p. 625-38.
5. Grewal, S.I. and S. Jia, *Heterochromatin revisited*. Nat Rev Genet, 2007. **8**(1): p. 35-46.
6. Jones, K.W. and G. Corneo, *Location of satellite and homogeneous DNA sequences on human chromosomes*. Nat New Biol, 1971. **233**(43): p. 268-71.
7. Jones, K.W., *Satellite DNA*. J Med Genet, 1973. **10**(3): p. 273-81.
8. Peters, A.H., et al., *Loss of the Suv39h histone methyltransferases impairs mammalian heterochromatin and genome stability*. Cell, 2001. **107**(3): p. 323-37.
9. Peters, A.H. and D. Schubeler, *Methylation of histones: playing memory with DNA*. Curr Opin Cell Biol, 2005. **17**(2): p. 230-8.
10. Muramatsu, D., et al., *Pericentric heterochromatin generated by HP1 protein interaction-defective histone methyltransferase Suv39h1*. J Biol Chem, 2013. **288**(35): p. 25285-96.
11. Daujat, S., et al., *H3K64 trimethylation marks heterochromatin and is dynamically remodeled during developmental reprogramming*. Nat Struct Mol Biol, 2009. **16**(7): p. 777-81.
12. Lange, U.C., et al., *Dissecting the role of H3K64me3 in mouse pericentromeric heterochromatin*. Nat Commun, 2013. **4**: p. 2233.
13. Balhorn, R., *A model for the structure of chromatin in mammalian sperm*. J Cell Biol, 1982. **93**(2): p. 298-305.
14. van der Heijden, G.W., et al., *Transmission of modified nucleosomes from the mouse male germline to the zygote and subsequent remodeling of paternal chromatin*. Dev Biol, 2006. **298**(2): p. 458-69.
15. Santos, F., et al., *Dynamic chromatin modifications characterise the first cell cycle in mouse embryos*. Dev Biol, 2005. **280**(1): p. 225-36.
16. Simon, J.A. and R.E. Kingston, *Mechanisms of polycomb gene silencing: knowns and unknowns*. Nat Rev Mol Cell Biol, 2009. **10**(10): p. 697-708.
17. Margueron, R. and D. Reinberg, *The Polycomb complex PRC2 and its mark in life*. Nature, 2011. **469**(7330): p. 343-9.
18. Merico, V., et al., *Epigenomic differentiation in mouse preimplantation nuclei of biparental, parthenote and cloned embryos*. Chromosome Res, 2007. **15**(3): p. 341-60.
19. Wongtawan, T., et al., *Histone H4K20me3 and HP1 alpha are late heterochromatin markers in development, but present in undifferentiated embryonic stem cells*. J Cell Sci, 2011. **124**(Pt 11): p. 1878-90.
20. van der Heijden, G.W., et al., *Parental origin of chromatin in human monopronuclear zygotes revealed by asymmetric histone methylation patterns, differs between IVF and ICSI*. Molecular reproduction and development, 2009. **76**(1): p. 101-108.
21. Avo Santos, M., et al., *A role for Aurora C in the chromosomal passenger complex during human preimplantation embryo development*. Hum Reprod, 2011. **26**(7): p. 1868-81.
22. Mantikou, E., et al., *Temporal and developmental-stage variation in the occurrence of mitotic errors in tripronuclear human preimplantation embryos*. Biol Reprod, 2013. **89**(2): p. 42.
23. Adenot, P.G., et al., *Differential H4 acetylation of paternal and maternal chromatin precedes DNA replication and differential transcriptional activity in pronuclei of 1-cell mouse embryos*. Development, 1997. **124**(22): p. 4615-25.
24. Feenan, K. and M. Herbert, *Can 'abnormally' fertilized zygotes give rise to viable embryos?* Hum Fertil (Camb), 2006. **9**(3): p. 157-69.

25. Hernandez-Munoz, I., et al., *Association of BMI1 with polycomb bodies is dynamic and requires PRC2/EZH2 and the maintenance DNA methyltransferase DNMT1*. Mol Cell Biol, 2005. **25**(24): p. 11047-58.
26. Zhang, A., et al., *Dynamic changes of histone H3 trimethylated at positions K4 and K27 in human oocytes and preimplantation embryos*. Fertil Steril, 2012. **98**(4): p. 1009-16.
27. van der Heijden, G.W., et al., *Asymmetry in Histone H3 variants and lysine methylation between paternal and maternal chromatin of the early mouse zygote*. Mechanisms of Development, 2005. **122**(9): p. 1008-1022.
28. Ross, P.J., et al., *Polycomb gene expression and histone H3 lysine 27 trimethylation changes during bovine preimplantation development*. Reproduction, 2008. **136**(6): p. 777-85.
29. Park, K.E., L. Magnani, and R.A. Cabot, *Differential remodeling of mono- and trimethylated H3K27 during porcine embryo development*. Mol Reprod Dev, 2009. **76**(11): p. 1033-42.
30. Santenard, A., et al., *Heterochromatin formation in the mouse embryo requires critical residues of the histone variant H3.3*. Nat Cell Biol, 2010. **12**(9): p. 853-62.
31. Zenzes, M.T., et al., *Abnormalities of sperm chromosome condensation in the cytoplasm of immature human oocytes*. Hum Reprod, 1990. **5**(7): p. 842-6.
32. Hammoud, S.S., et al., *Distinctive chromatin in human sperm packages genes for embryo development*. Nature, 2009. **460**(7254): p. 473-8.
33. Govin, J., et al., *Pericentric heterochromatin reprogramming by new histone variants during mouse spermiogenesis*. J Cell Biol, 2007. **176**(3): p. 283-94.
34. De Vries, M., et al., *Chromatin remodelling initiation during human spermiogenesis*. Biol Open, 2012. **1**(5): p. 446-57.
35. Chao, S.B., et al., *Heated spermatozoa: effects on embryonic development and epigenetics*. Hum Reprod, 2012. **27**(4): p. 1016-24.
36. van der Heijden, G.W., et al., *Sperm-derived histones contribute to zygotic chromatin in humans*. BMC developmental biology, 2008. **8**: p. 34.
37. Balhorn, R., B.L. Gledhill, and A.J. Wyrobek, *Mouse sperm chromatin proteins: quantitative isolation and partial characterization*. Biochemistry, 1977. **16**(18): p. 4074-80.
38. He, J., et al., *Kdm2b maintains murine embryonic stem cell status by recruiting PRC1 complex to CpG islands of developmental genes*. Nat Cell Biol, 2013. **15**(4): p. 373-84.
39. Casanova, M., et al., *Heterochromatin Reorganization during Early Mouse Development Requires a Single-Stranded Noncoding Transcript*. Cell Rep, 2013. **4**(6): p. 1156-67.
40. Posfai, E., et al., *Polycomb function during oogenesis is required for mouse embryonic development*. Genes Dev, 2012. **26**(9): p. 920-32.
41. Brykczynska, U., et al., *Repressive and active histone methylation mark distinct promoters in human and mouse spermatozoa*. Nat Struct Mol Biol, 2010. **17**(6): p. 679-87.
42. Bogliotti, Y.S. and P.J. Ross, *Mechanisms of histone H3 lysine 27 trimethylation remodeling during early mammalian development*. Epigenetics, 2012. **7**(9): p. 976-81.
43. Vassena, R., et al., *Waves of early transcriptional activation and pluripotency program initiation during human preimplantation development*. Development, 2011. **138**(17): p. 3699-709.
44. Jarmuz, M., et al., *The Evolution of satellite III DNA subfamilies among primates*. Am J Hum Genet, 2007. **80**(3): p. 495-501.
45. Sandqvist, A., et al., *Heterotrimerization of heat-shock factors 1 and 2 provides a transcriptional switch in response to distinct stimuli*. Mol Biol Cell, 2009. **20**(5): p. 1340-7.
46. Biamonti, G. and C. Vourc'h, *Nuclear stress bodies*. Cold Spring Harb Perspect Biol, 2010. **2**(6): p. a000695.
47. Miller, D., M. Brinkworth, and D. Iles, *Paternal DNA packaging in spermatozoa: more than the sum of its parts? DNA, histones, protamines and epigenetics*. Reproduction, 2010. **139**(2): p. 287-301.
48. Ramos, L., et al., *Incomplete nuclear transformation of human spermatozoa in oligo-astheno-teratospermia: characterization by indirect immunofluorescence of chromatin and thiol status*. Hum Reprod, 2008. **23**(2): p. 259-70.
49. Zhang, X., M. San Gabriel, and A. Zini, *Sperm nuclear histone to protamine ratio in fertile and infertile men: evidence of heterogeneous subpopulations of spermatozoa in the ejaculate*. J Androl, 2006. **27**(3): p. 414-20.

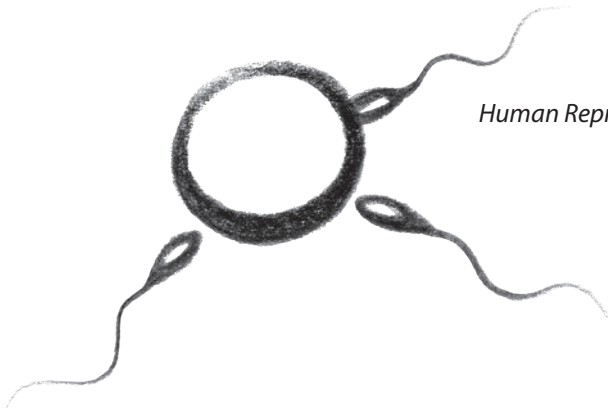
50. Hammoud, S.S., et al., *Genome-wide analysis identifies changes in histone retention and epigenetic modifications at developmental and imprinted gene loci in the sperm of infertile men*. Hum Reprod, 2011.
51. Probst, A.V. and G. Almouzni, *Heterochromatin establishment in the context of genome-wide epigenetic reprogramming*. Trends Genet, 2011. **27**(5): p. 177-85.
52. Fadloun, A., A. Eid, and M.E. Torres-Padilla, *Mechanisms and dynamics of heterochromatin formation during Mammalian development: closed paths and open questions*. Curr Top Dev Biol, 2013. **104**: p. 1-45.
53. Hohmann, F.P., N.S. Macklon, and B.C. Fauser, *A randomized comparison of two ovarian stimulation protocols with gonadotropin-releasing hormone (GnRH) antagonist cotreatment for in vitro fertilization commencing recombinant follicle-stimulating hormone on cycle day 2 or 5 with the standard long GnRH agonist protocol*. J Clin Endocrinol Metab, 2003. **88**(1): p. 166-73.
54. Kwiatkowski, N., et al., *Small-molecule kinase inhibitors provide insight into Mps1 cell cycle function*. Nat Chem Biol, 2010. **6**(5): p. 359-68.
55. Peters, A.H., et al., *Partitioning and plasticity of repressive histone methylation states in mammalian chromatin*. Mol Cell, 2003. **12**(6): p. 1577-89.
56. Atsuta, T., et al., *Production of monoclonal antibodies against mammalian Ring1B proteins*. Hybridoma, 2001. **20**(1): p. 43-6.
57. Isono, K., et al., *Mammalian polyhomeotic homologues Phc2 and Phc1 act in synergy to mediate polycomb repression of Hox genes*. Mol Cell Biol, 2005. **25**(15): p. 6694-706.
58. Hamer, K.M., et al., *A panel of monoclonal antibodies against human polycomb group proteins*. Hybrid Hybridomics, 2002. **21**(4): p. 245-52.
59. van de Werken, C., et al., *A universal method for sequential immunofluorescent analysis of chromatin and chromatin-associated proteins on chromosome spreads*. Chromosome Res, 2013. **21**(5): p. 475-89.
60. Kimura, Y. and R. Yanagimachi, *Intracytoplasmic sperm injection in the mouse*. Biol Reprod, 1995. **52**(4): p. 709-20.
61. Baart, E.B., et al., *Reduced oocyte activation and first cleavage rate after ICSI with spermatozoa from a sterile mouse chromosome mutant*. Human reproduction (Oxford, England), 2004. **19**(5): p. 1140-1147.
62. Perry, A.C., T. Wakayama, and R. Yanagimachi, *A novel trans-complementation assay suggests full mammalian oocyte activation is coordinately initiated by multiple, submembrane sperm components*. Biol Reprod, 1999. **60**(3): p. 747-55.
63. Cooke, H.J. and J. Hindley, *Cloning of human satellite III DNA: different components are on different chromosomes*. Nucleic Acids Res, 1979. **6**(10): p. 3177-97.
64. Tagarro, I., A.M. Fernandez-Peralta, and J.J. Gonzalez-Aguilera, *Chromosomal localization of human satellites 2 and 3 by a FISH method using oligonucleotides as probes*. Hum Genet, 1994. **93**(4): p. 383-8.
65. Moyzis, R.K., et al., *Human chromosome-specific repetitive DNA sequences: novel markers for genetic analysis*. Chromosoma, 1987. **95**(6): p. 375-86.
66. Lau, Y.F., *Detection of Y-specific repeat sequences in normal and variant human chromosomes using in situ hybridization with biotinylated probes*. Cytogenet Cell Genet, 1985. **39**(3): p. 184-7.
67. Waye, J.S., S.B. England, and H.F. Willard, *Genomic organization of alpha satellite DNA on human chromosome 7: evidence for two distinct alphoid domains on a single chromosome*. Mol Cell Biol, 1987. **7**(1): p. 349-56.
68. Willard, H.F., K.D. Smith, and J. Sutherland, *Isolation and characterization of a major tandem repeat family from the human X chromosome*. Nucleic Acids Res, 1983. **11**(7): p. 2017-33.
69. Baart, E.B., E. Martini, and D. Van Opstal, *Screening for aneuploidies of ten different chromosomes in two rounds of FISH: a short and reliable protocol*. Prenatal diagnosis, 2004. **24**(12): p. 955-961.

# CHAPTER 3

## **A role for Aurora C in the chromosomal passenger complex during human preimplantation embryo development**

Margarida Avo Santos, Christine van de Werken,  
Marieke de Vries, Holger Jahr, Martijn J.M. Vromans,  
Joop S.E. Laven, Bart C.J.M. Fauser, Geert J.P.L. Kops,  
Susanne M.A. Lens, Esther B. Baart

*Human Reproduction*, 2011. 26(7):  
p. 1868-81



## Abstract

**Background:** Human embryos generated by *in vitro* fertilization demonstrate a high incidence of chromosomal segregation errors during the cleavage divisions. To analyze underlying molecular mechanisms, we investigated the behavior of the chromosomal passenger complex (CPC) in human oocytes and embryos. This important mitotic regulatory complex consists of INCENP, survivin, Borealin and Aurora B, with the meiotic kinase Aurora C as a possible alternative subunit.

**Methods:** We analyzed mRNA expression by RT-qPCR of all members of the CPC in human oocytes, tripronuclear (3PN) zygotes, 2 cell and 4 cell embryos developed from 3PN zygotes, as well as good quality cryopreserved 8 cell, morula and blastocyst stage embryos. Protein expression and localization of CPC members was investigated by immunofluorescence in oocytes and embryos arrested at prometaphase, with a focus on Aurora B and Aurora C. Histone H3S10 phosphorylation, a known Aurora B kinase target, was investigated as an indicator of a functional CPC.

**Results:** INCENP, Survivin and Borealin were detected at the inner centromere of prometaphase chromosomes in oocytes and all stages of preimplantation development investigated. Whereas Aurora B and C are both present in oocytes, Aurora C becomes the most prominent kinase in the CPC during the first three embryonic cell cycles. Moreover, Aurora C mRNA was upregulated together with Aurora B after activation of the embryonic genome and both proteins were detected in early day 4 embryos. Subsequently, only Aurora B was detected in blastocysts.

**Conclusions:** In contrast to somatic cells, our results point to a specific role for Aurora C in the CPC during preimplantation embryo development. Although the presence of Aurora C in itself may not explain the high chromosome segregation error rate, differences between Aurora B and C, as well as regulation of the balance in expression of these kinases before and after activation of the embryonic genome, may help in identifying crucial factors.



## Introduction

The introduction of fluorescence *in situ* hybridization (FISH) for preimplantation genetic diagnosis has enabled screening of human embryos for chromosomal aneuploidies before transfer in *in vitro* fertilization (IVF). This has led to an increasing body of evidence demonstrating that, in IVF derived embryos, an estimate of 80% of all preimplantation embryos have chromosomally abnormal cells [1,2]. The majority of the aneuploidies observed at this stage have originated during the first mitotic divisions of early preimplantation development, resulting in chromosomally mosaic embryos [3-8]. A study using an array-based method allowing genome-wide screening of the copy number in single embryonic cells from cleavage stage embryos, found the high frequency of chromosomal instability to be similar to human cancers [9]. Furthermore, considerable percentages of chromosomal mosaicism have also been reported for bovine, equine, porcine and non human primate embryos [10-13], both for *in vitro* and *in vivo* produced embryos (bovine: [12]; porcine [13]). This indicates that chromosome segregation in preimplantation embryos is more error prone than in other dividing cells. The molecular mechanisms that control chromosome segregation in cleavage stage embryos are not well described [14], raising the question if these differ from somatic mitotic cells.

Correct segregation of chromatids to the two daughter cells during mitosis is crucial for maintaining genomic integrity and cells have a complex cell cycle machinery in place to regulate this process, including a checkpoint mechanism called the spindle assembly checkpoint (SAC) [15]. An important protein complex contributing to proper SAC functioning is the chromosomal passenger complex (CPC), named after its dynamic localization during mitosis. At the onset of mitosis, the CPC moves from the arms of the condensing chromosomes to the inner centromere. During the metaphase to anaphase transition, the CPC disassociates from the centromeres to localize to the microtubules of the central spindle in anaphase and telophase and to the midbody during cytokinesis. Parallel to its location, the CPC is involved in chromosome condensation, spindle assembly, the correction of erroneous microtubule-kinetochore interactions, signaling to the SAC, and the completion of cytokinesis (reviewed by [15]). The complex consists of four subunits: the inner centromere protein INCENP, Survivin, Borealin and the active enzymatic unit Aurora B kinase [16]. The role of the non-enzymatic CPC members is localization of the kinase at the right place and time (reviewed in [16,17]). Aurora B binds to the so-called IN-box region of INCENP and in turn, INCENP regulates the localization of Aurora B by interacting with Borealin and survivin [18-20].

Aurora B belongs to a family of serine/ threonine protein kinases, which in mammals also comprises the two other family members Aurora A and C. Although the three proteins share a high sequence similarity, each Aurora kinase has a specific localization pattern and function during cell division [21]. Aurora A is involved in centrosome maturation, bipolar spindle assembly and cell cycle progression in somatic cells [22-24] and oocytes [25]. Aurora C is the most recently described and least characterized family member that arose during mammalian evolution through gene duplication of Aurora B [26]. Expression was first described in the testis [27], where it is involved in chromatin condensation and proper attachment of homologous chromosomes during the first meiotic division [28]. Aurora C knockout mice are viable and males have normal testis weights, but reduced litter sizes with some males being sterile. Observed sperm abnormalities include

heterogeneous chromatin condensation, loose acrosomes and blunted heads. However, as multiple copies of the Aurora C gene (*AURKC*) are present in the mouse genome, a knockout approach is not reliable [29]. In contrast, male mice expressing a kinase-dead form of Aurora B as a transgene present with decreased testis weights, as well as severely impaired spermatogenesis and reduced litter size [30]. The relative importance of Aurora B vs C for male mouse meiosis remains uncertain, awaiting proper Aurora B and C knockout mouse models. Naturally occurring human mutations in *AURKC*, causing a severe truncation of the protein, have been described and are associated with male infertility [31]. This results from defective meiosis leading to the production of polyploid, multi-flagellar spermatozoa with abnormal acrosomes [32]. Two females carrying the same homozygous mutation were reported to be fertile, indicating that Aurora C may be dispensable for completion of meiosis in the human female, but not in the male [32]. However, transcript profiling of human oocytes points to a prominent role for Aurora C [33]. Moreover, a recent study in mouse demonstrated that microinjection of an mRNA coding for a kinase dead form of Aurora C disrupts meiosis I in *in vitro* matured oocytes, suggesting an essential role for Aurora C [34]. This result is in contrast to previous findings on Aurora B function during mouse female meiosis [35,36], indicating the importance of Aurora B for female meiosis.

Based on gonad specific expression and the homozygous mutation phenotype in man, Aurora C has been coined the germ cell specific homologue [35]. However, Aurora C is also expressed in various tumor lines [37], and its expression can be detected at a low level in other somatic tissues [38], including the pineal gland where it is implicated in circadian clock function [39]. Moreover, Aurora C was shown to fully support mitotic progression when replacing Aurora B in somatic cells [40]. It interacts with the other CPC proteins [41-43] and shares some substrates with Aurora B [42]. Therefore, in addition to a meiotic role, Aurora C may also have a tissue specific role in mitotic cells [40].

To obtain a better understanding of regulation of chromosome segregation in human primary oocytes, the early fertilization stage (female meiosis II), zygotes and preimplantation embryos, we have investigated the expression of CPC subunits, including both Aurora B and C, in a unique series of human oocytes and embryos. The high level of gene expression of *AURKC* in human and mouse oocytes [33,34] and the prominent role of Aurora C in human male meiosis lead us to hypothesize that Aurora C could act as the preferred enzymatic subunit of the CPC at the reductional divisions in oocytes. Moreover, as in the human the first cleavage divisions are maternally directed [44,45], Aurora C might well continue to play a role in the control of mitosis before activation of the embryonic genome.

We studied mRNA and *in situ* protein expression of all CPC members in human oocytes and all stages of human preimplantation embryo development. We observed that Aurora C can be detected at both the mRNA and protein level in oocytes and cleavage stage embryos. Yet, after the eight-cell stage and up to the morula stage, there was upregulation of both *AURKB* and *AURKC* mRNA and pericentromeric localization of both kinases on prometaphase chromosomes. In blastocysts Aurora C transcripts and protein were undetectable, and only Aurora B was found at the inner centromere of prometaphase chromosomes. Our results point to a specific role for Aurora C as the enzymatic subunit in the CPC during human female meiosis and preimplantation embryo development, up to complete replacement by Aurora B at the blastocyst stage.

## Materials and Methods

### Collection of human oocytes and spermatoocytes

Ovarian stimulation, oocyte retrieval and IVF procedures were performed as described previously [46,47]. At the day of oocyte retrieval (day 0), immature oocytes (metaphase I [MI]) were donated by couples undergoing ICSI treatment at the IVF laboratory of the University Medical Center Utrecht. Some mature oocytes (metaphase II [MII] stage) were donated in a case where on the day of oocyte retrieval no sperm cells could be obtained. MI oocytes were either processed immediately or allowed to mature in a 5% CO<sub>2</sub> atmosphere at 37°C in G-IVF Plus medium (Vitrolife) overnight (18 h) and fixed at the MII stage.

Testis material was obtained after testicular spermatozoa extraction from a man (age 47) of proven fertility with previous vasectomy and subsequent vaso-vasostomy that did not succeed. Remnant cellular material was used. A Johnson score of 9.5 (range 9-10) was determined at the pathology department of the Radboud University Nijmegen Medical Center. The patient signed an informed consent for participation in a project approved by the Dutch Central Committee on Research Involving Humans Subjects (CCMO – NL12408.000.06).

### Collection of human embryos

Under Dutch law, embryos are not allowed to be created for research. Therefore, human embryos are only available for research after embryo selection for transfer or cryopreservation. Exceptions to this rule are embryos resulting from abnormal fertilization, i.e. oocytes fertilized by two spermatozoa simultaneously or where the second polar body failed to extrude. Evaluation of the number of pronuclei 18-20h after insemination allows identification of such embryos, characterized by the presence of three pronuclei. This is observed in ~4% of all inseminated oocytes. To avoid potential triploid pregnancies these embryos normally are discarded [48]. We used triploid (3PN) embryos as a model for embryo development during the first cleavage divisions. Surplus good quality cryopreserved preimplantation embryos were used to study embryo developmental stages from day 3 to day 5 (Figure 1). Tripronuclear zygotes and surplus embryos were donated with written informed consent by couples undergoing routine IVF at the Erasmus MC University Medical Centre in the period between March and July 2010 and November 2000 and December 2007, respectively. The use of both types of surplus embryos was approved by the Dutch Central Committee on Research Involving Human Subjects (CCMO – NL28739.000.09) and the local institutional ethics committee.

Embryo culture and assessment of embryo morphology were performed as described previously [47]. Cryopreservation was performed in straws using a slow freezing standard protocol of 1.5 M dimethyl sulfoxide (DMSO) in culture medium containing 10% GPO (human plasma solution, CLB), as described previously [8]. Women donating cryopreserved embryos were aged between 29-41. A total of 90 embryos were thawed and 44 survived after consecutive washes in decreasing DMSO concentrations. Day 3 (8 cell) embryos were processed within 2 h after thawing. Early day 4 embryos (12-16 cell embryos) were randomized for either immediate processing, or culture until late day 4 (fully compacted morulas) or day 5 (blastocysts). After randomization, embryo morphology

was evaluated. Only those of good morphological quality and showing the stage-appropriate characteristics were used to avoid a selection bias in embryo quality.

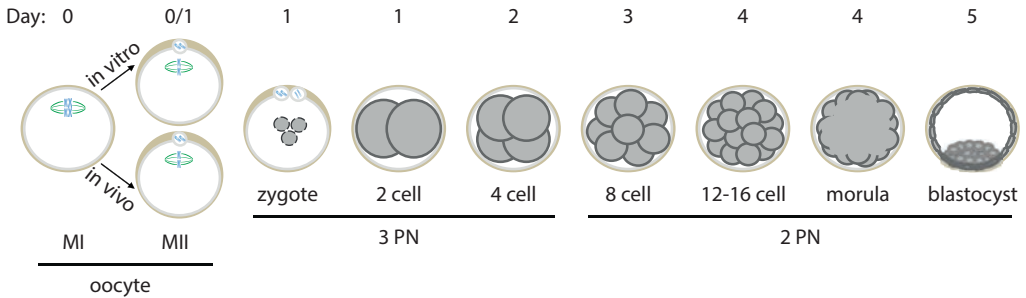


**Figure 1** — Schematic representation of the stages of oocyte and embryo development used in this study. MI and MII oocytes were fixed on the day of retrieval (day 0), or MI oocytes were left to mature to MII overnight. After fertilization, trippronuclear (3PN) zygotes were fixed at prometaphase of the first embryonic mitotic division or allowed to develop until 2 cell or 4 cell stage. Good quality diploid (2PN) 8 cell embryos or morulas that had been cryopreserved on day 3 or day 4 respectively, were thawed and immediately fixed or left in culture until reaching 12-16 cell, morula, or blastocyst stage.

### Single oocyte and embryo RT-qPCR

Quantification of mRNA levels was performed in individual single oocytes and preimplantation embryos of nine developmental stages (Figure 1): oocytes at MI (n=2) and MII (n=5), abnormally fertilized oocytes with three pronuclei (3PN; n=13), 2 cell embryos (3PN- 2 cell; n=10) and 4 cell embryos (3PN- 4 cell; n=4), both resulting from trippronuclear zygotes, and 8 cell embryos (n=12), 12-16 cell embryos (n=6), morulas (MOR; n=5), and blastocysts (BLAS; n=10), all good quality embryos cryopreserved at days 3 and 4 (Figure 1). For single oocyte/ embryo RT-qPCR, the Taqman® PreAmp Cells-to-Ct Kit (Applied Biosystems) was used according to the manufacturer's protocol with minor adjustments. The zona pellucida was removed from the oocytes and embryos by incubation in 0.1% protease (Sigma) in G-MOPS Plus medium (Vitrolife) for 3 min, prior to washing in G-MOPS Plus medium and 1X PBS. Lysis was performed for 5 min in 20 µl Taqman® PreAmp Cells-to-Ct lysis solution and terminated by addition of 2 µl of stop solution. After 2 min of incubation the lysate was stored at -20°C until further processing within one week. RNA was reverse transcribed to cDNA within an hour at 37°C by adding 25 µl of 2X RT Buffer and 2.5 µl of 20X RT Enzyme Mix to each lysate, prior to inactivating the enzyme for 5 min at 95°C. For sequence-specific preamplification of cDNA, Taqman Gene Expression Assays (Assays-on-demand, Applied Biosystems) were pooled and diluted 1:100 with 1X TE buffer (10 mM Tris-HCl, 5 mM EDTA; pH 7.5) to a final concentration of 180 nM of each primer. The following assays were used: *HPRT1* (Assay ID: Hs99999909\_m1; amplicon size 100bp), *AURKB* (Hs00177782\_m1; 130bp), *AURKC* (Hs00152930\_m1; 91bp), Borealin (*CDCA8*; Hs00216479\_m1; 127bp), Survivin (*BIRC5*; Hs00153353\_m1; 93bp), *INCENP* (Hs00220336\_m1; 62bp),

BRG1 (*SMARCA4*; Hs00231324\_m1; 106bp) and ZP3 (Hs00610623\_m1; 74bp). Assays were selected to recognize all validated (RefSeq) splice variants of each gene of interest, except for assays for *INCENP* (recognizing only NM\_020238.2) and *BIRC5* (recognizing NM\_001012271.1 and NM\_001168.2). To 12.5  $\mu$ l cDNA, 25  $\mu$ l Taqman<sup>®</sup> PreAmp Master Mix and 12.5  $\mu$ l of 0.2X pooled Taqman<sup>®</sup> Gene Expression Assays were added. After 10 cycles of preamplification (10 min at 95°C, followed by 10X 15 sec at 95°C and 4 min at 60°C), the preamplified cDNA (50 $\mu$ l) was diluted with 100  $\mu$ l 0.5X TE buffer. QPCR was performed on an ABI Prism 7000 Sequence Detecting System (Applied Biosystems) using 10 $\mu$ l 2X Taqman<sup>®</sup> Gene Expression Master Mix, 1  $\mu$ l Taqman<sup>®</sup> Gene Expression Assay and 5  $\mu$ l nuclease-free water added to 4 $\mu$ l diluted preamplified cDNA. The 2-step cycling parameters were as follows: one cycle of 2 min at 50°C, followed by one cycle of 10 min at 95°C to activate the polymerase and 40 cycles of 15 sec at 95°C and 1 min at 60°C.

Results were analyzed using Sequence Detection Software version 1.2.3 (Applied Biosystems) and expressed as cycle threshold (Ct) values. Presence of a single PCR-product of expected amplicon size was verified by 2% agarose gel electrophoresis. In order to be able to use a relative quantification approach to compare expression levels of *AURKB* and *AURKC*, we ensured that these commercial assays have similar amplification efficiencies, within the limits set by the supplier ( $E=100\pm 10\%$ ). Additionally, linearity during the preamplification reaction was tested on a series of 1:2 diluted cDNA from oocytes and blastocysts. The averaged expression level at the MII oocyte stage was used as a reference to calculate the relative levels in all other stages, according to the  $2^{-\Delta\text{CT}}$  method [49]. Differences in *AURKB* and *AURKC* expression across developmental stages were analyzed using the Mann-Whitney test in SPSS version 17.0. A p-value of 0.05 was considered statistically significant. To compare expression levels of *AURKB* directly to expression levels of *AURKC*, the relative expression for *AURKB* was calculated using *AURKC* as a reference.

### Antibodies

The following antibodies were used in this study: rabbit polyclonal antibodies against *AURKC* (ab38299, 1:100; Abcam), H3S10p (1:10,000; Cell Signalling), *INCENP* (1:1,000; Sigma), Borealin (1:2,000; kindly supplied by S. Wheatley, University of Nottingham Medical School, Nottingham, UK), Survivin (1:2,000, R&D Systems) and GFP (S.M.A. Lens, University Medical Centre Utrecht, The Netherlands). Mouse monoclonal antibodies against *AURKB* (1:250; BD Biosciences) and *INCENP* (1:1,000, Upstate). Human autoantibodies against the centromere (CREST, HCT-0100, 1:100, Immunovision and 1:2,000, Cortex Biochem). Primary antibodies were detected by labelling with the appropriate secondary antibodies conjugated with Alexa fluor 488, 555, 594 or 647 (Molecular Probes).

### Overexpression of Aurora A, B and C kinase in U2OS cells

Human osteosarcoma cells (U2OS) were grown at 37°C with 5% CO<sub>2</sub> in DMEM containing 6% FCS, glutamine, penicillin and streptomycin. Transfections were performed using a standard calcium phosphate protocol. U2OS cells were co-transfected with 1 $\mu$ g empty GFP vector, GFP-*AURKA*, GFP-*AURKB* or GFP-*AURKC* together with an empty pcDNA3 vector (9  $\mu$ g). Cells were first synchronized at the G1/S transition by incubation for 24 h with 2.5 mM thymidine and later arrested in mitosis by

incubation for 18 h with nocodazole (250 or 25 ng/ml; for harvesting or fixation of cells, respectively). Cells were harvested or fixed and used for cell lysis or immunofluorescence. Cell lysis and Western blotting was performed as described previously [50] and immunoprobed with anti-Aurora B and -C antibodies (1:250 and 1:500).

For immunofluorescence, U2OS cells were grown on slides and fixed with PFA buffer (4% w/v PFA in PBS). The slides were washed in PBS and dehydrated with ice-cold methanol. Subsequently, cells were blocked with 3% (w/v) BSA in PBS-T (PBS, 0.01% v/v Tween-20) for 30 min at RT, and incubated with anti-Aurora C and CREST antibodies overnight at 4°C. Slides were washed three times in PBS-T and then incubated with secondary antibodies for 1-2 h. After rinsing in PBS-T, slides mounted with vectashield containing DAPI for counterstaining (Vector Laboratories).

### **Fixation and immunofluorescence of spermatocytes**

Nuclear spreads were made as described previously [51], with minor modifications [52]. Briefly, a suspension of spermatogenic cells was made by pulverizing the testis tubuli with two ribbed forceps. After hypotonic treatment, cells were resuspended in 100 mM sucrose, pH 8.2 to obtain a cell concentration of about  $15 \times 10^6$  cells/ml. From this suspension 10  $\mu$ l was applied to a slide dipped in 1% (w/v) PFA solution, containing 0.15% (v/v) Triton X-100. After horizontal drying for 1.5 h in a humid chamber, slides were washed twice with 0.08% Kodak Photo-Flo and air-dried. Slides were stored at -80°C until use.

Surface spread preparations were processed for immunofluorescence as described [52]. Meiotic prophase I stages were approximated by DAPI staining annex nuclear morphology as based on previous experience with the synaptonemal complex marker SYCP3 (de Vries et al., unpublished results). Early and late pachytene substages were distinguished by the more prominent DAPI intense sex body present in late pachytene. Metaphase nuclei were recognised by separate bivalent chromosome domains and the absence of a DAPI intense sexbody. At least 50 early first meiotic division nuclei (leptotene, zygotene) and 100 pachytene nuclei were studied, as well as 5 first metaphase nuclei. Images were captured with a Zeiss AxioCam MR digital camera with Axiovision 3.1 software, using a Zeiss Axioplan fluorescence microscope (all Carl Zeiss).

### **Fixation and immunofluorescence of oocytes and embryos**

Ml and MII oocytes were incubated with nocodazole (500 ng/ml, Sigma) for 30 min before fixation. Trippronuclear zygotes were incubated with colcemid (1,5  $\mu$ g/ml) to arrest cells at prometaphase until pronuclei had disappeared. Good quality day 4 and 5 embryos were treated with nocodazole (500 ng/ml) for 4 h before fixation.

Oocytes and embryos were incubated in 0.1% Protease in G-IVF Plus medium (1-2 min) for removal of the zona pellucida and washed in G-IVF Plus medium. Fixation was performed as previously described, with minor modifications [53]. In short, cells were fixed in PFA buffer for 15 min at RT. After fixation, oocytes/embryos were rinsed in PBS-T and incubated with 0.2% (w/v) Triton X-100 in PBS for 15 min at RT for permeabilization. Oocytes and embryos were washed in PBS-TB (PBS-T, 2% w/v BSA), blocked with PBS-TB/ 5% NGS for 4h and incubated with primary antibodies at 4°C overnight. After washing with PBS-TB, oocytes and embryos were incubated with the appropriate

secondary antibodies conjugated with Alexa Fluor 488, 555, 594 or 647 (Invitrogen), washed with PBS-TB, and mounted on coverslips with vectashield mounting solution containing DAPI for DNA counterstaining (Vector Laboratories). To obtain chromosome spreads, arrested zygotes and day 4 embryos were (after zona removal) submitted to the same hypotonic treatment as spermatogenic cells. After brief transfer to 100 mM sucrose, cells were placed on a slide dipped in a 1% (w/v) PFA solution, containing 0.15% (w/v) Triton X-100. Slides were dried and processed as described for spermatogenic cell surface spreads.

Images were obtained using a Delta Vision microscope and deconvolution software (Applied Precision) or with an AxioCam MR digital camera with Axiovision 3.1 software, using an inverted Axio Observer fluorescence microscope equipped with an ApoTome (all Carl Zeiss) for optical sectioning.

## Results

### **Aurora C kinase is detected in human male and female meiotic cells**

A commercially available polyclonal antibody against Aurora C, raised against a synthetic peptide corresponding to amino acids within residues 1-50 of Human Aurora C was used. To confirm that this antibody does not cross-react with the other Aurora kinases, specificity was tested by immunofluorescence on U2OS cells overexpressing GFP-AURKA, GFP-AURKB and GFP-AURKC (Supplemental Figure 1a). The antibody did not detect Aurora A or B, but co-localized with the GFP-signal for Aurora C. We further tested the specificity of anti-Aurora C antibody using immunoblots on lysates of GFP-AURKA, -B and -C transfected U2OS cells. The antibody did not recognize GFP-AURKA or GFP-AURKB, but detected GFP-AURKC (Supplemental Figure 1b).

Since Aurora C is reported to be highly transcribed in mouse spermatocytes [27,29], the staining pattern and intensity of Aurora C was first studied in human primary spermatocyte nucleus spread preparations. From leptotene to early pachytene a faint, evenly distributed, dotted Aurora C kinase signal was observed (not shown). In later pachytene nuclei the Aurora C signal localized to chromosome regions adjacent to the centromeres (CREST antigen), probably reflecting the centromeric heterochromatin regions (Figure 2a). In early meiotic metaphase nuclei the Aurora C signal was more dispersed over the chromosomes and not solely localized to the centromeric heterochromatin regions as in late pachytene (Figure 2b). However, more intense spots surrounded the centromeric signal (Figure 2b, see insert).

We next investigated the localization of Aurora C during human female meiosis in MI and MII oocytes. MI oocytes were available 4-6 h after oocyte retrieval if they had failed to progress to the MII stage by the time the ICSI procedure was completed. As a consequence, synchronization was not optimal and oocytes could be at any stage between early prometaphase and metaphase of meiosis I. MI oocytes (n=13) were treated with nocodazole for 30 min and fixed immediately. We detected Aurora C along the chromosome arms in some oocytes, but in other MI oocytes, Aurora C signal was observed to localize near the centromere (Figure 2c). This is consistent with Aurora C staining recently described in mouse oocytes for prometaphase I and metaphase I, respectively [34]. In all MII oocytes (n=19), Aurora C staining was observed to localize to the chromosome regions adjacent to the centromeres (Figure 2d) and only weakly along the chromosome arms.

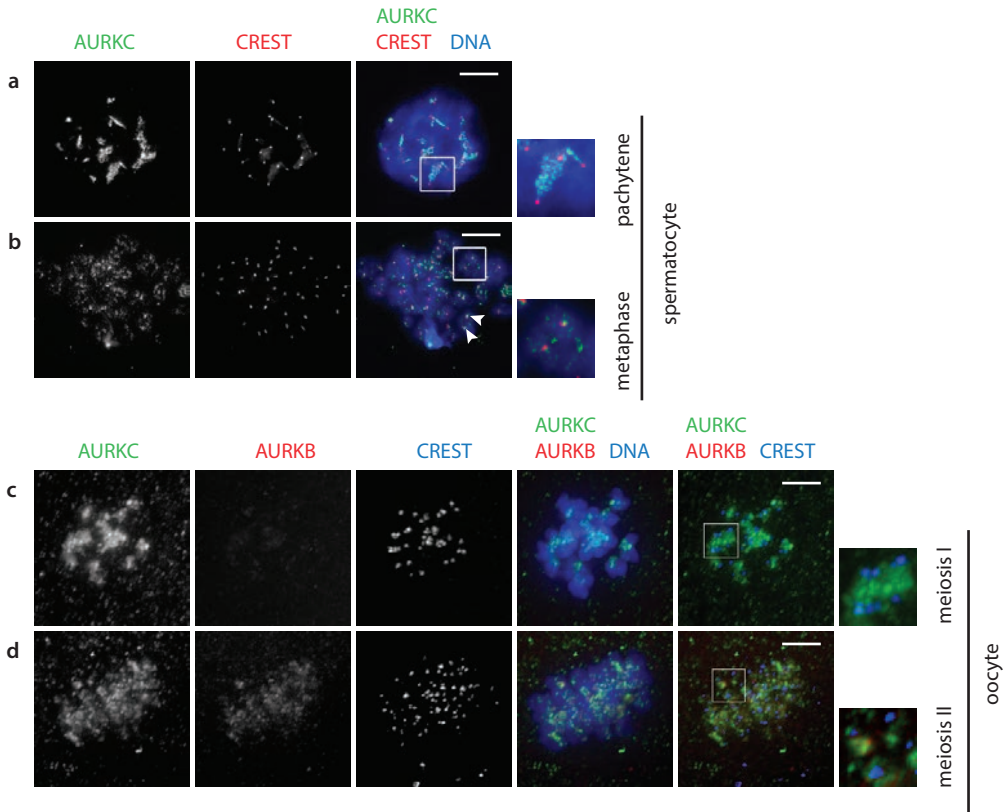


**Figure 2** — Immunolocalization of Aurora C in human primary spermatocytes and MI and MII oocytes. (a) Late pachytene spermatocyte nucleus, with Aurora C visible in concentrated clouds of various sizes. The merged image shows Aurora C localized adjacent to the centromeres (CREST antigen). (b) MI spermatocyte. Aurora C is not solely localized to the centromeric heterochromatin regions as in late pachytene, but also visible throughout the chromosome domains. In most of the dispersed clouds of Aurora C two intense spots colocalize with the centromeres (arrow heads). (c-d) MI and MII oocytes, with antibody staining for Aurora B and C and centromeric regions (CREST). (c) In MI oocytes, Aurora C was observed in a diffuse pattern surrounding the centromeres. (d) In MII oocytes, Aurora B localized more to the centromere, while Aurora C was observed in a more diffuse pattern surrounding the centromeres. DNA was counterstained with DAPI. Square boxes are blowups of each corresponding smaller box. Scale bars are 5  $\mu\text{m}$ .

Aurora B staining was also investigated together with Aurora C in MI and MII oocytes. In all MI oocytes investigated ( $n=10$ ), Aurora B staining was either not detected, or observed very weakly at chromosome regions adjacent to the centromeres (Figure 2c). In three MII oocytes, Aurora B staining showed a more intense signal than Aurora C (data not shown), but in most MII oocytes ( $n=12$ ), Aurora B staining was less intense than Aurora C (Figure 2d), with some oocytes showing no staining for Aurora B. This suggests that during female meiosis, both Aurora B and Aurora C are involved. However, in meiosis I Aurora B is hardly detected, while in meiosis II both kinases are found.



### mRNA expression and protein localization of INCENP, survivin and Borealin in human oocytes and embryos

To investigate if the CPC proteins INCENP, Borealin and survivin are expressed and functional in human oocytes and embryos, we first examined mRNA expression of these subunits in multiple individual oocytes and embryos of seven different preimplantation developmental stages (Figure 1). Normalization of gene expression is especially challenging in preimplantation embryos. Due to the absence of active transcription in the early embryo followed by activation of embryonic transcription later on, finding a reference gene with stable expression throughout all stages of development is problematic [54,55]. In rabbit embryos, where embryonic genome expression is activated at the same developmental stage as human embryos, *HPRT1* was shown to be a suitable reference gene for preimplantation development, when *in vivo* and *in vitro* produced embryos are compared [55]. We found *HPRT1* to be highly regulated during embryo development (Supplemental Figure 2a), similar to the pattern described for rabbit embryos [55]. Therefore, resulting gene expression levels were normalized using average expression levels of the gene in the metaphase II oocyte as a reference. As this method of normalization is not informative for the abundance of transcripts, average Ct values are presented for each gene investigated per developmental stage (Supplemental Table 1).

The expression levels of zona pellucida protein 3 (*ZP3*) and SWI/SNF related, matrix associated, actin dependent regulator of chromatin, subfamily a, member 4 (*SMARCA4*) were determined to further check the sensitivity of our single oocyte/ embryo RT-qPCR approach. *ZP3* expression is expected to be maternal only [56]. Our results demonstrate high expression in oocytes and a steady decrease in transcript levels until barely detectable at the blastocyst stage (Supplemental Figure 2b). *SMARCA4* has been described to be present as a maternal transcript [57] and subsequently to be one of the first genes transcribed after zygotic gene activation in mouse embryos [58]. In our series, expression of this gene was shown to decline from the oocyte to the 8-cell stage and then showed an increased expression from the 8 cell stage onwards (Supplemental Figure 2c). This confirms that transcripts detected up to the 8 cell stage are likely maternal, and activation of the embryonic genome occurring from the 8 cell stage on [44].

Normalized expression levels of *INCENP*, Survivin (*BIRC5*) and Borealin (*CDCA8*) were compared between the nine different stages of oocyte and preimplantation embryo development (Figure 3a-c). Transcript abundance for *INCENP* was low in oocytes and embryos up to the 8 cell stage, after which an increase occurred, starting at the 12-16 cell stage, with significant upregulation at the blastocyst stage (Figure 3a). Survivin and Borealin both showed a high transcript level at the MI oocyte stage, decreasing gradually until the 8 cell stage and increasing towards the morula and blastocyst stage (Figure 3b, c).

To investigate expression of these CPC subunits at the protein level, human oocytes and tripronuclear zygotes treated with nocodazole or colcemid were immunostained for *INCENP*, Survivin and Borealin. In both oocytes (data not shown) and zygotes (Figure 3d-f), each CPC protein was detected at the inner centromere in prometaphase and in a zygote escaping the nocodazole block, *INCENP* was also detected at the spindle midzone (Figure 3d'). These observations are consistent with findings in somatic mitotic cells. As *INCENP* forms the binding factor between the enzymatic subunit and Survivin and Borealin [18], double staining for Aurora C and *INCENP* was performed.

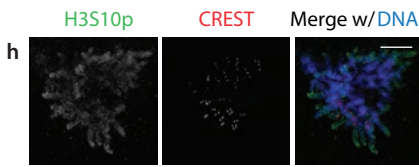
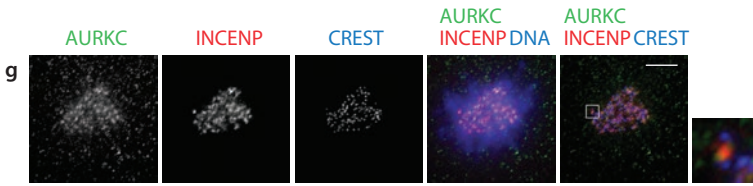
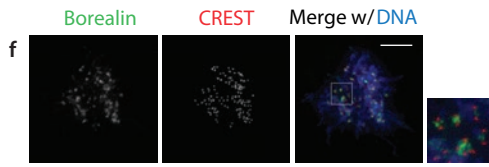
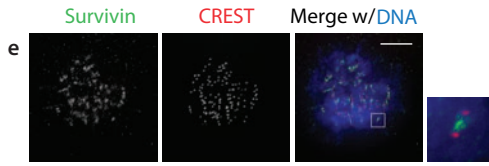
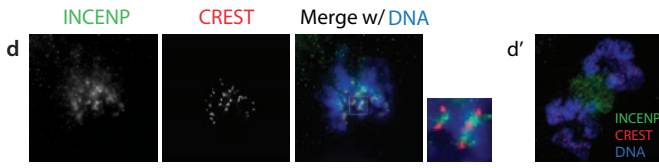
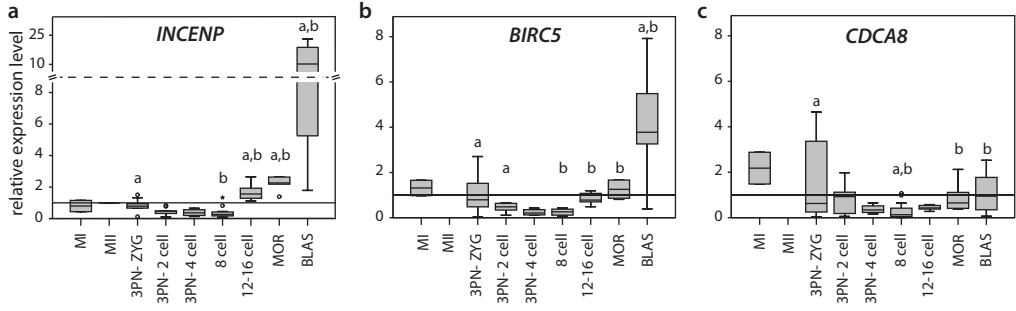


**Figure 3** — Expression of the CPC members *INCENP*, *Survivin* and *Borealin* in human oocytes and preimplantation embryos. Relative expression levels after RT-qPCR of (a) *INCENP*, (b) *BIRC5* (*Survivin*) and (c) *CDC48* (*Borealin*) in single oocytes and preimplantation embryos of nine developmental stages: oocytes at MI (n=2) and MII (n=5), zygotes (3PN, n=13), 2-cell embryos (3PN- 2 cell, n=10), 4-cell embryos (3PN- 4 cell, n=4), 8-cell embryos (n=12), 12-16-cell embryos (n=6), morulas (MOR, n=5), and blastocysts (BLAS, n=10). The mean expression level at the oocyte MII stage was taken as a reference to calculate the relative levels of the other stages. Note the scale of the y-axis differs. Boxes indicate 25th and 75th percentiles, with the horizontal line representing the median value. Whiskers span the range observed, open circles and asterisks represent outliers. Stages with average expression levels significantly different from the zygote stage (<sup>a</sup>) and the 8 cell stage (<sup>b</sup>) are indicated ( $p < 0.05$ ). (d-h) Immunolocalization of CPC proteins in human tripronuclear zygotes at prometaphase: *INCENP* (d), *Survivin* (e) and *Borealin* (f) relative to centromeres (CREST). (d') *INCENP* relocation to the midzone during anaphase. (g) Immunolocalization of Aurora C and *INCENP* in human tripronuclear zygotes showing colocalization of Aurora C and *INCENP* at the inner centromere. (h) Immunolocalization of H3S10p along the chromosome arms in human tripronuclear zygotes at prometaphase. Zygotes used for immunostaining were arrested in prometaphase after treatment with nocodazole. DNA was counterstained with DAPI. Square boxes are blowups of each corresponding smaller box. Scale bars are 5  $\mu\text{m}$ .

These two proteins co-localized on the inner centromere of prometaphase chromosomes in zygotes (Figure 3g). To investigate CPC function in these human zygotes, immunostaining with a H3S10p antibody was performed. This phosphorylation site is known to be targeted by active Aurora B, as well as Aurora C [37,41,43]. Histone H3S10 was phosphorylated along the chromosome arms, as previously described for somatic mitotic cells. These results suggest that a functional CPC is assembled in human oocytes and zygotes.

### Expression of *AURKB* and *AURKC* in human oocytes and preimplantation embryos

Aurora C has been described to fully compensate for loss of Aurora B as the enzymatic subunit of the CPC [40]. In oocytes, we detected both kinases in prometaphase of meiosis II (Figure 2). We therefore investigated the presence of Aurora B and Aurora C in human preimplantation embryos. First, mRNA expression of these kinases in nine different stages of oocyte and preimplantation embryo development was examined. *AURKB* mRNA levels were similar in MI and MII oocytes and then steadily decreased until the 8 cell stage, but increased significantly from the morula stage onwards (Figure 4a). *AURKC* mRNA levels were highest in MI oocytes and significantly decreased until the 4 cell stage. A gradual increase was observed starting from the 8-cell stage, with the morula stage reaching levels similar to the zygote. Subsequently, expression sharply decreased, until barely detectable at the blastocyst stage (Figure 4b). To better visualize differences in *AURKB* and *AURKC* expression patterns, the ratio between *AURKB* and *AURKC* was used. Both assays were verified to yield linear pre-amplification, as well as similar amplification efficiencies, enabling a direct comparison of transcript abundance in single oocytes and embryos. Plotting the levels of *AURKB* mRNA relative to levels of *AURKC* mRNA (Figure 4c) shows comparable levels of transcripts for *AURKC* and *AURKB* up to day 4 of embryo development, with an exception at the 4-cell stage, where *AURKC* transcripts

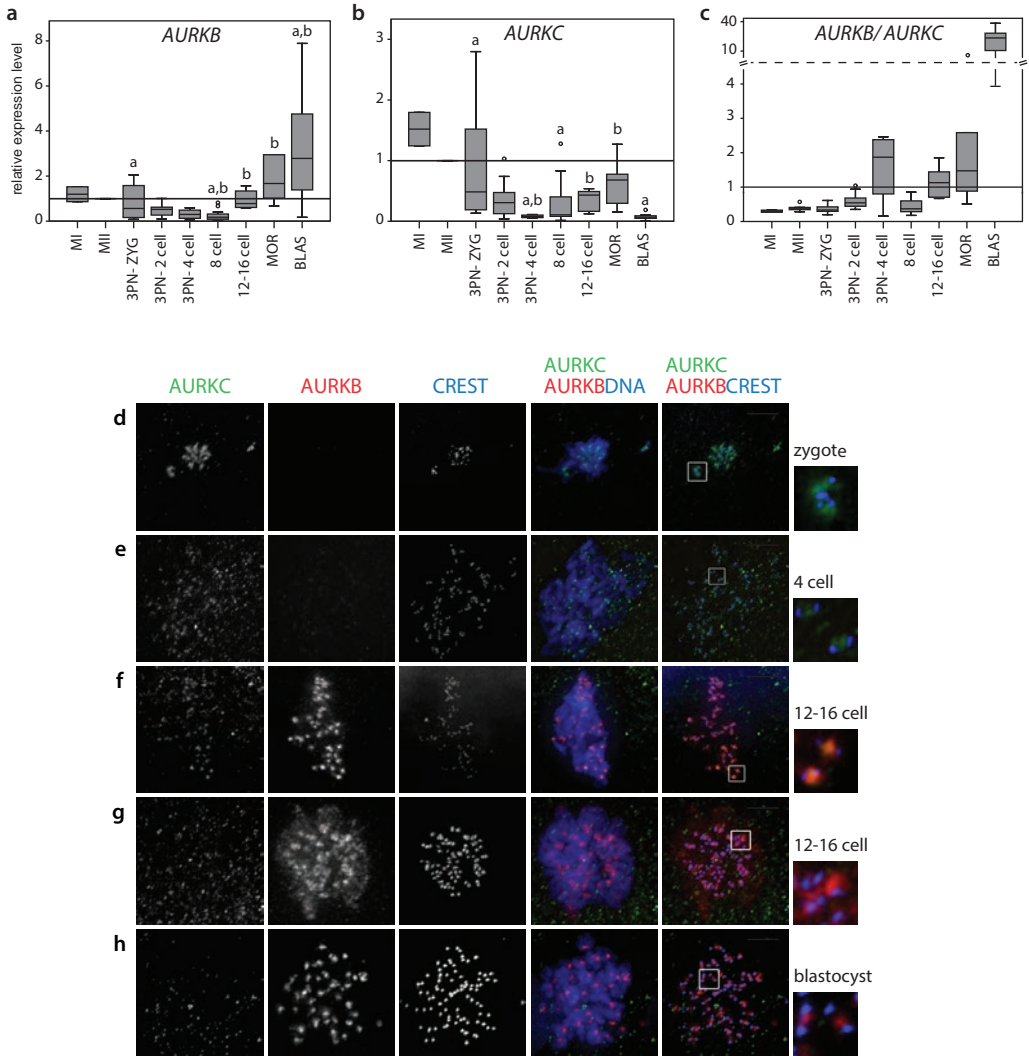


**Figure 4** — Expression of *AURKB* and *AURKC* in human oocytes and preimplantation embryos. Relative expression levels after RT-qPCR of (a) *AURKB* and (b) *AURKC* in single oocytes and preimplantation embryos of nine developmental stages: oocytes at MI (n=2) and MII (n=5), zygotes (3PN, n=13), 2-cell embryos (3PN-2 cell, n=10), 4-cell embryos (3PN-4 cell, n=4), 8-cell embryos (n=12), 12-16-cell embryos (n=6), morulas (MOR, n=5), and blastocysts (BLAS, n=10). The mean expression level at the oocyte MII stage was taken as a reference to calculate the relative levels of the other stages. Note the scale of the y-axis differs. Stages with average expression levels significantly different from the zygote stage (<sup>a</sup>) and the 8-cell stage (<sup>b</sup>) are indicated ( $p < 0.05$ ). (c) Relative expression of *AURKB* over *AURKC* for all developmental stages. (d-h) Immunolocalization of Aurora B and C relative to centromeres (CREST) in human preimplantation embryos: (d) haploid set of chromosomes in a tripronuclear zygote, (e) triploid 4-cell embryo, (f-g) diploid 12-16-cell embryo and (h) blastocyst. In zygotes (d) and 4-cell embryos (e) only Aurora C was detected near centromeric regions. In 12-16-cell embryos, relative intensity of Aurora B and C was variable, but in blastocysts only Aurora B was abundant around the centromere and in small amounts on the chromosome arms. All embryos used for immunostaining were arrested in prometaphase. DNA was counterstained with DAPI. Square boxes are blowups of each corresponding smaller box. Scale bars are 5  $\mu\text{m}$ .

are more severely depleted. After the 8 cell stage, *AURKB* expression increases rapidly, and together with the severe reduction of *AURKC* transcription by the blastocyst stage, results in a 16-fold higher expression of *AURKB* on day 5.

We next investigated the presence and localization of Aurora B and Aurora C in human preimplantation embryos. We performed triple immunolabeling for Aurora B, Aurora C and centromeric proteins in tripronuclear zygotes (n=17), 2 cell (n=4) and 4 cell (n=4) embryos from tripronuclear origin, as well as in good quality 8 cell (n=7), 12-16 cell embryos (n=10), and blastocysts (n=4). Aurora C was localized near the centromeres of prometaphase chromosomes from the zygote to the 12-16-cell stage (Figure 4d-f). In contrast, Aurora B was barely detectable up to the 8-cell stage. From the 8 cell stage onwards, staining intensity increased, with both Aurora B and C detected at prometaphase (Figure 5b) and one example where only Aurora B was detected. In 12-16-cell embryos, the ratio between Aurora B and C signal intensity was variable (Figure 4d-h). In most embryos, both kinases were found to co-localize at the centromeric regions (Figure 4f), but in one example only Aurora C was detected (data not shown). Other embryos revealed very little or no detectable Aurora C staining, but abundant Aurora B around the centromere and in small dispersed amounts along the chromosome arms (Figure 4g). In 23 prometaphases from 4 blastocysts, only Aurora B was found and abundantly present (Figure 4h).

To investigate in more detail if Aurora B and Aurora C proteins co-localize at prometaphase, chromosome spreads from tripronuclear zygotes, as well as diploid 8 cell and 12-16 cell stage embryos treated with colcemid or nocodazole were prepared, allowing higher resolution images (Figure 5a-c). On prometaphase chromosomes from zygotes, Aurora C staining was observed on the chromosome region surrounding the centromere and along the chromosome arms (Figure 5a). Aurora B staining was only weakly detected and more localized to the centromeric region. In 8-cell and 12-16-cell embryos, staining intensity of Aurora B and C was observed to be more similar, as was the localization of the signal (Figure 5b and c).

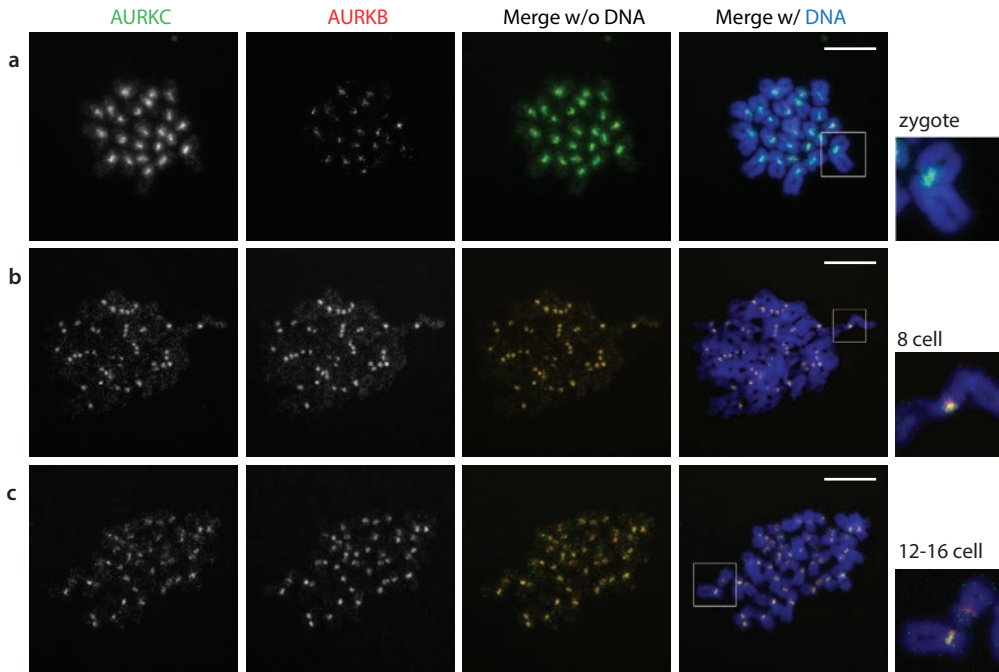


**Figure 5** — Immunolocalization of Aurora B and Aurora C on chromosome spreads from preimplantation human embryos: (a) tripronuclear zygote, (b) 8-cell embryo and (c) 12-16-cell embryo. In zygotes (a), Aurora C signal was abundant at centromeric regions and dispersed along the chromosome arms, whereas Aurora B was weakly detected at the inner centromere. In 8-cell (b) and 12-16-cell (c) embryos, relative abundance and localization of Aurora B and -C was similar. Embryos were arrested in prometaphase after treatment with colcemid. DNA was counterstained with DAPI. Square boxes are blowups of each corresponding smaller box. Scale bars are 5  $\mu$ m.

Although expression of *AURKB* mRNA was detected from the zygote to the 4-cell stage, Aurora B protein was weakly or not observed on prometaphase chromosomes. Immunofluorescence analysis from the 8-cell stage onwards confirms our observations at the mRNA level, with a joint performance for Aurora B and C from the 8 cell to the morula stage. After cavitation there is a progressive switch to Aurora B and at the blastocyst stage, Aurora B appears to be the only kinase involved in the CPC.

## Discussion

In this study, we analyzed localization of the different members of the CPC in human oocytes and preimplantation embryos, with a focus on the kinase subunits Aurora B and Aurora C. Contrary to INCENP, Survivin and Borealin that were detected in all stages investigated, Aurora B and C showed

dynamic expression patterns at both the *in situ* protein and transcript level. We hypothesized a role for Aurora C during mitosis in the early stages of embryo development. Here we show that Aurora C is indeed the more prominent Aurora kinase present in cleavage stage embryos, based on fluorescent staining intensity at prometaphase in zygotes, 2 cell and 4 cell embryos (Figure 4d,e; Figure 5a). Aurora B was either not detected, or expressed at significantly lower levels than found from the 8-cell stage onwards (Figure 4d-h). Although we did detect Aurora B transcripts, we did not observe significant amounts of protein on prometaphase chromosomes in zygotes, 2 cell and 4 cell stage embryos. Similarly, in mouse oocytes, although *AURKB* mRNA was present, western blot analysis failed to detect Aurora B, indicating regulation of expression at the translational level [34].

Since Aurora C overexpression can completely restore cell cycle progression in Aurora B deficient HeLa cells [40], Aurora C may be able to replace Aurora B and perform the same essential functions in cleavage stage embryos. Nevertheless, although Aurora B and Aurora C show high sequence similarities, structural differences exist [26]. The N- and C-terminal domains of Aurora C exhibit unique sequences and Aurora C lacks the so-called KEN-box and A-box sequences which target Aurora B for degradation via the anaphase-promoting complex/cyclosome (APC/C) after mitosis [59]. This implies that Aurora C is less susceptible to degradation, thus more stable throughout the cell cycle. In line with this, Aurora C protein levels were observed to peak after Aurora B during the later part of the M-phase [37]. Thus, as the first embryonic cell cycles lack active transcription, there might be a need for an Aurora kinase that is independent of degradation at the end of M-phase, but with otherwise overlapping functions. However, our data also suggests a possible complementary role of Aurora B and C during the first embryonic cell divisions. Aurora C was observed to cover a larger area on zygotic prometaphase chromosomes, whereas Aurora B was more constricted to the centromeric regions. Although we can not exclude the possibility that Aurora B is present on the chromosome arms at amounts that fall below detection levels, similar observations regarding differences in Aurora B and C localization have been made in mouse M1 oocytes [35,60]. This suggests that Aurora C may have a role during the first embryonic cell cycle that does not overlap with Aurora B. The observed association of Aurora C with pericentric heterochromatin in spermatocytes leads us to hypothesize that this function could be related to pericentric heterochromatin organization, an hypothesis that awaits further investigation.

We expected that the expression pattern of *AURKC* would be similar to *ZP3*, with maternal transcripts gradually disappearing during embryo development, to be replaced by *AURKB* after activation of the embryonic genome. However, we observed a brief upregulation of transcription of *AURKC* after embryonic gene activation, reaching similar levels as *AURKB*. The presence of both kinases was also detected on the protein level, but with a variation in staining intensity between day 3 and 4 (Figure 4f, g). Our data indicate that a switch in the Aurora B to Aurora C ratio is gradually made on day 4 of embryo development, and that Aurora B is the chromosomal passenger of choice only after cavitation.

Due to ethical limitations, we used embryos developed from tripronuclear zygotes as a model for embryo development up to the 4-cell stage. In human embryos, the first cleavage divisions are maternally directed until activation of the embryonic genome [44] and it is therefore unlikely that the extra set of chromosomes present has an impact on expression and localization of CPC

proteins in those early stages. Further in support of our findings on the presence of Aurora C during preimplantation embryo development, a recent study on mouse embryos carrying a targeted disruption of the *AURKB* gene showed that these embryos were able to develop up to the blastocyst stage (Fernandez-Miranda et al., personal communication). This is in contrast to mouse embryos that lack other components of the CPC, which are unable to progress beyond the cleavage stages [61-63]. Fernandez-Miranda et al. (personal communication) demonstrated that Aurora C was responsible for compensating loss of Aurora B function.

Although findings in most embryos investigated by us are consistent with an increase in the Aurora B/ Aurora C signal ratio from day 3 to day 4, we observed one prometaphase cell in a day 3 embryo showing clear Aurora B staining around the centromeres with no Aurora C, and the opposite in a day 4 (12-16 cell) embryo (data not shown). These variations are also visible at the mRNA level (Figure 4c) and may be related to a variation in timing and extent of activation of the embryonic genome. In human embryos, this is reported to start between the four- and eight cell stages of development [44], with a major outburst of transcription occurring at the 8 cell stage [45]. However, human IVF embryos have been shown to demonstrate a lack of synchronicity in making the switch from maternal to embryonic gene activity [64]. It was further observed in human and bovine embryos that development to the morula stage is possible without activation of the embryonic genome [64-66], but these embryos lack the ability to form a blastocyst [64,66].

In a previous study by us on the incidence of chromosomal abnormalities in human IVF embryos, we reported the proportion of aneuploid cells within an embryo to decline after cavitation [8]. This coincides with the time of disappearance of Aurora C mRNA and protein at the inner centromere we observe here. It is tempting to speculate that the presence of Aurora C may contribute to the observed high incidence of chromosome segregation errors during embryo development before compaction. However, Aurora C was shown to be able to fully compensate for the absence of Aurora B in mediating SAC function, as measured by cell cycle progression in HeLa cells [37,40] and mouse preimplantation embryos (Fernandez-Miranda et al., personal communication). A possible cause for the high error rate may be found in the variation in the Aurora B to Aurora C ratio between embryos as observed in this study. Ectopic overexpression of Aurora B in cell lines results in polyploidy [67] and over-expression of Aurora B has been shown to be associated with cancer cell lines and primary tumors [67,68], indicating that tight regulation of Aurora B expression levels is crucial for accurate chromosome segregation. Moreover, overexpression of an Aurora C kinase-deficient mutant disrupts the Aurora B-INCENP complex and induces polyploidy [69], and overexpression of Aurora C has been reported in several cancer cell lines [70]. So the question arises if maintaining the correct balance in expression of both kinases, before and after activation of the embryonic genome, is the underlying problem causing chromosome segregation errors.

Aurora C has already been described as an important kinase during human male meiosis [31], where lack of functional Aurora C severely disrupts the meiotic process. In the current study, we describe for the first time localization of Aurora C to the region surrounding the centromeres in human spermatocytes. Aurora C associates with pericentric heterochromatin during pachytene, then spreads onto the chromosome arms at diakinesis and condenses at the centromeres again at metaphase. In mouse spermatocytes, Aurora C has been described to appear at the diplotene stage



(an extremely short stage in the human male), following a similar pattern [28]. Our observations are also consistent with the phenotype observed in male patients carrying the Aurora C kinase c.144delC mutation [32] and a functional role for Aurora C during human male meiosis.

In agreement with the high mRNA expression of Aurora C reported in human oocytes [33], we also observed Aurora C on the region surrounding the centromeres in MI and MII oocytes. Although timing of fixation in these human oocytes can not be performed optimally due to ethical reasons, our observations are similar to those recently described in mouse oocytes [34], pointing to a conserved role for Aurora C in female mammalian meiosis. However, this function may be partly redundant in human oocytes, as the two female homozygous *AURKC* mutants are apparently fertile and without further phenotypes [32]. We also detected Aurora B transcripts in human IVF oocytes, although at a lower level than Aurora C. On (pro)metaphase chromosomes in MI oocytes, signal intensity of Aurora C was greater than Aurora B (Figure 2c), whereas in MII oocytes this signal ratio was more variable. Evidence in mouse as to the relative importance of Aurora B and C during meiosis I and II are contradictory [34-36]. The interpretation of these studies is complicated by the lack of specific inhibitors for Aurora B and C, as well as the possibility of the two kinases binding to each other *in vivo* [41]. Thus overexpression of a kinase dead form of one kinase may affect functioning of the other [69]. To complicate matters further, polymorphisms in the mouse *AURKC* gene that result in an amino acid sequence change have been described in inbred strains [29], underscoring the need for proper knockout models. However, taken together, the evidence indicates that there is room for plasticity in the balance of Aurora B and C in the female germline, with the two proteins able to compensate for each other. The fact that human male patients with a mutation in *AURKC* are sterile may indicate differences in this plasticity between the male and the female germline.

Interestingly, in rhesus macaque oocytes, Aurora B mRNA expression was observed to decrease significantly when IVM oocytes were compared to *in vivo* matured oocytes [71]. A similar observation was made in human oocytes [72], indicating that oocyte maturation conditions may contribute to regulation of Aurora B mRNA expression. In future studies it will be interesting to explore whether the variability in the levels of *AURKB* and *AURKC* we observe in the current study can be related to oocyte or embryo quality and patient characteristics, such as maternal age.

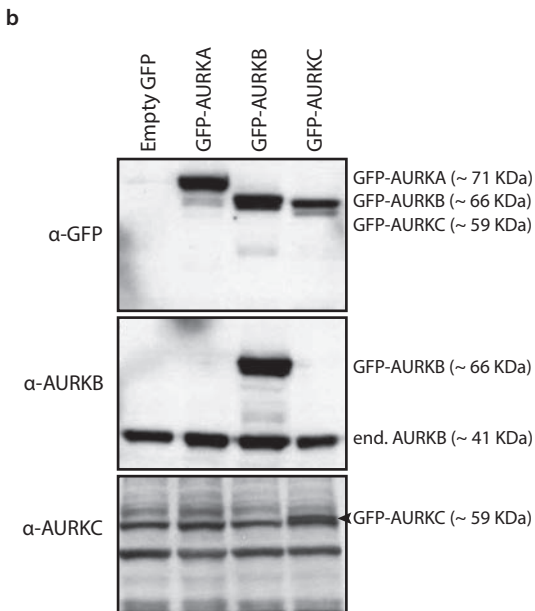
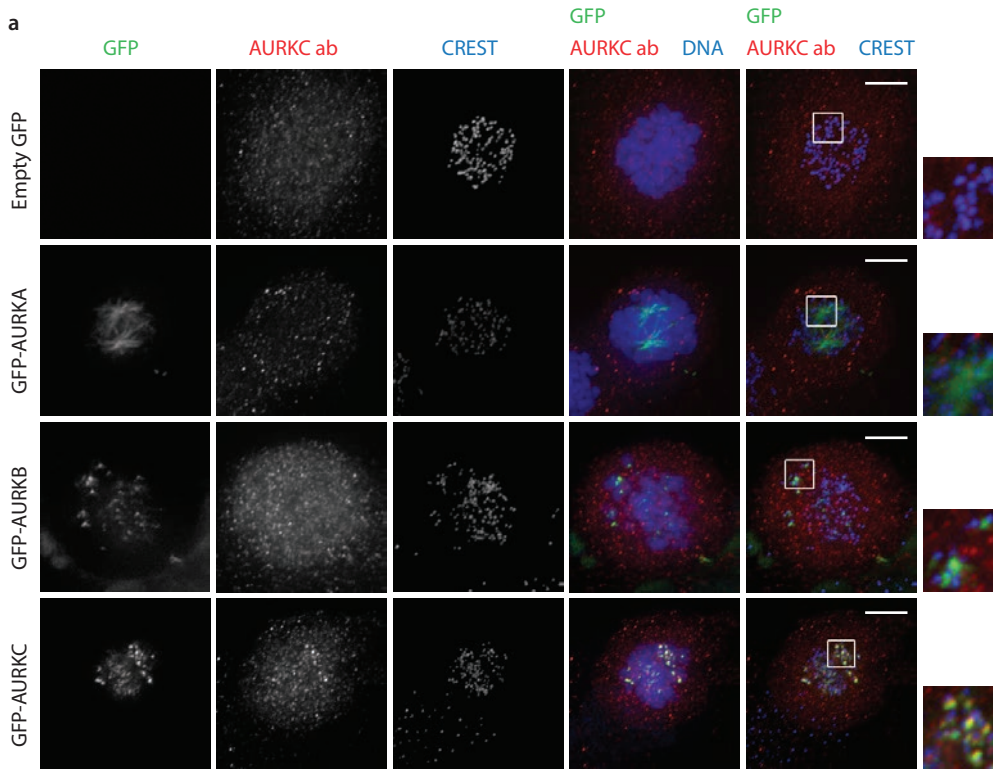
We set out to characterize the CPC in human preimplantation development, in order to identify causes for the observed high post-zygotic chromosome segregation error rate. Although known as a meiotic kinase, we present evidence that Aurora C is the main enzymatic subunit of the CPC during preimplantation embryo development up to the 8 cell stage, and continues to be present next to Aurora B during the compaction stage. This is in contrast to the constitution of the CPC in somatic mitotic cells, and indicates a role for Aurora C during preimplantation embryo development. Even though it is unlikely that the presence of Aurora C alone explains the high chromosome segregation error rate, the data presented here provide novel information regarding possible mechanisms. Further investigation of differences between Aurora B and C substrates and binding partners, as well as regulation of expression of these kinases before and after activation of the embryonic genome in relation to oocyte quality, may help identifying crucial factors.

### **Acknowledgements**

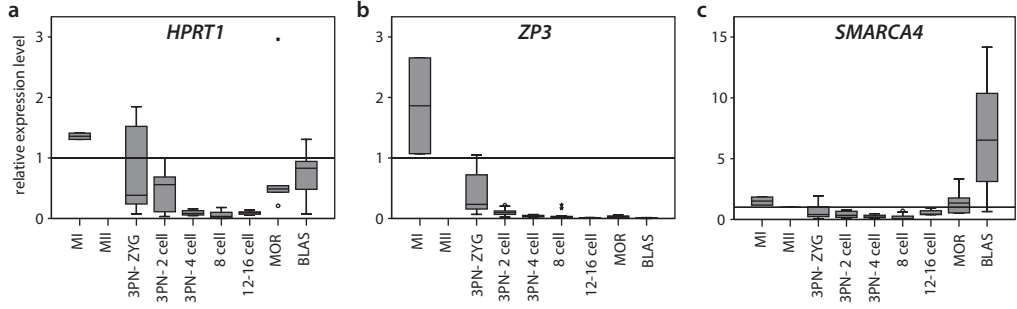
We are grateful to the patients of the IVF units at the Erasmus MC Medical Center and at the University Medical Center Utrecht, for participating in this study. Dr. P. de Boer, Radboud University Nijmegen Medical Centre, The Netherlands is gratefully acknowledged for critically reading the manuscript. We kindly thank Dr. Sally Wheatley, University of Nottingham Medical School, Nottingham, UK for the Borealin antibody.

Supplementary Table 1 — Average Ct-values after pre-amplification and RT-qPCR for indicated Taqman assays in single oocytes and preimplantation embryos of nine developmental stages: oocytes at MI (n=2) and MII (n=5), zygotes (3PN, n=13), 2-cell embryos (3PN- 2 cell, n=10), 4-cell embryos (3PN- 4 cell, n=4), 8-cell embryos (n=12), 12-16-cell embryos (n=6), morulas (MOR, n=5), and blastocysts (BLAS, n=10). Data are expressed as mean  $\pm$ SD.

	MI	MI I	3PN	3PN-2C	3PN-4C	8C	12-16C	MOR	BLAS
<i>AURKB</i>	26.67 $\pm$ 0.41	26.87 $\pm$ 1.18	27.95 $\pm$ 1.67	28.22 $\pm$ 1.09	29.09 $\pm$ 1.41	29.53 $\pm$ 1.44	27.06 $\pm$ 0.54	25.85 $\pm$ 1.36	25.75 $\pm$ 1.51
<i>AURKC</i>	24.93 $\pm$ 0.26	25.50 $\pm$ 1.37	26.50 $\pm$ 1.56	27.41 $\pm$ 1.33	29.18 $\pm$ 0.40	28.22 $\pm$ 1.72	27.17 $\pm$ 0.83	26.51 $\pm$ 1.09	29.87 $\pm$ 1.65
<i>BIRC5</i>	25.54 $\pm$ 0.38	25.89 $\pm$ 0.79	26.68 $\pm$ 1.84	27.27 $\pm$ 0.94	28.15 $\pm$ 0.77	27.93 $\pm$ 1.31	26.20 $\pm$ 0.42	25.32 $\pm$ 0.94	24.22 $\pm$ 1.24
<i>CDCA8</i>	23.64 $\pm$ 0.48	24.69 $\pm$ 1.57	25.38 $\pm$ 2.28	25.53 $\pm$ 1.59	26.26 $\pm$ 0.70	27.77 $\pm$ 2.17	25.92 $\pm$ 0.36	25.09 $\pm$ 0.93	25.11 $\pm$ 1.55
<i>HPRT1</i>	23.39 $\pm$ 0.06	23.83 $\pm$ 1.42	24.96 $\pm$ 1.50	25.47 $\pm$ 1.55	27.39 $\pm$ 0.65	29.07 $\pm$ 2.21	27.31 $\pm$ 0.45	24.59 $\pm$ 1.26	24.57 $\pm$ 1.19
<i>INCENP</i>	28.55 $\pm$ 0.69	28.06 $\pm$ 0.41	29.00 $\pm$ 1.54	29.47 $\pm$ 0.92	29.70 $\pm$ 0.87	29.93 $\pm$ 1.13	27.36 $\pm$ 0.41	26.62 $\pm$ 0.84	24.94 $\pm$ 1.19
<i>SMARCA4</i>	25.64 $\pm$ 0.32	26.20 $\pm$ 1.07	27.51 $\pm$ 1.58	28.09 $\pm$ 1.31	28.46 $\pm$ 0.80	29.41 $\pm$ 1.56	27.15 $\pm$ 0.48	25.97 $\pm$ 1.02	24.05 $\pm$ 1.56
<i>ZP3</i>	18.88 $\pm$ 0.66	19.63 $\pm$ 0.99	21.42 $\pm$ 1.27	23.17 $\pm$ 1.01	24.42 $\pm$ 0.58	25.01 $\pm$ 1.55	26.04 $\pm$ 0.28	24.97 $\pm$ 0.98	27.43 $\pm$ 1.46



**Supplementary Figure 1 — Validation of a rabbit polyclonal antibody against Aurora C (ab38299, Abcam).** (a) Immunolocalization of AURKC and CREST on U2OS cells transfected with empty GFP vector, GFP-AURKA, GFP-AURKB and GFP-AURKC. GFP-tagged AURKA was localized on microtubules near the spindle poles, whereas GFP-AURKB and GFP-AURKC were detected on the inner centromere of prometaphase chromosomes. AURKC antibody did not recognize GFP, GFP-AURKA or GFP-AURKB, but recognized GFP-AURKC. (b) Western blot of U2OS cells transfected with empty GFP vector, GFP-AURKA, GFP-AURKB and GFP-AURKC. Cell lysates were immunoprobed with antibodies to GFP, AURKB and AURKC. We are unsure as to the identity of the extra bands detected by AURKC antibody.



**Supplementary Figure 2** — Relative expression levels after *RT-qPCR* of (a) *HPRT1*, (b) *ZP3* and (c) *SMARCA4* in single oocytes and preimplantation embryos of nine developmental stages: oocytes at MI (n=2) and MII (n=5), zygotes (3PN, n=13), 2-cell embryos (3PN- 2 cell, n=10), 4-cell embryos (3PN- 4 cell, n=4), 8-cell embryos (n=12), 12-16-cell embryos (n=6), morulas (MOR, n=5), and blastocysts (BLAS, n=10). The mean expression level at the oocyte MII stage was taken as a reference to calculate the relative levels of the other stages. Note the scale of the y-axis differs.

## References

1. Voullaire, L., et al., *Chromosome analysis of blastomeres from human embryos by using comparative genomic hybridization*. Hum Genet, 2000. **106**(2): p. 210-7.
2. Wells, D. and J.D. Delhanty, *Comprehensive chromosomal analysis of human preimplantation embryos using whole genome amplification and single cell comparative genomic hybridization*. Mol Hum Reprod, 2000. **6**(11): p. 1055-62.
3. Baart, E.B., et al., *Preimplantation genetic screening reveals a high incidence of aneuploidy and mosaicism in embryos from young women undergoing IVF*. Human reproduction (Oxford, England), 2006. **21**(1): p. 223-233.
4. Daphnis, D.D., et al., *Detailed FISH analysis of day 5 human embryos reveals the mechanisms leading to mosaic aneuploidy*. Hum Reprod, 2005. **20**(1): p. 129-37.
5. Marquez, C., et al., *Chromosome abnormalities in 1255 cleavage-stage human embryos*. Reprod Biomed Online, 2000. **1**(1): p. 17-26.
6. Bielanska, M., S.L. Tan, and A. Ao, *Chromosomal mosaicism throughout human preimplantation development in vitro: incidence, type, and relevance to embryo outcome*. Hum Reprod, 2002. **17**(2): p. 413-9.
7. Coonen, E., et al., *Anaphase lagging mainly explains chromosomal mosaicism in human preimplantation embryos*. Hum Reprod, 2004. **19**(2): p. 316-24.
8. Santos, M.A., et al., *The fate of the mosaic embryo: chromosomal constitution and development of Day 4, 5 and 8 human embryos*. Hum Reprod, 2010. **25**(8): p. 1916-26.
9. Vanneste, E., et al., *Chromosome instability is common in human cleavage-stage embryos*. Nature medicine, 2009. **15**(5): p. 577-583.
10. Dupont, C., et al., *Incidence of chromosomal mosaicism in morphologically normal nonhuman primate preimplantation embryos*. Fertil Steril, 2010. **93**(8): p. 2545-50.
11. Rambags, B.P., et al., *Numerical chromosomal abnormalities in equine embryos produced in vivo and in vitro*. Mol Reprod Dev, 2005. **72**(1): p. 77-87.
12. Viuff, D., et al., *Chromosome aberrations in in vitro-produced bovine embryos at days 2-5 post-insemination*. Biol Reprod, 2000. **63**(4): p. 1143-8.
13. Zijlstra, C., et al., *Blastocyst morphology, actin cytoskeleton quality and chromosome content are correlated with embryo quality in the pig*. Theriogenology, 2008. **70**(6): p. 923-35.
14. Jones, G.M., et al., *Novel strategy with potential to identify developmentally competent IVF blastocysts*. Hum Reprod, 2008. **23**(8): p. 1748-59.
15. Vagnarelli, P. and W.C. Earnshaw, *Chromosomal passengers: the four-dimensional regulation of mitotic events*. Chromosoma, 2004. **113**(5): p. 211-222.
16. Vader, G., R.H. Medema, and S.M. Lens, *The chromosomal passenger complex: guiding Aurora-B through mitosis*. J Cell Biol, 2006. **173**(6): p. 833-7.
17. Ruchaud, S., M. Carmena, and W.C. Earnshaw, *Chromosomal passengers: conducting cell division*. Nature reviews.Molecular cell biology, 2007. **8**(10): p. 798-812.
18. Klein, U.R., E.A. Nigg, and U. Gruneberg, *Centromere targeting of the chromosomal passenger complex requires a ternary subcomplex of Borealin, Survivin, and the N-terminal domain of INCENP*. Mol Biol Cell, 2006. **17**(6): p. 2547-58.
19. Jeyapakash, A.A., et al., *Structure of a Survivin-Borealin-INCENP core complex reveals how chromosomal passengers travel together*. Cell, 2007. **131**(2): p. 271-85.
20. Vader, G., et al., *Survivin mediates targeting of the chromosomal passenger complex to the centromere and midbody*. EMBO Rep, 2006. **7**(1): p. 85-92.
21. Carmena, M., S. Ruchaud, and W.C. Earnshaw, *Making the Auroras glow: regulation of Aurora A and B kinase function by interacting proteins*. Curr Opin Cell Biol, 2009. **21**(6): p. 796-805.
22. Sugimoto, K., et al., *Molecular dynamics of Aurora-A kinase in living mitotic cells simultaneously visualized with histone H3 and nuclear membrane protein importin alpha*. Cell Struct Funct, 2002. **27**(6): p. 457-67.
23. Brittle, A.L. and H. Ohkura, *Centrosome maturation: Aurora lights the way to the poles*. Curr Biol, 2005. **15**(21): p. R880-2.

24. Barr, A.R. and F. Gergely, *Aurora-A: the maker and breaker of spindle poles*. J Cell Sci, 2007. **120**(Pt 17): p. 2987-96.
25. Yao, L.J., et al., *Aurora-A is a critical regulator of microtubule assembly and nuclear activity in mouse oocytes, fertilized eggs, and early embryos*. Biol Reprod, 2004. **70**(5): p. 1392-9.
26. Brown, J.R., et al., *Evolutionary relationships of Aurora kinases: implications for model organism studies and the development of anti-cancer drugs*. BMC Evol Biol, 2004. **4**: p. 39.
27. Bernard, M., et al., *Cloning of STK13, a third human protein kinase related to Drosophila aurora and budding yeast Ipl1 that maps on chromosome 19q13.3-ter*. Genomics, 1998. **53**(3): p. 406-9.
28. Tang, C.J., C.Y. Lin, and T.K. Tang, *Dynamic localization and functional implications of Aurora-C kinase during male mouse meiosis*. Dev Biol, 2006. **290**(2): p. 398-410.
29. Hu, H.M., et al., *Genomic organization, expression, and chromosome localization of a third aurora-related kinase gene, Aie1*. DNA Cell Biol, 2000. **19**(11): p. 679-88.
30. Kimmins, S., et al., *Differential Functions of the Aurora-B and Aurora-C Kinases in Mammalian Spermatogenesis*. Mol Endocrinol, 2007. **21**(3): p. 726-739.
31. Dieterich, K., et al., *Homozygous mutation of AURKC yields large-headed polyploid spermatozoa and causes male infertility*. Nature genetics, 2007. **39**(5): p. 661-665.
32. Dieterich, K., et al., *The Aurora Kinase C c.144delC mutation causes meiosis I arrest in men and is frequent in the North African population*. Hum Mol Genet, 2009. **18**(7): p. 1301-9.
33. Assou, S., et al., *The human cumulus-oocyte complex gene-expression profile*. Hum.Reprod., 2006. **21**(7): p. 1705-1719.
34. Yang, K.T., et al., *Aurora-C kinase deficiency causes cytokinesis failure in meiosis I and production of large polyploid oocytes in mice*. Mol Biol Cell, 2010. **21**(14): p. 2371-83.
35. Shuda, K., et al., *Aurora kinase B modulates chromosome alignment in mouse oocytes*. Mol Reprod Dev, 2009. **76**(11): p. 1094-105.
36. Vogt, E., A. Kipp, and U. Eichenlaub-Ritter, *Aurora kinase B, epigenetic state of centromeric heterochromatin and chiasma resolution in oocytes*. Reprod Biomed Online, 2009. **19**(3): p. 352-68.
37. Sasai, K., et al., *Aurora-C kinase is a novel chromosomal passenger protein that can complement Aurora-B kinase function in mitotic cells*. Cell Motil Cytoskeleton, 2004. **59**(4): p. 249-63.
38. Lin, Y.S., et al., *Gene expression profiles of the aurora family kinases*. Gene Expr, 2006. **13**(1): p. 15-26.
39. Price, D.M., et al., *Nocturnal activation of aurora C in rat pineal gland: its role in the norepinephrine-induced phosphorylation of histone H3 and gene expression*. Endocrinology, 2009. **150**(5): p. 2334-41.
40. Slattery, S.D., et al., *Aurora-C kinase supports mitotic progression in the absence of Aurora-B*. Cell Cycle, 2009. **8**(18): p. 2984-94.
41. Li, X., et al., *Direct association with inner centromere protein (INCENP) activates the novel chromosomal passenger protein, Aurora-C*. J Biol Chem, 2004. **279**(45): p. 47201-11.
42. Slattery, S.D., et al., *Aurora-C and Aurora-B share phosphorylation and regulation of CENP-A and Borealin during mitosis*. Cell Cycle, 2008. **7**(6): p. 787-95.
43. Yan, X., et al., *Aurora C is directly associated with Survivin and required for cytokinesis*. Genes Cells, 2005. **10**(6): p. 617-26.
44. Braude, P., V. Bolton, and S. Moore, *Human gene expression first occurs between the four- and eight-cell stages of preimplantation development*. Nature, 1988. **332**(6163): p. 459-61.
45. Tesarik, J., et al., *Activation of nucleolar and extranucleolar RNA synthesis and changes in the ribosomal content of human embryos developing in vitro*. J Reprod Fertil, 1986. **78**(2): p. 463-70.
46. Heijnen, E.M., et al., *A mild treatment strategy for in-vitro fertilisation: a randomised non-inferiority trial*. Lancet, 2007. **369**(9563): p. 743-9.
47. Hohmann, F.P., N.S. Macklon, and B.C. Fauser, *A randomized comparison of two ovarian stimulation protocols with gonadotropin-releasing hormone (GnRH) antagonist cotreatment for in vitro fertilization commencing recombinant follicle-stimulating hormone on cycle day 2 or 5 with the standard long GnRH agonist protocol*. J Clin Endocrinol Metab, 2003. **88**(1): p. 166-73.
48. Ulmer, R., et al., *Triploid embryo after in vitro fertilization*. Arch Gynecol, 1985. **237**(2): p. 101-7.



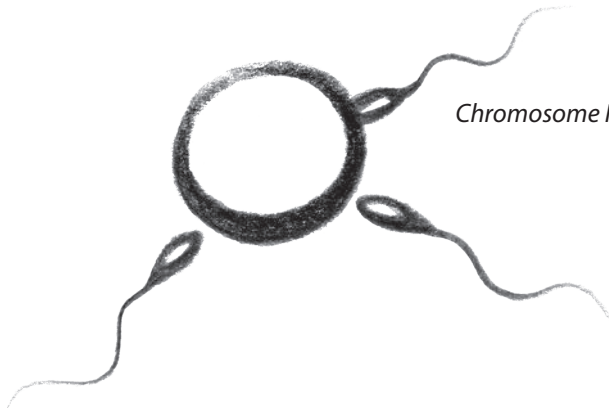
49. Livak, K.J. and T.D. Schmittgen, *Analysis of relative gene expression data using real-time quantitative PCR and the 2(-Delta Delta C(T)) Method*. Methods (San Diego, Calif.), 2001. **25**(4): p. 402-408.
50. Smits, V.A., et al., *p21 inhibits Thr161 phosphorylation of Cdc2 to enforce the G2 DNA damage checkpoint*. J Biol Chem, 2000. **275**(39): p. 30638-43.
51. Peters, A.H., et al., *A drying-down technique for the spreading of mammalian meiocytes from the male and female germline*. Chromosome Res, 1997. **5**(1): p. 66-8.
52. Baart, E.B., et al., *Distribution of Atr protein in primary spermatocytes of a mouse chromosomal mutant: a comparison of preparation techniques*. Chromosoma, 2000. **109**(1-2): p. 139-147.
53. Puschendorf, M., et al., *PRC1 and Suv39h specify parental asymmetry at constitutive heterochromatin in early mouse embryos*. Nature genetics, 2008. **40**(4): p. 411-420.
54. Kuijk, E.W., et al., *Validation of reference genes for quantitative RT-PCR studies in porcine oocytes and preimplantation embryos*. BMC Dev Biol, 2007. **7**: p. 58.
55. Mamo, S., et al., *Expression profiles of the pluripotency marker gene POU5F1 and validation of reference genes in rabbit oocytes and preimplantation stage embryos*. BMC Mol Biol, 2008. **9**: p. 67.
56. Rajkovic, A. and M.M. Matzuk, *Functional analysis of oocyte-expressed genes using transgenic models*. Mol Cell Endocrinol, 2002. **187**(1-2): p. 5-9.
57. Bultman, S.J., et al., *Maternal BRG1 regulates zygotic genome activation in the mouse*. Genes Dev, 2006. **20**(13): p. 1744-54.
58. Hamatani, T., et al., *Dynamics of global gene expression changes during mouse preimplantation development*. Dev Cell, 2004. **6**(1): p. 117-31.
59. Nguyen, H.G., et al., *Mechanism of Aurora-B degradation and its dependency on intact KEN and A-boxes: identification of an aneuploidy-promoting property*. Mol Cell Biol, 2005. **25**(12): p. 4977-92.
60. Sharif, B., et al., *The chromosome passenger complex is required for fidelity of chromosome transmission and cytokinesis in meiosis of mouse oocytes*. J Cell Sci, 2010. **123**(Pt 24): p. 4292-300.
61. Cutts, S.M., et al., *Defective chromosome segregation, microtubule bundling and nuclear bridging in inner centromere protein gene (Incenp)-disrupted mice*. Hum Mol Genet, 1999. **8**(7): p. 1145-55.
62. Uren, A.G., et al., *Survivin and the inner centromere protein INCENP show similar cell-cycle localization and gene knockout phenotype*. Curr Biol, 2000. **10**(21): p. 1319-28.
63. Yamanaka, Y., et al., *Loss of Borealin/Dasrab leads to defective cell proliferation, p53 accumulation and early embryonic lethality*. Mech Dev, 2008. **125**(5-6): p. 441-50.
64. Tesarik, J., *Involvement of oocyte-coded message in cell differentiation control of early human embryos*. Development, 1989. **105**(2): p. 317-22.
65. Schramm, R.D., A.M. Paprocki, and C.A. VandeVoort, *Causes of developmental failure of in-vitro matured rhesus monkey oocytes: impairments in embryonic genome activation*. Hum Reprod, 2003. **18**(4): p. 826-33.
66. Pavlok, A., et al., *Transcriptional activity and nuclear ultrastructure of 8-cell bovine embryos developed by in vitro maturation and fertilization of oocytes from different growth categories of antral follicles*. Mol Reprod Dev, 1993. **35**(3): p. 233-43.
67. Tatsuka, M., et al., *Multinuclearity and increased ploidy caused by overexpression of the aurora- and Ipl1-like midbody-associated protein mitotic kinase in human cancer cells*. Cancer Res, 1998. **58**(21): p. 4811-6.
68. Katayama, H., W.R. Brinkley, and S. Sen, *The Aurora kinases: role in cell transformation and tumorigenesis*. Cancer Metastasis Rev, 2003. **22**(4): p. 451-64.
69. Chen, H.L., et al., *Overexpression of an Aurora-C kinase-deficient mutant disrupts the Aurora-B/INCENP complex and induces polyploidy*. J Biomed Sci, 2005. **12**(2): p. 297-310.
70. Kimura, M., et al., *Cell cycle-dependent expression and centrosome localization of a third human aurora/Ipl1-related protein kinase, AIK3*. J Biol Chem, 1999. **274**(11): p. 7334-40.
71. Mtango, N.R. and K.E. Latham, *Differential expression of cell cycle genes in rhesus monkey oocytes and embryos of different developmental potentials*. Biology of reproduction, 2008. **78**(2): p. 254-266.
72. Jones, G.M., et al., *Gene expression profiling of human oocytes following in vivo or in vitro maturation*. Hum. Reprod., 2008. **23**(5): p. 1138-1144.



# CHAPTER 4

## **A universal method for sequential immunofluorescent analysis of chromatin and chromatin-associated proteins on chromosome spreads**

Christine van de Werken, Holger Jahr, Margarida Avo Santos, Cindy Eleveld, Joyce Schuilwerve, Joop S.E. Laven, Esther B. Baart



*Chromosome Research, 2013: p. 1-15*

## Abstract

Immunofluorescence has been widely used to study histone modification dynamics and chromosome-associated proteins that regulate the segregation of chromosomes during cell divisions. Since many of these regulatory proteins interact (in)directly to exert their proper function, it is of interest to detect these proteins simultaneously, to establish their spatiotemporal relation. However, the detection of multiple epitopes on the same material is limited by the availability of antibodies derived from different host species. For Western blot membranes, buffers were developed to remove antibodies after the first round of detection and enable a second round of detection. In this study, we establish that this “stripping” principle can also be applied for sequential immunofluorescence on chromosome preparations. We first adapted a drying down fixation technique for the use on cultured cells from different primary cells and cell lines. These chromosome spreads were subsequently used to optimize the stripping procedure for this application. We investigated feasibility and reliability of detection of histones and their posttranslational modifications as well as chromatin interacting proteins in two subsequent rounds of immunofluorescence. We conclude that this method is a reliable option when spatial resolution and co-expression need to be investigated and the material or the choice of antibodies is limited.

## Introduction

Immunofluorescence is a powerful tool to investigate protein expression and localization. By using this technique, our understanding of histone modification dynamics and different classes of chromosome-associated proteins that mediate the segregation of chromosomes during both meiotic and mitotic cell division has increased dramatically. A problem that had to be overcome in order to study chromosomes and chromosome-associated proteins in detail was that most such proteins are lost from the chromosomes during the fixation process in the conventional cytogenetic procedure, using methanol/acetic acid. Therefore, chromosome-associated proteins have been studied in whole mount fixed cells or in cells fixed by a cytospin procedure [1,2]. However, the cytospin method results in reduced chromosome resolution compared with the cytogenetic procedure. Chromosome analysis after whole mount fixation needs expensive imaging equipment for either confocal analysis or deconvolution techniques [3]. Chromosomal analysis of oocytes and preimplantation embryos is especially challenging, because of their large cytoplasmic volume that results in increased background staining and problems with antibody accessibility [4]. To circumvent these problems, a fixation technique was described for mouse oocytes and early cleavage stage embryos, with the aim to obtain analyzable chromosome preparations [5]. This method was developed by adapting the protocol established by Peters et al. [6] for male and female germline cells and shown to preserve chromosome-associated proteins [5]. In this method, cells are incubated in a hypotonic solution and subsequently transferred to 1% paraformaldehyde (PFA) containing 0.2% Triton on a glass slide, resulting in cell lysis and spread fixation of the chromatin after drying down. The application of this protocol allows the study of chromosomes and attached proteins in detail and has thereby increased our insight into chromosome segregation regulation in both mouse and human oocytes and preimplantation embryos [7,8].

Mounting evidence demonstrates the complex interplay between posttranslational histone modifications and protein complexes involved in regulation of chromosome segregation and mitosis, such as the chromosomal passenger complex (CPC) [9]. In order to further elucidate mechanisms that regulate these processes, it is of interest to detect these epitopes simultaneously on the same chromosome. In addition, when material under investigation is scarce and valuable, e.g. in case of surplus human oocytes or embryos from *in vitro* fertilization (IVF) treatments, it would be optimal to investigate as many epitopes as possible on the same preparation. However, detecting multiple proteins on the same material is limited by the availability of reliable antibodies raised in different host species. Most of the primary antibodies that work best for immunofluorescent studies are derived from either rabbit or mouse.

This difficulty is also known for Western blot procedures, for which “stripping” buffers were developed to remove the antibodies after detection and thereby enable a second round of detection. These buffers interfere with protein-protein interactions through high salt denaturing conditions, the use of detergent, or a low pH, without removing or damaging the epitope from the blotting membrane [10-12]. In this study, we aimed to evaluate the application of the stripping principle on chromosome spreads and investigate the feasibility of developing a protocol for sequential immunofluorescence. To this end, we first adapted the surface spreading protocol for the use on

cultured cells from different cell lines and species. We subsequently optimized the stripping protocol for this application and investigated reliability for different antibodies and antibody combinations. We further illustrate some possibilities this method can offer and critically discuss the limitations. We conclude that the method is a reliable option and offers a solution when spatial resolution and co-expression need to be investigated and the choice of antibodies is limited and/or when material is scarce.

## Methods

### Culture and collection of cells and germ cells

We cultured two different cell lines and two types of primary cells under routine conditions as described earlier: murine teratocarcinoma-derived chondrogenic cells (ATDC5) [13,14], immortalized human foetal osteoblasts (hFOB1.19) [15], primary porcine articular chondrocytes (PAC), and human articular chondrocytes (HAC) [16]. Cells were arrested by incubation with 250ng/mL nocodazole (Sigma) for 2h or overnight and harvested by mitotic shake-off.

Failed fertilized oocytes were donated for research 1 day post-insemination by patients undergoing IVF treatment at the outpatient clinic of the Department of Obstetrics and Gynaecology of the Erasmus MC, University Medical Center, Rotterdam, The Netherlands. Ovarian stimulation, oocyte retrieval and in vitro fertilization (IVF) procedures were performed as described previously [17].

### Surface spreading of different cell types

Mouse spermatocytes were obtained from the testis of an FVB male and nuclear spreads were prepared as described previously [6,18]. The spreads were made available to us by W. Baarends, Rotterdam, The Netherlands. Cultured primary cells and cell lines were also treated as described [6], but with minor modifications [19]. In short, cells obtained after mitotic shake-off in culture medium containing nocodazole were spun down for 10 minutes at 200 g. Supernatant was removed to leave 1 mL of medium and cells were resuspended. An equal volume of a hypotonic buffer (pH 8.2) containing 30 mM Tris-HCl, 17 mM trisodium citrate dihydrate, 50 mM sucrose, and 5 mM ethylenediaminetetraacetate (EDTA) was added. After 7 minutes incubation and spinning down for 7 minutes at 200xg, all supernatant was removed. Cells were resuspended in 100 mM sucrose (pH 8.2) to obtain a cell concentration of  $5\text{-}15 \times 10^6$  cells/mL. From this suspension 10  $\mu$ l was applied to a slide dipped in a freshly prepared and filtered (0.2  $\mu$ m) 1% PFA, pH 9.2 solution, containing 0.15% Triton X-100. The cell suspension was placed at the upper right corner of the slide and was slowly dispersed first in a horizontal direction, thereafter in a vertical direction, while exposing the cells to the fixative. After horizontal drying for 1.5-2 h in a humid chamber, slides were washed with 0.08% Kodak Photo-Flo and air dried.

Oocytes were fixed as described [7] with some minor modifications. After zona pellucida removal with Acidic Tyrode's Solution (Sigma), oocytes were incubated in hyposolution (25% FCS, 0.5% sodium citrate) for 5 minutes and subsequently transferred to a drop of fixative (1% PFA, 0.2% Triton

X-100, 0.1 mM dithiothreitol (DTT), pH 9.2) on a glass slide. After horizontal drying for 1 hour, slides were washed with 0.08% Photo-Flo (Kodak) and air dried.

All slides were stored at -20°C for a maximum of 3 months until further use.

## Antibodies

The following antibodies were used: rabbit polyclonal antibodies against H3K9me3 (1:500, Abcam), H2ApT120 (1:2500, Active Motif), H3pT3 (1:1,000, Upstate), H3pS10 (1:100, Cell Signaling) and SYCP3 (1:5000, Lammers et al., 1994 [20]), mouse monoclonal antibodies against AURKB (1:100, BD Biosciences), INCENP (1:1000; Upstate) and H3 (1:1000, Active Motif), and human anti-centromere antibodies (ACA) (human centromere antiserum; 1:1000, Fitzgerald Industries). Primary antibodies were detected by labelling with the appropriate secondary antibodies conjugated with Alexa Fluor 488, 594 or 633 (Invitrogen).

## Immunofluorescence

For immunofluorescence staining, chromosome spreads were rinsed in PBS-T (PBS with 0.01% v/v Tween-20), blocked with blocking solution (PBS-T, 2% w/v bovine serum albumin, 5% v/v normal goat serum) for 30 min and incubated with primary antibodies at 4°C overnight. After washing with PBS-T, chromosome spreads were incubated with the appropriate secondary antibodies for 1h, washed with PBS-T and mounted with Vectashield® mounting solution containing 750 ng/ml 4,6-diamidino-2-phenylindole (DAPI) for DNA counterstaining (Vector Laboratories).

## Stripping

To explore the feasibility of stripping, we tested different solutions for the ability to remove H3K9me3 staining from HAC chromosome spreads. We tested two different commercial stripping buffers: Restore™ PLUS Western Blot Stripping Buffer and Restore™ Fluorescent Western Blot Stripping Buffer (both Thermo Scientific). We also evaluated two stripping solutions described in the literature: a low pH glycine hydrochloride solution based on Legocki and Verma (0.1M GlyHCl, 0.15% Tween, pH 2.5) [21] and a guanidine hydrochloride solution based on Yeung and Stanley (6M GnHCl, 20mM Tris-HCl, 0.2% Triton, pH 7.5) [12].

After microscopic inspection of the immunofluorescent staining, coverslips were removed and slides were washed in PBS-T to remove the Vectashield® mounting solution. To test the commercial stripping buffers, slides were then incubated for 5 or 10 minutes in Restore™ PLUS Western Blot Stripping Buffer or for 10 or 20 minutes in 1x Restore™ Fluorescent Western Blot Stripping Buffer, at room temperature under constant shaking, according to manufacturer's protocol. To test the stripping solutions from literature, slides were incubated for 30 minutes in GlyHCl solution or for 10 minutes in GnHCl solution, both at room temperature, as described in literature. Slides were then washed twice in PBS-T and mounted with Vectashield®. Microscopic inspection of residual fluorescence was performed at a high (630x) magnification and evaluated as clearly distinguishable, faint, barely, or not visible. Differences between the stripping solutions were further quantified as described below.

After establishment of the optimal stripping procedure, slides in further experiments were treated as follows: after imaging the first round of immunofluorescent staining, coverslips were removed and slides were washed in PBS-T to remove the Vectashield® mounting solution. Slides were incubated in Restore™ PLUS Western Blot Stripping Buffer for 10 minutes. After stripping, slides were washed twice in PBS-T before use for a second immunofluorescent staining.

## Imaging

Images were obtained using a Zeiss Axio Imager M1 microscope (Carl Zeiss), CoolCube 1m camera (MetaSystems) and Isis FISH Imaging System software (version 5.4.7, MetaSystems). During the first round of imaging, positions of metaphases imaged were recorded in the form of the XY-position of the microscope table. These coordinates were used to find the same chromosome spread in subsequent rounds of imaging.

For quantifications (Figure 1b, 2b and Online Resource 1), we used spreads of HAC and ATDC5 cells. Images of the same metaphase before and after stripping and after a second round of immunostaining were acquired with identical microscope and illumination settings. Pixel intensities of areas containing chromosomes were determined in the various channels by using the Selection and Analyze-Measure tools in Image J (version 1.42n). For each set of chromosomes, the maximum fluorescence intensity was corrected for background intensities by subtracting the minimum fluorescence. The resulting pixel intensity after the first round of immunostaining was set to 1, and intensities after stripping and the second round of immunostaining were expressed as percentages. For each quantification experiment, 10 metaphase spreads were imaged sequentially. Significance was tested with the Wilcoxon Signed Rank Test using IBM SPSS Statistics (version 20.0.0.1).

For plotting the distribution of fluorescence intensities along one chromosome arm (Figure 3b), we used the images shown in Figure 3a. One chromosome arm was selected using the Segmented Line tool in Image J. This selection was copied to other images. Subsequently, using the Analyze-Plot Profile tool, the distribution of fluorescence intensities along the selected chromosome arm was obtained.

Images from different rounds of detection on the same chromosome spread were merged using the ROI Manager in Image J to copy a selected area of one image to the other images. Subsequently, selected areas were cropped and merged.

## Results

### **A universal method for surface spreading of different types of cells**

The surface spreading protocol could be successfully applied to a range of cultured cells and cell lines of human, murine and porcine origin (for examples see Online Resource 2). The quality of the spreads could be variable and we found this to be dependent on: 1) duration of prometaphase arrest, 2) cell density after resuspension in sucrose solution, and 3) the drying down procedure. Regarding the first, a shorter prometaphase arrest resulted in longer, less condensed chromosomes, but reduced the yield of mitotic cells. Regarding cell density, transferring too many cells onto the



slide resulted in poor spreading and compact chromatin. We found a density of  $5\text{-}15 \times 10^6$  cells/mL to work well. Variation induced by the drying down procedure has been described before [5,6,19] and depends on a slow drying process. When optimized, however, good chromosome morphology can be observed after DAPI-staining. Spread chromosomes of human, murine or porcine origin could be successfully immunostained for the presence of trimethylation of histone 3 at lysine 9 (H3K9me3), a well conserved marker for constitutive heterochromatin (Figures 1, 3, 5, Online Resource 2). This illustrates differences in size and distribution of chromosome regions enriched for this mark between species and cell types (Online Resource 2). We were also successful in detecting histone associating proteins (AURKB: Figure 2 and INCENP: Figures 3, 5), histone H3 (Figures 1, 3, 5) and different histone modifications (H3pT3, H2ApT120: Figures 2, 4, 5).

### Feasibility and optimization of the stripping protocol

Chromosomal spreads of human articular chondrocytes (HAC) were used to determine the optimal stripping protocol. As described in the Methods section, we tested four different stripping buffers and different durations of incubation. Residual fluorescence after incubation in Restore™ PLUS Western Blot Stripping Buffer was scored as faint to barely visible after 5 minutes incubation and as not or barely visible after 10 minutes incubation. Incubation in GnHCl solution for 10 minutes also resulted in an obvious reduction of staining intensity. In contrast, residual fluorescence after incubation in both Restore™ Fluorescent Western Blot Stripping Buffer and GlyHCl solution was scored as faint to clearly distinguishable in all cases. A five-fold increase in the concentration of Restore™ Fluorescent Western Blot Stripping Buffer and an increased incubation time of 30 minutes, as recommended in the manufacturer's protocol, improved stripping results. However, quantification of the decrease in fluorescence intensity on chromosome spreads of HAC cells shows incubation in Restore™ PLUS Western Blot Stripping Buffer for 10 minutes to be most efficient in signal removal (Online Resource 1). This buffer and incubation time were therefore used in subsequent stripping experiments.

To further illustrate the efficiency of stripping, chromosome spreads of HACs and ATDC5 cells were incubated with antibodies against histone H3 and H3K9me3 (Figure 1a). As expected, H3 was detected all over the chromosomes and H3K9me3 was detected mainly at the pericentric regions [22-24]. After stripping, chromosome morphology was still intact (Figure 1a, second panel). However, detected fluorescence of the secondary antibodies was significantly reduced. Subsequently, secondary antibodies were re-applied to investigate if stripping also removed primary antibodies. Imaging showed a slight increase of the signal, compared with the image directly after stripping, but still a convincing decrease of the initial signal (Figure 1a, third panel). Quantification of the decrease in fluorescence intensity on chromosome spreads of ATDC5 cells confirmed these observations, with a decrease to less than 10% of the initial intensity and a slight increase of intensity after re-application of the secondary antibodies for the epitopes tested (Figure 1b). This shows that stripping results in efficient removal of both the primary and the secondary antibody of an immunostaining.

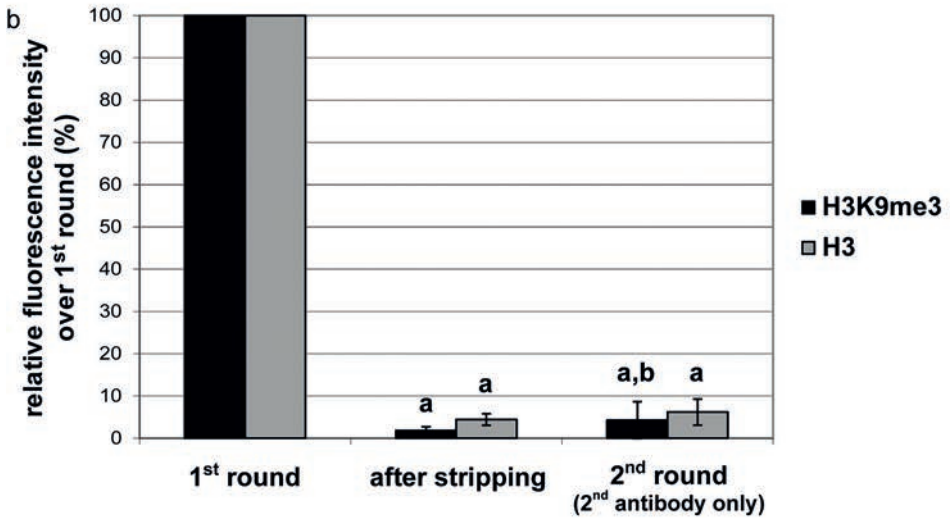
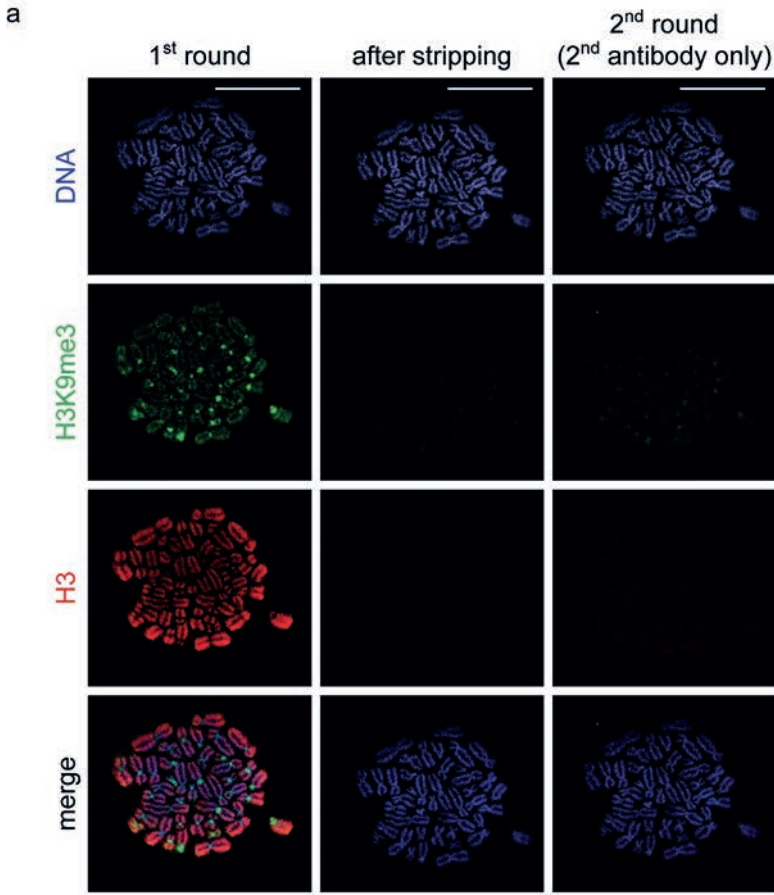


Figure 1 — (a) Efficiency of the stripping protocol, demonstrated by immunofluorescent detection of histone H3 and its trimethylation of lysine 9 (H3K9me3) on spread chromosomes from HACs. First, epitopes were visualized by immunofluorescent staining with primary and secondary antibodies (first panel). H3 can be observed all over the chromosomes and H3K9me3 was detected surrounding the centromeric area. After stripping, almost all signal had disappeared (second panel). Subsequent immunofluorescent staining with only secondary antibodies slightly increased the signal (third panel), indicating removal of most of the secondary, as well as the primary antibody. Scale bars are 25  $\mu\text{m}$ . (b) Relative fluorescence intensity of H3K9me3 and H3 after stripping and after re-application of the secondary antibodies. Shown are mean values and standard deviations of 10 ATDC5 chromosome spreads. Values significantly different from the first round (a) and after stripping (b) are indicated ( $p < 0.01$ ).

### Stripping does not compromise the epitopes investigated

As the stripping buffer is designed to interfere with protein-protein interactions, we investigated if epitopes are still present and intact after stripping. Chromosome spreads of ATDC5 cells were incubated with antibodies against H3pT3 and AURKB, followed by detection and imaging. After stripping, the same staining was repeated (Figure 2a). As expected [9,25], both H3pT3 and AURKB were detected at the centromeric region. Compared with the first staining, fluorescence intensity of the second round of immunolocalization was significantly reduced, but both epitopes were still clearly detectable. Quantification shows that the fluorescence intensity in the second round of detection still reached 59% and 78% of the original value for H3pT3 and AURKB, respectively (Figure 2b). From this, we conclude that these epitopes are not severely affected by the stripping procedure, but some loss of fluorescence intensity does occur.

### Stripping efficiency for different antibodies

Different types of antibodies are known to have large differences in epitope affinities that are hardly predictable [26]. Therefore, we tested if the stripping procedure is robust enough to not only remove low, but also high affinity antibodies. We therefore subjected antibodies directed against the following targets to the stripping procedure: H3K9me3, H3pT3, H3pS10, H2ApT120, H3, ACA, AURKB, INCENP, and SYCP3. The protocol efficiently removed all tested antibodies as shown by the prominent reduction in fluorescent signal intensities after stripping, to less than 10% of the original value when imaged with identical exposure settings (Figure 1b and data not shown). For the H3pT3 antibody, initial fluorescence intensities were very high, and we noticed that residual signal could still be detected in some metaphases. However, this was only obvious when imaging with increased exposure settings (Online Resource 3).

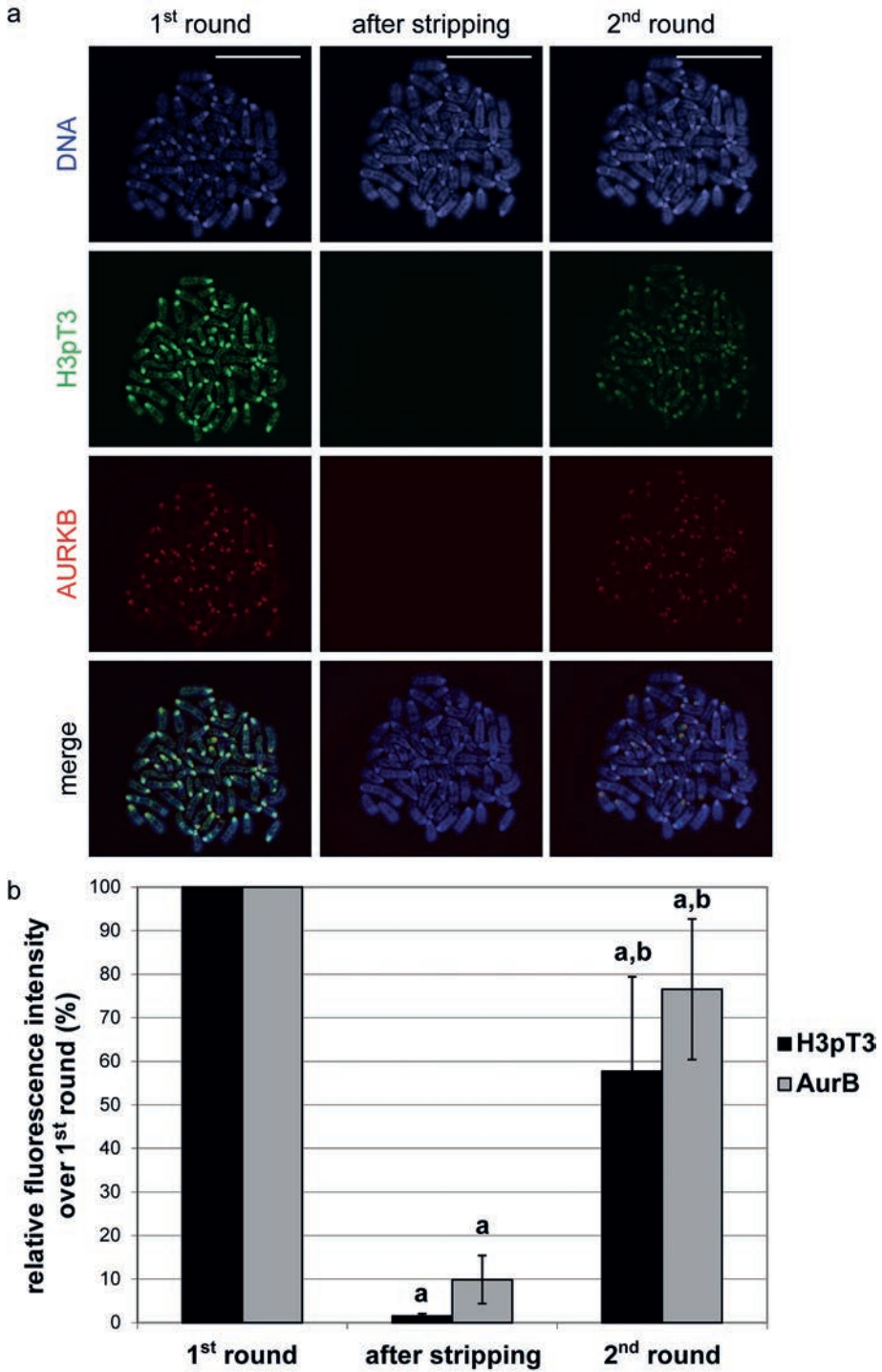


Figure 2 — (a) Immunofluorescent detection of H3pT3 and AURKB on chromosomes from ATDC5 cells. (first panel). After stripping, fluorescence is significantly reduced (second panel). In the subsequent second round of immunofluorescent detection, the same epitopes are again visualized (third panel). Scale bars are 25  $\mu\text{m}$ . (b) Relative fluorescence intensity of H3pT3 and AURKB after stripping and after the second round of immunofluorescent detection. Shown are mean values and standard deviations of 10 ATDC5 chromosome spreads. Values significantly different from the first round (a) and after stripping (b) are indicated ( $p < 0.01$ ).

### Stripping facilitates a second round of immunostaining

We next established if the stripping protocol facilitates a second round of immunostaining with different antibodies. We performed a first round of immunofluorescent detection and imaging, followed by stripping and a second round of immunostaining for different epitopes (Figure 3a). In the first round, we stained chromosomes of HACs with mouse-anti-INCENP antibodies and rabbit-anti-phosphorylation of histone H3 at serine 10 (H3pS10) antibodies. As previously described, H3pS10 was detected along the chromosome arms and INCENP at the inner centromere [27-29]. Stripping efficiently removed the signal of both antibodies. In the second round of detection, we used mouse-anti-H3 and rabbit-anti-H3K9me3 antibodies, and both epitopes were readily detected. When fluorescence intensities of all epitopes were plotted along the length of the chromosome, centromeric enrichment of INCENP (first round) and H3K9me3 (second round) were clearly visible as a peak in fluorescence intensity (Figure 3b).

This application of the stripping procedure illustrates that in these HAC cells trimethylation of H3 at lysine 9 might interfere with recognition of H3 by the mouse monoclonal antibody we used, since pericentric areas positive for H3K9me3 are negative for H3 (Figure 3a, arrowhead, and Figure 3b, second round). In contrast, phosphorylation of H3 on serine 10 does not interfere with H3 antibody binding, as both epitopes are detected abundantly on the chromosome arms of the same chromosome spread.

These results again show that stripping leaves epitopes intact for a second round of immunodetection and that we can successfully detect other epitopes in the second round.

### Applications of sequential immunofluorescent analysis

The combined recovery rate of chromosome spreads after imaging, stripping and a second round of immunostaining in the experiments above was 100% (30/30). The protocol can therefore be safely used on precious material. Next, we performed sequential immunofluorescent analysis on a variety of different cell types to demonstrate the broad applicability of the present stripping protocol.

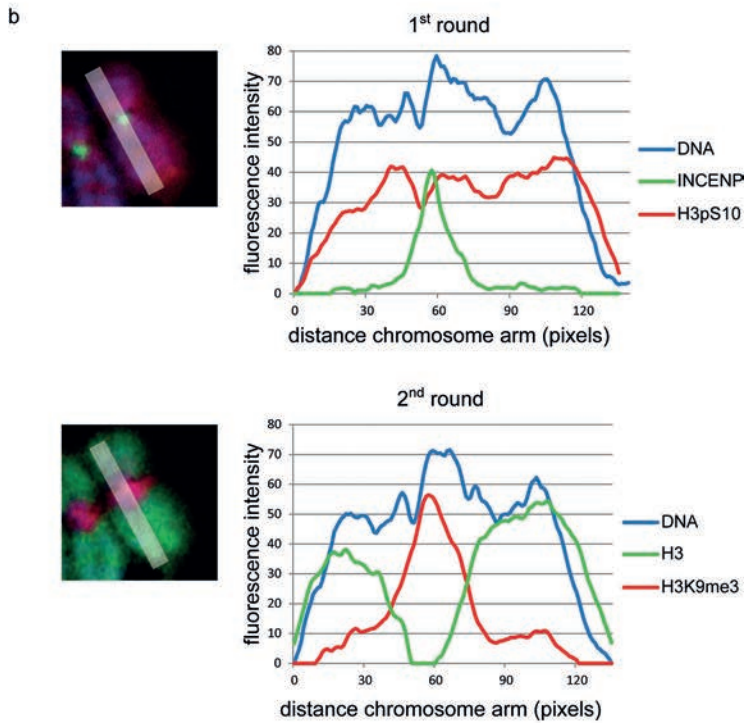
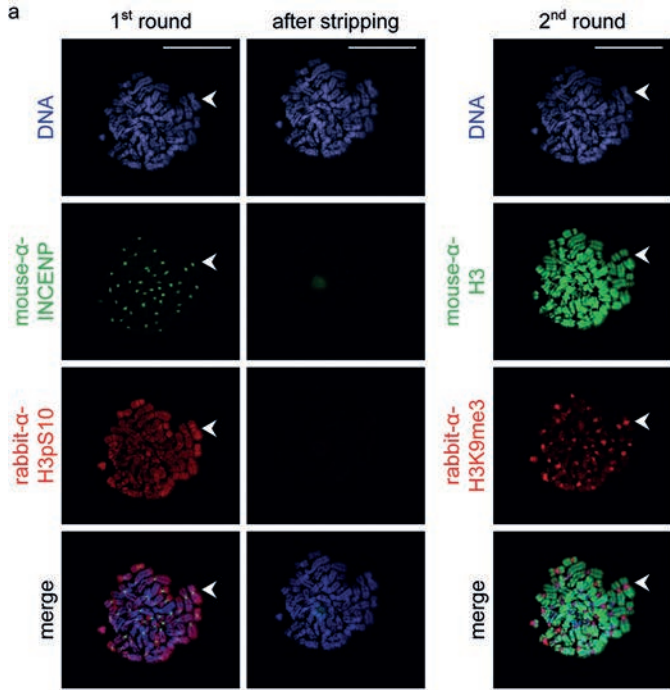


**Figure 3** — The stripping protocol enables sequential immunofluorescent analysis of 4 different epitopes on the same chromosome spread, as demonstrated by immunofluorescent detection of INCENP and H3pS10 on chromosomes from HACs (first panel), followed by stripping (second panel) and a second round of immunostaining for H3 and H3K9me3 (third panel). Note that it is likely that trimethylation of K9, but not phosphorylation of S10, interferes with recognition of histone H3 by the monoclonal antibody we used. Arrowheads indicate an example of a pericentric area where H3K9me3 and H3 are mutually exclusive. Scale bars are 25  $\mu\text{m}$ . **(b)** Distribution of fluorescence intensity over one chromosome arm of the chromosome indicated with an arrowhead in panel a, both after the first and second round of immunostaining. Centromeric enrichment of INCENP and H3K9me3 are clearly visible as a peak in fluorescence intensity.

First, ATDC5 chromosome spreads were incubated with rabbit-anti-H2ApT120 and human anti-centromere antibodies (ACA) (Figure 4). After stripping, the same slides were incubated with rabbit-anti-H3pT3 and ACA. Dynamic phosphorylation patterns described for H3pT3 and H2ApT120 during mitosis [9] can be observed simultaneously on the same chromosome spread. In early prometaphase, small H2ApT120 foci are found localizing to the centromeres, whereas H3pT3 is detected both on chromosome arms and around the centromeres. At late prometaphase, H2ApT120 signal size has increased and H3pT3 has disappeared from the arms and is concentrated at the inner centromere. These results illustrate that the stripping method allows spatio-temporal localization of different epitopes when only antibodies raised in the same host species are available.

Second, we stained chromosomes of human oocytes (Figure 5a) with mouse-anti-INCENP and H3K9me3 (rabbit) antibodies. After stripping, we immunostained these chromosomes using mouse-anti-H3 and rabbit-anti-H3pT3 antibodies. Oocyte chromosomes had the typical, highly condensed, appearance [30] and showed an overall staining for H3K9me3 and H3, similar to what has been described in mouse oocytes [31-33]. INCENP and H3pT3 seem to only partially colocalize (Figure 5b) at the pericentric region, different from what has been described for somatic cells [9,25]. These results show that when material is rare, it can successfully be used for two rounds of immunofluorescent staining.

Third, we stained nuclear spreads of mouse spermatocytes using rabbit-anti-SYCP3 antibodies (Figure 6). SYCP3 staining allows staging of meocytes by detecting formation of the synaptonemal complex [34], and the antibody derived by Lammers et al. [20] is widely used for this purpose and well-characterized [35-39]. After imaging of different stages of spermatocytes, the slides were stripped and stained for H3K9me3. This way we were able to determine both the stage of the cells during meiotic prophase and the distribution of the histone mark in those same cells, while using two antibodies raised in rabbit. Shown are pictures of spermatocytes of three meiotic stages: early pachytene, mid pachytene and diplotene. In early pachytene H3K9me3 was enriched on the XY-body, the transcriptionally silenced X and Y chromosomes in the meiotic prophase, followed by a reduction during mid pachytene, whereas by the diplotene stage, trimethylation levels on H3K9 were again increased on the X and Y chromosome [18,40]. Staging cells by an SYCP3 staining, followed by a staining for other proteins or epigenetic marks provides information about the presence and localization of these epitopes during specific stages of the meiotic prophase of spermatogenesis.

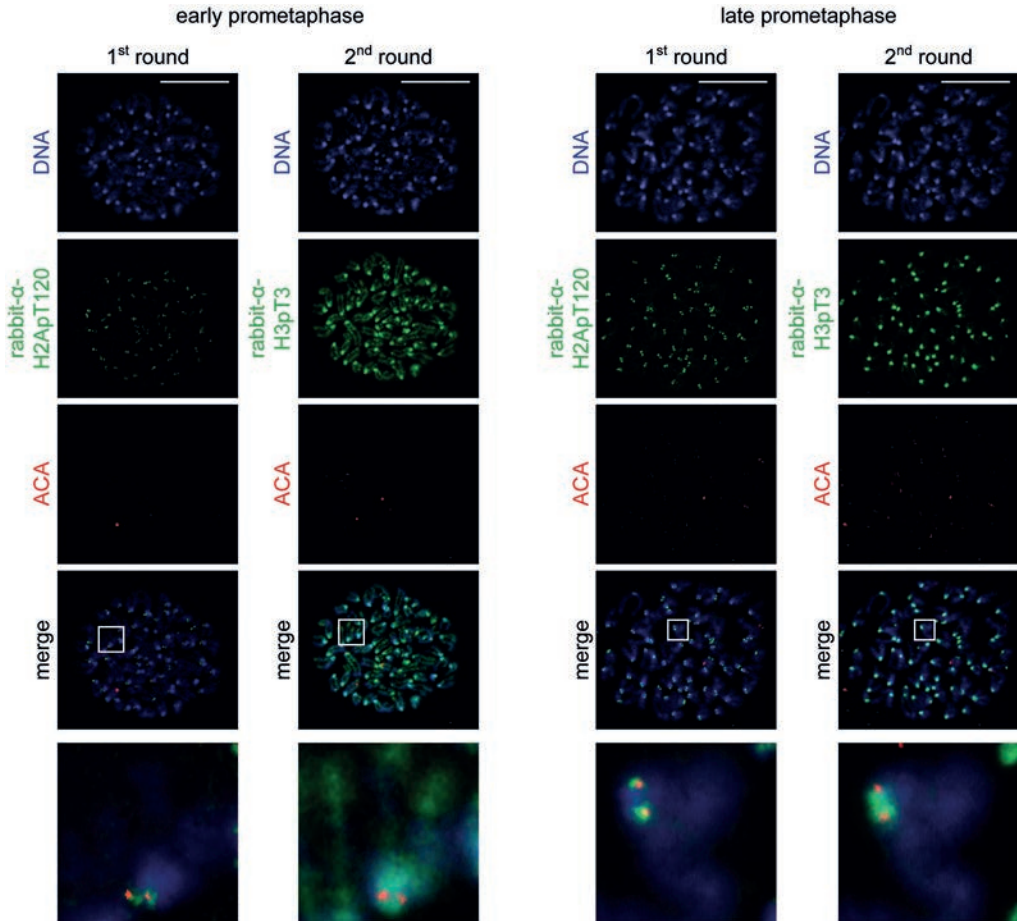
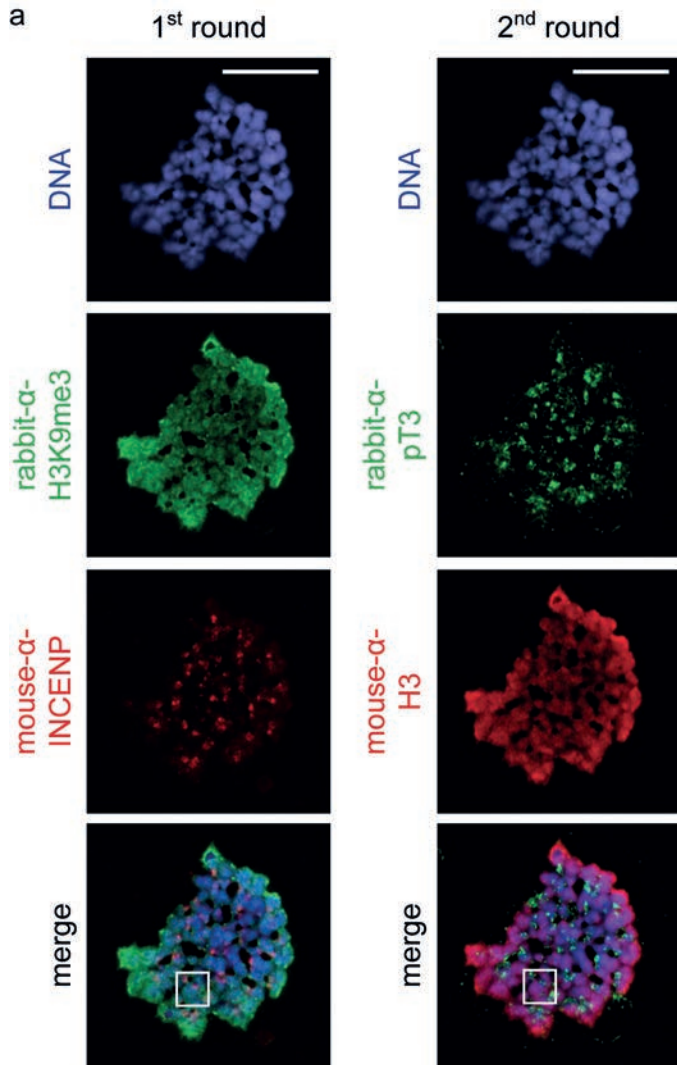


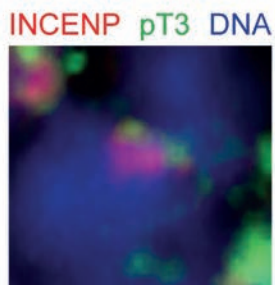
Figure 4 — Application of the stripping protocol, demonstrated by immunofluorescent detection of H2ApT120 and the centromeres (ACA) on chromosomes from ATDC5 cells, followed by stripping and a second round of immunostaining for H3pT3 and ACA. In early prometaphase (left), H2ApT120 was detected around the centromeres and H3pT3 both around the centromeres and on the chromosome arms. In late prometaphase (right), H2ApT120 signal size has increased at the centromeres and H3pT3 is enriched at the inner centromere. Enlarged regions at the bottom show a single chromosome. Scale bars are 25 μm.

Figure 5 — (a) Application of the stripping protocol, demonstrated by immunolocalization of INCENP and H3K9me3 on a chromosome spread from a human oocyte, followed by stripping and a second round of immunostaining for H3 and H3pT3. Chromosomes show typical condensed morphology and high levels of H3K9 trimethylation. Scale bars are 10 μm. (b) Zoom-in of a chromosome from a merged image showing INCENP and H3pT3 signal. INCENP is localized at the inner centromere and H3pT3 at the centromeres, with only limited signal overlap.





**b** merge of 1<sup>st</sup> and 2<sup>nd</sup> round



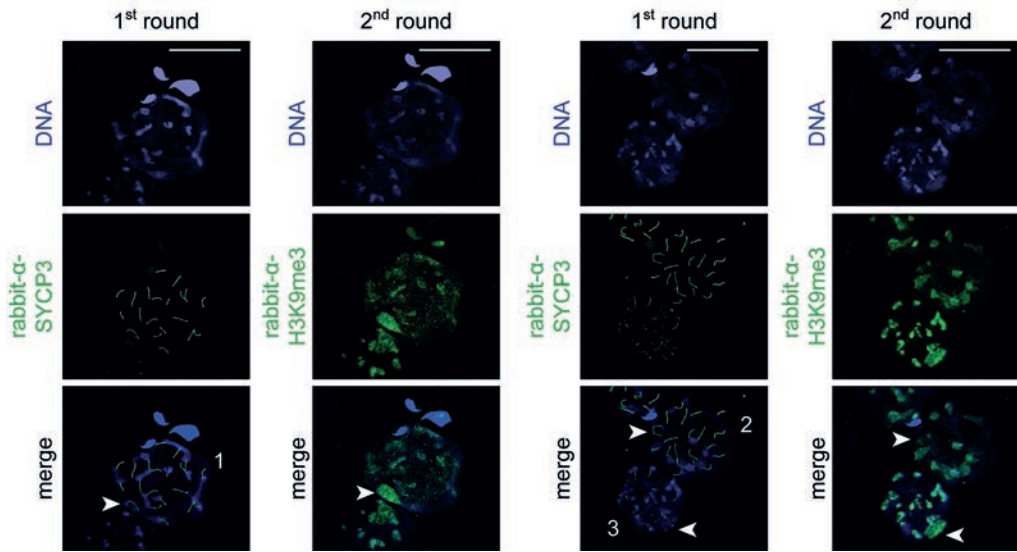


Figure 6 — Application of the stripping protocol, demonstrated by immunofluorescent detection of SYCP3 on mouse spermatocytes, followed by stripping and a second round of immunostaining for H3K9me3. Numbers indicate meiotic prophase stages (1: early pachytene, 2: mid pachytene, 3: diplotene) and arrowheads indicate XY-bodies. As expected, H3K9 trimethylation levels are high on sex body chromatin during early pachytene, decrease towards mid pachytene and are increased again at the diplotene stage. Scale bars are 25  $\mu\text{m}$ .

## Discussion

In this study we aimed to develop a protocol for sequential immunofluorescence on chromosome spreads. We were able to erase the first immunofluorescent staining using a stripping buffer designed for Western Blot membranes, while leaving chromosome morphology and epitopes intact for a second round of detection.

First, we optimized a surface spreading protocol described for gametes and embryos, for cultured cells from different cell lines and species. This protocol is a good alternative for the cytopsin technique; it is cheaper, does not require special equipment and gives good chromosome morphology. However, some care should be taken when interpreting results, as the drying down procedure results in removal of soluble proteins and loss of the 3D structure [19]. Furthermore, the spreading technique may cause stretching of the chromosome and increased signal sizes. This has also been described when comparing cytopsin preparations with whole mount preparations for localization of the chromosomal passenger complex for a chromosome with a neocentromere [41]. AURKB signal size was observed to be measurably increased after cytopsin, but found to be normal in whole mount preparations. Therefore, results from chromosome spread techniques should preferably be compared with findings in whole mount fixed cells, as these techniques can provide complementary information [19].

With chromosomes attached firmly to a microscope slide after surface spreading, we investigated if stripping buffers designed for Western Blots are able to remove antibodies from chromosome spreads. We tested four different stripping solutions and show that in our hands stripping with Restore™ PLUS Western Blot Stripping Buffer was most efficient, as well as fast, with an incubation time of only 10 minutes. Different stripping solutions have been described in literature, based on high salt concentrations, detergent or low pH, or a combination of those. The manufacturer did not provide details on the composition of the Restore™ PLUS Western Blot Stripping Buffer, but as the pH is 2.4, its formulation may be based on a low pH glycine hydrochloride solution. However, the GlyHCl solution we tested here, based on the solution described by Legocki and Verma [21], did not strip effectively. In contrast, the GnHCl solution we tested, based on the solution described by Yeung and Stanley [12], was almost as efficient as the Restore™ PLUS Western Blot Stripping Buffer. This suggests that the Restore™ PLUS Western Blot Stripping Buffer may combine a high concentration of chaotropic salts with a low pH. It also suggests that with some further optimization, a guanidine hydrochloride solution may constitute a cheaper alternative for this purpose.

Using the Restore™ PLUS Western Blot Stripping Buffer, we show that stripping does not severely affect chromosomes and attached proteins, as they could be readily detected in a second round of immunofluorescent staining. However, a small but significant reduction of fluorescence intensity could be observed after the second round of detection (Figure 2b), indicating that some loss of epitope or protein may occur after stripping. This should be taken into account when quantification of signal is desired.

Although we were able to efficiently remove every antibody tested, the stripping procedure shows some variation between different antibodies. As the reduction in fluorescence intensity we found was relative, antibodies with a very high epitope affinity and/or initial fluorescence intensity in the first round, may still be detectable after stripping, especially with increased exposure times. Stripping efficiency should thus be validated for every antibody separately. The problem of residual signals is known from Western blot membranes and can sometimes be remedied by increasing incubation times and temperatures of the stripping buffer. In general, we recommend that high affinity antibodies should be used in the second round of detection, or that interference of residual staining with interpretation of results from a second round of immunolocalization is otherwise excluded.

We anticipate that this stripping protocol will provide a versatile new tool for the study of chromosomes and chromatin, and envision many applications. We show sequential immunofluorescent stainings on different cell types, among which mouse spermatocytes and human oocytes. The ability to perform two immunofluorescent stainings on the same material is particularly useful in our studies on chromosome segregation and chromatin structure in human oocytes and preimplantation embryos, since this material is rare and valuable. Nonetheless, this protocol is useful for broad variety of cell types, because it creates the possibility to investigate the localization of proteins that are detected by antibodies from the same species. In this way, it is possible to show direct colocalization and protein dynamics in different cell cycle stages on the same chromosomes. This method will therefore greatly increase our insight into the complex

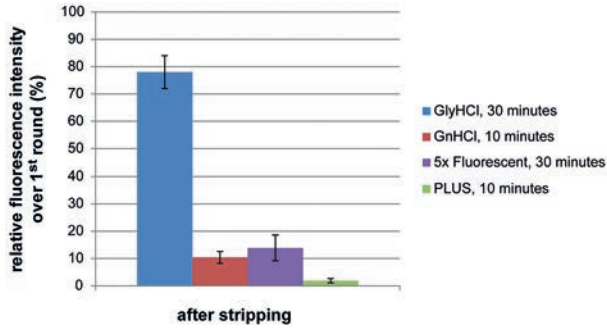
interplay of control mechanisms governing chromosome structure and regulation of segregation during mitosis.

### **Ethical standards**

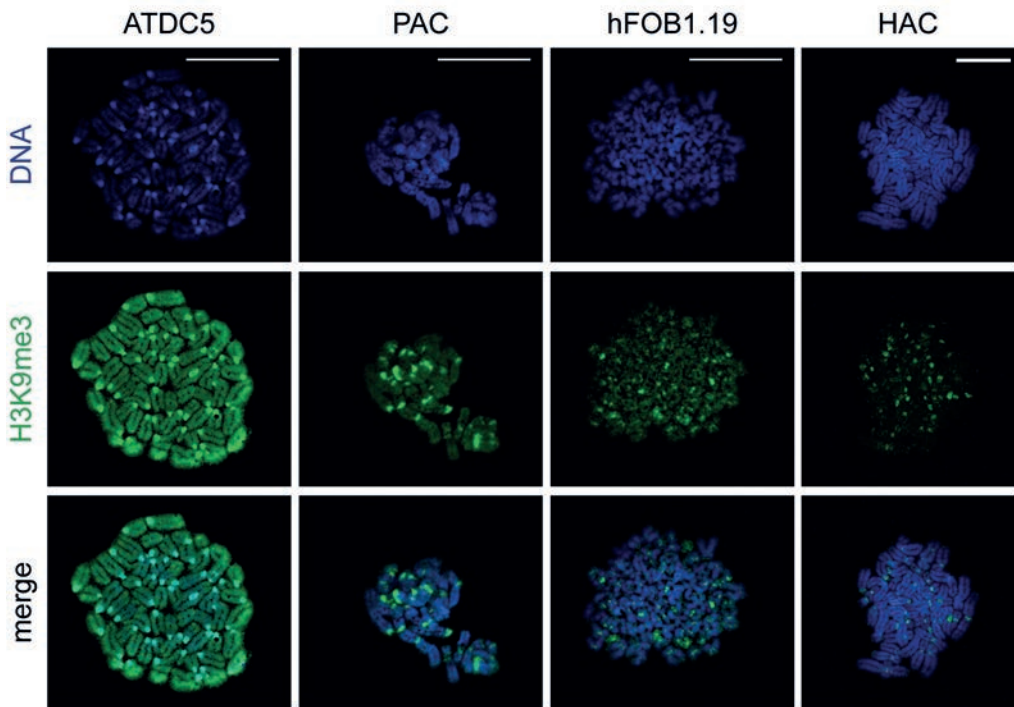
The experiments performed in this study comply with the current laws in The Netherlands. All procedures followed were in accordance with the ethical standards of the responsible committee on human experimentation and with the Helsinki Declaration of 1975, as revised in 2000. The use of surplus material for the derivation of human articular chondrocytes was approved by the local ethical committee (MEC2004-322). The use of human oocytes for research purposes was approved by the Dutch Central Committee on Research involving Human Subjects (CCMO NL38053.000.11). All institutional and national guidelines for the care and use of laboratory animals were followed.

### **Acknowledgments**

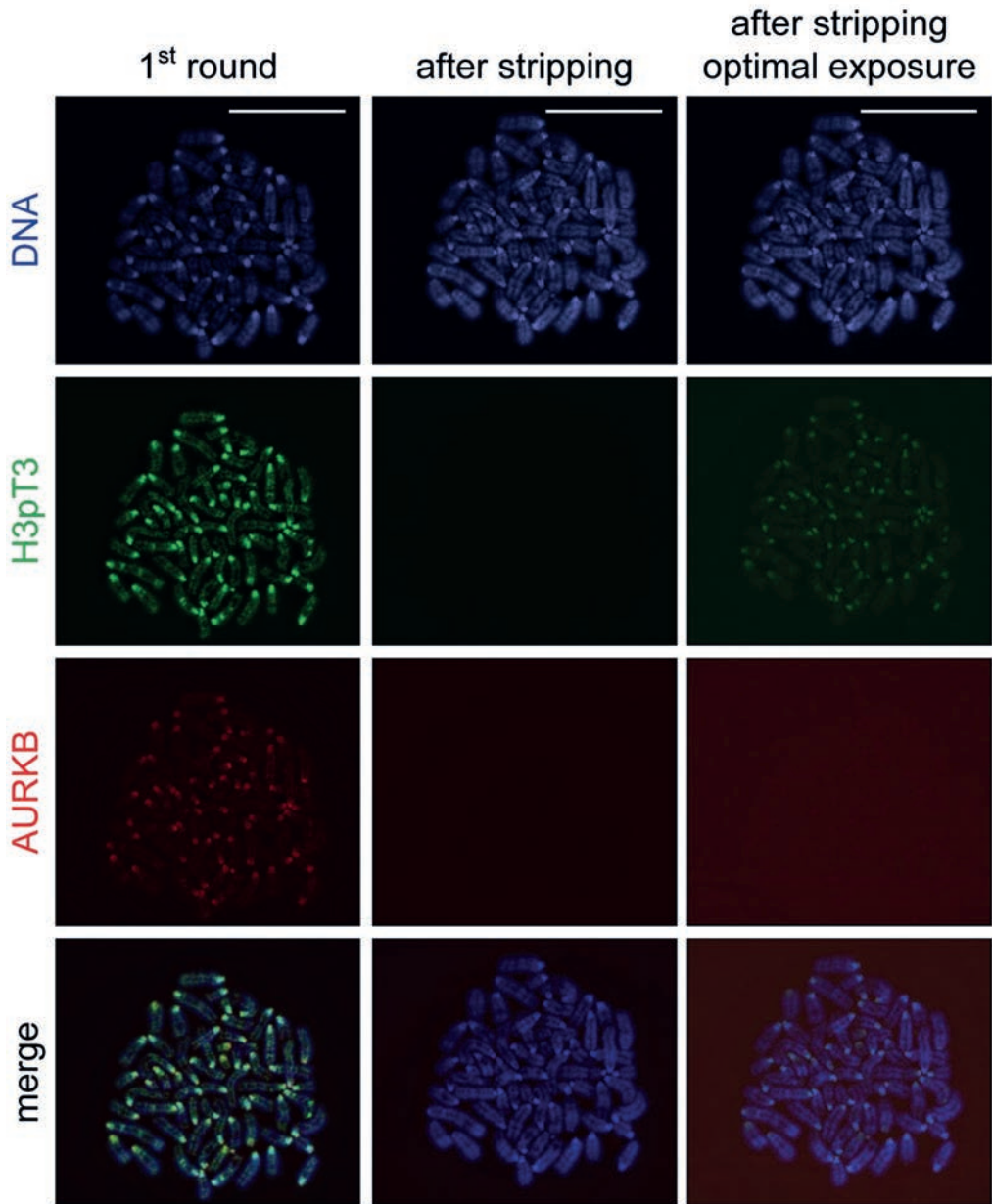
We thank W.M. Baarends (Erasmus MC, University Medical Center Rotterdam, The Netherlands) for the generous gift of nuclear spreads of spermatocytes, as well as the SYCP3 antibody. This work was funded by a grant from Fundação para a Ciência e Tecnologia (SFRH/BD/39 063/2007) to Margarida Avo Santos and from the Netherlands Organisation for Scientific Research (NWO-Veni: ZonMW 016.096.106) to Esther B. Baart. This research was performed within the framework of the Erasmus Postgraduate School Molecular Medicine.



Online Resource 1 — Relative fluorescence intensity of H3K9me3 after stripping with four different stripping solutions: GlyHCl, GnHCl, Restore™ Fluorescent Western Blot Stripping Buffer (Fluorescent), and Restore™ PLUS Western Blot Stripping Buffer (PLUS). Shown are mean values and standard deviations of 10 HAC chromosome spreads.



Online Resource 2 — Immunolocalization of H3K9me3 on chromosome spreads of four different cell types (ATDC5, PAC, hFOB1.19, and HAC) illustrating the applicability of the spreading protocol. Chromosome spreads show good chromosome resolution and differences in localization of regions enriched for the H3K9me3 mark between species. Scale bars are 25  $\mu$ m.



Online Resource 3 — Same figure as Figure 2, but with a panel added showing that when the exposure time was increased using optimal exposure settings in the Isis software, residual signal could be detected after stripping (third panel). Scale bars are 25  $\mu\text{m}$ .

## References

1. Stenman, S., M. Rosenqvist, and N.R. Ringertz, *Preparation and spread of unfixed metaphase chromosomes for immunofluorescence staining of nuclear antigens*. *Exp Cell Res*, 1975. **90**(1): p. 87-94.
2. Saffery, R., et al., *Human centromeres and neocentromeres show identical distribution patterns of >20 functionally important kinetochore-associated proteins*. *Hum Mol Genet*, 2000. **9**(2): p. 175-85.
3. Jelluma, N., et al., *Mps1 phosphorylates Borealin to control Aurora B activity and chromosome alignment*. *Cell*, 2008. **132**(2): p. 233-246.
4. Simerly, C. and G. Schatten, *Techniques for localization of specific molecules in oocytes and embryos*. *Methods Enzymol*, 1993. **225**: p. 516-53.
5. Hodges, C.A. and P.A. Hunt, *Simultaneous analysis of chromosomes and chromosome-associated proteins in mammalian oocytes and embryos*. *Chromosoma*, 2002. **111**(3): p. 165-9.
6. Peters, A.H., et al., *A drying-down technique for the spreading of mammalian meiocytes from the male and female germline*. *Chromosome Res*, 1997. **5**(1): p. 66-8.
7. Avo Santos, M., et al., *A role for Aurora C in the chromosomal passenger complex during human preimplantation embryo development*. *Hum Reprod*, 2011. **26**(7): p. 1868-81.
8. Chambon, J.P., K. Hached, and K. Wassmann, *Chromosome spreads with centromere staining in mouse oocytes*. *Methods Mol Biol*, 2013. **957**: p. 203-12.
9. Yamagishi, Y., et al., *Two histone marks establish the inner centromere and chromosome bi-orientation*. *Science*, 2010. **330**(6001): p. 239-43.
10. Kaufmann, S.H., C.M. Ewing, and J.H. Shaper, *The erasable Western blot*. *Anal Biochem*, 1987. **161**(1): p. 89-95.
11. Kar, P., et al., *A protocol for stripping and reprobing of Western blots originally developed with colorimetric substrate TMB*. *Electrophoresis*, 2012. **33**(19-20): p. 3062-5.
12. Yeung, Y.G. and E.R. Stanley, *A solution for stripping antibodies from polyvinylidene fluoride immunoblots for multiple reprobing*. *Anal Biochem*, 2009. **389**(1): p. 89-91.
13. Atsumi, T., et al., *A chondrogenic cell line derived from a differentiating culture of AT805 teratocarcinoma cells*. *Cell Differ Dev*, 1990. **30**(2): p. 109-16.
14. Caron, M.M., et al., *Osmolarity determines the in vitro chondrogenic differentiation capacity of progenitor cells via nuclear factor of activated T-cells 5*. *Bone*, 2013. **53**(1): p. 94-102.
15. Harris, S.A., et al., *Development and characterization of a conditionally immortalized human fetal osteoblastic cell line*. *J Bone Miner Res*, 1995. **10**(2): p. 178-86.
16. van der Windt, A.E., et al., *Inhibiting calcineurin activity under physiologic tonicity elevates anabolic but suppresses catabolic chondrocyte markers*. *Arthritis Rheum*, 2012. **64**(6): p. 1929-39.
17. Hohmann, F.P., N.S. Macklon, and B.C. Fauser, *A randomized comparison of two ovarian stimulation protocols with gonadotropin-releasing hormone (GnRH) antagonist cotreatment for in vitro fertilization commencing recombinant follicle-stimulating hormone on cycle day 2 or 5 with the standard long GnRH agonist protocol*. *J Clin Endocrinol Metab*, 2003. **88**(1): p. 166-73.
18. Baarends, W.M., et al., *Silencing of unpaired chromatin and histone H2A ubiquitination in mammalian meiosis*. *Mol Cell Biol*, 2005. **25**(3): p. 1041-53.
19. Baart, E.B., et al., *Distribution of Atr protein in primary spermatocytes of a mouse chromosomal mutant: a comparison of preparation techniques*. *Chromosoma*, 2000. **109**(1-2): p. 139-147.
20. Lammers, J.H., et al., *The gene encoding a major component of the lateral elements of synaptonemal complexes of the rat is related to X-linked lymphocyte-regulated genes*. *Mol Cell Biol*, 1994. **14**(2): p. 1137-46.
21. Legocki, R.P. and D.P. Verma, *Multiple immunoreplica Technique: screening for specific proteins with a series of different antibodies using one polyacrylamide gel*. *Anal Biochem*, 1981. **111**(2): p. 385-92.
22. Peters, A.H., et al., *Loss of the Suv39h histone methyltransferases impairs mammalian heterochromatin and genome stability*. *Cell*, 2001. **107**(3): p. 323-37.
23. Sullivan, B.A. and G.H. Karpen, *Centromeric chromatin exhibits a histone modification pattern that is distinct from both euchromatin and heterochromatin*. *Nat Struct Mol Biol*, 2004. **11**(11): p. 1076-83.

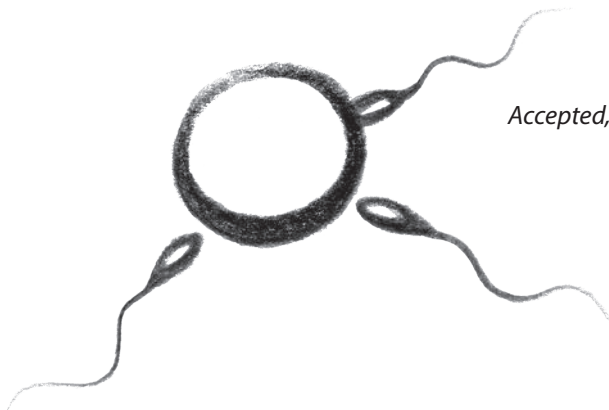
24. Alonso, A., et al., *A paucity of heterochromatin at functional human neocentromeres*. Epigenetics Chromatin, 2010. **3**(1): p. 6.
25. Wang, F., et al., *A positive feedback loop involving Haspin and Aurora B promotes CPC accumulation at centromeres in mitosis*. Curr Biol, 2011. **21**(12): p. 1061-9.
26. Kumagai, I. and K. Tsumoto, *Antigen–Antibody Binding*, in eLS. 2001, John Wiley & Sons, Ltd.
27. Hendzel, M.J., et al., *Mitosis-specific phosphorylation of histone H3 initiates primarily within pericentromeric heterochromatin during G2 and spreads in an ordered fashion coincident with mitotic chromosome condensation*. Chromosoma, 1997. **106**(6): p. 348-60.
28. Crosio, C., et al., *Mitotic phosphorylation of histone H3: spatio-temporal regulation by mammalian Aurora kinases*. Mol Cell Biol, 2002. **22**(3): p. 874-85.
29. Vagnarelli, P. and W.C. Earnshaw, *Chromosomal passengers: the four-dimensional regulation of mitotic events*. Chromosoma, 2004. **113**(5): p. 211-222.
30. Pellestor, F., et al., *Mechanisms of non-disjunction in human female meiosis: the co-existence of two modes of malsegregation evidenced by the karyotyping of 1397 in-vitro unfertilized oocytes*. Hum Reprod, 2002. **17**(8): p. 2134-45.
31. Santos, F., et al., *Dynamic chromatin modifications characterise the first cell cycle in mouse embryos*. Dev Biol, 2005. **280**(1): p. 225-36.
32. Meglicki, M., M. Zientarski, and E. Borsuk, *Constitutive heterochromatin during mouse oogenesis: the pattern of histone H3 modifications and localization of HP1alpha and HP1beta proteins*. Mol Reprod Dev, 2008. **75**(2): p. 414-28.
33. Puschendorf, M., et al., *PRC1 and Suv39h specify parental asymmetry at constitutive heterochromatin in early mouse embryos*. Nature genetics, 2008. **40**(4): p. 411-420.
34. Yang, F. and P.J. Wang, *The Mammalian synaptonemal complex: a scaffold and beyond*. Genome Dyn, 2009. **5**: p. 69-80.
35. Scully, R., et al., *Association of BRCA1 with Rad51 in mitotic and meiotic cells*. Cell, 1997. **88**(2): p. 265-75.
36. Eijpe, M., et al., *Association of mammalian SMC1 and SMC3 proteins with meiotic chromosomes and synaptonemal complexes*. J Cell Sci, 2000. **113** ( Pt 4): p. 673-82.
37. Baarends, W.M., et al., *Loss of HR6B ubiquitin-conjugating activity results in damaged synaptonemal complex structure and increased crossing-over frequency during the male meiotic prophase*. Mol Cell Biol, 2003. **23**(4): p. 1151-62.
38. de Boer, E. and C. Heyting, *The diverse roles of transverse filaments of synaptonemal complexes in meiosis*. Chromosoma, 2006. **115**(3): p. 220-34.
39. Schoenmakers, S., et al., *Female meiotic sex chromosome inactivation in chicken*. PLoS Genet, 2009. **5**(5): p. e1000466.
40. van der Heijden, G.W., et al., *Chromosome-wide nucleosome replacement and H3.3 incorporation during mammalian meiotic sex chromosome inactivation*. Nature genetics, 2007. **39**(2): p. 251-258.
41. Bassett, E.A., et al., *Epigenetic centromere specification directs aurora B accumulation but is insufficient to efficiently correct mitotic errors*. J Cell Biol, 2010. **190**(2): p. 177-85.



# CHAPTER 5

## **Chromosome segregation regulation in human zygotes: altered mitotic histone phosphorylation dynamics underlying centromeric targeting of the chromosomal passenger complex**

Christine van de Werken, Margarida Avo Santos,  
Joop S.E. Laven, Cindy Eleveld, Bart C.J.M. Fauser,  
Susanne M.A. Lens, Esther B. Baart



*Accepted, Human Reproduction*

## Abstract

**Study question:** Are the kinase feedback loops, that regulate activation and centromeric targeting of the chromosomal passenger complex (CPC), functional during mitosis in human embryos?

**Summary answer:** Investigation of the regulatory kinase pathways involved in centromeric CPC targeting revealed normal phosphorylation dynamics of Histone H2A at T120 (H2ApT120) by Bub1 kinase and subsequent recruitment of Shugoshin, but phosphorylation of Histone H3 at threonine 3 (H3T3) by Haspin failed to show the expected centromeric enrichment on metaphase chromosomes in the zygote.

**What is known already:** Human cleavage stage embryos show high levels of chromosomal instability. What causes this high error rate is unknown, as mechanisms used to ensure proper chromosome segregation in mammalian embryos are poorly described.

**Study design, size, duration:** In this study we investigated the pathways regulating CPC targeting to the inner centromere in human embryos. We characterized the distribution of the CPC in relation to activity of its two main centromeric targeting pathways: the Bub1-H2ApT120-Sgo-CPC and Haspin-H3pT3-CPC pathways.

**Participants/materials, setting, methods:** The study was conducted between May 2012 and March 2014 on human surplus embryos resulting from in vitro fertilization treatment and donated for research. In zygotes, nuclear envelope breakdown was monitored by time-lapse imaging to allow timed incubations with specific inhibitors to arrest at prometaphase and metaphase, and to interfere with Haspin and Aurora B/C kinase activity. Functionality of the targeting pathways was assessed through characterization of histone phosphorylation dynamics by immunofluorescent analysis, combined with gene expression by RT-qPCR and immunofluorescent localization of key pathway proteins.

**Main results and the role of chance:** Immunofluorescent analysis of the CPC subunit INCENP revealed the pool of stably bound CPC proteins not to be strictly confined to the inner centromere of prometaphase chromosomes in human zygotes, as observed in later stages of preimplantation development and somatic cells. Investigation of the regulatory kinase pathways involved in centromeric CPC targeting revealed normal phosphorylation dynamics of Histone H2A at T120 (H2ApT120) by Bub1 kinase and subsequent recruitment of Shugoshin. However, phosphorylation of Histone H3 at threonine 3 (H3T3) by Haspin kinase failed to show the expected centromeric enrichment on metaphase chromosomes in the zygote, but not at later stages. Inhibition of Haspin revealed this activity to be essential for proper MCC activation in human zygotes, thus demonstrating an active mitotic checkpoint under normal conditions. Abolishment of H3pT3 during zygotic prometaphase further shows that centromeric H2ApT120 alone is not sufficient for proper shugoshin and CPC localization. As removal of H3pT3 from the chromosome arms during

prometaphase normally contributes to further centromeric enrichment of the CPC in somatic cells, CPC targeting may be less accurate in human zygotes.

**Limitations, reasons for caution:** Due to ethical limitations, tripronuclear zygotes were used in functional experiments. Although it is the best available model, it is unknown if they are completely representative for dipronuclear zygotes. In addition, further research is needed to determine to what extent the differences we observed in H3T3 phosphorylation dynamics and CPC localization affect chromosome attachment.

**Wider implications of the findings:** In the zygote, paternal and maternal chromosomes coming from two separate pronuclei, and with contrasting epigenetic signatures, need to be aligned on a single metaphase plate. Our results suggest that adaptations in mechanisms regulating CPC targeting exist in the human zygote, to ensure symmetric recruitment despite the epigenetic asymmetry between maternal and paternal chromosomes. This adaptation may come at a price regarding chromosome segregation fidelity.

**Study funding/competing interest(s):** This study was funded by the Portuguese Fundação para a Ciência e Tecnologia and the Netherlands Organisation for Scientific Research. The authors have no conflicts of interest to declare.

**Key words:** human embryo research, chromosome segregation, Aurora kinase, Haspin kinase, histone phosphorylation

## Introduction

When cells divide, duplicated chromosomes (sister chromatids) have to be divided equally between the resulting daughter cells to ensure genome stability. Normally, errors in this process are rare, as cells are equipped with elaborate mechanisms that regulate and monitor chromosome segregation. Remarkably, chromosome aneuploidies are frequently observed in human pre-implantation IVF embryos [1-2]. Some of these aneuploidies are of meiotic origin, but we and others have shown that most of them occur post-meiotically, as a result of errors during the cleavage divisions [3-5]. The proportion of aneuploid cells within an embryo subsequently declines towards the blastocyst stage [4,6-8], suggesting that chromosome segregation mechanisms are especially error-prone during the cleavage divisions. This high error rate has been compared to that reported in human cancer cells [5], although the underlying molecular mechanisms contributing to errors during the cleavage divisions of human pre-implantation embryos remain largely unknown.

At the onset of mitosis, chromatin is rearranged into mitotic chromosomes, and multi-protein structures called kinetochores are assembled on the centromeres. Accurate chromosome segregation is dependent on the ability of these kinetochores to capture microtubules of the mitotic spindle and subsequently form bipolar attachments. Anaphase onset is controlled by the ubiquitin ligase anaphase-promoting complex/cyclosome (APC/C), together with cell division control protein 20 (CDC20) [9-11]. This complex initiates anaphase by targeting two proteins for degradation: Cyclin B that regulates cyclin dependent kinase 1 (CDK1) and securing that protects sister chromatid cohesion [12]. Until bi-orientation of all chromosomes is achieved, anaphase is delayed by action of the mitotic checkpoint (MC), also known as the spindle assembly checkpoint. The MC is formed by the kinases monopolar spindle protein 1 (Mps1) and budding uninhibited by benomyl 1 (Bub1), the pseudo-kinase Bub1-related 1 (BubR1) and the non-enzymatic components mitotic arrest deficient 1 (Mad1), Mad2 and Bub3. These proteins are recruited to unattached kinetochores, where they catalyze the formation of the mitotic checkpoint complex (MCC), consisting of CDC20 together with Mad2, Bub3 and BubR1. The MCC is released into the cytoplasm where it inactivates the APC/C (for review see [13-14]).

Chromosome attachment to the spindle is achieved through a stochastic trial-and-error process, whereby active destabilization of erroneous attachments is necessary to provide a new opportunity to attach in a bi-oriented fashion. Aurora B kinase is a key player in this mechanism of attachment-error-correction [15]. Aurora B belongs to a family of serine-threonine kinases that is conserved from yeast to humans. This kinase is a member of the Chromosomal Passenger Complex (CPC), together with the Inner Centromere Protein (INCENP), Borealin and Survivin [15-16]. However, in human cleavage stage embryos the main kinetic subunit of the CPC is an alternative subunit called Aurora C kinase [17]. Aurora C is capable to fully support mitotic progression in the absence of Aurora B in human somatic cells [18] and mouse embryo development [19]. Although the need for an alternative Aurora kinase remains poorly understood, Aurora C has been shown to have improved protein stability during the cleavage divisions in mouse embryos [20]. In addition, the function of Aurora C seems to be distinct from Aurora B during female mouse meiosis I, where loss of Aurora C function

results in erroneous microtubule attachments, but the mitotic checkpoint and cytokinesis remain undisturbed [21].

The mammalian CPC enriches at the inner centromere during prometaphase [22]. The inner centromere of the chromosome folds between the centromeres and within the pericentric heterochromatin (pHC). Pericentric HC is characterized by high levels of trimethylation on lysine residue 9 of histone H3 (H3K9me<sub>3</sub>; for review see [23] and disruption of this signature is associated with chromosome instability [24]. H3K9me<sub>3</sub> is known to recruit the three iso-forms of heterochromatin protein 1 (HP1 $\alpha$ ,  $\beta$ , and  $\gamma$ ), which are important for heterochromatin structure and function [25]. During mitosis, phosphorylation of serine residue 10 on histone H3 (H3pS10) by Aurora B disrupts the HP1-H3K9me<sub>3</sub> interaction and releases HP1 from chromatin [26] (Figure 1a). HP1 $\alpha$  also undergoes mitosis-specific phosphorylation, resulting in a population of HP1 $\alpha$  that remains at the inner centromere, independent of H3K9me<sub>3</sub> and possibly by interacting with INCENP [27-28]. This phosphorylated form of HP1 $\alpha$  facilitates the localization of the shugoshin protein 1 (Sgo1), which is crucial for protecting centromeric cohesion and the prevention of premature sister chromatid separation [28-29]. Next to their role in cohesion protection, both shugoshin proteins Sgo1 and Sgo2 are essential for CPC localization, as they bind to Borealin [30,31].

During mitosis, the inner centromere shows further dynamic phosphorylation of histones, further promoting CPC recruitment and localization [30-34]. It has been proposed that CPC targeting depends on two distinct histone modifications: phosphorylation of histone H3 at Thr 3 (H3pT3) by the kinase Haspin and phosphorylation of histone H2A at Thr 120 (H2ApT120) by Bub1 kinase (Figure 1a) [34]. Bub1, a mitotic kinase that localizes to the kinetochores, phosphorylates histone H2A on centromeric heterochromatin, creating a binding site for Sgo1 and Sgo2 that in turn recruit the CPC through Borealin [31,35-36]. Since Aurora B activity is needed to recruit Bub1 to the kinetochore, a positive feedback loop is created in this Bub1-H2ApT120-Sgo-CPC pathway, ensuring CPC recruitment to the inner centromere [15,37].

Phosphorylation of H3T3 by Haspin starts at late G2 / early prophase and by late prophase it has spread along the chromosome arms. This mark recruits the CPC, as Survivin binds to H3pT3 [32-33]. Phosphorylation of Haspin by Aurora B promotes full phosphorylation of H3pT3, creating a positive feedback loop between Aurora B and Haspin [37] (Figure 1a). At prometaphase, H3pT3 disappears from the arms and enriches at the inner centromeres [34,38]. The dephosphorylation of H3pT3 at the chromosome arms is specifically regulated by the phosphatase activity of protein phosphatase PP1 $\gamma$  together with its regulatory subunit Repo-Man [39]. Aurora B phosphorylates Repo-Man, thereby preventing its chromosomal targeting and supporting H3pT3 levels [40]. Repo-man also associates with the phosphatase PP2A, which opposes Aurora B phosphorylation of Repo-Man, thereby allowing the removal of H3pT3 from the chromosome arms during prometaphase [40]. These feedback loops between Aurora B and Haspin, as well as Aurora B and its opposing phosphatases regulate the levels of H3pT3 and ensure enrichment of the mark and the CPC at the inner centromere [22]. Mounting evidence also indicates that centromeric enrichment of the CPC through the Bub1-H2ApT120-Sgo-CPC pathway enhances the Haspin-H3pT3-CPC phosphorylation pathway and vice versa [15,37,41]. Thus, extensive and elaborate feedback mechanisms exist, resulting in precisely timed events leading to robust CPC localization to the inner centromeres.

Although the embryonic cleavage divisions are mitotic divisions, as opposed to the previous meiotic divisions, they differ from normal mitosis in many aspects [42]. In mammalian zygotes, the paternal and maternal genomes exist in an asymmetric chromatin configuration, where only the maternal chromatin has high levels of H3K9me3 [43]. For the paternal chromatin configuration, important species differences exist: in the mouse zygote, the paternal chromatin is mostly devoid of H3K9me3 and HP1, and pHC is formatted up to the 8-cell stage by an alternative mechanism involving the polycomb group proteins [44]. In contrast, human paternal pHC is marked by H3K9me3 that was transmitted to the zygote by the sperm [45]. During the first mitotic division, these asymmetric chromosomes, derived from two different pronuclei, need to align on the same metaphase plate. As described above, pHC structure underlies chromosome segregation regulation. We therefore hypothesize that the parental asymmetry in the early embryo may require adaptations in the mechanisms regulating chromosome segregation.

In this study, we aim to explore if the epigenetic asymmetry and the presence of Aurora C kinase affect the pathways regulating CPC targeting to the inner centromere in human embryos. We characterized CPC localization in relation to activity of the Bub1-H2ApT120-Sgo-CPC and Haspin-H3pT3-CPC pathways. In addition, we explore the contribution of the H3K9me3/HP1 $\alpha$  pathway to Sgo1 and CPC localization. Although our observations are mostly in line with the mechanisms described in somatic cells, the Haspin-H3pT3-CPC pathway is altered in zygotes and targeting of the CPC is less confined to the inner centromere. Furthermore, paternal and maternal chromosomes are differentially affected by interference with Haspin and Aurora kinase activity, leading us to hypothesize that the persisting Haspin activity on the arms is required for symmetrical CPC recruitment despite the underlying epigenetic asymmetry.

## Materials and Methods

### Ethical approval

The study was conducted between May 2012 and March 2014. The use of surplus embryos was approved by the Dutch Central Committee on Research Involving Human Subjects (CCMO NL38053.000.11) and the local institutional ethics committee.

### *Chemicals, reagents and inhibitors*

All chemicals and reagents were from Sigma-Aldrich (USA) unless otherwise stated. The following inhibitors and concentrations were used: colcemid (1.5  $\mu\text{g}/\text{ml}$ , Invitrogen, USA), MG132 (20  $\mu\text{M}$ ), 5-Iodotubercidin (Itu) (10  $\mu\text{M}$ , Tocris Bioscience, UK), ZM447439 (2  $\mu\text{M}$  or 20  $\mu\text{M}$ , Tocris Bioscience). Colcemid was dissolved in culture medium. Stock solutions for all other inhibitors were prepared at a 1000x concentration in DMSO, so the final concentration of DMSO in the culture medium never exceeded 0.1%.

### Culture, collection and treatment of human pre-implantation embryos

Tripronuclear embryos (3PN) were used to study the first and second cleavage divisions (days 1 and 2 post-fertilization). This type of abnormal fertilization occurs in ~4% of all inseminated oocytes and these embryos are unsuitable for transfer to the patient due to their triploid constitution [46]. 3PN zygotes mostly originate from an oocyte that is fertilized by two spermatozoa, resulting in one maternal pronucleus and two paternal pronuclei [47]. Since the first embryonic divisions are under maternal control [48] and 3PN zygotes are capable of implantation, they provide a relevant model for the first stages of pre-implantation embryo development [17,45]. To study embryo developmental stages on day 3 and day 5, surplus fresh or cryopreserved diploid embryos donated for research were (Figure 1b). Tripronuclear zygotes and surplus embryos were donated with written informed consent by couples undergoing routine IVF at the Erasmus MC University Medical Centre.

Embryo culture and assessment of embryo morphology were performed as described previously [49]. Embryos were cultured in G1 v5 PLUS medium (Vitrolife, Sweden) up to day 3 after fertilization and from there onwards in G2 v5 PLUS medium (Vitrolife, Sweden), according to the manufacturers' instructions. Cryopreservation was performed in straws using a slow freezing standard protocol and subsequent thawing was performed as described previously [4].

### Time-lapse imaging and treatment of zygotes and embryos

Tripronuclear human zygotes were transferred to a time-lapse embryo monitoring system (EmbryoScope™, Unisense Fertilitech, Denmark) at approximately 20h post-insemination (hpi) (Figure 1b). This allowed monitoring of nuclear envelope breakdown (NEB), which marks entry into prometaphase. Zygotes were cultured individually in EmbryoSlides™ (Unisense Fertilitech) in 25µl of G1 medium. In mouse embryos, metaphase plate formation occurs about 30 minutes after NEB and the first mitotic division is completed after 2h [50-51]. Our own time-lapse observations on human 3PN embryos have shown that the time interval between disappearance of pronuclei and completion of first cleavage was 2.83 +/- 0.73h (n=46). We estimated that incubation of human 3PN zygotes for 2h after NEB in G1 medium with colcemid would allow arrest at late prometaphase, whereas an incubation of only 30 minutes after NEB would correspond to early prometaphase.

All inhibitors were added to the culture drop within 5-25 min after NEB (Figure 1b). For the experiments in which the effect of Haspin kinase inhibition was investigated, 3PN zygotes were incubated for 1.5h in colcemid, followed by incubation for 1h in colcemid in combination with 5-iodotubercidin (Itu). For the experiments in which Aurora kinase inhibition was investigated, 3PN zygotes were incubated for 2h in colcemid in combination with ZM447439 (2 µM or 20 µM). All embryos were then processed for chromosome spreads, unless stated otherwise. To investigate the effect of colcemid treatment on our results, some zygotes were fixed 30 minutes in the absence of any inhibitor. To arrest zygotes at the metaphase stage, zygotes were incubated in G1 medium with MG132 for 3h after NEB.

Embryos at the 2-cell stage and later were incubated in medium containing colcemid in a standard incubator at 5,8% CO<sub>2</sub> in air. Tripronuclear 2-cell embryos were incubated in colcemid overnight. After thawing of cryopreserved embryos, day 3 (8-cell stage) embryos were cultured for 1-2h and then incubated for 5-8h with colcemid for cell cycle arrest at prometaphase. Thawed day 4 (morula

stage) embryos were cultured for 24h and embryos that had developed into blastocysts were then incubated for 5-8h with colcemid.

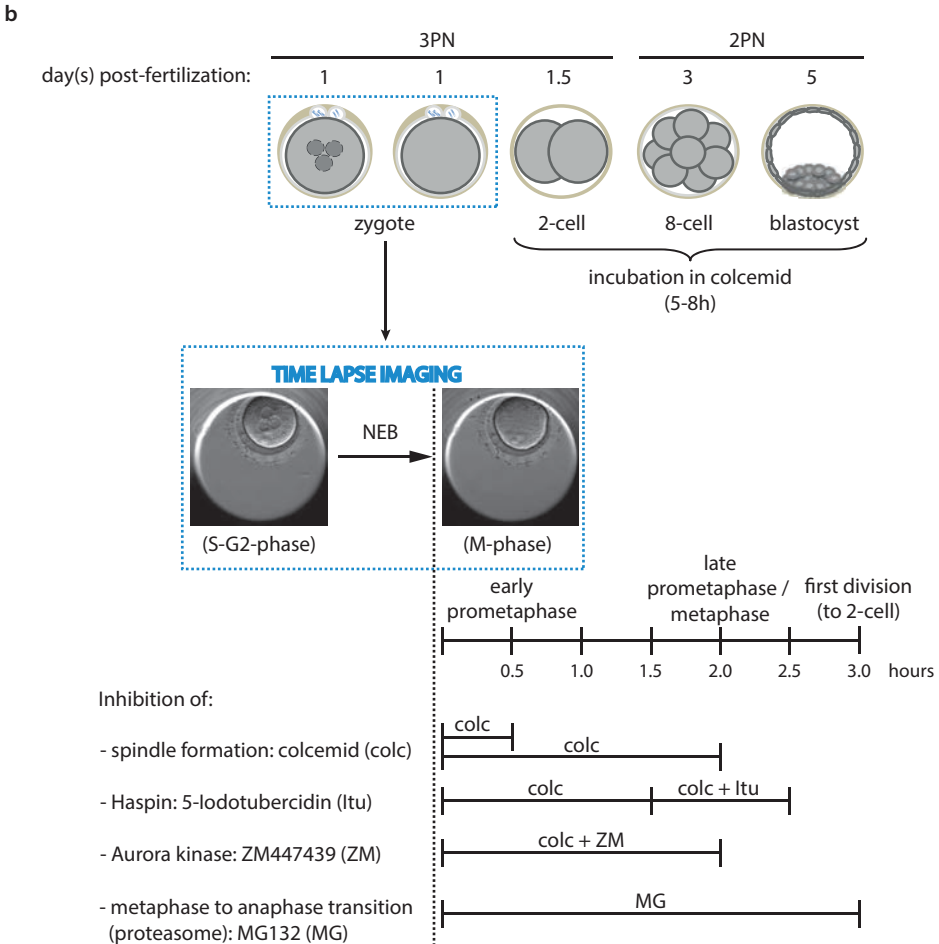
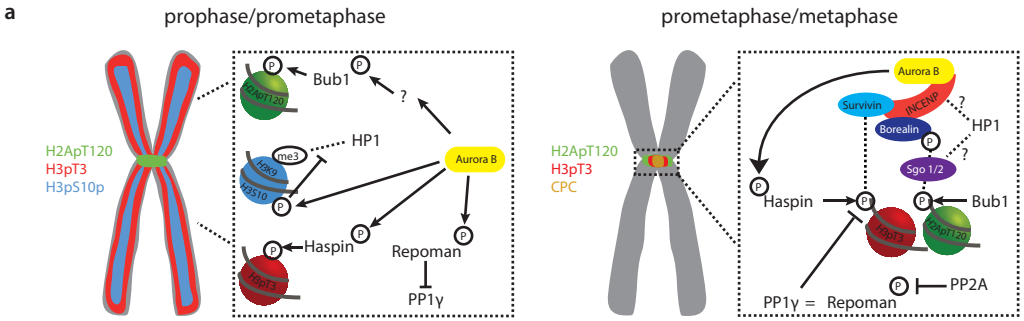




**Figure 1** — (a) Depiction of the models that explain the regulatory circuitry in somatic cells of recruitment of the CPC to chromatin at prophase and early prometaphase, and enrichment at the inner centromere at late prometaphase. Aurora B phosphorylates H3S10, dispelling HP1 from chromatin. Phosphorylation by Aurora B further activates Haspin and Bub1, and inhibits Repo-Man from binding to chromatin. Phosphorylation of H3T3 by Haspin acts to bring the CPC to chromosomes. The Survivin subunit of the CPC binds specifically to H3pT3. Furthermore, Bub1 phosphorylation of histone H2AT120 recruits Shugoshin (Sgo1). Sgo1 acts as a centromeric adaptor that binds the CPC via Borealin. Dephosphorylated Repo-Man binds to PP1 $\gamma$  resulting in removal of H3pT3 from chromosome arms. Intersection of H3pT3 and H2ApT120 defines CPC localization to the inner centromeres at prometaphase. Arrows indicate phosphorylation, dotted lines indicate direct binding and arrow to bar indicates inhibition. See main text for further explanation. (b) Fresh tripronuclear (3PN) embryos were used to study the zygote and 2-cell stages, whereas surplus fresh or cryopreserved (2PN) embryos were used to study the 8-cell and blastocyst stages. Nuclear envelope breakdown (NEB) was monitored by time-lapse imaging to allow immediate incubation of prometaphase zygotes in medium containing colcemid, colcemid+ltu, colcemid+ZM or MG. Embryos at the 2-cell stage and later were incubated in medium containing colcemid in a standard incubator. All embryos were fixed with 1% PFA to obtain chromosome spreads on glass slides, unless stated otherwise.

### Single embryo RT-qPCR

Quantification of mRNA levels was performed in individual single tripronuclear zygotes and blastocysts obtained after culture of day 3 or day 4 cryopreserved embryos in G2 medium, without addition of any of the cell cycle inhibitors mentioned above. Zygotes and blastocysts were incubated in EmbryoMax<sup>®</sup> Acidic Tyrode's Solution (Millipore) for 1-2 min for removal of the zona pellucida and rinsed in G-MOPS Plus medium (Vitrolife) before transfer to the lysis buffer solution provided in the Taqman<sup>®</sup> PreAmp Cells-to-Ct Kit (Applied Biosystems, USA). Lysis, preamplification and RT-qPCR were performed according to the manufacturer's protocol with minor adjustments, as described elsewhere [17]. The following Taqman Gene Expression Assays were used: *HPRT1* (Assay ID: Hs99999909\_m1; amplicon size 100bp); *BUB1* (Hs00177821\_m1; amplicon size 61bp); *GSG2*, Haspin (Hs01072471\_s1; amplicon size 89bp); *CDCA2*, Repo-Man (Hs00299250\_m1; amplicon size 93bp), *PPP1CC*, PP1 $\gamma$  (Hs01566021\_m1; amplicon size 83bp).

Results were analysed using Sequence Detection Software version 1.2.3 (Applied Biosystems) and expressed as cycle threshold (Ct) values. Gene expression levels were normalized over *HPRT1* gene expression, according to the 2<sup>- $\Delta$ CT</sup> method [52]. Differences in *BUB1*, *GSG2*, *CDC2A* and *PPP1CC* expression between zygotes and blastocysts were analysed using the Mann-Whitney test performed with GraphPad Prism software. A p-value of 0.05 was considered statistically significant.

### Antibodies for immunostaining

The following antibodies were used in this study: mouse monoclonal antibodies against INCENP (1:1000, Upstate, Germany), HP1 $\alpha$  (1:500, Euromedex) and Sgo1 (1:100, Abnova, Germany); rabbit polyclonal against H2ApT120 (1:2500, Active motif, USA), H3pT3 (1:1,000, Upstate), Repo-Man (CDCA2) (1:200, Abcam, UK), H3pS10 (1:100, Cell Signaling, USA), H3K9me3 (1:500, Abcam) and HP1 $\alpha$  (1:100, Bethyl Labs, USA); sheep polyclonal against Bub1 (1:100, a kind gift from G. Kops, The

Netherlands); human anticentromere antibodies (CREST) (human centromere antiserum; 1:1,000, Fitzgerald Industries). Primary antibodies were detected by labelling with the appropriate secondary antibodies conjugated with Alexa fluor 488, 594 or 633 (1:200, Molecular Probes, USA).

### **Chromosome spreads and whole mount fixation of embryos**

Before fixation, all embryos were subjected to zona pellucida removal with acidic Tyrode's solution (Millipore, Germany). Chromosome spreads of human embryos were prepared as described previously [17] and used for all the stainings shown, with the following exceptions. For immunofluorescent analysis of HP1 $\alpha$ , H2ApT120 and H3pT3 in zygotes at the pronuclear stage, and simultaneous detection of Sgo1 and H2ApT120, zygotes were fixed whole mount in 4% PFA as described [17]. For immunofluorescent analysis of Repo-Man, zygotes and 8-cell embryos were fixed whole mount for 15 minutes at RT using pre-extraction medium (PEM) containing 100 mM PIPES [pH 7.2], 5 mM MgCl<sub>2</sub>, 2.5 mM EGTA, 2% formaldehyde and 0.1% Triton X-100. Chromosome spread preparations were stored at -20°C, while whole mount-fixed embryos were stored in PBS/0.05% Sodium azide (NaN<sub>3</sub>) for a maximum of 3 months until used for immunostaining. For each embryonic stage and antibody investigated 5-12 embryos were analysed, unless otherwise stated.

### **Immunofluorescent imaging and antibody stripping**

For immunofluorescence stainings, chromosome spreads and whole embryos were rinsed in PBS-T (PBS, 0.01% v/v Tween-20) and blocked with blocking solution (PBS-T, 2% w/v bovine serum albumin (BSA), 5% v/v normal goat serum (NGS) for 30 minutes and incubated with primary antibodies at 4°C overnight. After washing with PBS-T, chromosome spreads or whole embryos were incubated with the appropriate secondary antibodies for 1h, washed with PBS-T and mounted with Vectashield mounting solution containing 750 ng/mL 4',6-diamidino-2-phenylindole (DAPI) for DNA counterstaining (Vector Laboratories, USA). Images were obtained using a Zeiss Axio Imager M2 confocal laser scanning microscope, equipped with four diode lasers (405, 488, 555, 639), an Axiocam camera, and Zen 2009 software (all Carl Zeiss, Germany). Images were processed with Image J (version 1.42n) and Adobe Photoshop CS3 (Adobe Systems, USA) software.

For antibody stripping of chromosome spreads, a western blot stripping buffer (Pierce Biotechnology, USA) was used as described [53]. After incubation of chromosome spreads with the stripping buffer for 3 minutes at RT, slides were washed twice in PBS-T before undergoing a second round of immunofluorescence.

### **Quantification of immunofluorescence and statistical analysis**

Quantification of immunofluorescence on chromosome spreads of human embryos from the zygote to the blastocyst stage was carried out using ImageJ (version 1.42n) and using images obtained at identical illumination settings. For assessment of spreading of the stably bound pool of the CPC beyond the inner centromeric region, the length of the (peri)centromeric INCENP pool was measured and expressed relative to CREST signal length. To do so, a vertical line was drawn following the chromosome arms and perpendicular to the axis connecting the two sister centromeres. The lengths of the INCENP pool and CREST foci were measured in pixels along this line. The ratio of

INCENP/CREST signal length was calculated for all chromosomes within each metaphase plate that were spread in a way that allowed accurate immunofluorescence quantification.

Statistical analyses were carried out using GraphPad Prism software (GraphPad Software, USA). One-way ANOVA followed by Bonferroni's multiple comparison test allowed comparison of INCENP/CREST signal length at the zygote, 8-cell and blastocyst stages. A p-value of 0.05 was considered statistically significant.

For assessment of the localization and distribution of H2ApT120 and H3pT3 relative to INCENP, the Freehand Line Selection Tool in ImageJ was used to draw a line following the whole length of a representative chromosome. The line width was adapted to match chromosome thickness. The average pixel intensity of H2ApT120, H3pT3 and INCENP stainings registered along this line were determined using ImageJ and resulting values were plotted in graphs using Excel (Microsoft, USA).

To compare H3pT3 and H3pS10 levels between maternal and paternal chromosomes within zygotes, parental chromosome sets were identified using the differences in H3K9me3 levels. Mean intensities of H3pT3 and H3pS10 in maternal and paternal chromosomes were measured using Image J, and the ratio between the two parental areas was calculated.

## Results

### **CPC localization at prometaphase becomes increasingly restricted to the inner centromere during development to the blastocyst stage**

Our previous work studying CPC constitution in human pre-implantation embryos suggested a difference in localization of the CPC in zygotes compared to blastocysts during prometaphase, with the CPC being less constricted to the inner centromere at the zygote stage [17]. We aimed to explore and quantify this difference further during embryo development at the zygote, 8-cell and blastocyst stage (Figure 1b). During the previous study, we confirmed co-localization of INCENP with Aurora B and C in the human zygote and blastocyst, respectively. We therefore used immunofluorescence of INCENP to evaluate CPC localization relative to the inner centromeric region as delimited by the height of the centromeres (detected by a human autoantibody against the centromere (CREST)). We determined the size of the INCENP signal relative to CREST signal size on chromosome spreads of human embryos arrested at prometaphase with colcemid (Figure 2a).

We observed a significant decrease of the relative size of the pool of INCENP stably bound to the inner centromeric region, when comparing the zygote to later stages of preimplantation embryo development. In zygotic prometaphases, INCENP was not confined to the inner centromere, but spread into the adjacent pericentric regions. At the blastocyst stage, however, INCENP was mostly confined to the inner centromeric region. These differences in INCENP localization were translated into a significantly higher mean ratio between the length of INCENP and CREST signals in the zygote compared to the blastocyst stage (Figure 2b). The mean INCENP/CREST length ratio in 8-cell embryos, although lower than in zygotes, was also significantly higher than in blastocysts. Together these results suggest that CPC localization at prometaphase becomes increasingly confined to the inner centromeres as embryo development progresses in time.

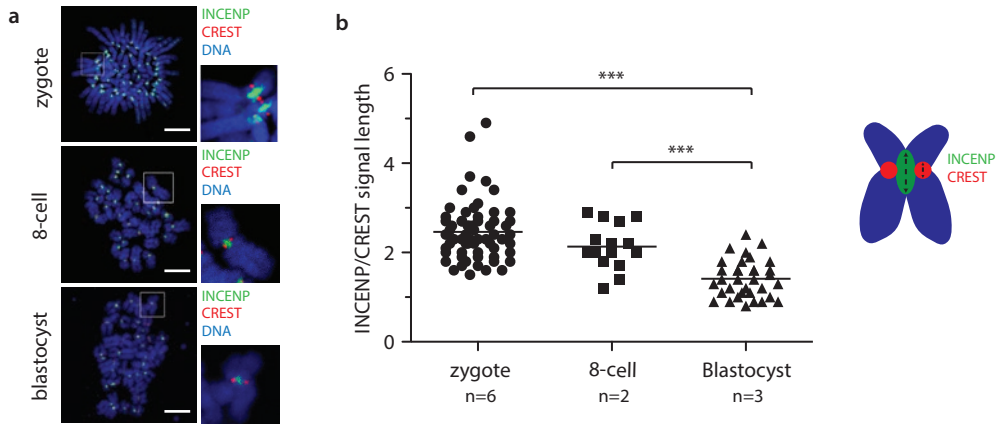


**Figure 2** — (a) Immunolocalization of INCENP and centromeres (CREST) on chromosome spreads of colcemid arrested human embryos at the zygote, 8-cell and blastocyst stage. DNA was counterstained with DAPI. Square boxes are blow-ups of each corresponding smaller box. Scale bars represent 10  $\mu\text{m}$ . (b) Grouped scatter plot showing the relative length of INCENP signal normalized over the diameter of the CREST signal as measured in pixels. Each dot represents the relative INCENP length measured on a single chromosome, as measured in six zygotes, two 8-cell embryos and three blastocysts, respectively ( $n$ =number of embryos analysed). Horizontal bars represent mean values. \*\*\* $p$ <0.05.

### Normal localization of H2ApT120, Bub1 and Sgo1 in human pre-implantation embryos

To investigate the mechanisms that determine CPC localization at the inner centromere in human zygotes, we first investigated the Bub1-H2ApT120-Sgo-CPC pathway. Immunolocalization of H2ApT120 together with INCENP was performed on colcemid induced prometaphase chromosomes in zygotes, 8-cell and blastocyst stage human embryos. Similar to somatic cells [31], phosphorylation of H2AT120 in all embryonic stages was strongly enriched at centromeric regions along the interkinetochore axis, but spreading to the pericentromere was also observed (Figure 3a). Quantification of H2ApT120 staining intensities along the whole length of representative chromosomes showed that peak intensities of H2ApT120 co-localized with those of INCENP (Figure 3a). To more accurately analyse H2AT120 phosphorylation dynamics during mitosis in zygotes, H2ApT120 was investigated by immunofluorescence at late G2-phase (zygotes at 20h post-insemination with pronuclei still visible), early prometaphase (30 minutes after NEB) and at metaphase (3h after NEB in the presence of the proteasome inhibitor MG132). H2AT120 phosphorylation was observed from late G2-phase until metaphase, with enrichment along the interkinetochore axis from early prometaphase to metaphase (Supplemental Figure 1). CPC dynamics as observed by immunolocalization of INCENP followed the expected pattern: it was found to be present at pericentric regions at G2 phase and spread to the chromosome arms at prophase/early prometaphase. INCENP subsequently enriched at the pericentromere at late prometaphase/metaphase. Gene expression analysis of *BUB1*, the kinase responsible for phosphorylation of

H2AT120, showed similar levels of relative mRNA expression in zygotes and blastocysts (Figure 3b). Consistent with these results and to what has been published before for somatic cells [31,36,54], we readily detected Bub1 at the kinetochores (Figure 3c).

Recently, it was shown that before bi-orientation of chromosomes is achieved, two distinct pools of Sgo1 exist: one at the inner centromere recruited by cohesins and another at the kinetochore recruited by H2ApT120 [35,55]. In human zygotes treated with colcemid (non-bioriented chromosomes) we observed Sgo1 as expected at both the kinetochore and inner centromeres co-localizing both with Bub1 and H2ApT120 (Figure 3c).

Next to H2ApT120 and cohesins, in somatic cells HP1 $\alpha$  is also implicated in Sgo1 recruitment [28-29]. Interestingly, early mouse embryos do not express HP1 $\alpha$  until after implantation [44,56]. To investigate if HP1 $\alpha$  has a role in Sgo1 recruitment in human embryos, we performed immunofluorescent analysis of HP1 $\alpha$  in zygotes. At late G2 phase, we detected HP1 $\alpha$  in an asymmetric pattern similar to H3K9me3, with high global levels on maternal chromatin and enrichment at heterochromatic regions at paternal chromatin (Figure 3d, arrowheads, [45]). In colcemid arrested zygotes at early prometaphase, HP1 $\alpha$  localization was observed to become unrelated to parental origin and to become weakly associated with the centromeric regions (Figure 3d).

Together, these findings suggest a functional Bub1-H2ApT120-Sgo-CPC feedback loop in human zygotes and later stages investigated, including a possible interaction with HP1 $\alpha$  for INCENP and Sgo1 recruitment [27-28,31,34].

### **H3pT3 fails to enrich at the inner centromere on (pro)metaphase chromosomes in human zygotes**

In somatic cells it has been shown that Haspin phosphorylates H3T3, providing a chromatin binding site for the CPC required for centromeric enrichment [37]. In HeLa and U2OS cells, phosphorylation of H3T3 becomes enriched at the inner centromere during prometaphase [34,38]. Similar enrichment was readily observed on colcemid-induced prometaphase chromosomes of 2-cell, 8-cell and blastocyst stage embryos (Figure 4a). However, on colcemid-induced prometaphase chromosomes in zygotes, immunolocalization of H3pT3 revealed ubiquitous phosphorylation on the whole length of the chromosome, without enrichment at the centromere (Figure 4a). To exclude an effect of incubation in colcemid or timing of fixation on this aberrant finding in zygotes, H3pT3 dynamics were further investigated in zygotes at late G2-phase, early prometaphase without spindle poison, and at MG132 induced metaphase arrest (Supplemental Figure 2). The absence of H3pT3 staining in late G2-phase zygotes indicates that H3T3 phosphorylation is probably initiated at the onset of mitosis as expected [38]. Subsequently, ubiquitous phosphorylation of H3T3 was consistently observed on chromosomes at prometaphase and metaphase, without centromeric enrichment. Simultaneous detection of INCENP revealed pericentric enrichment at metaphase, although H3pT3 failed to enrich at centromeric regions.

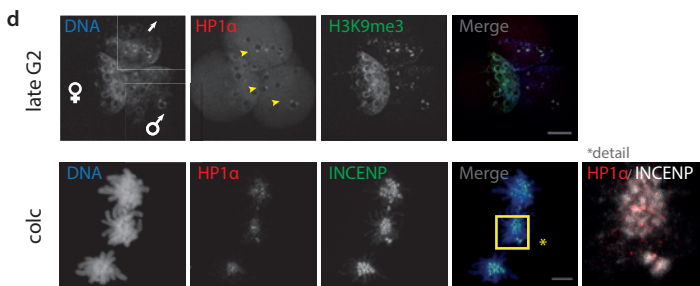
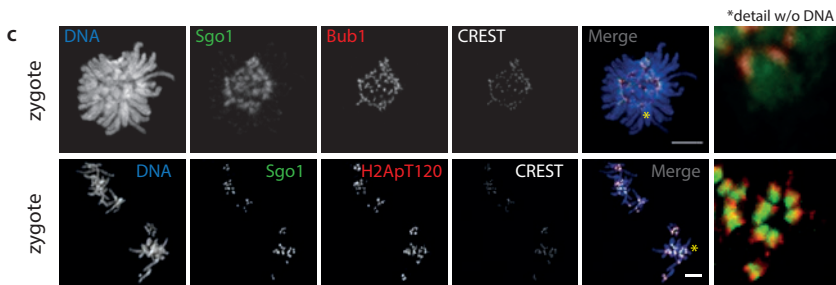
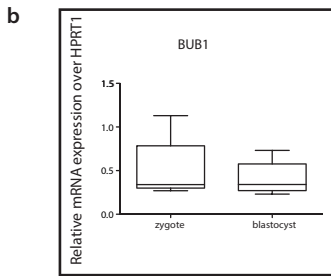
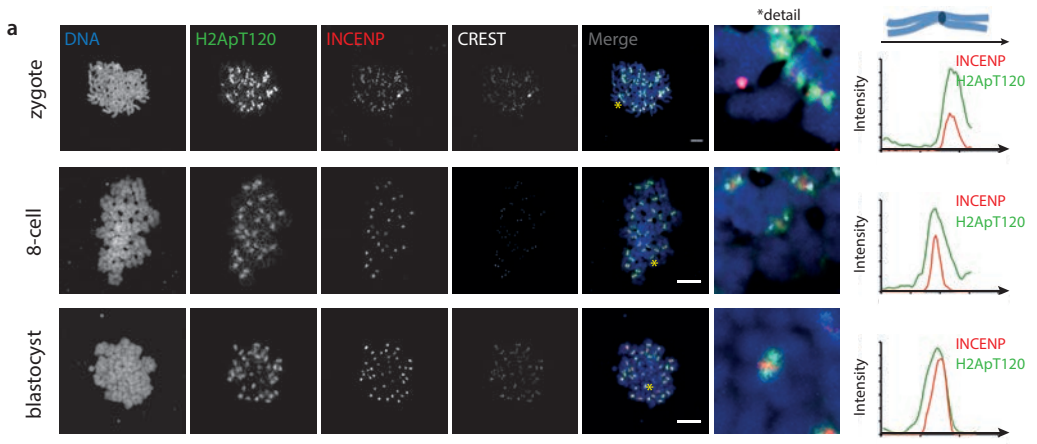


**Figure 3** — (a) Immunolocalization of H2ApT120, INCENP and centromeres (CREST) on chromosome spreads of colcemid arrested human embryos at the zygote, 8-cell and blastocyst stage. DNA was counterstained with DAPI. All scale bars represent 10µm. Asterisks indicate the area that is shown enlarged in the detail panel. For each stage of development, a graph was plotted representing the distribution of fluorescent intensity for H2ApT120 and INCENP along the entire length of a representative chromosome (\*). Intensity was measured in arbitrary units and distance in pixels. (b) Relative mRNA expression of *BUB1* over *HPRT1* in human zygotes (n=5) and blastocysts (n=5). (c) Upper panel: immunolocalization of Bub1, Sgo1 and centromeres (CREST) on chromosome spreads of colcemid arrested human zygotes, 2h after NEB. Lower panel: immunolocalization of H2ApT120, Sgo1 and centromeres (CREST) on chromosomes of colcemid arrested human zygotes, fixed whole mount 2h after NEB. Shown is a full projection of Z-sections. DNA was counterstained with DAPI. Scale bars represent 10µm. Asterisk indicates the area that is shown enlarged in the detail panel. (d) Upper panel: immunolocalization of HP1α and H3K9me3 in human zygotes at late G2 stage, fixed whole mount 20h post insemination. Shown is a full projection of Z-sections. Lower panel: immunolocalization of HP1α and INCENP on chromosome spreads of colcemid arrested human zygotes. DNA was counterstained with DAPI. Scale bars represent 20 µm (upper panel) and 10 µm (lower panel). Asterisk indicates the area that is shown enlarged in the detail panel.

In U2OS cells the joint action of PP1γ and Repo-Man was shown to dephosphorylate H3T3 during prometaphase, ensuring centromeric H3pT3 enrichment [39,57]. The persistent phosphorylation of H3T3 on the chromosome arms at prometaphase and metaphase in human zygotes is reminiscent of the phenotype of Haspin overexpression or Repo-Man knockdown [39]. As the balance between PP1γ/Repo-Man and Haspin expression was demonstrated to be important for correct localization of the CPC, we analysed mRNA expression in human zygotes and blastocysts. Contrary to expectations, quantification of Haspin mRNA (*GSG2*) levels revealed low relative expression of Haspin in human zygotes, whereas Repo-Man mRNA (*CDCA2*) expression levels between zygotes and blastocysts were not significantly different (Figure 4b). However, this does not exclude the possibility of Haspin protein accumulation in the cytoplasm of human oocytes, as evidenced by the presence of H3pT3 on the chromatin. Immunodetection of Repo-Man showed similar levels of this protein on the chromosome arms of prometaphase-arrested zygotes, when H3pT3 is ubiquitous, and later embryonic stages, when H3pT3 is absent from the chromosome arms (Figure 4c). Interestingly, expression levels of PP1γ mRNA (*PPP1CC*) were found to be significantly lower in the zygote compared to the blastocyst stage (Figure 4c). However, removal of H3pT3 from the chromosome arms appears to occur normally during mitosis at the 2-cell stage (Figure 4a). As transcription is limited to only a handful of genes between the zygote and the 2-cell stage [48], transcription activation of Repo-Man or PP1γ in this interval is unlikely. The observed persistent phosphorylation of H3T3 on the chromosome arms of zygotes is therefore not likely to be explained by lack of Repo-Man or PP1γ expression. During prophase, Aurora B phosphorylates Repo-Man, preventing its recruitment to chromatin. The phosphatase PP2A normally counteracts this phosphorylation during prometaphase, allowing the targeting of Repo-Man to chromosomes and the removal of H3pT3. Our findings suggest this mechanism to be altered in human zygotes, as centromeric enrichment of H3pT3 is not necessary for inner centromeric localization of INCENP in the zygote.

### **Haspin activity is needed for mitotic checkpoint establishment and centromeric targeting of the CPC in the zygote**

To further investigate the importance of Haspin mediated H3T3 phosphorylation for CPC localization in human zygotes, we incubated zygotes with colcemid in combination with the Haspin inhibitor 5-iodotubercidin (Itu) (Figure 1b). Colcemid inhibits spindle formation and chromosome attachment, normally leading to prometaphase arrest due to sustained mitotic checkpoint activity. Whereas human zygotes normally have completed cytokinesis by 3 hours after NEB, colcemid treatment induces cell cycle arrest for >24h (Supplemental Figure 3). However, when Itu was added directly after NEB, the presence of colcemid did not result in prometaphase arrest. Zygotes incubated with colcemid and Itu showed faster cell cycle progression and had cleaved already around 2 hours after NEB (n=5; Supplemental Figure 3). A similar effect of Itu addition on mitotic progression was reported in HeLa and U2OS cells, reportedly caused by the inability of Aurora B to efficiently recruit the MC subunits Bub1 and BubR1 to kinetochores during prophase [41,58]. In analogy to this, Haspin activity appears to be similarly needed for MC establishment in the zygote.

To further study the effect of Haspin inhibition on CPC activity and localization, zygotes were first treated with colcemid for 1.5h to induce prometaphase arrest and subsequently Itu was added. Immunolocalization of H3pT3 in these zygotes showed that Haspin inhibition at this stage results in a severe decrease of H3pT3 along the chromosome arms (Figure 5a) in comparison with zygotes arrested with colcemid only (Figure 4a). As levels of H3pT3 are already high on early prometaphase chromosomes in untreated zygotes (Supplemental Figure 2), the observed decrease in H3pT3 levels in Itu-treated zygotes is probably secondary and due to existing phosphatase activity, that is no longer be counterbalanced by Haspin activity. Further, Haspin inhibition also resulted in a reduction of centromeric INCENP levels, with a more diffuse localization when compared to untreated zygotes (compare Figure 4a and Figure 5a). Aurora B/C kinase phosphorylates H3S10 along the chromosome arms, as shown in colcemid treated zygotes (Figure 5b). Haspin inhibition by Itu addition at prometaphase does not obviously affect overall H3pS10 levels, however, different levels of H3pS10 were observed between chromosomes within a single prometaphase spread (Figure 5b). We hypothesized that this difference was related to the parental origin of the chromosomes. Therefore, after detection of H3pS10 and image analysis, we performed antibody stripping followed by a second round of immunostaining to detect trimethylation of H3K9 [53]. This allows distinction between maternal (enriched for H3K9me3) and paternal (low levels of H3K9me3) chromosomes [47]. Indeed, altered levels of H3pS10 after Itu treatment correlate with parental origin of chromosomes: mean immunofluorescent intensities on maternal chromosomes were 63% ( $\pm 19\%$ , n=7) of that on paternal chromosomes (Figure 5b). Thus, Haspin inhibition and/or the reduction in H3pT3 levels results in lower levels of Aurora B/C activity on maternal chromatin.

To determine the effect of Itu treatment during prometaphase on Bub1 activity, H2ApT120 was investigated. This mark was detected at the kinetochores, comparable to zygotes treated with only colcemid (compare Figures 3a with 5c). This is in line with previous findings in somatic cells, where Haspin activity is important for recruitment of Bub1 to kinetochores, but not for Bub1 activity once it localizes to the kinetochore [41,58]. Notably, in the absence of H3pT3, the presence of H2ApT120 alone was not enough to fully target the CPC to the inner centromere. Altogether, these data show



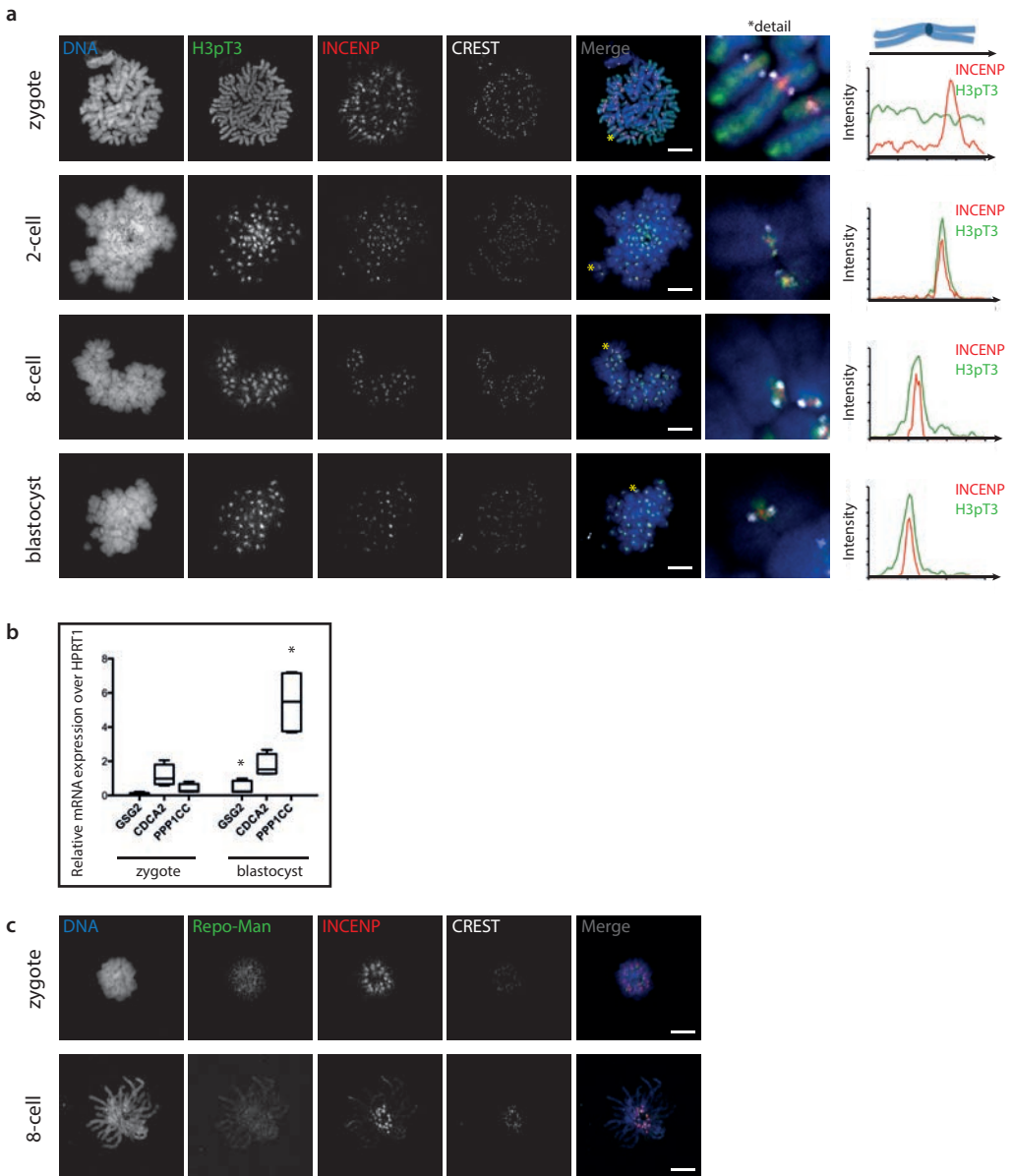


**Figure 4** — (a) Immunolocalization of H3pT3, INCENP and centromeres (CREST) on chromosome spreads of colcemid arrested human embryos at the zygote, 2-cell, 8-cell and blastocyst stage. DNA was counterstained with DAPI. All scale bars represent 10  $\mu$ m. Asterisks indicate the area that is shown enlarged in the detail panel. For each stage of development, a graph was plotted representing the distribution of fluorescent intensity for H3pT3 and INCENP along the entire length of a representative chromosome (\*). Intensity was measured in arbitrary units and distance in pixels. (b) Relative mRNA expression of Haspin (*GSG2*) (n=5), Repo-Man (*CDCA2*) (n=4) and PP1 $\gamma$  (*PPP1CC*) (n=4) over *HPRT1* in human zygotes and blastocysts. \* $p < 0.05$  compared to the zygote stage. (c) Immunolocalization of Repo-Man, INCENP and centromeres (CREST) on prometaphase-arrested human embryos, fixed whole mount at the zygote (n=2) and 8-cell (n=3) stage. DNA was counterstained with DAPI. Shown is a full projection of Z-sections. All scale bars represent 10  $\mu$ m.

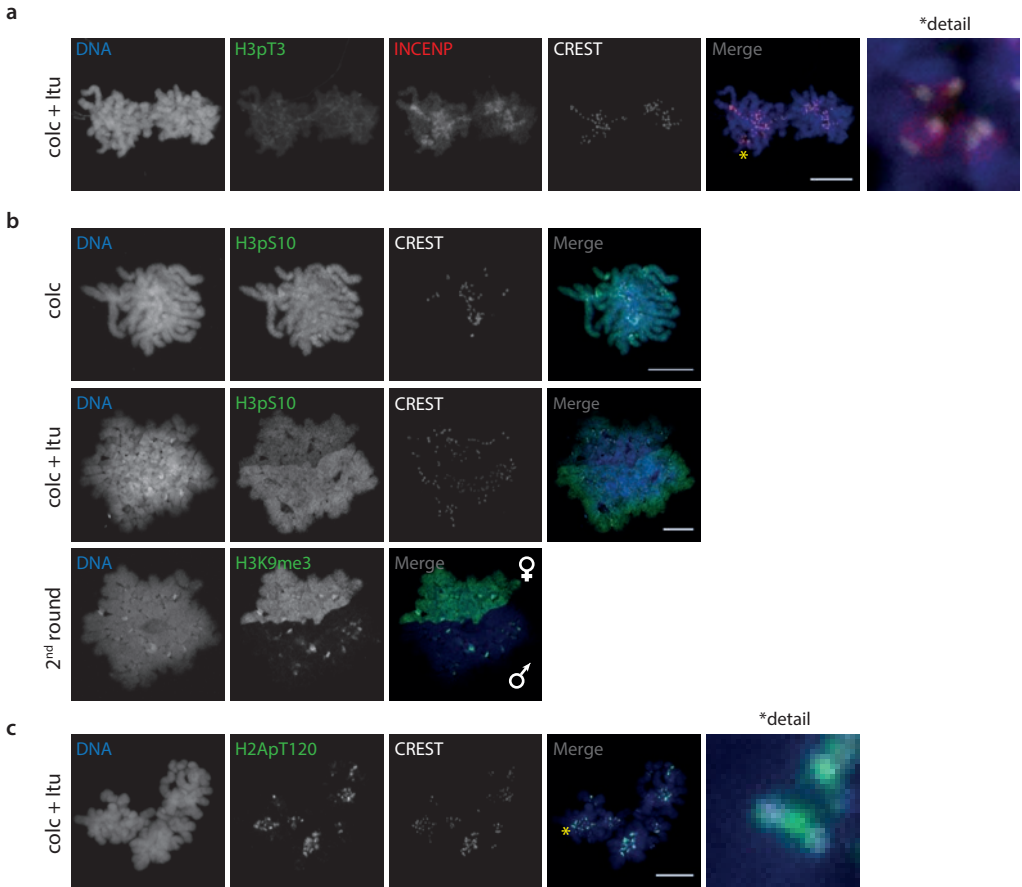


**Figure 5** — (a) Immunolocalization of H3pT3, INCENP and centromeres (CREST) on chromosome spreads of human zygotes 2.5h after NEB, after culture with colcemid and the Haspin inhibitor 5-iodotubercidin (Itu). DNA was counterstained with DAPI. Scale bar represents 10  $\mu\text{m}$ . Asterisk indicates area that is shown enlarged in the detail panel. (b) Immunolocalization of H3pS10 and centromeres (CREST) on chromosome spreads of human zygotes 2.5h after NEB after culture with colcemid only or with colcemid and the Haspin inhibitor 5-iodotubercidin (Itu). Lower panel: immunolocalization of H3K9me3 after stripping and a second round of immunofluorescence on the zygote treated with colcemid and Itu. DNA was counterstained with DAPI. Scale bars represent 10  $\mu\text{m}$ . (c) Immunolocalization of H2ApT120 and centromeres (CREST) on chromosome spreads of human zygotes 2.5h after NEB, after culture with colcemid and the Haspin inhibitor 5-iodotubercidin (Itu). DNA was counterstained with DAPI. Scale bar represents 10  $\mu\text{m}$ . Asterisk indicates area that is shown enlarged in the detail panel.

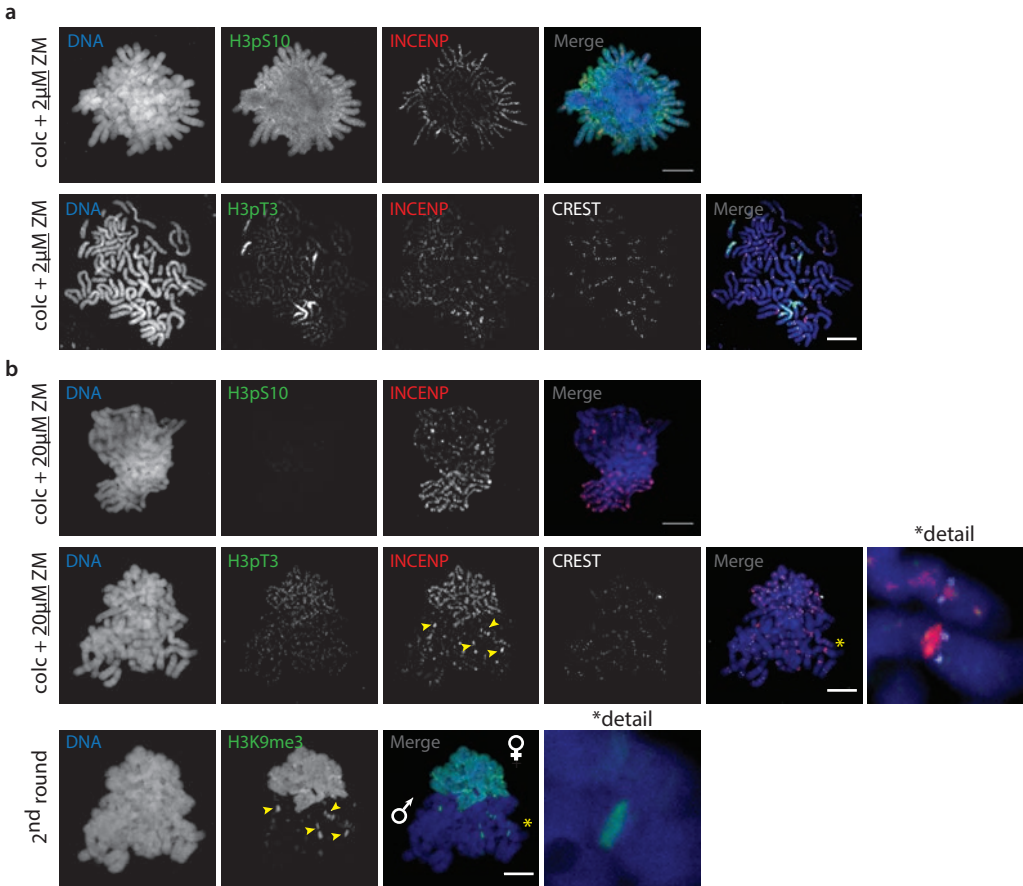


**Figure 6** — (a) Immunolocalization of H3pS10 and INCENP and of H3pT3, INCENP and centromeres (CREST) on chromosome spreads of human zygotes 2h after NEB, after culture with colcemid and 2  $\mu$ M of the Aurora inhibitor ZM447439 (ZM). DNA was counterstained with DAPI. Scale bars represent 10  $\mu$ m. (b) Immunolocalization of H3pS10 and INCENP and of H3pT3, INCENP and centromeres (CREST) on chromosome spreads of human zygotes 2h after NEB, after culture with colcemid and 20  $\mu$ M of the Aurora inhibitor ZM447439 (ZM). Lower panel: immunolocalization of H3K9me3 after stripping and a second round of immunofluorescence on the zygote of the middle panel, treated with colcemid and 20 $\mu$ M ZM. DNA was counterstained with DAPI. Scale bars represent 10  $\mu$ m. Asterisks indicate the area that is shown enlarged in the detail panel.

that Haspin-mediated H3pT3 is required for CPC localization, but centromeric enrichment of H3pT3 may not be.

### **Aurora kinase inhibition reveals a functional feedback loop between Aurora B/C and Haspin in zygotes**

In somatic cells, the CPC binds to H3pT3, where in return Aurora B phosphorylates Haspin to promote further phosphorylation of H3T3 [37]. The same authors showed that this positive feedback loop is disturbed when cells are treated with the Aurora kinase inhibitor ZM447439 (ZM), which leads to reduced phosphorylation of endogenous Haspin and concomitant reduction of H3pT3. As Aurora C is the main kinetic subunit of the CPC in human zygotes, we investigated whether a similar feedback loop is active.

As ZM treatment inhibits all Aurora kinase activity [59], we are not able to distinguish Aurora B from Aurora C kinase activity. To test the effect of ZM treatment on Aurora kinase activity in zygotes, we first applied a concentration that is commonly used in somatic cells [2  $\mu$ M ZM; [59]] in combination with colcemid directly after NEB, and determined the levels of H3pS10 at late prometaphase. H3pS10 signal was high and well defined (Figure 6a), similar to what was observed in non-treated zygotes (Figure 5b). However, simultaneous detection of INCENP showed disturbed centromeric enrichment of INCENP with displacement to the chromosome arms (compare Figure 3a with Figure 6a). In addition, ZM treatment resulted in reduced levels of H3T3 phosphorylation on most, but not all chromosomes (Figure 6a). This reduction of H3pT3 levels after Aurora B/C inhibition indicate a functional positive feedback loop between Aurora B/C and Haspin in human zygotes, similar to what has been described in somatic cells.

### **Abolishment of H3pS10 reveals differences in Haspin activity and CPC recruitment on maternal and paternal chromatin**

The high levels of H3pS10 and residual Haspin activity may indicate an insufficient level of Aurora B/C inhibition at 2  $\mu$ M ZM. We next tested a concentration previously shown to efficiently abolish H3pS10 in mouse zygotes (20  $\mu$ M ZM, [60]). At this concentration, a complete loss of H3pS10 was observed on human zygotic prometaphases (Figure 6b). This concentration also reduced H3T3 phosphorylation levels on all chromosomes, with a more severe reduction on a subset of chromosomes within a spread. INCENP localization reflected the asymmetric pattern of H3pT3: it was observed to locate along the arms on chromosomes with higher levels of H3pT3, whereas on the other chromosomes only some INCENP foci were observed (Figure 6b). Comparable to the effect of Haspin inhibition on H3pS10 levels, we investigated if the observed differences between chromosomes within one zygote after high concentration ZM treatment was related to their parental origin. Using a second round of immunofluorescence for H3K9me3, we observed that the effect of complete Aurora B/C inhibition on H3pT3 levels was less pronounced on maternal compared to paternal chromatin (Figure 6b): mean immunofluorescent intensities of H3pT3 on paternal chromosomes were 33% ( $\pm$ 6%, n=4) of that on maternal chromosomes. Thus, in the presence of a concentration of ZM that abolishes H3S10ph phosphorylation, maternally and paternally derived chromosomes have different levels of residual Haspin activity.

Notably, foci of accumulated INCENP did not localize to the inner centromere, but to H3K9me3-positive regions of constitutive heterochromatin on the paternal chromosomes (arrows, Figure 6b). We have recently shown these regions to correspond to constitutive, pericentric heterochromatin

containing DNA Satellite II/III repeats in human zygotes [45]. In somatic cells, inhibition of Aurora B with the concomitant reduction in H3pS10, has been shown to result in retention of HP1 proteins on mitotic chromosomes [26,61]. As in the absence of H3pS10, HP1 is not evacuated from the chromatin and remains bound to H3K9me3, we asked whether the observed asymmetric distribution of INCENP in ZM-treated zygotes was due to an association to H3K9me3-anchored HP1 $\alpha$ . Indeed, after disruption of H3pS10 with ZM treatment, HP1 $\alpha$  fails to redistribute and is detected at high levels in the same asymmetric distribution on the parental chromosomes as H3K9me3 and as observed at G2-phase (Compare Figure 3d with Figure 7a). In addition, Sgo1 did not localize to the (inner) centromere after ZM treatment, but followed the same asymmetric pattern as HP1 $\alpha$  and INCENP, with enrichment at H3K9me3 positive pericentric regions on paternal chromosomes (Figure 7a,b).

ZM treatment was previously shown also to abolish phosphorylation of H2AT120 at the centromeres in U2OS cells [15]. However, our immunofluorescence analysis shows that in 7 out of 10 zygotes ZM treatment did not abolish centromeric H2ApT120 (Figure 7c). Nevertheless, Sgo1 and INCENP still consistently failed to show centromeric enrichment indicating that H2ApT120 alone is not sufficient for their recruitment after Aurora B/C inhibition. These results are consistent with a role for HP1 $\alpha$  in facilitating both Sgo1 and INCENP recruitment to chromatin.

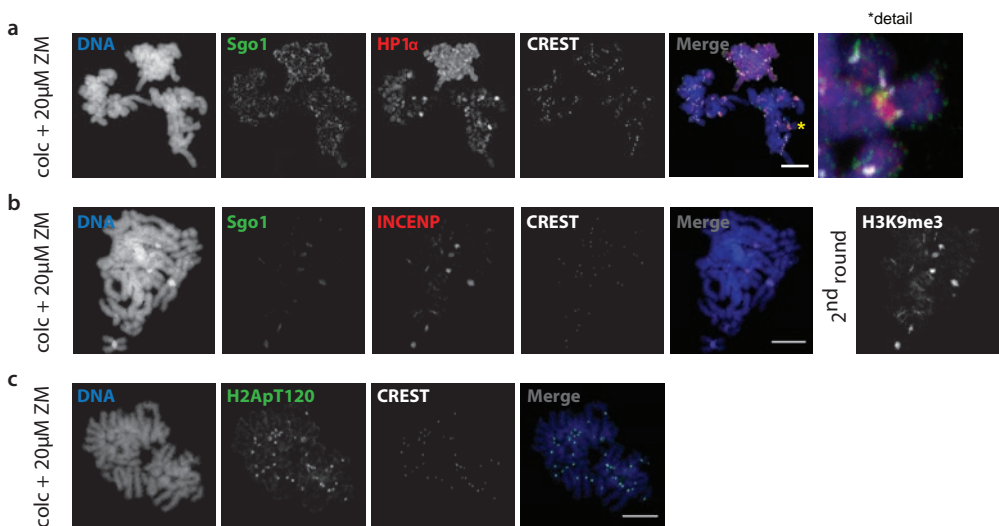


**Figure 7** — (a) Immunolocalization of Sgo1, HP1 $\alpha$  and centromeres (CREST) on chromosome spreads of human zygotes 2h after NEB, after culture with colcemid and 20  $\mu$ M of the Aurora inhibitor ZM447439 (ZM). DNA was counterstained with DAPI. Scale bar represent 10  $\mu$ m. Asterisk indicates the area that is shown enlarged in the detail panel. (b) Immunolocalization of Sgo1, INCENP and centromeres (CREST) on chromosome spreads of human zygotes 2h after NEB, after culture with colcemid and 20  $\mu$ M of the Aurora inhibitor ZM447439 (ZM). Only the paternal chromosome set is shown. 2<sup>nd</sup> round panel: immunolocalization of H3K9me3 after stripping and a second round of immunofluorescence of the same zygote. DNA was counterstained with DAPI. Scale bars represent 10  $\mu$ m. (c) Immunolocalization of H2ApT120 and centromeres (CREST) on chromosome spreads of human zygotes 2h after NEB, after culture with colcemid and 20  $\mu$ M of the Aurora inhibitor ZM447439 (ZM). DNA was counterstained with DAPI. Scale bars represent 10  $\mu$ m.

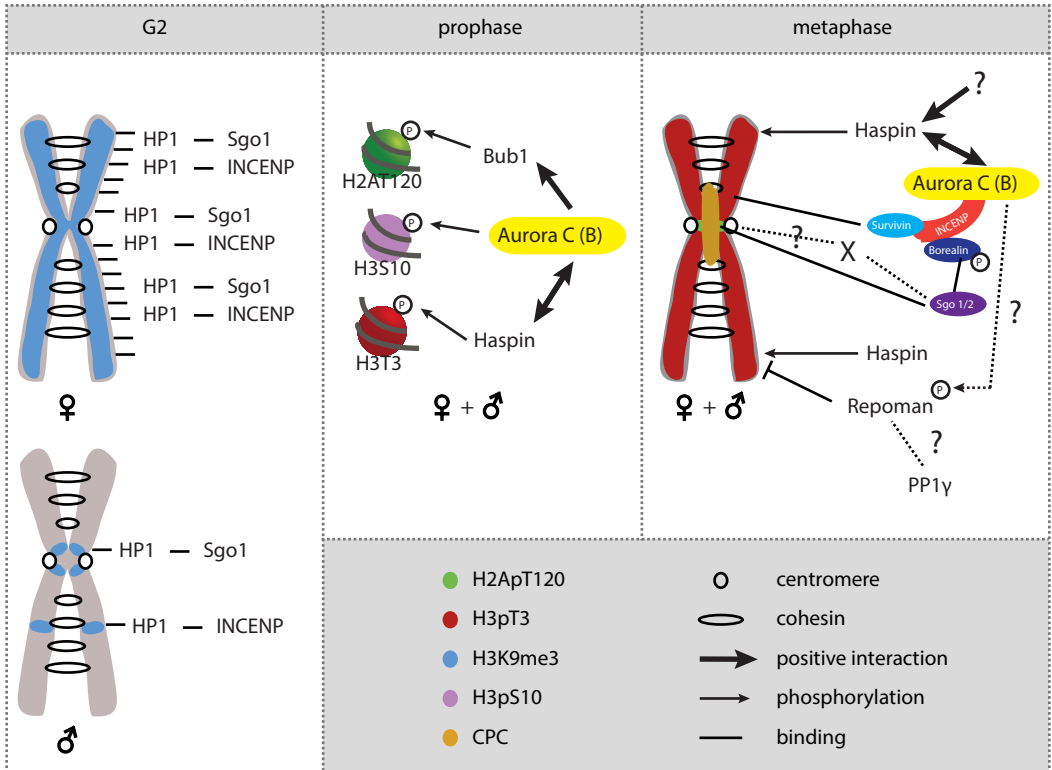


**Figure 8** — Schematic representation of the main findings, highlighting the altered CPC targeting pathways in zygotes. The distribution of HP1, Sgo1 and INCENP at the G2 phase-prophase transition follows the epigenetic asymmetry for H3K9me3 on maternal and paternal chromosomes. Whereas the asymmetry for H3K9me3 remains, HP1a, Sgo1 and INCENP redistribute in a symmetric fashion during prometaphase by action of the mitotic kinases. The Haspin-H3pT3-CPC pathway remains active on the chromosome arms until metaphase, while the CPC is enriched around the pericentromeric area. H2ApT120 alone seems insufficient for CPC localization, suggesting the existence of additional recruitment factors, where HP1a is a candidate for X. See Discussion for further details.

## Discussion

Cells of the early human embryo frequently mis-segregate chromosomes during cell division. What causes embryos to be so error-prone at this crucial stage during the formation of a new individual is largely unknown, as the mechanisms for chromosome segregation used by pre-implantation embryos are poorly described. In this work we aimed to explore CPC localization in human embryos and assess the functionality of the main kinase pathways regulating CPC targeting as described in somatic cells. By interfering in these pathways using specific kinase inhibitors, we demonstrate that they are functional in human cleavage stage embryos and we provide indirect evidence for a

functional mitotic checkpoint. Similar to somatic cells, CPC localization in cleavage stage embryos follows phosphorylation of H3T3 and H2ApT120. We also show that the feedback interactions between the three kinases are as expected: Haspin activity is crucial for Aurora kinase activation, and in turn Aurora kinase activity is needed for full Haspin activity. In addition, Aurora activity is needed for Bub1 recruitment, but not for Bub1 activity once properly located. Thus, the presence of Aurora C in zygotes does not seem to alter the described feedback interactions with Bub1 and Haspin. However, we did observe an important difference in Haspin activity specifically in the zygote: phosphorylation levels of H3T3 on the chromosome arms remain high until metaphase. Notably, when persistent H3pT3 on chromosome arms is induced by either Haspin overexpression or phosphatase inhibition in somatic cells, this immediately results in severe CPC displacement to the chromosome arms [39,62]. Surprisingly, in zygotes pericentric enrichment of INCENP was already observed at early prometaphase, despite ubiquitous presence of H3pT3 on the arms. However, we did observe INCENP to be less confined to the pericentromere and we hypothesize that the persisting H3pT3 levels on the arms does interfere with precise CPC targeting.

The CPC is a key player in ensuring accurate chromosome attachment and alignment and also has a function in localizing and sustaining mitotic checkpoint complex activity. In all model organisms studied, the CPC becomes increasingly enriched at the inner centromeric region during prometaphase of normal mitosis. This enrichment is important for its proper function, as experimentally induced CPC displacement results in chromosome alignment defects [22]. Even subtle displacement of the CPC, as observed on chromosomes carrying a neocentromere and the concomitant lack of the typical pHC epigenetic signature, appears to affect the efficiency of such a chromosome to form bipolar attachments and align at the metaphase plate [63]. However, the importance of (inner)centromeric CPC enrichment has been recently questioned in budding yeast [64], where each kinetochore attaches to a single microtubule. Human kinetochores attach to several microtubules, creating the possibility of one kinetochore to attach to both spindle poles (merotelic attachment). It is hypothesized that centromeric CPC enrichment may be specifically needed for efficient resolution of merotelic attachments [22]. This type of erroneous attachment is not sensed by the MC and leads to anaphase lagging [65]. Interestingly, analysis of the type of chromosomal abnormalities observed within human pre-implantation embryos show them to be most frequently consistent with anaphase lagging events [66-69]. It is thus tempting to speculate that the “sloppy” CPC localization we observe here may contribute to an increase in merotelic attachments that escape correction, thus leading to chromosome mis-segregation.

Due to experimental limitations when working with human embryos, we were unable to resolve the underlying mechanism for persisting H3pT3 on metaphase chromosome arms. Net levels of H3pT3 are determined by the equilibrium between the phosphorylating activity of Haspin and the dephosphorylating activity of Repo-Man, together with the phosphatase PP1 $\gamma$ . Recruitment of Repo-Man-PP1 $\gamma$  to chromosome arms is opposed by the presence of Aurora B during prophase/early prometaphase, but it is recruited to chromosome arms as the CPC becomes centromerically enriched (Figure 1a; [39-40]). Our results show similar levels of Repo-Man on chromosome arms in prometaphase arrested zygotes and 8-cell embryos. This may indicate that dephosphorylation dynamics may not be different between these stages, but that the persistent high levels of H3pT3

are the consequence of sustained Haspin activity on chromosome arms in human zygotes. Recent reports identified three different kinases to be involved in increased activation of Haspin: during interphase it is initially phosphorylated by Cdk1, followed at prophase by Polo-like kinase 1 (Plk1) and subsequently Aurora B [70-71]. It is not known if during prometaphase Haspin is subsequently dephosphorylated/deactivated at the chromosome arms to ensure centromeric enrichment of H3pT3.

Cohesion between sister chromatids, mediated by proteins called cohesins, is essential for accurate chromosome alignment, but needs to be resolved at anaphase onset. In vertebrate cells, cohesins are removed during mitosis in two steps [72]. Cohesins are removed from chromosome arms during prophase, while centromeric cohesins are protected from this removal by a mechanism involving Sgo1 until they are cleaved by the protease Separase at anaphase onset. Cohesin removal during prophase involves phosphorylation of cohesins and the cohesion binding protein Sororin, involving the same mitotic kinases responsible for activating Haspin (Cdk1, Plk1 and Aurora B) [73-76]. Interestingly, overexpression of Haspin and concomitant persisting high levels of H3pT3 on chromosome arms is associated with persistent arm cohesins during prometaphase in HeLa cells [62]. In our series of both prometaphase and metaphase chromosome spreads prepared from human zygotes, we consistently observed chromosomes with closed chromosome arms (Supplemental Figures 1 and 2), as opposed to chromosomes with the typical X-shape observed at later developmental stages (compare stages in Figures 3 and 4). This observation indicates persistence of chromosome arm cohesins until zygotic metaphase and is in line with similar observations in mouse zygotes [77]. We hypothesize that the persisting high levels of H3pT3 on chromosome arms may have a role in protecting arm cohesins from the prophase removal pathway, although the purpose of this odd phenomenon and its consequences for chromosome segregation remain unknown.

When H3pS10 was completely abolished by inhibition of Aurora B/C an asymmetry in H3pT3 levels between chromosomes of maternal and paternal origin was revealed. Maternal H3K9me3-rich chromosomes were able to attract higher levels of residual H3pT3 on the chromosome arms, whereas H3pT3 foci co-localized with the few H3K9me3-positive regions of constitutive HC on paternal chromatin. Due to the lack of specific antibodies for Haspin, little is known about Haspin localization and how it is targeted to chromatin [78]. Our findings suggest an association of Haspin with constitutive heterochromatin. This is in line with recent findings suggesting the cohesin binding protein Pds5B to promote cohesion establishment and maintenance at pericentric heterochromatin. In addition, Pds5B was also found to be required for Haspin recruitment [79]. Alternatively, maternal chromatin contains higher levels of HP1 $\alpha$  and may thus be able to recruit higher levels of CPC proteins through the HP1 $\alpha$ -INCENP interaction. This may lead to higher levels of residual Aurora B/C activity able to activate Haspin on maternal chromatin. However, when abolishing H3pT3 by inhibiting Haspin activity, we observed lower levels of H3pS10 on maternally derived chromatin. Although we have no conclusive explanation for this phenomenon, our findings illustrate the importance of full Haspin and Aurora B/C activity in ensuring accurate CPC localization in the face of the epigenetic parental asymmetry present in the zygote. It is thus conceivable that the observed persisting Haspin activity during prometaphase is an adaptation to the asymmetry. It is further conceivable that oocyte quality or culture condition-related disturbances in Aurora B/C or Haspin kinase activity



have differential effects on maternal and paternal chromosomes. As H3K9me3-rich maternal chromatin appears to have an advantage in recruitment of INCENP and Haspin, CPC recruitment to paternal chromosomes may be more easily compromised under conditions of suboptimal mitotic kinase activity. This may render paternal chromosomes more prone to attachment errors and mis-segregation, a question that is currently under investigation.

We observed that inhibition of Aurora and Haspin kinase at prometaphase did not affect Bub1 activity at the kinetochore, and H2AT120 phosphorylation was consistently observed at the centromeres. However, under these conditions this mark alone was not sufficient for full centromeric CPC enrichment, suggesting the existence of additional recruitment mechanisms. H2ApT120 normally ensures CPC localization through recruitment of Sgo1. Research in somatic cells suggests that recruitment of INCENP and Sgo1 by HP1 $\alpha$  at interphase is needed for their subsequent centromeric recruitment at prometaphase, but this matter is still under debate [27-28,80]. Under high ZM conditions, where H3pS10 was completely abolished in human zygotes, HP1 $\alpha$  remained localized to H3K9me3, and did not relocate to the centromeric region at prometaphase. Both Sgo1 and INCENP remained co-localized to H3K9me3/HP1 $\alpha$ , suggesting that these proteins bound directly or indirectly to H3K9me3-anchored HP1 $\alpha$ . These findings support a role for HP1 $\alpha$  in recruitment of INCENP and Sgo1 at interphase and indicate that displacement of HP1 $\alpha$  through Aurora kinase activity is needed to enable relocation of INCENP and Sgo1 to the centromeric region.

Using a more accessible model such as mouse embryos would enable more conclusive experiments. However, chromosome segregation regulation in mouse embryos may not be representative, as mouse embryos have very low spontaneous mitotic error rates [81]. Also, in the mouse zygote alternative mechanisms are used to format paternal pHC that do not rely on the H3K9me3 pathway [44]. As mouse embryos also lack HP1 $\alpha$  expression [44], it is likely that different mechanisms have evolved for INCENP and Sgo1 recruitment. Therefore, despite the ethical and practical limitations, this study yields valuable insight into the possible origins of human embryo aneuploidy that could not have been obtained by the study of mouse embryos.

Our findings indicate differences in the dynamics of the Haspin-H3pT3-CPC feedback loop and H3pT3 dephosphorylation by Repo-Man/PP1 $\gamma$  during prometaphase in human zygotes compared to later embryonic stages and normal mitosis (Figure 8). It is conceivable that the observed persisting Haspin activity is an adaptation needed to ensure symmetric CPC recruitment, despite the parental epigenetic asymmetry. As removal of H3pT3 from the chromosome arms during prometaphase normally contributes to further centromeric enrichment of the CPC in somatic cells [40], we hypothesize that this adaptation may come at a price concerning accurate CPC targeting in zygotes. However, further research is needed to what extent the differences we observed in CPC localization affect the prevention and/or correction of erroneous attachments. In future studies it will be interesting to assess if the error correcting ability of the CPC is compromised in the zygote and if differences exist in this aspect between maternal and paternal chromosomes.

### **Author's roles**

C.v.d.W. and M.A.S. performed experiments and data analysis, contributed to discussion and drafted the manuscript. C.E. performed experiments. J.S.E.L. was responsible for IVF patients and informed consent for donated human embryos. B.C.J.M.F. contributed to manuscript drafting and critical discussion. S.M.A.L. contributed to study design, manuscript drafting and critical discussion. E.B.B. designed the study, performed data analysis, writing and critical review of the manuscript and final approval of the version to be published. All authors have reviewed the final version of the manuscript and approved it for publication.

### **Acknowledgments**

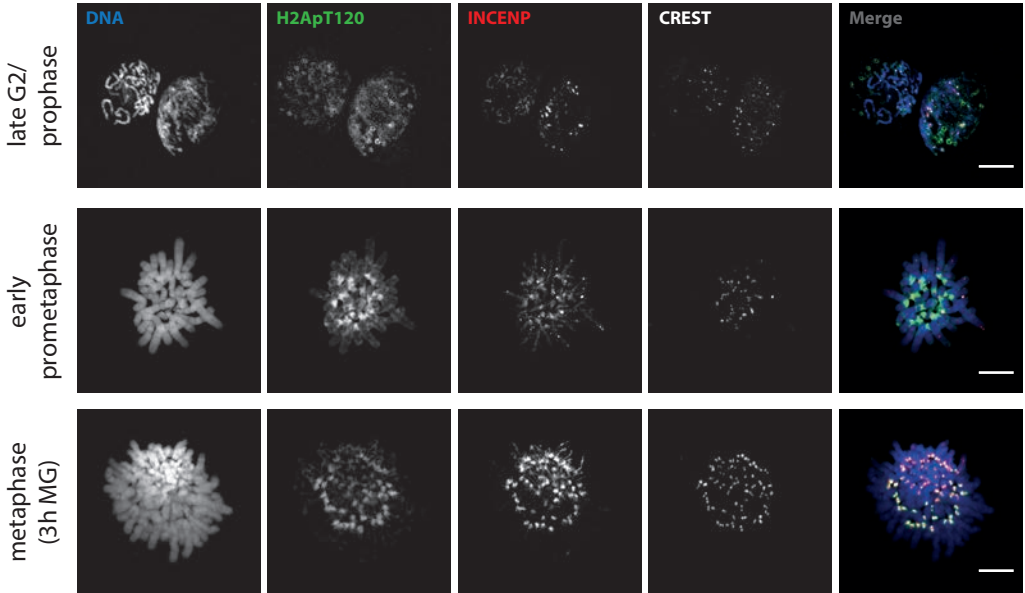
We are grateful to the patients of the IVF unit at the Erasmus MC, University Medical Center for donating embryos for this study. We thank G. Kops for a generous gift of antibodies. J. Speksnijder and A. Dons are gratefully acknowledged for technical assistance, and Dr. G. van Cappellen from the Erasmus Optical Imaging Centre for advice on methods for quantification of immunofluorescence.

### **Funding**

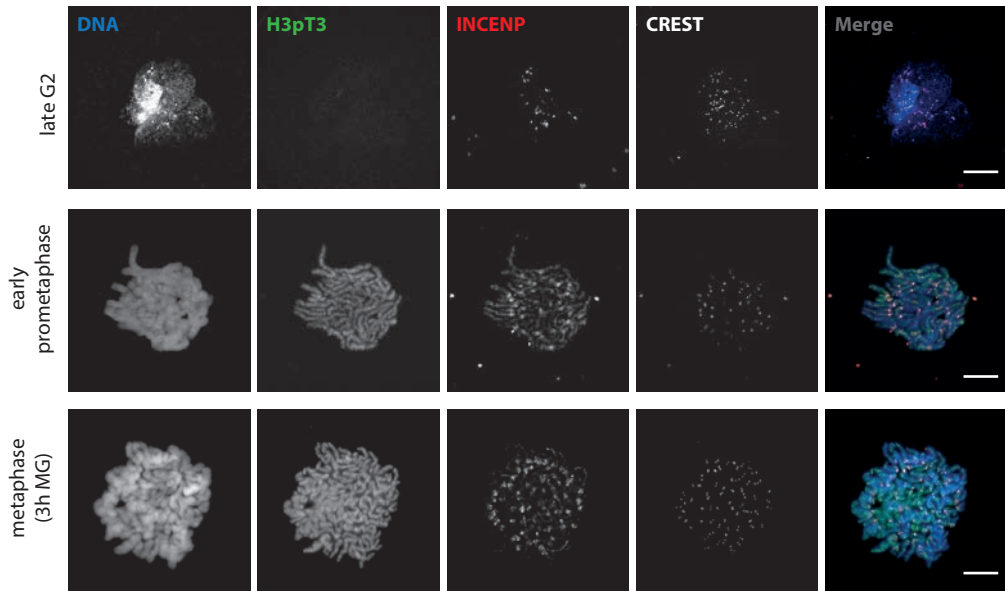
This study was funded by a grant from Fundação para a Ciência e Tecnologia (SFRH/BD/39 063/2007) to M.A.S. and from the Netherlands Organisation for Scientific Research (NWO-Veni: ZonMW 016.096.106) to E.B.B.

### **Conflict of interest**

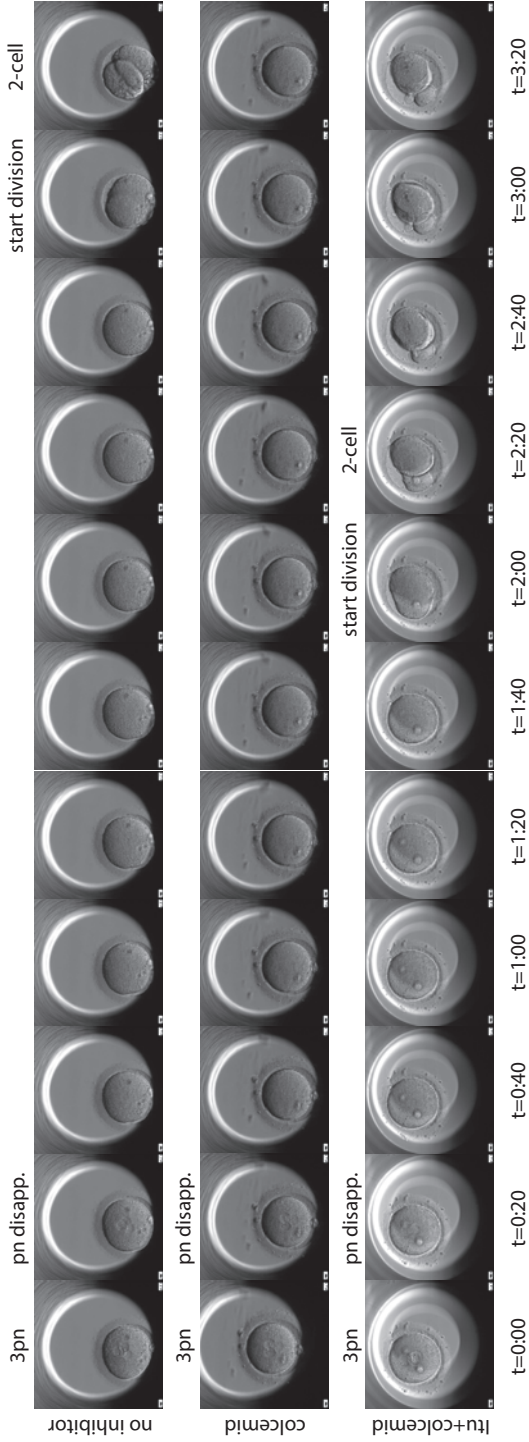
The authors declare that there is no conflict of interest that would prejudice the impartiality of this scientific work.



**Supplementary Figure 1** — Immunolocalization of H2ApT120, INCENP and centromeres (CREST) on whole mount human zygotes at late G2/prophase, and chromosome spreads prepared at the early prometaphase and metaphase stage. Zygotes at early prometaphase were fixed 30 min after NEB in the absence of cell cycle inhibitors. Zygotes at metaphase were cultured directly after NEB in the presence of the proteasome inhibitor MG132 and fixed 3h later. DNA was counterstained with DAPI. Scale bars represent 10  $\mu$ m.



**Supplementary Figure 2** — Immunolocalization of H3pT3, INCENP and centromeres (CREST) on whole mount human zygotes at late G2/prophase, and chromosome spreads prepared at early prometaphase and metaphase stage. Zygotes at early prometaphase were fixed 30 min after NEB in the absence of cell cycle inhibitors. Zygotes at metaphase were cultured directly after NEB in the presence of the proteasome inhibitor MG132 and fixed 3h later. DNA was counterstained with DAPI. Scale bars represent 10  $\mu\text{m}$ .



Supplementary Figure 3 — Sequential images obtained by time-lapse imaging comparing mitotic progression in human 3PN embryos incubated without cell cycle inhibitors, with colcemid, or with colcemid and 5-iodotubercidin (Itu). 3PN embryos without any inhibitor complete cytokinesis 3 hours after disappearance of the pronuclei (nuclear envelope breakdown, NEB). Treatment with colcemid inhibits division for >24h. Treatment with colcemid+Itu reduced the time between cleavage and NEB to within 2 hours.

## References

1. Mantzouratou, A. and J.D. Delhanty, *Aneuploidy in the human cleavage stage embryo*. Cytogenet Genome Res, 2011. **133**(2-4): p. 141-8.
2. Voet, T., E. Vanneste, and J.R. Vermeesch, *The human cleavage stage embryo is a cradle of chromosomal rearrangements*. Cytogenet Genome Res, 2011. **133**(2-4): p. 160-8.
3. Baart, E.B., et al., *Preimplantation genetic screening reveals a high incidence of aneuploidy and mosaicism in embryos from young women undergoing IVF*. Human reproduction (Oxford, England), 2006. **21**(1): p. 223-233.
4. Santos, M.A., et al., *The fate of the mosaic embryo: chromosomal constitution and development of Day 4, 5 and 8 human embryos*. Hum Reprod, 2010. **25**(8): p. 1916-26.
5. Vanneste, E., et al., *Chromosome instability is common in human cleavage-stage embryos*. Nature medicine, 2009. **15**(5): p. 577-583.
6. Bielanska, M., S.L. Tan, and A. Ao, *Chromosomal mosaicism throughout human preimplantation development in vitro: incidence, type, and relevance to embryo outcome*. Hum Reprod, 2002. **17**(2): p. 413-9.
7. Ruangvutitert, P., et al., *FISH analysis on day 5 post-insemination of human arrested and blastocyst stage embryos*. Prenat Diagn, 2000. **20**(7): p. 552-60.
8. Mantikou, E., et al., *Temporal and developmental-stage variation in the occurrence of mitotic errors in tripronuclear human preimplantation embryos*. Biol Reprod, 2013. **89**(2): p. 42.
9. Chao, W.C., et al., *Structure of the mitotic checkpoint complex*. Nature, 2012. **484**(7393): p. 208-13.
10. Eytan, E., et al., *Roles of different pools of the mitotic checkpoint complex and the mechanisms of their disassembly*. Proc Natl Acad Sci U S A, 2013. **110**(26): p. 10568-73.
11. Kops, G.J., B.A. Weaver, and D.W. Cleveland, *On the road to cancer: aneuploidy and the mitotic checkpoint*. Nature reviews.Cancer, 2005. **5**(10): p. 773-785.
12. Oliveira, R.A., et al., *Cohesin cleavage and Cdk inhibition trigger formation of daughter nuclei*. Nat Cell Biol, 2010. **12**(2): p. 185-92.
13. Foley, E.A. and T.M. Kapoor, *Microtubule attachment and spindle assembly checkpoint signalling at the kinetochore*. Nat Rev Mol Cell Biol, 2013. **14**(1): p. 25-37.
14. London, N. and S. Biggins, *Signalling dynamics in the spindle checkpoint response*. Nat Rev Mol Cell Biol, 2014. **15**(11): p. 736-47.
15. van der Waal, M.S., et al., *Cell division control by the Chromosomal Passenger Complex*. Exp Cell Res, 2012. **318**(12): p. 1407-20.
16. Carmena, M., et al., *The chromosomal passenger complex (CPC): from easy rider to the godfather of mitosis*. Nat Rev Mol Cell Biol, 2012. **13**(12): p. 789-803.
17. Avo Santos, M., et al., *A role for Aurora C in the chromosomal passenger complex during human preimplantation embryo development*. Hum Reprod, 2011. **26**(7): p. 1868-81.
18. Slatery, S.D., et al., *Aurora-C kinase supports mitotic progression in the absence of Aurora-B*. Cell Cycle, 2009. **8**(18): p. 2984-94.
19. Fernandez-Miranda, G., et al., *Genetic disruption of aurora B uncovers an essential role for aurora C during early mammalian development*. Development, 2011. **138**(13): p. 2661-72.
20. Schindler, K., et al., *Maternally recruited Aurora C kinase is more stable than Aurora B to support mouse oocyte maturation and early development*. Proceedings of the National Academy of Sciences of the United States of America, 2012. **109**(33): p. E2215-22.
21. Balboula, A.Z. and K. Schindler, *Selective disruption of aurora C kinase reveals distinct functions from aurora B kinase during meiosis in mouse oocytes*. PLoS Genet, 2014. **10**(2): p. e1004194.
22. van der Horst, A. and S.M. Lens, *Cell division: control of the chromosomal passenger complex in time and space*. Chromosoma, 2014. **123**(1-2): p. 25-42.
23. Boyarchuk, E., R. Montes de Oca, and G. Almouzni, *Cell cycle dynamics of histone variants at the centromere, a model for chromosomal landmarks*. Curr Opin Cell Biol, 2011. **23**(3): p. 266-76.

24. Peters, A.H., et al., *Loss of the Suv39h histone methyltransferases impairs mammalian heterochromatin and genome stability.* Cell, 2001. **107**(3): p. 323-37.
25. Bannister, A.J., et al., *Selective recognition of methylated lysine 9 on histone H3 by the HP1 chromo domain.* Nature, 2001. **410**(6824): p. 120-4.
26. Hirota, T., et al., *Histone H3 serine 10 phosphorylation by Aurora B causes HP1 dissociation from heterochromatin.* Nature, 2005. **438**(7071): p. 1176-80.
27. Kang, J., et al., *Mitotic centromeric targeting of HP1 and its binding to Sgo1 are dispensable for sister-chromatid cohesion in human cells.* Mol Biol Cell, 2011. **22**(8): p. 1181-90.
28. Chakraborty, A., K.V. Prasanth, and S.G. Prasanth, *Dynamic phosphorylation of HP1alpha regulates mitotic progression in human cells.* Nat Commun, 2014. **5**: p. 3445.
29. Yamagishi, Y., et al., *Heterochromatin links to centromeric protection by recruiting shugoshin.* Nature, 2008. **455**(7210): p. 251-5.
30. Tsukahara, T., Y. Tanno, and Y. Watanabe, *Phosphorylation of the CPC by Cdk1 promotes chromosome bi-orientation.* Nature, 2010. **467**(7316): p. 719-23.
31. Kawashima, S.A., et al., *Phosphorylation of H2A by Bub1 prevents chromosomal instability through localizing shugoshin.* Science, 2010. **327**(5962): p. 172-7.
32. Kelly, A.E., et al., *Survivin reads phosphorylated histone H3 threonine 3 to activate the mitotic kinase Aurora B.* Science, 2010. **330**(6001): p. 235-9.
33. Wang, F., et al., *Histone H3 Thr-3 phosphorylation by Haspin positions Aurora B at centromeres in mitosis.* Science, 2010. **330**(6001): p. 231-5.
34. Yamagishi, Y., et al., *Two histone marks establish the inner centromere and chromosome bi-orientation.* Science, 2010. **330**(6001): p. 239-43.
35. Liu, H., L. Jia, and H. Yu, *Phospho-H2A and cohesin specify distinct tension-regulated Sgo1 pools at kinetochores and inner centromeres.* Curr Biol, 2013. **23**(19): p. 1927-33.
36. Kitajima, T.S., et al., *Human Bub1 defines the persistent cohesion site along the mitotic chromosome by affecting Shugoshin localization.* Curr Biol, 2005. **15**(4): p. 353-9.
37. Wang, F., et al., *A positive feedback loop involving Haspin and Aurora B promotes CPC accumulation at centromeres in mitosis.* Curr Biol, 2011. **21**(12): p. 1061-9.
38. Dai, J., et al., *The kinase haspin is required for mitotic histone H3 Thr 3 phosphorylation and normal metaphase chromosome alignment.* Genes Dev, 2005. **19**(4): p. 472-88.
39. Qian, J., et al., *PP1/Repo-man dephosphorylates mitotic histone H3 at T3 and regulates chromosomal aurora B targeting.* Curr Biol, 2011. **21**(9): p. 766-73.
40. Qian, J., et al., *Aurora B defines its own chromosomal targeting by opposing the recruitment of the phosphatase scaffold Repo-Man.* Curr Biol, 2013. **23**(12): p. 1136-43.
41. Wang, F., et al., *Haspin inhibitors reveal centromeric functions of Aurora B in chromosome segregation.* J Cell Biol, 2012. **199**(2): p. 251-68.
42. Clift, D. and M. Schuh, *Restarting life: fertilization and the transition from meiosis to mitosis.* Nat Rev Mol Cell Biol, 2013. **14**(9): p. 549-62.
43. Burton, A. and M.E. Torres-Padilla, *Chromatin dynamics in the regulation of cell fate allocation during early embryogenesis.* Nat Rev Mol Cell Biol, 2014. **15**(11): p. 723-35.
44. Puschendorf, M., et al., *PRC1 and Suv39h specify parental asymmetry at constitutive heterochromatin in early mouse embryos.* Nature genetics, 2008. **40**(4): p. 411-420.
45. van de Werken, C., et al., *Paternal heterochromatin formation in human embryos is H3K9/HP1 directed and primed by sperm-derived histone modifications.* Nat Commun, 2014. **5**: p. 5868.
46. Ulmer, R., et al., *Triploid embryo after in vitro fertilization.* Arch Gynecol, 1985. **237**(2): p. 101-7.
47. van der Heijden, G.W., et al., *Parental origin of chromatin in human monopronuclear zygotes revealed by asymmetric histone methylation patterns, differs between IVF and ICSI.* Molecular reproduction and development, 2009. **76**(1): p. 101-108.
48. Vassena, R., et al., *Waves of early transcriptional activation and pluripotency program initiation during human preimplantation development.* Development, 2011. **138**(17): p. 3699-709.

49. Hohmann, F.P., N.S. Macklon, and B.C. Fauser, *A randomized comparison of two ovarian stimulation protocols with gonadotropin-releasing hormone (GnRH) antagonist cotreatment for in vitro fertilization commencing recombinant follicle-stimulating hormone on cycle day 2 or 5 with the standard long GnRH agonist protocol*. J Clin Endocrinol Metab, 2003. **88**(1): p. 166-73.
50. Ciemerych, M.A., B. Maro, and J.Z. Kubiak, *Control of duration of the first two mitoses in a mouse embryo*. Zygote, 1999. **7**(4): p. 293-300.
51. Sikora-Polaczek, M., et al., *The first mitosis of the mouse embryo is prolonged by transitional metaphase arrest*. Biol Reprod, 2006. **74**(4): p. 734-43.
52. Livak, K.J. and T.D. Schmittgen, *Analysis of relative gene expression data using real-time quantitative PCR and the 2(-Delta Delta C(T)) Method*. Methods (San Diego, Calif.), 2001. **25**(4): p. 402-408.
53. van de Werken, C., et al., *A universal method for sequential immunofluorescent analysis of chromatin and chromatin-associated proteins on chromosome spreads*. Chromosome Res, 2013. **21**(5): p. 475-89.
54. Kitajima, T.S., S.A. Kawashima, and Y. Watanabe, *The conserved kinetochore protein shugoshin protects centromeric cohesion during meiosis*. Nature, 2004. **427**(6974): p. 510-7.
55. Nerusheva, O.O., et al., *Tension-dependent removal of pericentromeric shugoshin is an indicator of sister chromosome biorientation*. Genes Dev, 2014. **28**(12): p. 1291-309.
56. Wongtawan, T., et al., *Histone H4K20me3 and HP1alpha are late heterochromatin markers in development, but present in undifferentiated embryonic stem cells*. J Cell Sci, 2011. **124**(Pt 11): p. 1878-90.
57. Vagnarelli, P., et al., *Repo-Man coordinates chromosomal reorganization with nuclear envelope reassembly during mitotic exit*. Developmental cell, 2011. **21**(2): p. 328-42.
58. De Antoni, A., et al., *A small-molecule inhibitor of Haspin alters the kinetochore functions of Aurora B*. J Cell Biol, 2012. **199**(2): p. 269-84.
59. Ditchfield, C., et al., *Aurora B couples chromosome alignment with anaphase by targeting BubR1, Mad2, and Cenp-E to kinetochores*. The Journal of cell biology, 2003. **161**(2): p. 267-280.
60. Teperek-Tkacz, M., et al., *Phosphorylation of histone H3 serine 10 in early mouse embryos: active phosphorylation at late S phase and differential effects of ZM447439 on first two embryonic mitoses*. Cell Cycle, 2010. **9**(23): p. 4674-87.
61. Fischle, W., et al., *Regulation of HP1-chromatin binding by histone H3 methylation and phosphorylation*. Nature, 2005. **438**(7071): p. 1116-22.
62. Dai, J., B.A. Sullivan, and J.M. Higgins, *Regulation of mitotic chromosome cohesion by Haspin and Aurora B*. Developmental cell, 2006. **11**(5): p. 741-50.
63. Bassett, E.A., et al., *Epigenetic centromere specification directs aurora B accumulation but is insufficient to efficiently correct mitotic errors*. J Cell Biol, 2010. **190**(2): p. 177-85.
64. Campbell, C.S. and A. Desai, *Tension sensing by Aurora B kinase is independent of survivin-based centromere localization*. Nature, 2013. **497**(7447): p. 118-21.
65. Cimini, D., et al., *Merotelic kinetochore orientation is a major mechanism of aneuploidy in mitotic mammalian tissue cells*. J Cell Biol, 2001. **153**(3): p. 517-27.
66. Coonen, E., et al., *Anaphase lagging mainly explains chromosomal mosaicism in human preimplantation embryos*. Hum Reprod, 2004. **19**(2): p. 316-24.
67. van Echten-Arends, J., et al., *Chromosomal mosaicism in human preimplantation embryos: a systematic review*. Hum Reprod Update, 2011. **17**(5): p. 620-7.
68. Capalbo, A., et al., *Sequential comprehensive chromosome analysis on polar bodies, blastomeres and trophoblast: insights into female meiotic errors and chromosomal segregation in the preimplantation window of embryo development*. Hum Reprod, 2013. **28**(2): p. 509-18.
69. Mantikou, E., et al., *Molecular origin of mitotic aneuploidies in preimplantation embryos*. Biochim Biophys Acta, 2012. **1822**(12): p. 1921-30.
70. Ghenoïu, C., M.S. Wheelock, and H. Funabiki, *Autoinhibition and Polo-dependent multisite phosphorylation restrict activity of the histone H3 kinase Haspin to mitosis*. Mol Cell, 2013. **52**(5): p. 734-45.
71. Zhou, L., et al., *Polo-like kinase-1 triggers histone phosphorylation by Haspin in mitosis*. EMBO reports, 2014. **15**(3): p. 273-81.

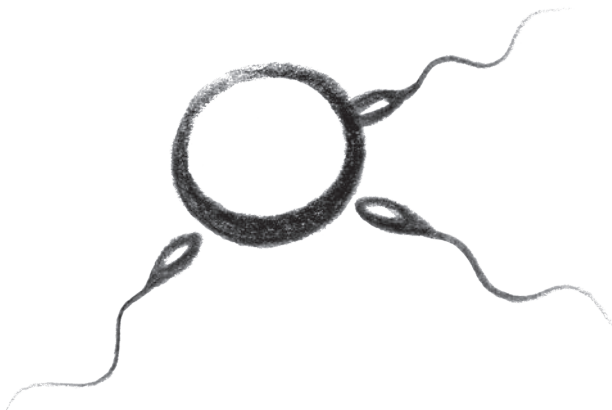


72. Waizenegger, I.C., et al., *Two distinct pathways remove mammalian cohesin from chromosome arms in prophase and from centromeres in anaphase*. Cell, 2000. **103**(3): p. 399-410.
73. Nishiyama, T., et al., *Aurora B and Cdk1 mediate Wapl activation and release of acetylated cohesin from chromosomes by phosphorylating Sororin*. Proceedings of the National Academy of Sciences of the United States of America, 2013. **110**(33): p. 13404-9.
74. Dreier, M.R., M.E. Bekier, 2nd, and W.R. Taylor, *Regulation of sororin by Cdk1-mediated phosphorylation*. J Cell Sci, 2011. **124**(Pt 17): p. 2976-87.
75. Sumara, I., et al., *The dissociation of cohesin from chromosomes in prophase is regulated by Polo-like kinase*. Mol Cell, 2002. **9**(3): p. 515-25.
76. Hauf, S., et al., *Dissociation of cohesin from chromosome arms and loss of arm cohesion during early mitosis depends on phosphorylation of SA2*. PLoS Biol, 2005. **3**(3): p. e69.
77. Tachibana-Konwalski, K., et al., *Rec8-containing cohesin maintains bivalents without turnover during the growing phase of mouse oocytes*. Genes Dev, 2010. **24**(22): p. 2505-16.
78. Dai, J. and J.M. Higgins, *Haspin: a mitotic histone kinase required for metaphase chromosome alignment*. Cell Cycle, 2005. **4**(5): p. 665-8.
79. Carretero, M., et al., *Pds5B is required for cohesion establishment and Aurora B accumulation at centromeres*. EMBO J, 2013. **32**(22): p. 2938-49.
80. Higgins, J.M., *Chromosome segregation: learning to let go*. Curr Biol, 2013. **23**(19): p. R883-5.
81. Tateno, H., H. Kusakabe, and Y. Kamiguchi, *Structural chromosomal aberrations, aneuploidy, and mosaicism in early cleavage mouse embryos derived from spermatozoa exposed to gamma-rays*. Int J Radiat Biol, 2011. **87**(3): p. 320-9.



# CHAPTER 6

## General discussion



Many cellular processes in pre-implantation embryos are clearly different from what has been described in somatic cells. Our interest in chromosomal abnormalities in human pre-implantation embryos [1-4] has led us to investigate two of these differences: the establishment of constitutive heterochromatin and the composition and targeting of the chromosomal passenger complex. In this chapter, we discuss the main findings of our studies and the implications of those findings for future clinical procedures and research.

## **Modified histones retained in human spermatozoa contribute to the establishment of embryonic chromatin structure**

Chromatin structure re-establishment is one of the most important processes after fertilization, as chromatin structure is essential for the regulation of gene expression, differentiation and chromosome segregation (see **chapter 1**). In **chapter 2** we describe our investigation on the re-establishment of a prominent heterochromatin domain, constitutive heterochromatin (cHC), and the possible contribution of sperm chromatin to this process.

Our results show that histones carrying canonical cHC modifications (H3K9me3, H4K20me3, H3K64me3) are retained in spermatozoa and transmitted to the embryo. These modified histones contribute to the formation of paternal embryonic cHC, as they are recognized by maternal chromatin modifiers of the SUV39H/HP1 pathway and propagated over the embryonic cleavage divisions. These results indicate transgenerational epigenetic inheritance of cHC structure in human embryos and identify an additional role of sperm in embryo development.

The mechanism of cHC re-establishment has been studied extensively in mouse embryos and findings in this animal model are frequently assumed to be generally applicable for all mammalian species [5-8]. However, we now have shown that the mechanism in human embryos differs significantly from what has been described for mice. Mouse paternal cHC lacks canonical cHC marks and is formatted by a backup mechanism (Polycomb proteins) during the first stages of embryo development [9]. In contrast, we find human cHC to be transmitted in the canonical configuration from the spermatozoon to the embryo, which not appear to possess – or need – the backup mechanism. This indicates that in human embryos there is no need for complete chromatin structure re-establishment, as the canonical cHC structure is never entirely lost. This might also be true for other chromatin domains. We therefore hypothesize that the epigenetic contribution of the human spermatozoon allows human pre-implantation embryos to maintain a canonical-like chromatin structure and might thereby obviate the need for a complete epigenetic reprogramming. This may explain observations in stem cells research; human embryonic stem cells have shown reduced plasticity when compared to mouse embryonic stem cells [10-11]. Whether these species differences relate to differences in chromatin structure remains to be investigated. Importantly, our results show that mouse pre-implantation embryos are not a representative animal model to study epigenetic regulation of human pre-implantation embryo development. This underlines the importance of research on human embryos, which will improve our understanding of human

embryo development, embryonic stem cells and the influence of *in vitro* culture conditions during IVF treatments.

The epigenetic contribution of spermatozoa to embryo development raises the question whether there are variations between spermatozoa that might have an impact on embryo developmental potential. During mammalian spermiogenesis, histones are replaced by protamines. In humans, 5-15% of the DNA appears to be protected against this histone removal and retains a nucleosomal structure (for review see [12]). Some studies have shown that modified histones are retained at promoters of genes involved in early embryo development [13-15]. In one of these studies, the authors describe that in infertile men, the number of retained histones is both higher and more variable than in fertile men, and that the histones are retained in a more dispersed pattern throughout the genome [15]. Another study demonstrated that there is an increase in the nucleosome/protamine ratio in spermatozoa from male factor subfertility patients [16]. Variations like these may interfere with the function of a specific histone retention pattern and thereby affect embryo development. As chromatin structure is important for regulation of gene expression and chromosome segregation, we hypothesize that variation in histone content between spermatozoa may have an impact on embryonic chromatin and thereby on developmental potential. It would be interesting to study the variation in chromatin structure between spermatozoa in more detail and to investigate whether it correlates with factors such as sperm quality based on morphological examination and patient characteristics, e.g. age, weight and lifestyle. These kind of studies might result in a marker for male fertility and lead to the development of new diagnostic, or even prognostic, tests which enable patient-tailored counseling and treatment. If future techniques provide tools to detect subtle differences in sperm chromatin structure, sperm selection could be based on sperm content, in addition to sperm morphology. This would be a novel approach to optimize IVF outcome.

## Chromosomal passenger complex composition and localization are different in the first stages of human embryo development

In somatic cells, the chromosomal passenger complex (CPC) plays a crucial role in the prevention of chromosome missegregation by ensuring accurate chromosome attachment and regulating mitotic checkpoint complex (MCC) activity (see **chapter 1**). In human pre-implantation embryos, chromosomal abnormalities are detected at high frequencies [1,4,17-26], which suggest impaired functionality of these mechanisms. Therefore, we investigated composition (**chapter 3**) and localization (**chapter 5**) of the CPC in human pre-implantation embryos derived from IVF.

In **chapter 3**, we describe a difference in composition of the CPC during the first embryonic cleavage divisions, as compared to somatic cells. In somatic cells, Aurora B is the kinetic subunit of the CPC. In pre-implantation embryos, from the zygote (embryonic day 1) up to the 8- to 16-cell stage (embryonic day 3 and 4), we found Aurora C to be the main kinetic subunit present in the CPC. Around the morula stage (embryonic day 4), Aurora C levels at the inner centromere decrease and at the blastocyst stage (embryonic day 5) Aurora C is completely replaced by Aurora B.

Aurora C has been known as the meiotic counterpart of Aurora B and is thus present in oocytes. Due to different mRNA and protein characteristics, Aurora C is less susceptible to degradation in comparison with Aurora B [27-29]. This might explain why Aurora C is still present after meiosis, whereas Aurora B is degraded. Possibly, this also explains why Aurora C is needed during the first mitotic divisions of the embryo; before embryonic genome activation, embryos rely on maternal transcripts, which are stored in the oocyte.

As Aurora C is present only during the first cleavage divisions of embryos, which are more prone to segregation errors than mitotic division later during development [4], it is tempting to speculate about a link between Aurora C and chromosome missegregation. Aurora C has been shown to compensate for the absence of Aurora B in HeLa cells [30-31] and mouse pre-implantation embryos [32], enabling normal progression of mitosis. Although possible subtle aneuploidies were not examined in these cells, there was no indication of reduced error-correction activity of Aurora C. However, several studies have shown that overexpression of the Aurora kinases and an imbalance in expression of Aurora B and Aurora C lead to chromosome segregation errors [33-35]. In our study, we detected varying ratios of Aurora B and Aurora C in human oocytes. Therefore, we hypothesize that these differences in concentration, rather than the presence of Aurora C, might influence the accuracy of the error-correction mechanism. Investigation of the differences between the two Aurora kinases, for example of their substrates and binding partners, and the regulation of their expression might provide some clues to understand the function of these kinases in the regulation of chromosome segregation in pre-implantation embryos. Also, since it is known that female age is an important factor in oocyte quality [36-37], it would be of interest to determine whether the Aurora B/C ratio is influenced by maternal age.

Precise inner centromeric CPC localization is crucial for accurate function of the error-correction mechanism [38-39]. In **chapter 5** we describe our investigation into the localization of the CPC in the first embryonic divisions. For this investigation, we made use of the technique we developed and described in **chapter 4**. With this 'stripping' technique, we were able to perform sequential immunofluorescent analysis on the same chromosome preparation, which allowed us to investigate co-localization of several proteins and histone modifications that play a role in CPC localization. The ability to perform two immunofluorescent analyses on the same material is particularly useful in our studies on chromosome segregation and chromatin structure in human oocytes and pre-implantation embryos, since this material is rare and valuable.

Previously, it was hypothesized that the extremely high incidence of chromosomal abnormalities in human embryos were due to a lack of a functional mitotic checkpoint [21]. Using different kinase inhibitors in our investigation of CPC localization pathways (**chapter 5**), we demonstrate that feedback loops between CPC and MCC proteins, as described in somatic cells [40-43], are functional and that the checkpoint is active. Therefore, we hypothesize that chromosomal abnormalities in human embryos do not arise because of a total lack of mitotic checkpoint function activity. However, this does not rule out the possibility of more subtle differences in checkpoint functionality.

In **chapter 5**, we found CPC localization to be less confined to the inner centromeric region in zygotes than at later developmental stages. Also, we found that in the zygote stage, one of the pathways for CPC targeting (see **chapter 1**) is different; H3T3 phosphorylation failed to enrich at the

centromeric region on metaphase chromosomes in human zygotes. From the 2-cell stage onwards, H3pT3 was detected in a normal pattern and towards the blastocyst stage, CPC localization slowly normalized too. These findings suggest that centromeric targeting of the CPC is controlled differently and possibly less accurate in zygotes and to a lesser extent also in cleavage stage embryos. It is tempting to speculate that altered CPC targeting and localization contribute to the occurrence of chromosomal abnormalities. Future research should elucidate if this is the case, for example by investigating the error-correcting ability of the CPC in the first mitotic division of embryos.

Despite abundant H3pT3 on chromosome arms in zygotes, the CPC still localizes to the centromeric area, suggesting that centromeric CPC localization is not completely dependent on centromeric enrichment of H3pT3. Still, CPC localization is less restricted to the centromere, so the different H3pT3 pattern may have an impact on the accuracy of the CPC targeting. Studies in somatic cells support this hypothesis, as induced abundant H3pT3 on the chromosome arms leads to CPC mislocalization [44]. However, the pattern of H3pT3 normalizes already in the 2-cell stage, whereas CPC localization normalizes slowly towards the blastocyst stage. Thus, more factors will probably underlie the less accurate CPC localization during the cleavage divisions. Differences in the pathways that regulate CPC targeting may be an explanation for chromosome missegregation in embryos, as subtle changes in CPC localization are known to affect chromosome alignment and the error-correction mechanism [38-39,43]. Next to this, high levels of H3pT3 on chromosome arms were shown to affect mechanisms responsible for cohesion resolution in somatic cells [45], which leads to chromosome segregation defects. Thus, the observed difference in H3pT3 localization in human zygotes may have different consequences for the regulation of chromosome segregation and might cause chromosome segregation to be more error prone.

Taken together, results described in **chapter 3** and **chapter 5** show that there are differences in both CPC composition and localization in the first mitotic divisions of embryos, compared with mitotic divisions in later embryonic stages and somatic cells. Presence of Aurora C as the main CPC kinase and different targeting and localization of the CPC might lead to a less accurate regulation of chromosome segregation. Further research is needed to determine if the differences we observed indeed affect the prevention and correction of erroneous chromosome segregation, for example by assessing if the error correcting ability of the CPC is different in the first cleavage divisions.

Our knowledge on the high rate of chromosomal abnormalities is almost exclusively derived from embryos generated by IVF. It is possible that our observations are induced by the IVF procedure, for example through influence of hormonal treatment or *in vitro* embryo culture. However, chromosomal abnormalities are also observed after natural cycle IVF and in *in vivo* fertilized porcine and bovine embryos, indicating that embryos of certain mammalian species are predisposed to chromosome segregation errors. Whether (suboptimal) IVF procedures increase the chance on these errors is very hard to examine, because of ethical and practical difficulties in obtaining human *in vivo* pre-implantation embryos. Still, our increasing knowledge on chromosome segregation in IVF-derived embryos is relevant for daily IVF practice and future optimization of IVF procedures.

## Is altered chromosomal passenger complex composition and localization an adaptation to epigenetic asymmetry between maternal and paternal chromatin?

As described in **chapter 3** and **chapter 5**, both the composition and the localization of the CPC in pre-implantation embryos differ from what has been described in somatic cells. Next to that, there are differences in the structure of chromatin, most prominent of which is the asymmetry between paternal and maternal chromatin, as described in **chapter 2**. In our investigation of CPC localization (**chapter 5**), we revealed an effect of this epigenetic asymmetry on CPC localization under certain experimental conditions.

To investigate the mechanism of CPC targeting, we used an inhibitor of Aurora kinase activity. As a result, the histone modifications induced by Aurora kinase directly (H3pS10) and indirectly via Haspin activation (H3pT3) were dramatically reduced. Surprisingly, maternal and paternal chromosomes showed different effects of the inhibitor. On maternal chromosomes, which are H3K9me3-positive along the whole chromosome, both residual H3pT3 and CPC levels were higher, and CPC localization was less restricted to the inner centromere. On paternal chromosomes, which are H3K9me3-positive at cHC regions only, H3pT3 and the CPC were detected at lower levels and the CPC mainly localized to the cHC, which is localized not only pericentrically, but also in large blocks on certain chromosomes, referred to as knobs [46]. Based on these results, we propose that Aurora kinase activity, possibly Aurora C activity specifically, and the altered Haspin-H3pT3 pathway are necessary to compensate for the epigenetic asymmetry in zygotes. Possibly, Aurora C-mediated H3pS10 and Haspin-mediated H3pT3 equalize maternal and paternal chromatin, for example by inhibiting the binding of chromatin regulators to the DNA, and thereby cover the difference in H3K9me3 and related cHC marks. Hence, these mechanisms might be an adaptation to the extreme parental epigenetic asymmetry in zygotes, in order to ensure similar CPC localization on maternal and paternal chromosomes. As a consequence of these mechanisms having to deal with epigenetic asymmetry, chromosome segregation might become more error-prone. Therefore, the altered CPC targeting and the epigenetic asymmetry between parental chromosomes might together explain the high rates of chromosome segregation errors in human pre-implantation embryos.

Similar to human embryos, extreme parental asymmetry has been described in mouse embryos. Also, Aurora C seems to be involved in early mouse development [29], and we detected persisting H3pT3 in mouse zygotes (unpublished observations). Interestingly, these features do not result in high rates of chromosomal abnormalities in mouse embryos. Possibly, different mechanisms for CPC targeting or the Polycomb backup mechanism for marking paternal cHC [9] create a more reliable error-correction mechanism. Therefore, the transfer and maintenance of H3K9me3 in paternal chromatin of human embryos may be an underlying cause of error-prone chromosome segregation.

Until recently, research into the origin of chromosomal abnormalities has focused mainly on causative factors in the oocyte. Future research should focus on the possible contribution of the spermatozoon. It would be of interest to investigate the possible variation in the epigenetic signature of cHC in human spermatozoa, and to determine whether this variation is transferred to paternal embryonic chromatin. Since cHC is important for correct chromosome segregation



[47-48], we hypothesize that variations in the histone retention pattern of spermatozoa might affect chromosome segregation mechanisms in embryos. Analyzing the variation in the epigenetic make-up of spermatozoa and the consequences of this for the regulation of chromosome segregation in early embryos, hope to underlying causes of aneuploidy in human embryos. Knowledge of the influence of sperm quality on embryo developmental potential may provide clues to further optimize IVF procedures in the future.

## Concluding remarks

The first embryonic cleavage divisions are mitotic divisions, but they differ from somatic mitosis in many aspects [49]. Paternal and maternal chromosomes coming from two epigenetically different gametes need to be aligned on a single metaphase plate, a situation likely to require adaptations in chromosome segregation regulation. Our findings show that the mechanisms that regulate CPC function and localization are altered in the first cleavage divisions of human embryos and we hypothesize that this is related to the epigenetic asymmetry between maternal and paternal chromatin. Although these mechanisms may be altered to ensure the best possible CPC targeting in a situation that is very different from somatic cells, CPC localization and function may be less accurate and that may lead to a reduced efficiency of the error-correction mechanism. This might be an explanation for the high rates of chromosome segregation errors in human pre-implantation embryos. Our hypothesis is supported by the observation that both the normalization of CPC composition and localization and the equalization of paternal and maternal chromatin marks around the morula stage (embryonic day 4) coincide with a decrease in chromosome segregation errors. Since we show that spermatozoa make a significant contribution to chromatin structure in embryos, it would be interesting to investigate the influence of sperm quality on chromosomal abnormalities and developmental competence of embryos.

## References

1. Baart, E.B., et al., *Preimplantation genetic screening reveals a high incidence of aneuploidy and mosaicism in embryos from young women undergoing IVF*. Human reproduction (Oxford, England), 2006. **21**(1): p. 223-233.
2. Baart, E.B., *Aneuploidy screening of human IVF embryos: cytogenetic aspects and clinical implications*. 2007.
3. Baart, E.B., et al., *Milder ovarian stimulation for in-vitro fertilization reduces aneuploidy in the human preimplantation embryo: a randomized controlled trial*. Human reproduction (Oxford, England), 2007. **22**(4): p. 980-988.
4. Santos, M.A., et al., *The fate of the mosaic embryo: chromosomal constitution and development of Day 4, 5 and 8 human embryos*. Hum Reprod, 2010. **25**(8): p. 1916-26.
5. Probst, A.V. and G. Almouzni, *Heterochromatin establishment in the context of genome-wide epigenetic reprogramming*. Trends Genet, 2011. **27**(5): p. 177-85.
6. Fadloun, A., A. Eid, and M.E. Torres-Padilla, *Mechanisms and dynamics of heterochromatin formation during Mammalian development: closed paths and open questions*. Curr Top Dev Biol, 2013. **104**: p. 1-45.
7. Nestorov, P., M. Tardat, and A.H. Peters, *H3K9/HP1 and Polycomb: Two Key Epigenetic Silencing Pathways for Gene Regulation and Embryo Development*. Curr Top Dev Biol, 2013. **104**: p. 243-91.
8. Duffie, R. and D. Bourc'his, *Parental epigenetic asymmetry in mammals*. Curr Top Dev Biol, 2013. **104**: p. 293-328.
9. Puschendorf, M., et al., *PRC1 and Suv39h specify parental asymmetry at constitutive heterochromatin in early mouse embryos*. Nature genetics, 2008. **40**(4): p. 411-420.
10. Tesar, P.J., et al., *New cell lines from mouse epiblast share defining features with human embryonic stem cells*. Nature, 2007. **448**(7150): p. 196-9.
11. Nichols, J. and A. Smith, *Naive and primed pluripotent states*. Cell Stem Cell, 2009. **4**(6): p. 487-92.
12. Miller, D., M. Brinkworth, and D. Iles, *Paternal DNA packaging in spermatozoa: more than the sum of its parts? DNA, histones, protamines and epigenetics*. Reproduction, 2010. **139**(2): p. 287-301.
13. Hammoud, S.S., et al., *Distinctive chromatin in human sperm packages genes for embryo development*. Nature, 2009. **460**(7254): p. 473-8.
14. Brykczynska, U., et al., *Repressive and active histone methylation mark distinct promoters in human and mouse spermatozoa*. Nat Struct Mol Biol, 2010. **17**(6): p. 679-87.
15. Hammoud, S.S., et al., *Genome-wide analysis identifies changes in histone retention and epigenetic modifications at developmental and imprinted gene loci in the sperm of infertile men*. Hum Reprod, 2011.
16. Ramos, L., et al., *Incomplete nuclear transformation of human spermatozoa in oligo-astheno-teratospermia: characterization by indirect immunofluorescence of chromatin and thiol status*. Hum Reprod, 2008. **23**(2): p. 259-70.
17. Magli, M.C., et al., *Chromosome mosaicism in day 3 aneuploid embryos that develop to morphologically normal blastocysts in vitro*. Hum Reprod, 2000. **15**(8): p. 1781-6.
18. Wells, D. and J.D. Delhanty, *Comprehensive chromosomal analysis of human preimplantation embryos using whole genome amplification and single cell comparative genomic hybridization*. Mol Hum Reprod, 2000. **6**(11): p. 1055-62.
19. Bielanska, M., S.L. Tan, and A. Ao, *Chromosomal mosaicism throughout human preimplantation development in vitro: incidence, type, and relevance to embryo outcome*. Hum Reprod, 2002. **17**(2): p. 413-9.
20. Coonen, E., et al., *Anaphase lagging mainly explains chromosomal mosaicism in human preimplantation embryos*. Hum Reprod, 2004. **19**(2): p. 316-24.
21. Los, F.J., D. Van Opstal, and C. van den Berg, *The development of cytogenetically normal, abnormal and mosaic embryos: a theoretical model*. Hum Reprod Update, 2004. **10**(1): p. 79-94.
22. Delhanty, J.D., *Mechanisms of aneuploidy induction in human oogenesis and early embryogenesis*. Cytogenet Genome Res, 2005. **111**(3-4): p. 237-44.
23. Baart, E.B., et al., *FISH analysis of 15 chromosomes in human day 4 and 5 preimplantation embryos: the added value of extended aneuploidy detection*. Prenatal diagnosis, 2007. **27**(1): p. 55-63.
24. Vanneste, E., et al., *Chromosome instability is common in human cleavage-stage embryos*. Nature medicine, 2009. **15**(5): p. 577-583.

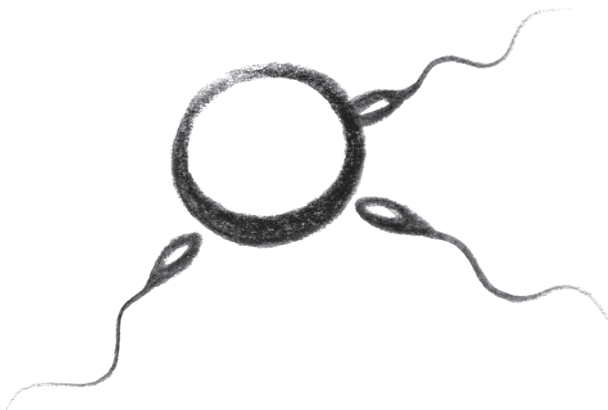
25. van Echten-Arends, J., et al., *Chromosomal mosaicism in human preimplantation embryos: a systematic review*. Hum Reprod Update, 2011. **17**(5): p. 620-7.
26. Dekel-Neftali, M., et al., *Chromosomal integrity of human preimplantation embryos at different days post fertilization*. J Assist Reprod Genet, 2013. **30**(5): p. 633-48.
27. Brown, J.R., et al., *Evolutionary relationships of Aurora kinases: implications for model organism studies and the development of anti-cancer drugs*. BMC Evol Biol, 2004. **4**: p. 39.
28. Nguyen, H.G., et al., *Mechanism of Aurora-B degradation and its dependency on intact KEN and A-boxes: identification of an aneuploidy-promoting property*. Mol Cell Biol, 2005. **25**(12): p. 4977-92.
29. Schindler, K., et al., *Maternally recruited Aurora C kinase is more stable than Aurora B to support mouse oocyte maturation and early development*. Proceedings of the National Academy of Sciences of the United States of America, 2012. **109**(33): p. E2215-22.
30. Sasai, K., et al., *Aurora-C kinase is a novel chromosomal passenger protein that can complement Aurora-B kinase function in mitotic cells*. Cell Motil Cytoskeleton, 2004. **59**(4): p. 249-63.
31. Slattery, S.D., et al., *Aurora-C kinase supports mitotic progression in the absence of Aurora-B*. Cell Cycle, 2009. **8**(18): p. 2984-94.
32. Fernandez-Miranda, G., et al., *Genetic disruption of aurora B uncovers an essential role for aurora C during early mammalian development*. Development, 2011. **138**(13): p. 2661-72.
33. Tatsuka, M., et al., *Multinuclearity and increased ploidy caused by overexpression of the aurora- and lpl1-like midbody-associated protein mitotic kinase in human cancer cells*. Cancer Res, 1998. **58**(21): p. 4811-6.
34. Kimura, M., et al., *Cell cycle-dependent expression and centrosome localization of a third human aurora/lpl1-related protein kinase, AIK3*. J Biol Chem, 1999. **274**(11): p. 7334-40.
35. Chen, H.L., et al., *Overexpression of an Aurora-C kinase-deficient mutant disrupts the Aurora-B/INCENP complex and induces polyploidy*. J Biomed Sci, 2005. **12**(2): p. 297-310.
36. Hassold, T. and P. Hunt, *To err (meiotically) is human: the genesis of human aneuploidy*. Nature reviews.Genetics, 2001. **2**(4): p. 280-291.
37. van den Berg, I.M., et al., *Defective deacetylation of histone 4 K12 in human oocytes is associated with advanced maternal age and chromosome misalignment*. Hum Reprod, 2011. **26**(5): p. 1181-90.
38. Bassett, E.A., et al., *Epigenetic centromere specification directs aurora B accumulation but is insufficient to efficiently correct mitotic errors*. J Cell Biol, 2010. **190**(2): p. 177-85.
39. Becker, M., et al., *Centromere localization of INCENP-Aurora B is sufficient to support spindle checkpoint function*. Cell cycle, 2010. **9**(7): p. 1360-72.
40. Wang, F., et al., *Haspin inhibitors reveal centromeric functions of Aurora B in chromosome segregation*. J Cell Biol, 2012. **199**(2): p. 251-68.
41. De Antoni, A., et al., *A small-molecule inhibitor of Haspin alters the kinetochore functions of Aurora B*. J Cell Biol, 2012. **199**(2): p. 269-84.
42. van der Waal, M.S., et al., *Cell division control by the Chromosomal Passenger Complex*. Exp Cell Res, 2012. **318**(12): p. 1407-20.
43. van der Horst, A. and S.M. Lens, *Cell division: control of the chromosomal passenger complex in time and space*. Chromosoma, 2014. **123**(1-2): p. 25-42.
44. Qian, J., et al., *PP1/Repo-man dephosphorylates mitotic histone H3 at T3 and regulates chromosomal aurora B targeting*. Curr Biol, 2011. **21**(9): p. 766-73.
45. Dai, J., B.A. Sullivan, and J.M. Higgins, *Regulation of mitotic chromosome cohesion by Haspin and Aurora B*. Developmental cell, 2006. **11**(5): p. 741-50.
46. Grewal, S.I. and S. Jia, *Heterochromatin revisited*. Nat Rev Genet, 2007. **8**(1): p. 35-46.
47. Peters, A.H., et al., *Loss of the Suv39h histone methyltransferases impairs mammalian heterochromatin and genome stability*. Cell, 2001. **107**(3): p. 323-37.
48. Slee, R.B., et al., *Cancer-associated alteration of pericentromeric heterochromatin may contribute to chromosome instability*. Oncogene, 2012. **31**(27): p. 3244-53.
49. Clift, D. and M. Schuh, *Restarting life: fertilization and the transition from meiosis to mitosis*. Nat Rev Mol Cell Biol, 2013. **14**(9): p. 549-62.



# CHAPTER 7

**Summary**

**Samenvatting**



# Summary

## Chapter 1

Currently, the average pregnancy rate per embryo transfer after *in vitro* fertilization (IVF) is around 32%. In order to achieve better results in the future, we need to gain knowledge on all aspects of the treatment, including pre-implantation embryo development.

In this thesis, we describe the research we performed into epigenetics and chromosome segregation in human pre-implantation embryos derived from IVF. The term 'epigenetics' refers to heritable marks on the genome, such as DNA methylation and histone modifications. These marks are essential for chromosome structure, chromosome segregation and gene expression. Chromosome segregation is the process in which duplicated chromosomes are equally separated over two cells during cell division.

Chromosomal abnormalities are detected at high frequencies in human pre-implantation embryos. This suggests that mechanisms regulating chromosome segregation are less functional during the first cell divisions of an embryo. Next to that, epigenetic marks, which are also important for correct chromosome segregation, are different in oocytes and spermatozoa and need to be re-established in early embryos. The research described in this thesis aimed to investigate both the mechanisms regulation chromosome segregation and the re-establishment of epigenetics marks in human pre-implantation embryos, in order to shed light on the causes of chromosomal abnormalities.

## Chapter 2

DNA is wrapped around histones, together forming chromatin. Epigenetic marks like histone modifications determine the structure of chromatin and define certain chromatin domains. Oocytes and spermatozoa have a very different chromatin structure, both from each other and from somatic cells, and after fertilization, canonical chromatin domains need to be re-established. In this chapter we investigated the re-establishment of a chromatin domain important for chromosome segregation, constitutive heterochromatin (cHC), in human pre-implantation embryos derived from IVF.

We describe that human spermatozoa carry histones with canonical cHC modifications (H3K9me3, H4K20me3, H3K64me3). After fertilization, these modified histones contribute to the formation of paternal embryonic cHC. The histone modifications are recognized by maternal chromatin regulators (e.g. HP1, SUV39H) and propagated over the embryonic cell divisions. These results indicate transgenerational epigenetic inheritance of cHC structure in human embryos and show that there is an important contribution of the spermatozoon to embryo development.

Until now, this process was studied only in mouse embryos, in which paternal cHC in spermatozoa and embryos lacks canonical modifications and is transiently established by other mechanisms, present in the oocyte. Often these results are assumed to be applicable for all mammalian species.

However, we now show that the mechanism in human embryos differs significantly from what has been described for mice. This points out that mouse embryos are not a representative animal model and underlines the need for research on human embryos.

## Chapter 3

One of the most important players in the regulation of chromosome segregation is a protein complex named chromosomal passenger complex (CPC). The CPC consists of the proteins Survivin, Borealin, INCENP and Aurora kinase B in somatic cells divisions (mitosis). In this chapter we investigated presence and composition of the CPC in human pre-implantation embryos derived from IVF.

We describe that the composition of the CPC in the first embryonic cell divisions is different from what has been described for somatic cells. In somatic cells, Aurora B is the kinetic subunit of the CPC. In pre-implantation embryos, from the zygote (day 1 of embryonic development) up to the 8- to 16-cell stage (day 3), we found Aurora C to be the main kinetic subunit present in the CPC. Until now, Aurora C has been described only in the cell divisions of germ cells, which result in oocytes and spermatozoa (meiosis). Around the morula stage (day 4), Aurora C levels decreased and at the blastocyst stage (day 5) Aurora C was completely replaced by Aurora B again. As subtle differences between the Aurora kinases might lead to less accurate regulation of chromosome segregation, the different composition of the CPC may contribute to chromosome segregation errors, which lead to chromosomal abnormalities, in the first cell divisions of human embryos.

## Chapter 4

Immunofluorescence has been widely used to study histone modifications and proteins involved in the regulation of chromosome segregation. Although it is important to study co-localization of these modifications and proteins, this is very difficult due to the limited availability of antibodies derived from different host species. For Western blot membranes, buffers were developed to remove antibodies after the first round of detection, called 'stripping', and thereby enable a second round of detection.

In this chapter, we describe that we were able to apply the stripping principle for sequential immunofluorescence on chromosome preparations of diverse cell types and human embryos. We show feasibility and reliability of detection of histone modifications and proteins in two rounds of immunofluorescence. This method is a reliable option when co-localization needs to be investigated and the choice of antibodies or the material, for example in case of human embryos, is limited.

## Chapter 5

Precise localization of the CPC at the inner centromeric area of chromosomes is crucial for accurate regulation of chromosome segregation. This localization is regulated by two histone modifications, H2ApT120 and H3pT3, which are catalyzed by the proteins Bub1 and Haspin respectively. In this chapter we investigated the localization of the CPC during the first cell divisions of human pre-implantation embryos derived from IVF.

We describe that CPC localization is less restricted to the inner centromere in the first embryonic cell division and that during the subsequent cell divisions, it becomes increasingly restricted, comparable with its localization in somatic cells. Of the two pathways that regulate inner centromeric localization of the CPC, we found the Bub1-H2ApT120 pathway to be comparable with what has been described for somatic cells. However, the Haspin-H3pT3 pathway was different in zygotes, during the first cell division of the embryo; instead of only centromeric, it was detected along the whole chromosome. This difference in the regulation of CPC localization may explain the less restricted CPC localization during the first cell divisions of embryos, which might be an explanation for chromosome segregation errors.

We also describe that the (partly altered) distribution of histone modifications involved in CPC localization and function, such as H3pT3 and H3pS10, in human pre-implantation embryos seems to be related to the epigenetic asymmetry between maternal and paternal chromosomes. Possibly, all these differences together lead to less accurate chromosome segregation and thereby may be a cause of chromosomal abnormalities in human pre-implantation embryos.

## Chapter 6

Our results show altered, and thereby probably less accurate, mechanisms that are involved in the prevention of chromosome segregation errors in human pre-implantation embryos. Also, our results show that human spermatozoa have an epigenetic contribution to embryo development. The altered error-correction mechanism and the epigenetic asymmetry between maternal and paternal chromosomes might together explain the high rates of chromosome segregation errors in human pre-implantation embryos. In our future research, we want to focus on the possible contribution of the spermatozoon to chromosome abnormalities in embryos. Knowledge of the influence of sperm quality on embryo developmental potential may lead to the optimization of IVF procedures in the future.



# Nederlandse samenvatting

## Hoofdstuk 1

De laatste jaren is het gemiddelde aantal zwangerschappen na terugplaatsing van een embryo ontstaan na in vitro fertilisatie (IVF) ongeveer 32%. Om nog betere resultaten te behalen in de toekomst, moeten we meer inzicht krijgen in alle aspecten van de IVF behandeling, inclusief de ontwikkeling van pre-implantatie embryo's.

In dit proefschrift beschrijven we het onderzoek dat we hebben gedaan op het gebied van epigenetica en chromosoomsegregatie in humane pre-implantatie embryo's ontstaan na IVF. Het begrip 'epigenetica' verwijst naar erfelijke markeringen op het genoom, zoals DNA methylatie en histon modificaties. Deze markeringen zijn cruciaal voor de structuur van chromosomen, chromosoomsegregatie en genexpressie. Chromosoomsegregatie is het proces waarbij verdubbelde chromosomen gelijk verdeeld worden over twee cellen tijdens een celdeling.

Chromosomale afwijkingen komen zeer frequent voor in humane pre-implantatie embryo's. Dit doet vermoeden dat de mechanismen die chromosoomsegregatie reguleren minder goed functioneren tijdens de eerste celdelingen van een embryo. Daarnaast zijn epigenetische markeringen, die ook belangrijk zijn voor correcte chromosoomsegregatie, heel verschillend in eicellen en zaadcellen, waardoor ze opnieuw moeten worden opgebouwd in embryo's. De studies die worden beschreven in dit proefschrift hadden als doel het onderzoeken van zowel mechanismen die chromosoomsegregatie reguleren als de opbouw van epigenetische markeringen in humane pre-implantatie embryo's, om meer inzicht te krijgen in de oorzaken van chromosomale afwijkingen.

## Hoofdstuk 2

DNA is opgerold rond speciale eiwitten, histonen, en samen wordt dat chromatine genoemd. Epigenetische markeringen, zoals histon modificaties, bepalen de structuur van het chromatine en specificeren bepaalde chromatine domeinen. Eicellen en zaadcellen hebben een heel andere chromatine structuur, die in beide cellen ook afwijkt van somatische cellen. Na de bevruchting moeten de normale chromatine structuur en domeinen opnieuw worden opgebouwd. In dit hoofdstuk onderzochten we de opbouw van een chromatine domein dat belangrijk is voor chromosoomsegregatie, constitutief heterochromatine (cHC), in humane pre-implantatie embryo's ontstaan na IVF.

We beschrijven dat humane zaadcellen histonen bevatten met modificaties die in somatische cellen cHC specificeren (H3K9me3, H4K20me3, H3K64me3). Na de bevruchting, in het embryo, dragen deze gemodificeerde histonen bij aan de opbouw van cHC in paternale chromosomen (chromosomen van de vader). De histon modificaties worden herkend door maternale eiwitten (eiwitten van de moeder, aanwezig in de eicel) die een rol hebben in de opbouw van de chromatine structuur (b.v.

HP1, SUV39H). Vervolgens worden de modificaties behouden gedurende de celdelingen van het embryo. Deze resultaten wijzen erop dat er bij mensen sprake is van overerving van cHC structuur over generaties en laten zien dat humane zaadcellen een belangrijke bijdrage leveren aan embryo-ontwikkeling.

Tot op heden was dit proces alleen bestudeerd in muizenembryo's. Bij de muis ontbreken de cHC modificaties in zaadcellen en op paternale chromosomen in het embryo, waardoor de opbouw van cHC tijdelijk gereguleerd wordt door andere mechanismen, die aanwezig zijn in de eicel. Vaak wordt aangenomen dat de resultaten verkregen in onderzoek naar muizenembryo's ook van toepassing zijn op alle andere soorten zoogdieren. We laten nu echter zien dat het mechanisme voor cHC opbouw in humane embryo's enorm verschilt van wat is beschreven voor muizenembryo's. Dit toont aan dat muizenembryo's geen representatief diermodel zijn en benadrukt het belang van onderzoek naar humane embryo's.

### Hoofdstuk 3

Een van de meest belangrijke onderdelen van het mechanisme dat chromosoomsegregatie reguleert, is een eiwitcomplex genaamd chromosomal passenger complex (CPC). Het CPC bestaat uit de eiwitten Survivin, Borealin, INCENP en Aurora kinase B tijdens de celdelingen (mitose) van lichaamscellen (somatische cellen). In dit hoofdstuk onderzochten we de aanwezigheid en samenstelling van het CPC in humane pre-implantatie embryo's die ontstaan zijn na IVF.

We beschrijven dat de samenstelling van het CPC in de eerste embryonale celdelingen verschilt van wat is beschreven voor somatische cellen. In somatische cellen is Aurora B de enzymatische component van het CPC. We ontdekten dat in pre-implantatie embryo's, van de bevruchte eicel (zygote, dag 1 van de embryonale ontwikkeling) tot en met het 8- tot 16-cellig stadium (dag 3), voornamelijk Aurora C aanwezig is als enzymatische component van het CPC. Tot op heden was beschreven dat Aurora C alleen een rol speelt in de celdelingen van geslachtscellen (meiose), die resulteren in eicellen en zaadcellen. Rond het morula stadium (dag 4) neemt de hoeveelheid Aurora C af en in het blastocyst stadium (dag 5) is Aurora C weer helemaal vervangen door Aurora B. Aangezien subtiele verschillen tussen de twee Aurora kinases zouden kunnen leiden tot een verminderde nauwkeurigheid van de regulatie van chromosoomsegregatie, zou de veranderde samenstelling van het CPC kunnen bijdragen aan fouten in chromosoomsegregatie, die leiden tot het ontstaan van chromosomale afwijkingen in de eerste celdelingen van humane embryo's.

### Hoofdstuk 4

Immunofluorescentie (kleuren met een fluorescerende antistof) is een vaak gebruikte techniek om histon modificaties en eiwitten die betrokken zijn bij de regulatie van chromosoomsegregatie te bestuderen. Hoewel het belangrijk is om co-lokalisatie (op dezelfde plek voorkomen) van deze modificaties en eiwitten te onderzoeken, is dit erg moeilijk, omdat antilichamen vaak worden

opgewekt in dezelfde diersoorten (b.v. muis, konijn) en daardoor niet te combineren zijn in één kleuring. Voor Western blot experimenten zijn vloeistoffen ontwikkeld die het mogelijk maken om antilichamen na een eerste ronde van detectie te verwijderen, "stripping" genoemd, en daarna nog een tweede ronde van kleuring en detectie te doen.

In dit hoofdstuk beschrijven we dat we in staat zijn om het stripping principe toe te passen voor het uitvoeren van meerdere rondes immunofluorescentie op chromosoompreparaten van diverse typen cellen en humane embryo's. We laten zien dat het haalbaar en betrouwbaar is om histon modificaties en eiwitten te detecteren in twee rondes immunofluorescentie. Deze methode is een betrouwbare optie als co-lokalisatie bestudeerd moet worden, maar de keuze van antilichamen of de beschikbaarheid van materiaal, zoals in het geval van humane embryo's, beperkt is.

## Hoofdstuk 5

Precieze lokalisatie van het CPC in het 'inner centromere' gebied van chromosomen is cruciaal voor nauwkeurige regulatie van chromosoomsegregatie. Deze lokalisatie wordt gereguleerd door twee histon modificaties, H2ApT120 en H3pT3, die gemaakt worden door respectievelijk de enzymen Bub1 en Haspin. In dit hoofdstuk onderzochten we de lokalisatie van het CPC gedurende de eerste celdelingen van humane pre-implantatie embryo's ontstaan na IVF.

We beschrijven dat CPC lokalisatie in mindere mate is beperkt tot alleen het inner centromere gebied tijdens de eerste embryonale celdeling en dat de lokalisatie gedurende de volgende delingen steeds preciezer wordt, tot het vergelijkbaar is met CPC lokalisatie in somatische cellen. Van de twee mechanismen die CPC lokalisatie reguleren, is het Bub1-H2ApT120 mechanisme vergelijkbaar met wat eerder beschreven is voor somatische cellen. Echter, het Haspin-H3pT3 mechanisme is anders in zygoten, tijdens de eerste celdeling; in plaats van alleen in het inner centromere gebied, detecteerden we H3pT3 op het hele chromosoom. Dit verschil in de regulatie van CPC lokalisatie zou de oorzaak kunnen zijn van de minder precieze CPC lokalisatie tijdens de eerste celdelingen van embryo's, en dit zou kunnen verklaren hoe de fouten in chromosoomsegregatie ontstaan.

We beschrijven ook dat de (deels veranderde) lokalisatie van histon modificaties die betrokken zijn bij CPC lokalisatie en functie, zoals H3pT3 en H3pS10, in humane pre-implantatie embryo's gerelateerd lijkt te zijn aan de epigenetische asymmetrie tussen maternale en paternale chromosomen. Mogelijk leiden al deze verschillen samen tot een minder nauwkeurige regulatie van chromosoomsegregatie en zouden daardoor een oorzaak kunnen zijn van chromosomale afwijkingen in humane pre-implantatie embryo's.

## Hoofdstuk 6

Onze resultaten laten zien dat er veranderde, en daardoor wellicht minder nauwkeurige mechanismen zijn om fouten in chromosoomsegregatie te voorkomen in humane pre-implantatie embryo's. Ook laten we zien dat humane zaadcellen een epigenetische bijdrage leveren aan embryo-

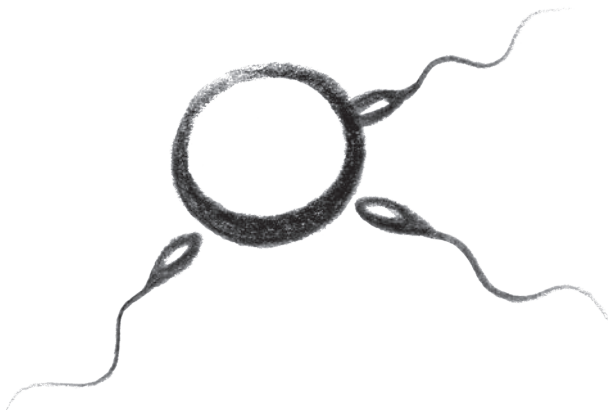
ontwikkeling. De veranderde mechanismen voor het voorkomen van fouten en de epigenetische asymmetrie tussen maternale en paternale chromosomen zouden samen een verklaring kunnen zijn voor de hoge frequentie van fouten in chromosoomsegregatie in humane pre-implantatie embryo's. In toekomstig onderzoek willen we ons richten op de mogelijke bijdrage van de zaadcel aan chromosoomafwijkingen in embryo's. Kennis over de invloed van zaadkwaliteit op embryo-ontwikkeling kan in de toekomst leiden tot de optimalisatie van IVF procedures.

# ADDENDUM

**PhD portfolio**

**Dankwoord**

**Curriculum Vitae**





## PhD portfolio

Name PhD student: Christine van de Werken  
 Research School: Molecular Medicine  
 PhD period: 01/10/2009 - 31/12/2013

### Courses

Basic Introduction Course on SPSS (Molecular Medicine)	2010
Update on Pluripotent Stem Cells, Barcelona, Spain (ESHRE)	2010
Course on Molecular Medicine (Molecular Medicine)	2010
Biomedical English Writing and Communication	2011
Presenting Skills for PhD-students (Molecular Medicine)	2011
Microscopic Image Analysis: From Theory to Practice (Molecular Medicine)	2011
Loopbaanoriëntatie voor wetenschappers	2012

### Workshops

Workshop EndNote (Medical Library)	2010
Workshop Photoshop (Molecular Medicine)	2010
Erasmus MC PhD Day	2010
EmbryoScope Embryo Monitoring System User Workshop, Aarhus, Denmark	2010
Get out of your lab Days (Molecular Medicine)	2011

### (Inter)national conferences

Stem Cells in Development and Disease, Amsterdam, The Netherlands	2009
Vergadering Vereniging voor Fertilitestsstudie, Tilburg, The Netherlands	2009
MolMed Day, Rotterdam, The Netherlands	2010
Dutch Stem Cell Meeting (DSSCR), Utrecht, The Netherlands	2010
ESI Opening Symposium, Rotterdam, The Netherlands	2010
ESHRE 26 <sup>th</sup> Annual Meeting, Rome, Italy	2010
8 <sup>th</sup> Dutch Chromatin Meeting, Leiden, The Netherlands	2010
Vergadering Vereniging voor Fertilitestsstudie, Nijmegen, The Netherlands	2010
MolMed Day, Rotterdam, The Netherlands	2011
The EMBO Meeting, Vienna, Austria	2011

Vergadering Vereniging voor Fertilitestsstudie, Utrecht, The Netherlands	2011
Wetenschapsmiddag KLEM, Nijmegen, The Netherlands	2012
ESHRE 28 <sup>th</sup> Annual Meeting, Istanbul, Turkey	2012
Ovarian Club II, Prague, Czech	2012
MolMed Day, Rotterdam, The Netherlands	2013

## Presentations

### Posters

ESHRE 26th Annual Meeting, Rome, Italy	2010
MolMed Day, Rotterdam, The Netherlands	2011
The EMBO Meeting, Vienna, Austria	2011
Ovarian Club II, Prague, Czech	2012
ESHRE 29th Annual Meeting, London, United Kingdom	2013

### Orals

Vergadering Vereniging voor Fertilitestsstudie, Nijmegen, The Netherlands	2010
Wetenschapsdag Voortplantingsgeneeskunde, Erasmus MC	2011
Vergadering Vereniging voor Fertilitestsstudie, Utrecht, The Netherlands	2011
ESHRE 28 <sup>th</sup> Annual Meeting, Istanbul, Turkey	2012
Jaarlijkse Onderzoeksmiddag Verloskunde en Gynaecologie, Erasmus MC	2012
Science meeting Verloskunde & Gynaecologie en Urologie, Erasmus MC	2013
MolMed Day, Rotterdam, The Netherlands	2013

## Travel grants

The EMBO Meeting: Stichting Simonsfonds, Nijmegen, The Netherlands	2011
ESHRE 28th Annual Meeting: Trustfonds Erasmus	2012

## Teaching activities

Supervising student internship (Keuzeonderzoek Bachelor Geneeskunde)	2010
Supervising student internship (Master Molecular Medicine)	2011
Supervising student internship (Master Molecular Medicine)	2012
Supervising student internship (afstudeerstage HLO)	2012
Supervising student internship (Keuzeonderzoek Bachelor Geneeskunde)	2012



## Dankwoord

Een boekje als dit schrijf je absoluut niet alleen en daarom wil ik hier iedereen bedanken die heeft bijgedragen aan de inhoud van mijn proefschrift, mijn tijd als onderzoeker en mijn leven naast het onderzoek.

Allereerst wil ik alle IVF patiënten die hun restembryo's hebben gedoneerd voor onderzoek bedanken. Zonder die embryo's zou ik dit onderzoek niet hebben kunnen doen en zouden we niet steeds meer te weten komen over pre-implantatie embryo-ontwikkeling, iets dat van groot belang is voor het verbeteren van IVF behandelingen.

Beste Joop, bedankt dat je me de kans gaf om na mijn afstudeerstage te starten aan een promotietraject. Het was een ontzettend leerzame tijd. Je was altijd oprecht geïnteresseerd in mijn resultaten en gaf me alle vertrouwen, ook als de door jou zo geliefde deadlines weer eens niet gehaald werden, dankjewel!

Beste Esther, jij was de spil in dit alles. Al tijdens mijn stage wist je mij enthousiast te maken voor je onderzoek en vakgebied. Ik ben ontzettend blij dat ik onder jouw leiding mocht promoveren. Ook tijdens mijn promotie, als ik soms even pessimistisch was, wist je altijd weer mijn enthousiasme aan te wakkeren. Bedankt voor al je hulp, geduld en vriendschap.

Geachte prof.dr. J.H. Gribnau, prof.dr. R.M.W. Hofstra en prof.dr. S.M.A. Lens, hartelijk dank dat u zitting heeft willen nemen in de leescommissie.

Beste Godfried, bedankt voor al je hulp; van de 'freaky' ICSI's in het begin tot de begeleiding in de afrondende fase. Jij was er toen Esther er even niet kon zijn, dankjewel!

Beste Margarida, ik vond het ontzettend leuk dat ik met jou kon samenwerken. Je was een collega om alles mee te bespreken, ook naast het onderzoek. Bedankt voor alle hulp bij de experimenten en bij het schrijven van de papers!

Beste Cindy, wat was ik blij dat je onderzoek kwam doen bij ons in de 'groep'! Je kwam precies op het juiste moment en nam me al het praktische werk uit handen, zodat ik me kon concentreren op het schrijven van de inhoud van dit boekje. Ik had ook meteen weer iemand om tegenaan te kletsen (en zeuren soms...), dankjewel voor je steun en de gezelligheid! Ontzettend leuk dat je als paranimf naast me wilt staan!

Beste Hánah, Miriam, Joyce, Michelle en Line, wat leuk dat jullie onze groep uitkozen voor een stage. Toen iedereen weer weg was, was het wel erg stil. Ik heb jullie met veel plezier begeleid en op mijn beurt erg veel geleerd van jullie slimme vragen. Bedankt voor al het werk dat jullie gedaan hebben!

Beste Amy, Claudia, Jeroen, Karin van der Horn, Karin van Veen, Miranda, Nel, Nicole, Samantha, Sanne en Shirley, bedankt voor al jullie hulp. Wat ik ook vroeg, welk materiaal ik ook nodig had, het was nooit een probleem. In het bijzonder Amy, Jeroen en Karin van Veen bedankt voor alle keren dat jullie weer inhibitors in de EmbryoScope-wells pipetteerden en Karin van Veen natuurlijk ook voor alle heterologe ICSI's die je hebt gedaan. Jullie zijn een ontzettend leuk IVF-team, waarin ik me altijd welkom voelde, dank jullie wel!

Beste collega's van de IVF afdeling, alle gynaecologen, fertiliteitsartsen en verpleegkundigen, bedankt voor de prettige samenwerking, ook op de maandelijkse informatieavond.

Beste Hikke, Ilse, Willy, Federica, Fabrizia, Maureen, Aristeia en Catherine, bedankt voor jullie interesse, het meedenken, de antilichamen, de muizeneicellen, en alle andere hulp. Zulke samenwerkingen zijn ontzettend waardevol! Catherine, ook al kregen we het niet voor elkaar om blastocysten te kleuren met die kit, we hebben toch hele gezellige uren gehad op het lab, dankjewel!

Beste Holger, al tijdens mijn afstudeerstage leerde je me alles over de RT-qPCR en ook bij mijn promotietraject was je weer nauw betrokken. Zonder jou was die 'stripping' paper er niet gekomen! Bedankt voor al je begeleiding!

Beste Peter, Marieke, Heleen en Liliana, bedankt voor de goede samenwerking. We hebben erg veel profijt gehad van het decondensatie protocol!

Beste medeonderzoekers van de 22<sup>e</sup> en andere delen van het gebouw, door de jaren heen o.a. Marieke, Jinke, Jennifer, John, Marijana, Fatima, Kim, Evelyne, Babette, Irene, Matthijs, Emilie, Nicole, Caroline, Nina, Zoe, Leonie, Bas en Ruben (sorry als ik iemand vergeet te noemen), allemaal bedankt voor de goede sfeer, alle kopjes thee en de leuke 'onderzoekers-lunches'.

Lieve Yvonne en Wendy, van Istanbul tot Eindhoven 'de gekste'... met jullie was het altijd ontzettend gezellig. Daarnaast waren jullie er ook voor de praktische zaken rondom mijn promotie, super! Dank jullie wel!

Beste Jolanda, bedankt voor alle keren dat je afspraken voor me plande in de agenda van Joop en voor het verwerken van allerlei formulieren en andere praktische zaken.

Beste Marjan, Jolanda, Hannie & co., bedankt voor alle gezellige lunches. Ontzettend leuk dat jullie me zo gastvrij opnamen in de 'klinische genetica'-groep.

Beste Ank, Anne, Annelieke, Else, Hanneke en Lisette, bedankt voor de leuke cursus en de daaropvolgende lunches en heel veel succes in jullie verdere carrière!

Beste collega's van Synthon, bedankt voor de warme ontvangst, super goede werksfeer en al jullie interesse in en begrip voor het afmaken van mijn proefschrift.

Beste Rianne en Ronald, als 'kleuterjuf' en 'groep 8 meester' stonden jullie aan het begin van mijn loopbaan en later bleven jullie altijd geïnteresseerd. Ik vind het dan ook erg leuk om jullie nu dit resultaat te laten zien. Ronald, bedankt voor mijn 10<sup>e</sup> stelling; ik ben het er al die jaren al helemaal mee eens!

Lieve Sandra, Julia (en Peter natuurlijk: zoals je zo graag wilde, staat jouw naam nu ook in dit proefschrift, haha), Emilie en Marijke, bedankt voor jullie vriendschap. Ik geniet van al die keren dat we samen eten, thee drinken en uren kletsen!

Lieve Ton, Ans, Niels en Petra, wat een super schoonfamilie heb ik getroffen! Bij jullie voelde ik me meteen thuis. Bedankt voor alle gezelligheid, interesse en zorgzaamheid.

Lieve Ada, dit is het dan, de eerste mijlpaal in mijn leven waar Gert niet meer bij is. Wat was hij teleurgesteld toen bij de uitreiking van mijn Master diploma bleek dat de docenten geen toga en baret droegen en wat zou hij deze ceremonie graag gezien hebben. In mijn hart zal hij altijd overal bij zijn. Bedankt voor alle gezelligheid die we bij jullie mochten en nog steeds bij jou mogen beleven!

Lieve opa en oma, wat fijn dat jullie hier nog bij kunnen zijn. Dank jullie wel voor al het plezier dat Elisa en ik door de jaren heen met jullie gehad hebben, het was altijd geweldig. Betere grootouders kunnen we ons niet wensen!

Lieve Elisa, je vond de tekst ooit zelf: "geen betere vriendin dan een zus en geen betere zus dan jij". Treffender kan ik het niet zeggen! Bij jou kan ik altijd helemaal m'n 'rare zelf' zijn en ik kan alles met je delen. Of we nou samen op de bank hangen, winkelen of op vakantie gaan, het is altijd genieten. Onze band is onverwoestbaar en dat jij mijn paranimf zou zijn, stond al vast voor ik aan dit onderzoek begon.

Lieve pap en mam, hoe zou ik jullie ooit kunnen bedanken; het is gewoon niet in woorden uit te drukken. Dank jullie wel voor jullie grenzeloze liefde, steun en zorgzaamheid. Zonder jullie was ik nooit zo ver gekomen!

Lieve Martijn, jij bent het allermooiste resultaat van dit promotietraject. Als ik soms dacht "was ik hier maar nooit aan begonnen", dacht ik meteen daarna "gelukkig maar, anders had ik Martijn nooit ontmoet". Samen met jou werd Rotterdam de mooiste stad van het land en na onze verhuizing naar Ede weet ik dat ik me met jou overal thuis voel. Jij bent het perfecte maatje om alle leuke en soms moeilijke dingen mee te delen. Je bent geweldig, ik houd van je!

Christine  
mei 2015



## Curriculum Vitae

Christine van de Werken was born on May 3<sup>rd</sup> 1986 in Werkendam. After finishing her secondary school (VWO) at CSG Oude Hoven in Gorinchem, in 2004, she started her study Biomedical Sciences at Utrecht University. In October 2009, she graduated from the Master Cancer Genomics & Developmental Biology. From October 2009 until December 2013 she worked on the research described in this thesis, performed at the Department of Obstetrics & Gynaecology of the Erasmus MC University Medical Center Rotterdam. In May 2014, she started working as a Regulatory Affairs Manager at Synthon in Nijmegen.

Christine van de Werken werd geboren op 3 mei 1986 in Werkendam. Na het behalen van haar VWO diploma op CSG Oude Hoven in Gorinchem, in 2004, begon zij aan haar studie Biomedische Wetenschappen aan de Universiteit Utrecht. In oktober 2009 haalde zij het diploma voor de Master Cancer Genomics & Developmental Biology. Van oktober 2009 tot december 2013 werkte ze aan het onderzoek dat is beschreven in dit proefschrift, op de afdeling Verloskunde & Gynaecologie van het Erasmus MC Rotterdam. In mei 2014 begon zij als Regulatory Affairs Manager bij Synthon in Nijmegen.



